DISSERTATION

ACETAL-FUNCTIONALIZED ENCAGED COPPER(I) COMPLEXES AND POLYMER ENCAPSULATED REVERSE MICELLE COMPOSITES

Submitted by

Joseph J. Kremer

Department of Chemistry

In partial fulfillment of the requirements
For the Degree of Doctor of Philosophy
Colorado State University
Fort Collins, CO 80523
Fall 2006

ProQuest Information and Learning Company
300 North Zeeb Road
P.O. Box 1346
Ann Arbor, MI 48106-1346

COLORADO STATE UNIVERSITY

JULY 25, 2006

WE HEREBY RECOMMEND THAT THE DISSERTATION PREPARED UNDER OUR SUPERVISION BY JOSEPH J. KREMER ENTITLED "ACETAL-FUNCTIONALIZED ENCAGED COPPER(I) COMPLEXES AND POLYMER ENCAPSULATED REVERSE MICELLE COMPOSITES" BE ACCEPTED AS FULFILLING, IN PART, REQUIREMENTS FOR THE DEGREE OF DOCTOR OF PHILOSOPHY.

Committee on Graduate Work

Amy L Prieto

C. Michael Elliott

Adviser

Department Head

ABSTRACT OF DISSERTATION

ACETAL-FUNCTIONALIZED ENCAGED COPPER(I) COMPLEXES AND POLYMER ENCAPSULATED REVERSE MICELLE COMPOSITES

This work describes synthetic methods for encaging coordination complexes within ligand frameworks and polymer encapsulated reverse micelle composites. Caging coordination complexes in this manner can preserve some facets of the complexes' chemical identity and behavior while simultaneously changing others.

Chapter 1 considers the methodologies employed towards preparing encaged copper(I) complexes through performing interligand cyclizations with diacetal-derivitized 5,5'-dicarboxaldehyde-2,2'-bipyridine bischelated precursor complexes ($[Cu^I(NN)_2]X$). Encaging copper(I) protects it both from oxidation and from axially directed nucleophilic attack. The prepared copper(I) complexes displayed long emission lifetimes (> 0.50 μs), thus enabling them to store and ultimately transfer both electrons and energy.

Chapter 2 addresses many unresolved issues surrounding the production of tris(bipyridine)ruthenium(II) chloride ($[Ru(bpy)_3]Cl_2$) chromophore-sequestered polymer encapsulated reverse micelle composite (PERMC) materials. Styrene:divinylbenzene composite precursor reverse micellar solution (CPRMS) nonpolar phases are polymerized in order to prepare the PERMC materials. Desired 'bulk solution-like behavior' of the sequestered polar chromophores is realized upon their PERMC sequestration.

Chapter 3 presents the conclusion of research performed on phenoxazine (POZ) donor-based Donor-Chromophore-Acceptor ($D\text{-}C^{2+}\text{-}A^{2+}$, or triad)-sequestered PERMC materials. Triad-sequestered PERMCs can serve as optically addressable solid-state sensors for the detection of external magnetic fields. Upon triad photoexcitation, a series of electron transfer steps occurs which produces a spectroscopically detectable triplet biradical Charge Separated State (^{3}CSS, $D^{+\bullet}$-C^{2+}-$A^{+\bullet}$) but only in solution. The ^{3}CSS lifetimes (τ_{CSS}) of the sequestered triads lengthen and become biexponential in quality as magnetic field strength increases. Such behavior constitutes a magnetic field effect (MFE). The composite nature of the PERMCs allows for such MFEs to be detected.

Chapter 4 provides a forum for the introduction of $[Ru(bpy)_3]Cl_2$ chromophore-sequestered PERMCs of the following cationic, zwitterionic, and anionic surfactant:cosurfactant systems: cetyltrimethylammonium bromide:1-octanol (1 CTAB: 5 C_8OH), cetyldimethylbenzylammonium bromide (CDBA), hexadecylpyridinium bromide (HDPB), phosphatidylcholine extracted from soy lecithin, and Aerosol-OT:trioctylphosphine oxide (3 AOT:2 TOPO). Chapter 5 builds on the above work by characterizing POZ donor-based triad-sequestered PERMC magnetic field sensors of different surfactant:cosurfactant systems.

Joseph J. Kremer
Department of Chemistry
Colorado State University
Fort Collins, CO 80523
Fall 2006

ACKNOWLEDGEMENTS

I am indebted to the following people who made this work possible. First and foremost, I am grateful to my graduate research advisor, Dr. C. Michael Elliott. He has invited me to attend a Gordon Research Conference to be a poster presenter and has shown me how to write and communicate more effectively. It was not an easy process by any means, but I sincerely thank him for help with writing. I also thank him for laboratory help which ranged from setting up a Fischer-Porter bottle apparatus to conducting experiments on some of my PERMC samples at The Universität of Konstanz in Germany. I know that Mike truly enjoys graduate research advising. He devises very interesting projects, and I have enjoyed my time working on two of them. Lastly, I thank him for letting me pet-sit his cat Mr. Earl. It was a pleasure.

Dr. Oren Anderson took a personal interest in my early success and for that I thank him. Also, Dr. Vijaya Sampath and Dr. Agnete LaCôur were my immediate supervisors when I was a C-344 teaching assistant. I thank them for patiently helping me transition into teaching assistant responsibilities.

The Elliott Research Group can take credit for the success that I have enjoyed. In particular, I thank Matthew Rawls for the help he gave me when I was preparing the phenoxazine donor-based triad. I thank Mike Scott for his help with transient absorption experiments. I thank Shawn, John, Corey, and Brian for their help. I will miss Tashi Herzmark's 'crazy-train' laugh. Last but not least, I thank the remaining Elliott Research Group members--especially for the farewell party that they threw for me.

I have had the pleasure of developing new students' laboratory skills as a graduate research assistant in Mike's group. Leah Reid, a Rocky Mountain High School graduate,

assisted me over the span of a year. I appreciated her cheerful demeanor everyday when she arrived for work in that she always said 'hi,' and asked how I was doing. Ryan Davis, a Colorado State University senior, has worked diligently on the polymer encapsulated reverse micelle thin film project which is not presented in this dissertation. I credit both Leah and Ryan, and I thank them for their efforts.

I thank Dr. Karsten Hötzer from The Universität of Konstanz. His willingness to perform experiments on some PERMCs when our time-resolved transient absorption system was in flux is invaluable. I also thank Yunfeng Lu who helped me to perform surface analysis experiments on the composites. Both Karsten and Yunfeng are duly co-authors of the corresponding publications.

I thank the following faculty members who have been active in my success. It was a pleasure working with Dr. Nancy Levinger after she took such a vested interest in the PERMC project. I am honored to have worked with her, and I am so thankful to have consulted with her on many issues. I thank both Dr. Bruce Parkinson for reviewing surface analysis interpretations and Dr. Carl Patton for coping with a broken gaussmeter.

I thank the chemistry department personnel. In particular, I thank machinist Elden Burk. It is noteworthy that Elden assisted with the installation of our group's electromagnet. I thank Bob Kraus for helping me ship international parcels. I thank Mike Olsen for state-of-the-art glassblowing services and for great conversation. I thank "The Two Don's", Don Heyse and Don Dick, and also Chris Rithner for their help with both nuclear magnetic resonance and mass spectroscopy experiments. I especially want to thank Don Dick, because I tested his patience a few times regarding the tendency of the perchlorate salts of the copper complexes to hinder instrumental performance.

I thank the chemistry department business assistants. I thank Jan Moder, Kathy Martinolich, and Cindy Ungerman for preparing letters of recommendation for me on behalf of my references. I thank Tach Costello for looking after two of my plants and for ‘dropping everything’ and helping me send faxes. I thank Shelly Shaeffer for helping me compose letters to financial institutions.

My family has a lasting impact on my work. This dissertation is dedicated to them. My mother and father didn’t know a lot about graduate school culture, but they nevertheless provided the same direction and comfort that they always have in the past. I thank Aunt Patti especially for her emails which were an invaluable centering point for me. I am grateful for the trips I took to see my brother Matthew in California and the places that we visited like Yosemite, brine shrimp- and alkali fly-infested Mono (Mŏw′′nō) Lake, the ghost town Bodie (Bō′′dē), and The Big Sur. I thank my brother Dan for being an equally good friend. Lastly, I thank Gram Kennedy for her support. I am glad that she can see me graduate.

In closing, Ft. Collins was a wonderful place to live. Colorado is a prime locality for trout fishing. I will miss my weekend outings to Carter and Red Feather Lakes. The ‘Pittsburgh Steeler Bar’ at the County Cork was always lively-win or lose. I will miss watching the Steeler games with John, Eric, Freddie Franz, Steve Cullen, and the other 75+ Steeler fans after doing so for four seasons. While waiting for ‘Steeler Bar’ or fishing weekends, I was fortunate to come home to my black & white tuxedo cat Cornelius every night. He is the coolest cat but watch your ankles.

**This dissertation is dedicated to Mom, Dad, Matt, Dan,
Aunt Patti, Big Z, Aunt Andrea, Uncle John, Gram
and the memory of Pap Kennedy and Pap & Gram Kremer**

TABLE OF CONTENTS

Chapter 1. Acetal-functionalized Encaged Bis(bipyridine)copper(I) Complexes

Chapter 2. Chromophore-sequestered Polymer Encapsulated Aerosol-OT Reverse Micelle Composite Materials of Aqueous and Nonaqueous Polar Phase Constitutions

Chapter 3. Triad-sequestered Polymer Encapsulated Reverse Micelle Composite Materials as Optical Magnetic Field Sensors

Chapter 4. Chromophore-sequestered Polymer Encapsulated Reverse Micelle Composite Materials of Cationic, Zwitterionic, and Mixed Surfactant Systems

Chapter 5. Triad-sequestered Polymer Encapsulated Reverse Micelle Composite Materials of Cationic and Mixed Surfactant Systems as Optical Magnetic Field Sensors

LIST OF ILLUSTRATIONS

Tables:

Figures:

LIST OF ABBREVIATIONS AND SYMBOLS

[Chromophore]	chromophore molar concentration
[Cosurfactant]	cosurfactant molar concentration
$[Cu(dmp)_2]ClO_4$	bis(2,9-dimethyl-1,10-phenanthroline)copper(I) perchlorate
$[Cu(dpp)_2]ClO_4$	bis(2,9-diphenyl-1,10-phenanthroline)copper(I) perchlorate
$[Cu(CH_3CN)_4]ClO_4$	tetrakis(acetonitrile)copper(I) perchlorate
$[Cu(NN)_2]X$	a generic bischelated copper(I) complex with α,α-diimine ligands
$[CuL_2]X$	a generic bischelated copper(I) complex
[Polar phase]	polar phase concentration
$[Ru(bpy)_3]Cl_2$	tris(2,2'-bipyridine)ruthenium(II) chloride
[Surfactant]	surfactant molar concentration
[Triad]	triad molar concentration
1a	pyridinium *para*-toluenesulfonate acid catalyst
1c	bis(2,2'-bipyridine-5,5'-tetrakis(1,4-*trans*-dimethanolcyclohexane)acetal)copper(I) perchlorate
1l	(4,4′,4″,4‴-(2,2′-bipyridine-5,5′-diylbis(methanetriyl)tetrakis(oxy)tetrakis(methylene) tetrakis(trans-cyclohexane-4,1-diyl)))tetramethanol
1u	bis(4,4′,4″,4‴-2,2′-bipyridine-5,5′-diylbis(methanetriyl)tetrakis(oxy)tetrakis(methylene) tetrakis(trans-cyclohexane-4,1-diyl)tetramethanol)copper(I) perchlorate
^{1}CSS	charge separated state of singlet multiplicity (where multiplicity is the quantity (2S+1) and S is the spin quantum number)
^{1}CTS	charge transfer state of singlet multiplicity
^{1}H NMR	proton nuclear magnetic resonance

2a	*iso*-propylammonium *para*-toluenesulfonate acid catalyst
2c	bis(2,2′-bipyridine –5,5′-tetrakis(1,4-dimethanolbenzene)acetal)copper(I) perchlorate
2l	(4,4′-((5-((3-(hydroxylmethyl)benzyloxy)(4-(hydroxylmethyl)benzyloxy)methyl)-2,2′-bipyridin-5'-yl)methylene)bis(oxy)bis(methylene)bis(4,1-phenylene))dimethanol
2u	bis(4,4′-((5-((3-(hydroxylmethyl)benzyloxy)(4-(hydroxylmethyl)benzyloxy)methyl)-(2,2′-bipyridin-5′-yl)methylene)bis(oxy)bis(methylene)bis(4,1-phenylene))dimethanol)copper(I) perchlorate
^{3}CSS	charge separated state of triplet multiplicity
^{3}CTS	charge transfer state of triplet multiplicity
^{3}MLCT	metal-to-ligand charge-transfer state of triplet multiplicity
4-DQ^{2+}	diquaternary bipyridine acceptor containing a three-carbon $(CH_2)_n$ bridge with a two-carbon methylene linker $(CH_2)_n$ to the *para* (4) position of the 2,2'-bipyridine ligand of the chromophore
A	absorbance
A$^{+\bullet}$	reduced electron acceptor moiety
A^{2+}	electron acceptor moiety
A$_0$	set-point amplitude
ACN	acetonitrile
ADPN	2,2'-azobis(2,4-dimethylpentanenitrile)
A$_{fast}$	weighting factor for the fast component of the triplet charge separated state biexponential decay
AgNO$_3$	silver nitrate
AIBN	2,2'-azobis(isobutyronitrile)
AOT	Aerosol-OT, or sodium bis(2-ethylhexyl)sulfosuccinate

ASCII	American Standard Code for Information Interchange
A_{slow}	weighting factor for the slow component of the triplet charge separated state biexponential decay
ASTM	American Society of Testing and Materials
bpy	2,2'-bipyridine
B_{app}	externally applied magnetic field strength
BPO	benzoyl peroxide
cmc	critical micelle concentration below which micelles cannot form
c_{plr}	concentration of the polar phase solvent in a composite precursor reverse micellar solution
c_{surf}	concentration of the surfactant in a composite precursor reverse micellar solution
C^{2+}	chromophore moiety
C_8OH	1-octanol
CCl_4	carbon tetrachloride
CD-ROM/R/RW	compact disc-random operating memory/read/read and write (record)
CDBA	cetyldimethylbenzylammonium chloride
$CDCl_3$	deuterated chloroform (not deuterated methyl chloride)
CD_3CN	deuterated acetonitrile
CE	counter electrode
$CHCl_3$	chloroform
CH_3CN	acetonitrile
ClO_4^-	perchlorate
CPRMS	composite precursor reverse micellar solution

CSS	charge separated state (D$^{+\bullet}$-C^{2+}-A$^{+\bullet}$)
CT	radical polymerization chain transfer agent
CTAB	cetyltrimethylammonium bromide
CTS	charge transfer state (D-C^{3+}-A$^{+\bullet}$)
Cu^{I}(bpy)$_2^+$	**bis(2,2'-bipyridine)copper(I)**
Cu^{I}(ClO$_4$)$_2$	copper(II) perchlorate
Cu^{I}(phen)$_2^+$	bis(1,10-phenanthroline)copper(I)
CV	cyclic voltammetry
dvb	divinylbenzene
D	electron donor moiety
D$^{+\bullet}$	oxidized electron donor moiety
D-C^{2+}-A^{2+}	donor-chromophore-acceptor supramolecular triad
D$_{2d}$	dihedral point group with a C$_2$ symmetry axis
D$_2$NND$_2$	deuterated hydrazine
D$_2$O	deuterated water
D$_{4h}$	square planar point group
DCM	dichloromethane
DDI	doubly deionized water
DLS	dynamic light scattering particle sizing
DMB	5,5'-dimethyl-2,2'-bipyridine
DMSO	dimethylsulfoxide
DVD-ROM/RAM	digital video disc-random operating memory/random access memory
eq.	molar equivalent (mol ratio)

eV	electron volt
$E_{1/2}$	half-wave potential
$E_{1/2}^{(Cu(I)/Cu(II))}$	half-wave potential of the copper(I)/copper(II) redox couple
EC	electrochemical process-chemical reaction
$E_{encapsulation}$	energy of an encaged copper(I) complex
$E_{hydrogenated}$	energy of an uncaged precursor copper(I) complex
$E_{pa}^{(Cu(I)/Cu(II))}$	anodic (oxidation) wave potential of the copper(I)/copper(II) redox couple
ES	excited state
ESI^+	cationic electrospray ionization mass spectrometry
EtOAc	ethyl acetate
E_Y	Young's Modulus (tensile stress divided by tensile strain)
f	focal length of a lens
f. w.	formula weight
F	applied tensile force
$Fe(ClO_4)_2 \bullet x\ H_2O$	ferrous perchlorate hydrate
FPT	freeze-pump-thaw degassing
GS	ground state ($D-C^{2+}-A^{2+}$)
H_2NNH_2	hydrazine
H_2O	water
Hz	hertz or reciprocal second
i_{cmc}	induced critical micelle concentration
isc	intersystem crossing

I	intensity at time t (corresponds to the difference between the offset and the signal)
I_{em}	maximum emission intensity
I_o	baseline intensity (corresponds to the vertical offset magnitude)
IPTS	*iso*-propylammonium *para*-toluenesulfonate acid catalyst
k_1	rate of formation of the charge transfer state
k_1'	reverse rate of formation of the charge transfer state
k_2	rate of formation of the charge separated state
k_3	rate of spin-allowed relaxation of the singlet charge separated state
k_4	rate of spin-forbidden relaxation of the triplet charge separated state
l	length
LFSE	ligand field stabilization energy
LUMO	lowest unoccupied molecular orbital
m/z	mass-to-charge ratio
mol %	mol percent
M	magnetization
MeOH	methanol
MFE	magnetic field effect
MLCT	metal-to-ligand charge-transfer photoexcited state
MO	magnetooptical
MP	melting point
n	methylene unit (-CH_2-) chain length

n-POZ	phenoxazine donor with a methylene linker ($(-CH_2-)_n$) of length n bridged at the *para* (4) position of the 2,2'-bipyridine chromophore ligands
N_2	nitrogen gas
N_A	Avogadro's number
Na_2CO_3	sodium carbonate
$NaHCO_3$	sodium bicarbonate
NaOH	sodium hydroxide
NBS	N-bromosuccinimide
Nd:YAG	neodymium-doped yttrium aluminum garnet
NH_4^+	ammonium
NH_4PF_6	ammonium hexafluorophosphate
NO_3^-	nitrate
phen	1,10-phenanthroline
pS-DVB	poly(styrene-*co*-divinylbenzene)
P	molar ratio of cosurfactant to surfactant
PDI	averaged polydispersity index of a reverse micelle population determined from particle sizing experiments
PERMC	polymer encapsulated reverse micelle composite material
PF_6^-	hexafluorophosphate
PMT	photomultiplier
POZ	phenoxazine
PPTS	pyridinium *para*-toluenesulfonate acid catalyst
r	averaged radius of a reverse micelle population determined from dynamic light scattering particle sizing experiments

R	rheostat
R. M.	reverse micelle
R^2	linear regression (goodness of fit)
RE	reference electrode
RE'	rare earth element
R_f	retention factor
$[Ru^{3+}(bpy)_2(bpy^{\bullet-})]X$	tris(bipyridine)ruthenium(II) electronic structure after metal-to-ligand charge transfer photoexcitation
RT	room temperature (298.15 K)
sty	styrene
S:N	signal-to-noise ratio
SEM	scanning electron microscopy
SSCE	saturated sodium calomel electrode (a reference electrode)
t	time
t_p	composite precursor reverse micellar solution nonpolar phase polymerization time
T	temperature
T_0	median energy level of the nondegenerate triplet charge separated state
$T_\pm$	highest and lowest energy levels of the nondegenerate triplet charge separated state
T_1	spin-spin (longitudinal) relaxation time
T1	$[Ru(II)(4\text{-}POZ)_2(4\text{-}DQ^{2+})](NO_3^-)_4$, a $D\text{-}C^{2+}\text{-}A^{2+}$ triad
T_c	magnetic coercivity temperature
T_d	tetrahedral point group

T_{dec}	polymer or composite thermal decomposition temperature
TLC	thin layer chromatography
TGA	thermalgravimetric analysis
TIFF	tagged image file format
TM-AFM	tapping mode-atomic force microscopy
T_p	composite precursor reverse micellar solution nonpolar phase polymerization temperature
UV	ultraviolet
UV-vis	ultraviolet-visible
vol. %	volume percent
V	voltage
Vis	visible
V_{nplr}	total volume of the nonpolar phase of a composite precursor reverse micellar solution
V_{plr}	total volume of the polar phase of a composite precursor reverse micellar solution
$V_{R.M.}$	volume of a spherical reverse micelle fluid core
V_{tot}	total volume of a reverse micellar solution
wt. %	weight percent
W	watt
W_0	molar ratio of polar phase to surfactant
WD	working distance between the electron beam and sample in scanning electron microscopy experiments
WE	working electrode
XPS	x-ray photocorrelation spectroscopy

δ	chemical shift (ppm)
ε	tensile strain
λ	wavelength
λ_{em}	emission maximum wavelength
λ_{max}	absorption or emission maximum wavelength
ρ	density
σ	one standard deviation unit
σ (nm)	polydispersity of micellar radii
τ	process lifetime
τ_{CSS}	the triplet charge separated state lifetime
$\tau_{CSS(fast)}$	fast component of the triplet charge separated state biexponential lifetime
$\tau_{CSS(slow)}$	slow component of the triplet charge separated state biexponential lifetime
τ_{em}	emission lifetime
Δ	change in
Δl	change in sample length with applied tensile force
ΔA	change in absorption
ΔE_p	voltage difference between oxidative and reductive wave peaks in cyclic voltammetry experiments
ΔI	change in intensity at time t = 0 (corresponds to the signal)
$\Delta \Phi$	phase difference in TM-AFM phase images
Θ_K	Kerr angle
Ω	ohm

©	copyright
°	degree
↑	magnetization vector
→, ←, ↑, and ↓	molecular motion vectors
*	photoexcited state
®	restricted
™	trademark

FUNDING

Financial support for the work contained in this dissertation was provided by the National Science Foundation (CHE 0113112 and CHE 0139637).

Chapter 1.

Acetal-functionalized Encaged Bis(bipyridine)copper(I) Complexes.

Introduction.

There is longstanding interest in optimizing the photochemistry of inorganic complexes for applications which require efficient conversion of light energy to facilitate either energy- or electron-transfer.[1-4] Tris(bipyridine)ruthenium(II), $[Ru(bpy)_3]Cl_2$, and tris(phenanthroline)ruthenium(II), $[Ru(phen)_3]Cl_2$, have long-lived photoexcited triplet metal-to-ligand charge transfer (MLCT) states that are conducive for such energy- and electron-transfer.[5-7] Their chemical behavior is well- understood because of the tremendous efficiency of the complexes in transforming light into useful work. However, ruthenium(II) complexes are expensive to produce, because ruthenium is not as naturally-abundant on earth as other transition metals.[8] Therefore, G. Meyer and coworkers [9-11] and competing researchers[12-13] initiated studies of bischelated α,α-diimine ligated copper(I) species, $[Cu^{I}(NN)_2]X$. The photoexcitation of a $[Cu^{I}(NN)_2]X$ species forms the MLCT state, $[Cu^{II}(NN^{-}\bullet)(NN)]^{*}X$, whereupon an electron is transferred from the T_d (t_2) orbital of copper(I) to the π* orbitals (e, t_1, t_2) of the α,α'-diimine ligands. Consequently, tetrahedral d^{10} copper(I) oxidizes to the Jahn-Teller distorted square planar d^9 copper(II) excited complex (exciplex) (Figure 1. 1).[14]

There are three problems exclusive to $[Cu^{I}(NN)_2]X$ species intended for energy- and electron-transfer capacities. The worst problem follows from nucleophilic exciplex quenching which decreases MLCT lifetimes.[15] Such exciplex quenching of the D_{4h} $[Cu^{II}(NN^{-}\bullet)(NN)]^{*}X$ MLCT occurs upon solvent molecule or counteranion axial coordination. The nucleophilic attack yields the five-coordinate $[Cu^{II}(NN)_2X]$ which cannot facilitate energy- or electron-transfer. The second problem follows from the facile oxidation of the $[Cu^{I}(NN)_2]X$ ground state yielding $[Cu^{II}(NN)_2]X$ species which also cannot facilitate energy- or electron-transfer. Third, the ligand lability of the $[Cu^{I}(NN)_2]X$ ground state is large, because there is no ligand field stabilization energy (LFSE) of d^{10} copper(I).

In a measured response to these problems, G. Meyer and coworkers used 2,9-alkyl disubstituted bis(phenanthroline)copper(I) species to nullify exciplex quenching and thus achieve energy- and electron-transfer.[16] The 2,9-substituents facilitated steric clashes between alkyl groups on opposite ligands upon D_{4h} exciplex formation thereby making such geometries harder to attain. This in turn decreased the rate of exciplex quenching and increased the MLCT excited state lifetime.[17] For example, MLCT lifetimes of 83 and 243 ns were reported for bis(2,9-dimethyl-1,10-phenanthroline)copper(I) perchlorate ($[Cu^{I}(dmp)_2]ClO_4$) and bis(2,9-diphenyl-1,10-phenanthroline)copper(I) perchlorate, ($[Cu^{I}(dpp)_2]ClO_4$) respectively, at 298 K in degassed dichloromethane.[16-17] In contrast, dichloromethane solutions of underivitized bis(1,10-phenanthroline)copper(I), $Cu^{I}(phen)_2^{+}$, and bis(2,2'-bipyridine)copper(I), $Cu^{I}(bpy)_2^{+}$, have no appreciable MLCT lifetime even at 77 K.[16-17] Despite G. Meyer's initial success, both copper(I) complex oxidation and ligand lability problems persisted.

As an alternative, a copper(I) ligand 'encapsulation strategy' can prohibit exciplex quenching while simultaneously preventing copper(I) oxidation and ligand lability.[18-19] Upon photoexcitation, the encaged complex remains in a tetrahedrally-distorted D_{2d} symmetry and cannot achieve a more-distorted D_{4h} geometry.[20] The encaged ligand framework is less labile than bischelated $[Cu^I(NN)_2]X$ species, because the former contains a tetradentate ligand.

Acetal functionalities can be used to form a caged structure about a metal center. Acetals are stable in base, and are often subject to self-assembly and cyclization.[21-22] As such, novel encaged $[Cu^I(NN)_2]X$ species can be formed from the acid-catalyzed interligand cyclization of acyclic diacetal-derivitized moieties on the 2,2'-bipyridine ligands in a precursor bischelated copper(I) complex. Bulky cyclic diol components, like 1,4-cyclohexanedimethanol and 1,4-benzenedimethanol, theoretically can further protect the ground state of the encaged $[Cu^I(NN)_2]X$ species from both nucleophilic attack and oxidation. A D_{4h} flattening distortion is never attained for such encaged complexes.

The work herein describes efforts towards synthesizing and characterizing acetal-functionalized encaged copper(I) complexes. These complexes have unique and not altogether unexpected qualities in the rudimentary proton nuclear magnetic spectra and positive ion electrospray mass spectra. Results from theoretical modeling studies are considered in conjunction with the both the encaged copper(I) complexes' anodic oxidation waves from cyclic voltammetry and the emission lifetimes (τ_{em}).

Experimental Section.

General. Pyridinium *para*-toluenesulfonate (**1a**) and tetrakis(acetonitrile)copper(I) perchlorate $[Cu^I(CH_3CN)]ClO_4$ were prepared according to literature procedures.[23-24] The preparation of each is described in brief. An equimolar diethyl ether solution of pyridine and *para*-toluenesulfonic acid were combined to isolate **1a**. Copper(II) perchlorate, $Cu(ClO_4)_2$, was dissolved in acetonitrile. Copper metal was added to the solution. The aqua blue solution was refluxed for three days. The resulting dark green colored solution was hot-filtered. A green precipitate and a clear filtrate were obtained. The filtrate was refrigerated to collect $[Cu^I(CH_3CN)_4]ClO_4$ platelet crystals. The crystals were recrystallized two times from acetonitrile.

Purification of *trans*-1,4-cyclohexanedimethanol. The ratio of *trans*:*cis* 1,4-cyclohexanedimethanol (98 %, Aldrich) was 5:2 as received according to proton nuclear magnetic resonance spectroscopy.[25] Approximately 100.0 g of the *trans*:*cis* diol mixture was recrystallized four times in 250 mL of ethyl acetate. Flaky white crystals were obtained and kept in a desiccator. The final *trans:cis* ratio was 80:1 as determined by proton nuclear magnetic resonance spectroscopy. MP: (64.0, 65.5) °C; (^{1}H NMR ($CDCl_3$, 300 MHz)): $\delta = 3.3$(t, 4H), $\delta = 2.9$(t, 2H), $\delta = 1.8$(d, 4H), $\delta = 1.6$(s, 2H), $\delta = 0.9$(t, 4H).

Purification of 1,4-benzenedimethanol. Approximately 100.0 g of 1,4-benzenedimethanol obtained from Aldrich was dissolved in 200 mL of acetonitrile. Then, 2.0 g of activated charcoal was added to the solution which was then hot filtered over ca. 20.0 g of Celite® before its recrystallization upon cooling to room temperature. Needle-shaped crystals were obtained and kept in a desiccator. MP: (117.0, 125.0) °C; (^{1}H NMR ($CDCl_3$, 300 MHz)): $\delta = 7.7$(s, 4H), $\delta = 2.9$(s, 4H), $\delta = 1.9$(s, 4H).

Synthesis of *iso*-propylammonium *para*-toluenesulfonate acid catalyst (2a). *Iso*-propyl amine (1.06 g, 0.0235 mol) was added to *para*-toluenesulfonic acid (4.05 g, 0.0235 mol) in diethyl ether. The precipitate was collected under vacuum filtration, washed with diethyl ether and dried *in vacuo*. A mass of 0.980 g of flaky white crystals were obtained and kept in a desiccator. MP: (128.5, 130.5) °C; (^{1}H NMR ($CDCl_3$, 300 MHz)): $\delta = 7.4$(d, 2H), $\delta = 3.2$(sep, 1H), $\delta = 2.3$ (s, 3H), $\delta = 1.2$(d, 6H).

Synthesis of 5,5'-bis(bromomethyl)-2,2'-bipyridine. The starting compound 5,5'-dimethyl-2,2'-bipyridine (DMB) was synthesized using a modification of the Rainey nickel method.[26-27] It is noteworthy that yields of 5,5'-dimethyl-2,2'-bipyridine syntheses have been recently improved.[28-30] The 5,5'-dimethyl-2,2'-bipyridine was recrystallized from ethyl acetate three times and dried *in vacuo* for 24 hours at room temperature before use (Mp: 172.0, 175.0 °C). The 99 % N-bromosuccinimide (NBS) was obtained from Aldrich. The NBS was recrystallized once from 9:1 water:acetone to obtain white flaky crystals which were then stored in a dark refrigerator. Five grams of DMB (0.02716 mol, 1.0 eq.) was charged into a 50 mL round bottom flask equipped with a stir bar. The DMB was dissolved in 25 mL of 99 % carbon tetrachloride (Baker Analyzed). Then, 9.668 g of NBS (0.05432 mol, 2.0 eq.) was added as a solid into the DMB solution at 25 °C. The round bottom was capped with a septum and then placed in a tungsten/halogen visible light source (240-2500 nm) belonging to an overhead projector for two days while stirring. During this time, the reaction mixture became turbid and changed from clear into an orange color. Over time the succinimide solid byproduct floated on the top. The reaction's progress was monitored by thin layer chromatography (TLC). Plates were eluted with 1:1 dichloromethane:ethyl acetate in a jar where the headspace was saturated with ammonium hydroxide vapors. The eluted plates (Aldrich) were then developed by spraying them with an aqueous solution of iron(II) perchlorate hydrate often removing the ammonia by gentle heating. The desired product had the third-highest R_f value when there was still unreacted DMB in the reaction mixture. The product turned a pinkish-red color upon developing the plates. Unreacted DMB had the highest R_f and turned a burnt-orange color. After the DMB was consumed according to TLC, the reaction mixture was filtered to obtain a yellow powder that precipitated during the reaction. The powder consisted of both the product and succinimide. This powder was dissolved in methylene chloride and extracted with three 100 mL water portions. The organic layer was collected after separatory extractions and dried with anhydrous sodium sulfate. Evaporation to dryness gave crude 5,5′-bis(bromomethyl)-2,2′-bipyridine. The solid was recrystallized three times from chloroform to obtain 2.2 g of a cream-white powder. MP: (206.0, 210.5) °C; (^{1}H NMR ($CDCl_3$, 300 MHz)): 7.85 ppm(d, 2H), 8.45 ppm(d, 2H), 8.75 ppm(s, 2H), 4.55 ppm(s, 4H); (ESI^+ (CH_2Cl_2)): 342.0 (M+H).

Synthesis of 5,5'-dicarboxyaldehyde-2,2'-bipyridine. The procedure below followed the Kornblüm oxidation as reported by Oâe and coworkers[31] A mass of 1.000 g of 5,5′-bis(bromomethyl)-2,2′-bipyridine (2.923 x 10^{-4} mol, 1.0 eq.) was dried *in vacuo* before being charged into a 50 mL round bottom flask equipped with a stirbar. This mass was then dissolved in 10 mL of 99.8 % dimethylsulfoxide (DMSO) used as received from Fisher. Then, 1.050 g of 99.9999 % silver nitrate (6.169 x 10^{-4} mol, 2.1 eq.) used as received from Aldrich was added to the reaction mixture and allowed to stir at 25 °C for ten minutes. A faint yellow-green colored solution resulted. The reaction mixture was then placed in a 90 °C oil bath for thirty minutes. Then, 0.845 mL of 99+ % 2,6-lutidine (0.004341 mol, 2.5 eq.) used as received from Aldrich was added to the reaction mixture using a 1.00 mL glass syringe. The stirred reaction mixture turned turbid dark green during which time a black precipitate formed. Hydrogen sulfide gas evolved upon venting the reaction mixture. After two hours at 90 °C, the reaction mixture was then allowed to cool to 30 °C before dispensing all of the contents of the round bottom flask into a 500 mL separatory funnel containing 150 mL of chloroform (Fisher) and 150 mL of a 10 wt. % aqueous potassium chloride solution. The aqueous layer was extracted three times with 25 mL of chloroform. A dark green aqueous layer and a dark-colored emulsion remained in the separatory funnel. The organic layer was extracted three times with 50 mL of water, and then dried with anhydrous sodium sulfate. The organic layer was rotary evaporated to dryness to obtain 0.48 g of a yellow-colored powder. The solid was re-dissolved in chloroform and eluted through a chromatographic column with 95:5 dichloromethane:acetone eluent. The eluate was rotary evaporated once again to obtain a faint yellow powder. The powder was recrystallized from acetonitrile three times then dried in air to yield 0.40 g 5,5'-dicarboxyaldehyde-2,2'-bipyridine as a light yellow powder. MP: (225.0, 230.0) °C; (^{1}H NMR, ($CDCl_3$, 300 MHz)): 8.36 ppm(d, 2H), 8.75 ppm(d, 2H), 9.25 ppm(s, 2H), 10.20 ppm(s, 2H); (ESI^+ (CH_2Cl_2)): 213.1 (M+H).

Synthesis of (4,4′,4″,4‴-(2,2′-bipyridine-5,5′-diylbis(methanetriyl)tetrakis(oxy)tetrakis(methylene)tetrakis(*trans*-cyclohexane-4,1-diyl)tetramethanol (1l). Consult Figure 1. 2. Acetalizations reactions followed those previously described by Li and coworkers and Fraser-Reid and coworkers[32-33] Solid *trans*-1,4-cyclohexanedimethanol (9.50 g, 0.066 mol, 140 eq.) was charged into a 50 mL round bottom flask equipped with a magnetic stirbar, and melted at 120 °C. Then, ca. 5.0 g of 4-8 mesh 4 Å molecular sieves (Acros) previously activated in a heated vacuum oven were added to the molten diol. After one minute, solid 2,2′-bipyridine-5,5′-dicarbaldehyde (0.100 g, 4.71×10^{-4} mol, 1 eq.) was added to the reaction mixture. After five minutes, **1a** (0.050 g, 2.00×10^{-4} mol, 0.42 eq.) was added as a solid to the reaction mixture. The reaction mixture developed a slight pinkish-yellow color. The contents were refluxed for one hour at 165 °C. The reaction was monitored by TLC with the plates eluted in 1:1 acetone:dichloromethane, and developed with a water solution of iron(II) perchlorate hydrate. The component which turned red after spraying was the diacetal-functionalized bipyridine. Any purple component was the hemiacetal- or monoacetal-functionalized bipyridine which had larger R_f values than the product. After one hour, solid sodium bicarbonate was added to the reaction mixture to neutralize PPTS catalyst before diluting the mixture with ethyl acetate. The hot reaction mixture was decanted from the sieves and the bicarbonate. The excess 1,4-*trans*-cyclohexanediol precipitated under refrigeration. The mother liquor was rotary evaporated to dryness then reconstituted with 100 mL of dichloromethane for liquid phase extraction three times with 100 mL saturated $NaHCO_3$ in doubly deionized water. This removed the pinkish hue from the organic layer. The organic layer was dried with sodium sulfate and then rotary evaporated to dryness to obtain 0.240 g of a solid bone-white powder which was stored under inert atmosphere. MP: (93.0, 101.7) °C; (^{1}H NMR ($CDCl_3$, 300 MHz)): δ = 8.5(m, 6H), δ = 5.6(s, 2H), δ = 3.6(d, 8H), δ = 3.4(t, 8H), δ = 1.8(m, 16H), δ = 1.7(d, 4H), δ = 1.5(d, 4H), δ = 1.3(s, 4H), δ = 1.0(t, 16H); (ESI^+ (CH_2Cl_2)): 759.7 (M+H).

Synthesis of (4,4'-((5'-((3-(hydroxylmethyl)benzyloxy)(4-(hydroxylmethyl)benzyloxy)methyl)-2,2'-bipyridine-5-yl)methylene)bis(oxy)bis(methylene)bis(4,1-phenylene))dimethanol (2l). Consult Figure 1. 2. Solid 1,4-benzenedimethanol (9.00 g, 0.0651 mol, 132 eq.) was charged into a 50 mL round bottom flask with a magnetic stirbar. The diol was melted at 160 °C and then stirred. Approximately 5.0 g of 4 – 8 mesh 4 Å molecular sieves (Acros) previously activated in a heated vacuum oven were added to the molten diol. After one minute, solid 2,2'-bipyridine-5,5'-dicarboxaldehyde (0.100 g, 4.91 x 10^{-4} mol, 1 eq.) was added as a solid into the reaction mixture. The synthesis then follows that of ligand **1l**. A mass of 0.145 g of ligand **2l** was obtained. MP: (224.0, 226.5) °C; (^{1}H NMR ($CDCl_3$, 300 MHz)): $\delta = 8.7$(m, 6H), $\delta = 5.5$(s, 2H), $\delta = 1.9$ (m, 32H), $\delta = 1.4$(t, 16H), $\delta = 1.0$(m, 8H); (ESI$^+$ (CH_2Cl_2)): 729.9 (M+H).

Synthesis of [bis((4,4′,4″,4‴-(2,2′-bipyridine-5,5′-diylbis(methanetriyl)tetrakis(oxy)tetrakis(methylene)tetrakis(*trans*-cyclohexane-4,1-diyl)tetramethanol)copper(I)] perchlorate (1u). Consult Figure 1. 2. In an inert atmosphere glovebox, solid [$Cu^I(CH_3CN)_4$]ClO_4 (0.0077 g, 2.35 x 10^{-5} mol, 1 eq.) was added into a 25 mL round bottom flask equipped with a stir bar containing 15 mL of degassed Optima acetonitrile (Aldrich). Ligand **1l** (0.0734 g, 9.772 x 10^{-5} mol, 4.1 eq.) was added as a solid, causing the reaction mixture to immediately turn dark brown. The four-fold excess of ligand **1l** is required to fully form the bischelated complex. Complex **1u** was made and characterized at this point. (^{1}H NMR (CD_3CN, 300 MHz)): δ =8.0-9.0 (m, 12H), δ =5.7(s, 4H), $\delta = 3.4$ (d, 16 H), $\delta = 2.4$ (m, 8H), $\delta = 1.9$ (m, 32H), $\delta = 1.6$ (broad s, 8H), $\delta = 1.6$ (d, 16H), $\delta = 0.9$ (m, 32H); (ESI$^+$ (CH_3CN)): 1567.1 (M-ClO_4^+).

Synthesis of [bis(2,2'-bipyridine-5,5-tetrakis((1,4-*trans*-dimethanolcyclohexane)acetal)copper(I)] perchlorate (1c). Consult Figure 1. 2. *Iso*-propylammonium *para*-toluenesulfonate acid catalyst (IPTS) (**2a**) (0.00054 g, 2.35 x 10^{-6}, 0.1 eq.) acid catalyst was added as a solid into a 15 mL acetonitrile optima solution of complex **1u** containing a two-fold excess of ligand **1l**. The reaction mixture was refluxed under stirring action for seven days in an inert atmosphere glovebox. During the reaction period, a fine white powder precipitated which increased the turbidity of the reaction mixture. This powder was analyzed later by ^{1}H NMR, and showed a broad peak at 1.4

ppm which is consistent with the diol. After the reaction was determined to be complete, the contents were decanted away from this solid, and evaporated to dryness to yield more of the white powder and a thin brown film. Column chromatography and water extractions would instantly hydrolyze all of the acetal moieties of complex **1c**, so these purification methods were not chosen. Instead, 20 mL of dry toluene was added to these contents and was brought to a slow boil--at which time the toluene was pipetted out of the round bottom flask. This toluene extraction was repeated once more to separate the four diol equivalents. A brown film remained (**1c**). (^{1}H NMR (CD_3CN, 300 MHz)): δ =8.0-9.5 (m, 12H, broad), δ = 5.3 (s, 4H), δ = 1.9(t, 16H), δ = 1.8 (d, 8H), δ = 1.2 (m, 16H), δ = 0.9 (m, 16H); UV-vis(CH_3CN) λ, nm: 444; (ESI$^+$ (CH_3CN/MeOH)): Consult Table I. 1.

Synthesis of [bis((4,4'-((5'-((3-(hydroxylmethyl)benzyloxy)(4-(hydroxylmethyl)benzyloxy)methyl)-2,2'-bipyridine-5-yl)methylene)bis(oxy)bis(methylene)bis(4,1-phenylene))dimethanol)copper(I)] perchlorate (2u). Consult Figure 1. 2. In an inert atmosphere glovebox, $[Cu^I(CH_3CN)_4]ClO_4$ (0.0107 g, 3.27×10^{-5} mol, 1 eq.) was added into a 25 mL round bottom flask equipped with a stir bar containing 15 mL of acetonitrile. Ligand **2l** (0.1011 g, 1.34×10^{-4} mol, 4.1 eq.) was added as a solid, causing the reaction mixture to immediately turn dark brown. The four-fold excess of ligand is required to completely form the bischelated species. Complex **2u** was synthesized at this point. (^{1}H NMR, CD_3CN): δ = 8.0-9.0(m, broad, 12H), δ = 7.3 (d, 32H), δ = 5.5(s, 4H), δ = 4.6(s, 16H), δ = 4.5(s, 16H); (ESI$^+$ (CH_3CN)): 1519.4 (M-ClO_4^+).

Synthesis of [bis(2,2′-bipyridine –5,5′-tetrakis((1,4-dimethanolbenzene)acetal)copper(I)] perchlorate (2c). Consult Figure 1. 2. Acid catalyst **2a** (0.00071 g, 3.27 x 10^{-6} mol, 0.1 eq.) was added to a 15 mL acetonitrile solution of **2u**. The reaction mixture was refluxed under stirring action for seven days in an inert atmosphere glove box. During the reaction period, a fine brown-white powder precipitated. This powder was analyzed later by ^{1}H NMR, and showed a broad peak at 1.9 ppm which is consistent with the diol. The turbid reaction mixture was decanted from this solid, and evaporated to dryness to obtain a thin brown film which was covered by another cake-like powdery solid. Column chromatography and water extractions would have instantly hydrolyzed the acetal moieties on complex **2c**, so these purification methods were again not chosen. Instead, 20 mL of dry toluene was added to these contents and was brought to a slow boil--at which time the toluene was pipetted out of the round bottom flask. This toluene extraction was repeated to remove condensed four diol equivalents. A brown thin film remained (**2c**). (^{1}H NMR ($CDCl_3$, 300 MHz)): δ = 8.0-10.0 (m, 12H, broad), δ = 7.2(s, 16H), δ = 5.6(s, 4H), δ = 4.6 (s, 16H); UV-vis(CH_3CN) λ, nm: 448; (ESI^+ (MeOH)): Consult Table I. 1

Instrumental. Molecular modeling of encaged copper complexes was performed using Cerius$^{2®}$ 5.0 modeling program.[34] Ten annealing cycles over the range of 300 K to 500 K with 50 K temperature increments were carried out on ligands **1l** and **2l** as well as complexes **1u, 1c, 2u,** and **2c.** The annealed models were then minimized in energy, and this energy was reported (Table I. 2). The total energy consisted of contributions from torsional strain, van der Waals, electrostatic, and bond energy components.

The ^{1}H NMR spectra were recorded at room temperature on a Varian® Inova 300 MHz spectrometer using deuterated solvents with residual protonated solvents serving as internal standards (for ^{1}H NMR spectra, for the ligands **1l** and **2l**, δ = 7.72 for $CDCl_3$ and

δ =1.5 for $CHCl_3$; and for the complexes **1u**, **1c**, **2u**, and **2c**, δ = 1.9 ppm for CD_3CN, δ = 2.1 ppm for CH_3CN). For T_1 relaxation investigations of complex **1c**, deuterated hydrazine (D_2NND_2), a liquid reductant, was prepared by mixing 2.0 mL of deuterated methanol (CD_3OD) with 2.0 mL of hydrazine followed by the rotary evaporation of CD_3OD. This process was iterated four times. Approximately 0.05 mL of D_2NND_2 was added into an NMR tube containing complex **1c** in CD_3CN. The T_1 relaxation experiment was carried out by a standard T_1 analysis program (Varian). Positive ion electrospray ionization (ESI^+) mass spectra of complexes **1u**, **1c**, **2u**, and **2c** were recorded on a Fisons® VG Quattro-SQ spectrometer. Concentrations of analyzed solutions were approximately 10 μM. The solvent was either methanol or acetonitrile.

Cyclic voltammograms were recorded on an x-y plot recorder. An EG&G Model 175 potentiostat was used. A 0.10 M tetrabutylammonium hexafluorophosphate ($TBAPF_6$) background electrolyte acetonitrile optima solution was used. All voltammograms were collected using a polished glassy carbon working electrode (WE) with a diameter of 3.0 μm (a microelectrode), a saturated sodium calomel electrode (SSCE) as the reference electrode, and a platinum coil as the counter electrode (CE). The scan rate for all collected voltammograms was 50 mV/sec.

Spectroscopic analyses were performed as follows. Ultraviolet-visible absorption spectra were collected on a Hewlett Packard® 8452A spectrophotometer over 200 to 600 nm by recording the absorbance every 0.5 nm. Fluorescence spectra were recorded using right angle collection on a Fluorolog® 19 spectrometer over 550 to 650 nm with an integration time of 1.0 second recording every 0.5 nm. The absorption maxima (λ_{abs}) and emission maxima (λ_{em}) for the **1c** and **2c** species were collected in acetonitrile. Dark cell effects were observed for all fluorescence spectra presented. The emission lifetimes of complexes **1c** and **2c** were determined at room temperature in solutions of acetonitrile. The solutions were freeze-pump-thawed (FPT) four times to remove dissolved oxygen using a specially-designed freeze-pump-thaw cell equipped with spectroscopic-grade optical glass, a cold arm for FPT operations, and a Kontes Teflon® screwable seal. The laser system used for time-resolved emission spectroscopy was previously reported.[35]

Results and Discussion.

Chemical Modeling Studies. The energy of the encaged bischelated copper(I) complexes was determined as a function of both the acetal diol component and the α,α-diimine ligand (Table I. 2). The Cerius^2 modeling program[34] calculated the complexes' energies after five consecutive [300 K → 500 K → 300 K] annealing cycles and energy minimizations. The calculated energies presented herein consist of van der Waals, electrostatic, bond, angle, and torsional strain.

The choice concerning which terminal diols (1,n-diols) would be selected as constituent members of the ligand diacetal functionalities depended on both chain length and steric bulk. The encaged copper(I) complex of lowest energy contained 1,6-hexanediol acetal moieties (Table I. 2). Diols of shorter chain length can not fully extend over the void space between opposing ligands without greatly increasing bond strain. Diols of longer chain lengths were coincident with considerable linker torsional strain upon bridging the void space. Regardless of the modeling results, there were persistent ligand synthesis problems with 1,6-hexanediol diacetal-derivitized α,α-diimine precursor ligand preparation. Namely, cyclized diacetal functionalities formed on the precursor ligands. Such cyclic diacetal ligands cannot encage copper(I).

Ligand cyclic diol moieties have more favorable features than 1,n-diols. Such bulky diol components preclude both the formation of cyclized diacetal functionalities on precursor ligands and axially directed attack of copper(I) exciplexes through steric encumbrance (Table I. 2). This time, ligand synthesis acetalizations incorporating 1,4-benzenedimethanol and 1,4-dimethanolcyclohexane diols were successful. Note, these cyclic diols also have six carbons in the main chain, as does 1,6-hexanediol. Therefore, the bulky diols were chosen for copper(I) interligand diacetal cyclization syntheses. The remaining issue regarded which geometric isomer of 1,4-dimethanolcyclohexane, *cis* or *trans*, corresponded to the lower energy encaged copper(I) complex. The encaged copper(I) complex employing the *trans*-1,4-dimethanolcyclohexane alcohol constituent had the lowest energy. The *cis* isomer is consistent with shorter distance between the two hydroxyl functionalities consequently increasing torsional strain.

The choice concerning which α,α-diimine ligand would be the constituent member of the ligand was then investigated. The 1,10-phenanthroline (phen) ligand, with the acetal moieties on the 3 and 8 positions, is a more structurally rigid ligand than 2,2'-bipyridine (bpy), with the acetal functionalities on the 5 and 5' positions. The modeled energy difference between the precursor non-cyclized and cyclized complexes is 1.8 kcal greater for phen than bpy. Therefore, bpy ligands were used to facilitate a less energetically demanding copper(I) encapsulation even though the τ_{em} values of phen-ligated copper(I) complexes longer. Diacetal functionalities located at the *meta* positions

(5,5'), with respect to the nitrogen heteroatoms in 2,2'-bipyridine, contributed less strain in the encaged complex than the *ortho* or *para* analogs.

Complex Synthesis and Purification Methodologies. Acetalization of 5,5'-dicarboxaldehyde-2,2'-bipyridine with the *trans*-1,4-cyclohexanedimethanol and 1,4-dimethanolbenzene diols in the presence of pyridinium *para*-toluenesulfonate (PPTS) produced ligands **1l** and **2l**, respectively (Figure 1. 2). The equilibrium is shifted towards ligand production given both the large excess of diol and the water-absorbing qualities of molecular sieves. Only the separation of the excess alcohol and the neutralization of the PPTS ammonium acid catalyst were required to isolate ligands **1l** and **2l**. Solvent extractions were performed with an excess of potassium carbonate to avoid acetal hydrolysis.[33] Ligands **1l** and **2l** cannot be isolated using chromatographic separation methods, because acetal functionalities hydrolyze at the acidic sites of the silica stationary phase and decompose back to the aldehyde precursors. Molecular models of ligands **1l** and **2l** exhibit the spatial orientation of the diol moieties positioned in such a way as to avoid steric clashes and to promote pi-stacking, respectively (Figure 1. 3).[36]

There are several synthetic requirements that must be met to prepare diacetal-encaged copper(I) species. First, tetrakis(acetonitrile)copper(I) perchlorate ($[Cu^I(CH_3CN)_4]ClO_4$) was used instead of tetrakis(acetonitrile)copper(I) tetrafluoroborate ($[Cu^I(CH_3CN)_4]BF_4$), because of the latter's capability to hydrolyze acetal functionalities in acetonitrile.[37] According to the work of Albrecht-Gary and coworkers, the equilibrium-based syntheses of precursor complexes **1u** and **2u** require four-fold excesses of ligands **1l** and **2l**, respectively, to form the bischelated complex $[Cu^I(NN)_2]X$ and not the monochelated complex $[Cu^I(NN)]X$.[38] Subsequently, *iso*-propylammonium *para*-

toluenesulfonate (**2a**) is added to complexes **1u** and **2u** to effect encaged complexes **1c** and **2c**, respectively. As with ligands **1l** and **2l**, no column chromatography or aqueous extraction can be used to purify complexes **1u**, **1c**, **2u**, or **2c** (Figure 1. 2). Instead, a boiling toluene extraction was performed to separate the two equivalents of excess ligand and four equivalents of condensed diol from the complexes.

The engagement follows the S_{N2} and acetal cyclization mechanisms. Accordingly, only the internal oxygen atoms of the acetals' diol moieties are protonated by the ammonium acid **2a** (Figure 1. 4). Then, the acetal terminal oxygen atom nucleophiles attack the methine carbon electrophiles on opposing ligands to complete the copper(I) encapsulation. The high local concentration of the terminal oxygens about the activated methine electrophiles facilitates encapsulation. It is crucial that trace water does not act as a nucleophile; reaction between **1u** and **2u** and trace water yields bis(5,5'-dicarboxyaldehyde-2,2'-bipyridine)copper(II) perchlorate. The encapsulation equilibrium is shifted toward products because of the large entropy increase coincident with the loss of four diol equivalents upon the conversion of complexes **1u** and **2u** to complexes **1c** and **2c**, respectively.

Complexes **1c** and **2c** can only be isolated as brown films. The encapsulation of copper(I) inhibits pi-pi stacking of bipyridine rings among complexes which would facilitate crystal growth.[36] The films are stable in ambient environment for months before the intensity of the complexes' brown color (MLCT) decreases.

Proton Nuclear Magnetic Resonance Spectra. The proton nuclear magnetic spectrum (^{1}H NMR) spectrum of complex **1c** partially confirms synthesis success. First, there are no broad hydroxyl resonances for **1c**. This engenders confidence that the hydroxyl terminal groups of complex **1u** were converted into inter-ligand cyclic diacetal moieties in **1c** (Figure 1. 5). Second, the integrated area of the alkane protons in complex **1c** (at 0 - 4 ppm) is ca. one half that of the integrated area of the alkane protons in complex **1u**. This result is consistent with the loss of half of the diol moieties upon encapsulation. Note, unresolved alkane resonances are attributable to boat and chair interconversions of 1,4-*trans*-dimethanolcyclohexane moieties.[39]

It is disturbing that the bipyridine proton resonances are broadened for both complexes **1u** and **1c**. Since the complexes are diamagnetic, trace amounts of contaminant oxidants cause a paramagnetic shift which by definition both broadens resonances and shifts them downfield.[40-41] The bipyridine proton resonances, and only these resonances, are broadened but in fact are not shifted downfield with respect to the bipyridine resonances of **1u** and **2u**. Therefore, T_1 tumbling, instead of strictly paramagnetic effects, causes the broadening of the bipyridine proton resonances.

A T_1 experiment determined the cause of unresolved aromatic proton resonances (Table I. 3). The T_1 values of the three bipyridine proton resonances were determined be in the range of 1.3 to 9.9 s^{-1}. Such values contrast to the much shorter T_1 values of the upfield diol-based proton resonances which are on the order of 0.05 s^{-1}. To explain this disparity, the rigid bipyridine ring protons are conformationally locked. Thus, their T_1 values are large, because these protons can only tumble in space. The T_1 lengthening can also be caused by intra- or intermolecular dipole-dipole interactions.[42] In contrast, the remaining protons from the diol cage structure can tumble as well as wag and rotate about sigma bonds. Moreover, the tumbling of these diol-based protons is faster, because they are located on the periphery of the complex.

The validity of the prevalent T_1 tumbling effect exerted on complex **1c** causing the peak broadening was corroborated by an experiment wherein a reductant was added to complex **1c**. If paramagnetic effects were active, then the bipyridine proton resonances should be both sharpened and shifted upfield upon copper(II) reductant addition. Deuterated hydrazine, D_2NND_2, was chosen as the reductant for the sake of having homogeneous reagents. Under inert atmosphere, ca. 10 μL D_2NND_2 liquid reductant was added into an nmr tube containing a 1.0 mL of a CD_3CN solution of complex **1c**. Neither sharpening nor upfield shifting of the bipyridine proton resonances was observed once the D_2NND_2 was added. This result negates paramagnetic broadening.

The ^{1}H NMR of complex **2c** has fewer resonances than complex **1c**, because it is more symmetric (Figure 1. 5). For example, the aromatic and methylene protons are equivalent. The bipyridine proton resonances are again broadened for complex **2c**.

Electrospray Ionization Mass Spectra. Ligands **1l** and **2l** and complexes **1u**, **1c**, **2u**, and **2c** were diluted to concentrations of ca. 10 μM for positive ion electrospray ionization mass spectral analysis (ESI^+). Protonated parent ions for ligands **1l** and **2l** were detected (Figure 1. 6 and Figure 1.7, respectively). The parent ions for the precursor caged complexes **1u** and **2u** were detected (Figure 1. 8 and Figure 1. 9, respectively).[43] The peaks in the isotopic distribution series are separated by one m/z indicating the presence of copper(I) (Figure 1. 10). The interligand acetal cyclization caged complexes **1c** and **2c** had the correct isotopic splitting pattern but the incorrect m/z values (Figure 1. 11 and Figure 1. 12, respectively). In fact, there was no detection of the 967.5 m/z and 991.5 m/z parent peaks for either complex **1c** or **2c**, respectively. Instead, complex-solvent adducts were detected (Figure 1. 11 and Figure 1. 12, respectively).

The detection of **1c** and **2c** solvates can be justified. The acetal oxygen atoms can orient solvent molecules. In this way, the cage's oxygen atoms induce the nucleophilic attack on the complexes at copper(I). The solvates have been reproduced over different days and for different samples. Consult Table I. 1.

Unfortunately, complexes **1c** and **2c** were never isolated at more than 75 % purity with respect to the ^{1}H NMR and positive ion electrospray characterizations. It is difficult to isolate such complexes by conventional methods, vide supra. Still, the ultraviolet-visible absorption spectroscopy, cyclic voltammetry, and the emission spectroscopy of **1c** and **2c** are discussed because of their novel nature. Accordingly, **1c** and **2c** will henceforth be referred to as **1c'** and **2c'**, respectively.

Ultraviolet-visible (UV-vis) Absorption Spectroscopy. Ultraviolet-visible (UV-vis) absorption spectroscopy was performed on complexes **1c'** and **2c'** to determine both the relative population of bischelated to monochelated complex, as well as to determine the degree of tetrahedral distortion in the copper(I) ligation sphere. The absorption spectra were recorded for deaerated acetonitrile solutions of the complexes (Figure 1. 13). Complexes **1c'** and **2c'** are both entirely bischelated, because there is no absorption maximum centered at ca. 350 nm (Figure 1. 13).[38]

Theoretically, the degree of tetrahedral distortion of the copper(I) ligation sphere in complex **1c'** can be determined by assessing the number of resolved MLCT bands. In general, the triply-degenerate t_2 orbitals progressively split into the b_2 and e orbitals corresponding to the sterically strained D_{2d} geometry as the tetrahedral geometry becomes more distorted.[44] Thus, two MLCT absorption bands of different energies are produced due to electron excitations from the D_{2d} (b_2 and e) metal-centered orbitals to ligand π^* (e, t_1, and t_2) orbitals. These excitations correspond to distinct absorption maxima (λ_{max}) for Band I centered near 525 nm and the more intense Band II centered at 450 nm.[45-46] The number of MLCT bands observed, therefore, indicates whether the complex is T_d or D_{2d}-distorted. Recall, molecular modeling studies on the two encaged complexes concluded that no such distortions can occur in the ground state. Therefore, no sharp Band I absorptions are expected for either complex. Yet, complex **1c'** exhibits a small absorption band at 538 nm. The 538 nm absorption occurs as a shoulder on the λ_{max} of Band II centered at 444 nm. Therefore, complex **1c'** is contaminated because of the presence of the D_{2d}-distorted Band at 538 nm. Complex **2c'** has λ_{max} Band II centered at 448 nm and does not exhibit Band I (Figure 1. 13).

Variable temperature UV-vis absorption spectroscopy on the precursor complex bis(5,5'-dicarboxaldehyde-2,2'-bipyridine)copper(I) perchlorate and complex **1c** in acetonitrile determined the ratio of bischelated to monochelated copper(I) complex. As the temperature increases, the MLCT absorbance of the former decreases, of ligand lability issues.[47-48] In contrast, complex **1c'** remains coordinated to copper(I) over a 50 °C temperature range, because the A(λ_{max}(Band II)) remains constant (Figure 1. 14). The tetradentate cage ligand is not labile in acetonitrile solution at elevated temperatures due to a substantial kinetic chelate effect.

Oxidative Wave Cyclic Voltammetry. Cyclic voltammetry experiments were performed on complexes **1c'** and **2c'** to determine the half-wave potential of copper(I) oxidation to copper(II) ($E_{1/2}^{(Cu(I)/Cu(II))}$). The oxidation potential is directly proportional to the strain barrier impeding a $[Cu^{II}(NN^{-}\bullet)(NN)]^{*}X$ D_{4h} flattening distortion.[49-50] A more positive $E_{1/2}^{(Cu(I)/Cu(II))}$ value therefore corresponds to a greater degree of complex stability in the copper(I) oxidation state over that of copper(II). An oxidative wave cyclic voltammogram was obtained for complex **1c'** in 0.10 M tetrabutylammonium hexafluorophosphate (TBAPF$_6$) using a glassy carbon electrode (Figure 1. 15). An anodic copper(I)/copper(II) oxidation voltage peak vs. SSCE ($E_{pa}^{(Cu(I)/Cu(II))}$) value is reported instead of an $E_{1/2}^{(Cu(I)/Cu(II))}$ half- wave potential since the process is irreversible. The $E_{pa}^{(Cu(I)/Cu(II))}$ of complex **1c'** is +1360 mV v. SSCE. This is substantially shifted to more oxidizing potentials versus the +0.153 mV formal potential ($E_0^{(Cu(I)/Cu(II))}$) for unligated copper(I). No reversible cathodic wave is observed; thus, a coupled Electrochemical oxidation-Chemical reaction (EC) mechanism is active.[51-52] The strain induced in complex **1c'** geometry is relieved at +1360 mV vs. SSCE whereupon acetal oxygen atoms attack electrochemically-generated trace hydronium ions, consequently disintegrating the cage structure. The return Cu(II)/Cu(I) reduction was not detected in the examined potential range. The $E_{pa}^{(Cu(I)/Cu(II))}$ of complex **2c'** is +1055 mV v. SSCE in 0.10 M TBAPF$_6$ using a glassy carbon electrode (Figure 1. 15). An EC mechanism also holds for complex **2c'** (Figure 1. 15). According to electrochemical data, a D4h flattening distortion is never attained for complexes **1c'** and **2c'**.

Emission Spectroscopy. The static emission photochemistry of complexes **1c'** and **2c'** in acetonitrile were characterized to determine if the species exhibited MLCT photoexcited states at 25 °C. Emission spectra of complexes **1c'** and **2c'** were taken using an MLCT excitation wavelength of 450 nm which approximates λ_{max}(Band II) (Figure 1. 16). The corresponding emission maxima (λ_{em}) of **1c'** and **2c'** are centered at 610 and 627 nm, respectively. These λ_{em} are blue-shifted with respect to literature values of 640 nm for uncaged [Cu^I(NN)$_2$]X species.[53] According to the energy gap law, complex **1c'**

should have a slower rate of nonradiative decay (k_{nr}) and a longer emission lifetime (τ_{em}) than complex **2c'**.[54]

Emission Lifetime. The decay of fluorescence intensity over time was monitored at the λ_{em} of each complex to determine the efficiency of energy- and electron-transfer. The time-resolved emission decays of both complexes are intensity-normalized. The emission decay of complex **1c'** [τ_{em}(**1c'**)] followed single exponential kinetics and is 1.592 ± 0.018 μs (Figure 1. 17). The linear regression factor is 0.9777 with accompanying nonharmonic residuals (Figure 1. 17 inset). The τ_{em}(**2c'**) also follows single exponential decay kinetics but is shorter at 0.593 ± 0.024 μs (Figure 1. 17). The linear regression factor is 0.9952 with accompanying nonharmonic residuals.

It is particularly remarkable that the long MLCT lifetimes for complexes **1c'** and **2c'** are achieved by using bipyridine ligands instead of phenanthroline ligands and in acetonitrile instead of dichloromethane. *Ortho*-substituted derivatives of 2,2′-bipyridine copper(I) complexes have lower τ_{em} values compared to *Ortho*-substituted derivatives of 1,10-phenanthroline copper(I) complexes by a factor of ca. four.[44,54] Accordingly, the majority of investigators select the more rigid 1,10-phenanthroline ligand derivatives to engineer long-lived MLCT states.[16-20] More importantly, standard literature lifetimes are commonly reported in non-exciplex quenching dichloromethane solution.[9-13,16-20,47-48] The τ_{em} values reported herein were assessed in the more nucleophilic exciplex-quenching acetonitrile solvent. This was initially done to ensure solubility. In general, MLCT lifetimes in dichloromethane are expected to be five to ten times longer than those in acetonitrile.[55] To conclude, it is undoubtedly an added advantage of encaged copper(I) species that such long-lived MLCT lifetimes can be observed in solvents of higher dielectric constants. This increases the viability and practicality of such encaged copper(I) complexes as energy- and electron-transfer candidates.

Agreement Between Modeling and Experimental Characterizations. Complex **1c'** which has greater modeled strain energy than **2c'** also has the greatest experimentally determined E_{pa} and MLCT lifetime.

Conclusions.

The brown films of complexes **1c'** and **2c'** do not oxidize in ambient air over a period of weeks. The cage is effectively a tetradentate ligand which shows no lability as demonstrated by no changes in the absorption maximum of **1c** over a 50 °C temperature increase. The encapsulation of the copper(I) also protects it against exciplex quenching and molecular oxygen oxidation. Both the large E_{pa} voltages and long MLCT lifetimes of these complexes in high dielectric solvents constitute highly desired qualities in copper(I) complexes.

Applications. Two synthetic fronts can be pursued to optimize the photochemical qualities of encaged copper(I) species characterized herein. First, the syntheses of 1,10-phenanthroline diacetal-derivitized ligated encaged copper(I) analogs can be prepared. In doing so, the k_{nr} decreases, because the 1,10-phenanthroline fused aromatic ring system is more rigid than 2,2′-bipyridine ligands. In this vein, 3,8-dibromo-1,10-phenanthroline has been synthetically prepared from 1,10-phenanthroline. This derivative can thereby undergo palladium-catalyzed formylation as refined by Okano and coworkers to effect the carboxaldehyde functionalities required for the interligand acetal cyclization.[56]

Chapter 1.

Tables

Table I. 1. Theoretical and experimental parent m/z of encaged acetal-functionalized copper(I) complexes.

Complex	Experimental	Theoretical[a]	Adduct[b]
1c	(c)	**991.5**	None
1c	1025.0	1023.5	MeOH
1c	1027.4	1027.4	Cl^-
1c	(c)	1032.5	MeCN
1c	1041.0	1041.5	MeOH and H_2O
1c	1075.5	1073.5	2 MeCN
1c	1091.4	1091.42	ClO_4^-
2c	(c)	**967.5**	None
2c	1001.7	999.3	MeOH
2c	(c)	1008.3	MeCN
2c	1017.7	1017.3	MeOH and H_2O
2c	1033.7	1031.3	2MeOH
2c	1049.7	1049.3	2MeCN
2c	1065.6	1066.2	ClO_4^-

(a) Determined by an isotopic distribution modeling program on the FISONS Quattro-SQ single quadrupole mass spectrometer software.[43]

(b) Adduct is postulated to bind to complex during experimental timescale.

(c) No parent ion peak was detected for the adduct.

Table I. 2. Energies of precursor and encaged acetal-functionalized copper(I) complexes.

alcohol[a]	$E_{(encagement)}$ (kcal/mol)[b]	$E_{(hydrogenated)}$ (kcal/mol)[c]	$E_{(hydrogenated)}$-$E_{(encagement)}$ (kcal/mol)[d]
1,4-butanediol	1273.1	1408.0	85.6
1,5-pentanediol	1410.7	1513.4	53.1
1,6-hexanediol	1527.8	1615.7	38.7
1,7-heptanediol	1618.8	1673.7	54.9
1,8-octanediol	1652.6	1710.2	57.6
1,4-benzenedimethanol	1121.5	1207.7	37.0
trans-1,4-dimethanolcyclohexane	1658.2	1746.8	39.3

(a) Alcohol constituent of the 5,5'-diacetal-2,2'-bipyridine ligand.

(b) Energy of the encaged copper(I) complex, analogous to **1c**.

(c) Energy of the uncaged precursor copper(I) complex, analogous to **1u**.

(d) Energy required to encage copper(I) in the ligand framework.

(e) All α,α-diimine ligands are 2,2'-bipyridine.

Table I. 3. The T_1 determination of the aromatic protons of **1c**.

δ (ppm)[a]	T_1 (s^{-1})[b]
9.3	0.0662
8.7	0.0865
8.5	0.0719

(a) The reported T_1 values correspond to the aromatic proton resonances presented in Figure 1. 4.

(b) The reported T_1 values were obtained from a T_1 experiment performed on the Varian Inova 300 MHz NMR.

Chapter 1.

Figures

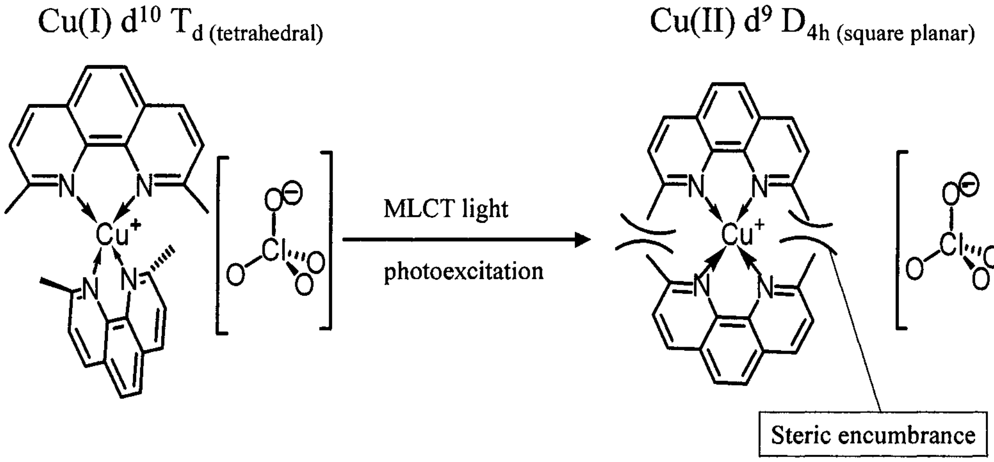

Figure 1. 1. Exciplex quenching of copper(I) complexes by solvent and counteranion axially directed nucleophilic attack. Bis(2,9-dimethyl-1,10-phenanthroline)copper(I) perchlorate is depicted.

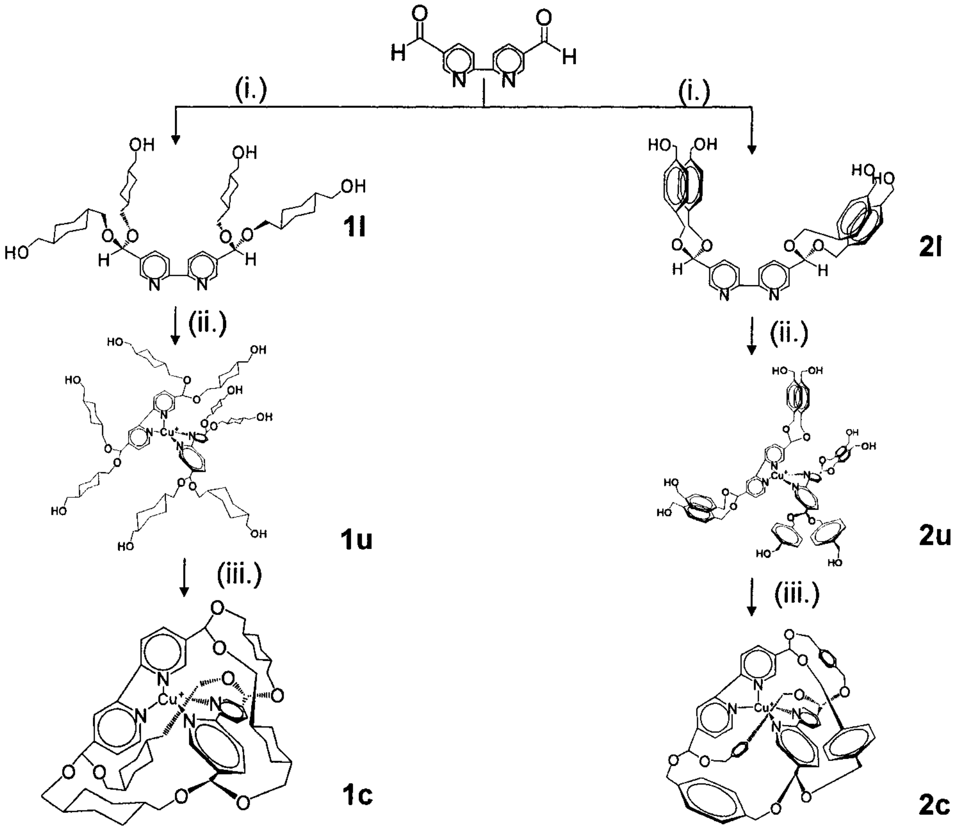

Figure 1. 2. Synthetic scheme used to prepare acetal-functionalized encaged bis(bipyridine)copper(I) complexes. The diacetal 2,2'-bipyridine ligands **1l** and **2l** are prepared in step (i.) by dissolving the precursor 5,5'-dicarboxaldehyde-2,2'-bipyridine in the neat diols, 1,4-*trans*-cyclohexanedimethanol and 1,4-benzenedimethanol, respectively, with dried 4 Å molecular sieves and trace pyridinium *para*-toluenesulfonate (**1a**) acid catalyst. Water byproduct (not represented in the above figure) is separated. The precursor complexes **1u** and **2u** are prepared in step (ii.) by adding four-fold excesses of ligands **1l** and **2l**, respectively, to tetrakis(acetonitrile)copper(I) perchlorate ($[Cu^I(CH_3CN)_4]ClO_4$) in CH_3CN under inert atmosphere conditions. Acetonitrile byproduct (not represented in the above figure) is separated. The encaged copper complexes **1c** and **2c** are prepared in step (iii.) by adding trace *iso*-propylammonium *para*-toluenesulfonate (**2a**) under inert atmosphere conditions to refluxing acetonitrile solutions of **1u** and **2u**, respectively; the encapsulation reactions are complete upon the condensation of four diol equivalents (not represented in the above figure).

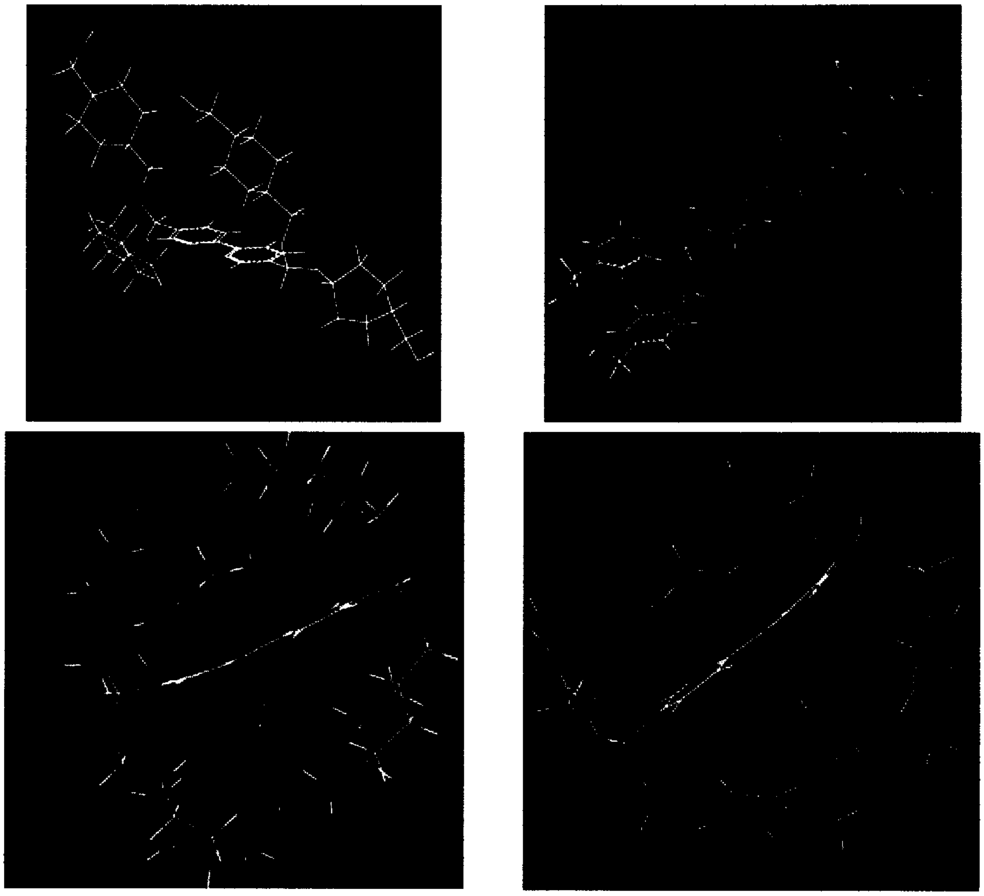

Figure 1. 3. Molecular modeling presentations of acetal-functionalized encaged bis(bipyridine)copper(I) complexes and corresponding ligands.[34] Clockwise from the upper left: ligand **1l**, ligand **2l**, complex **2c**, and complex **1c**.

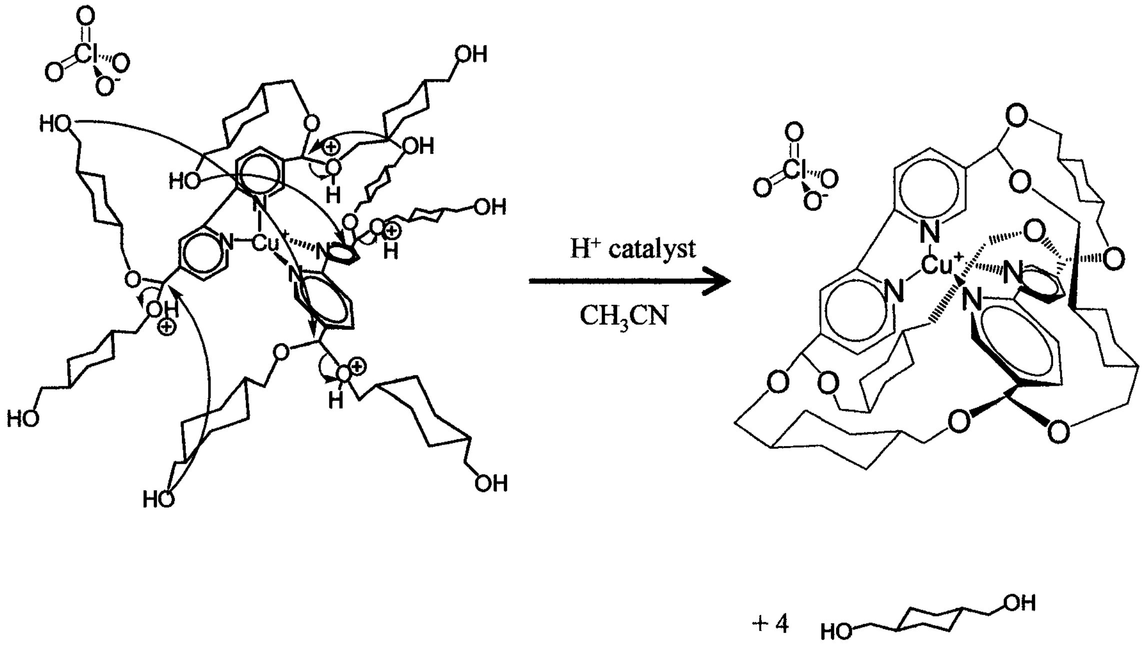

Figure 1. 4. Electron arrow mechanism showing the formation scheme of complex **1c** from **1u**. The reaction follows a generic S_N2 mechanism where the terminal acetal oxygen nucleophiles attack methine carbon electrophiles as represented by the blue arrows. The (acid-catalyzed) protonated alcohols are stable leaving groups as represented by the red arrows. Water must be excluded from the cyclization reaction to prevent ligand hydrolysis. The synthesis of complex **2c** from **2u** follows the same mechanism.

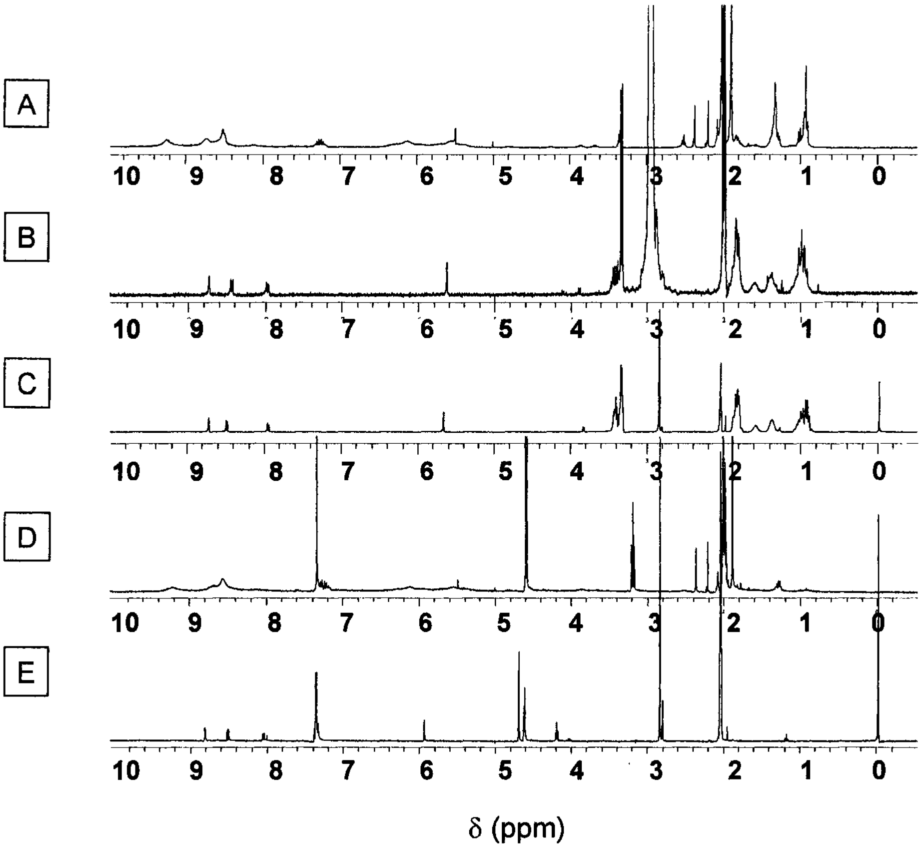

Figure 1. 5. Proton nuclear magnetic resonance (^{1}H NMR) spectra of encaged copper complexes and the corresponding precursor complexes and ligands. The presented ^{1}H NMR spectra are as follows: complex **1c'** (A), complex **1u** (B), ligand **1l** (C), complex **2c'** (D), and ligand **2l** (E). The resonances corresponding to the bipyridine peaks are broadened in complexes **1c'** and **2c'** for reasons explained in the text. Full spectral reports (including integrations) are included in the experimental section.

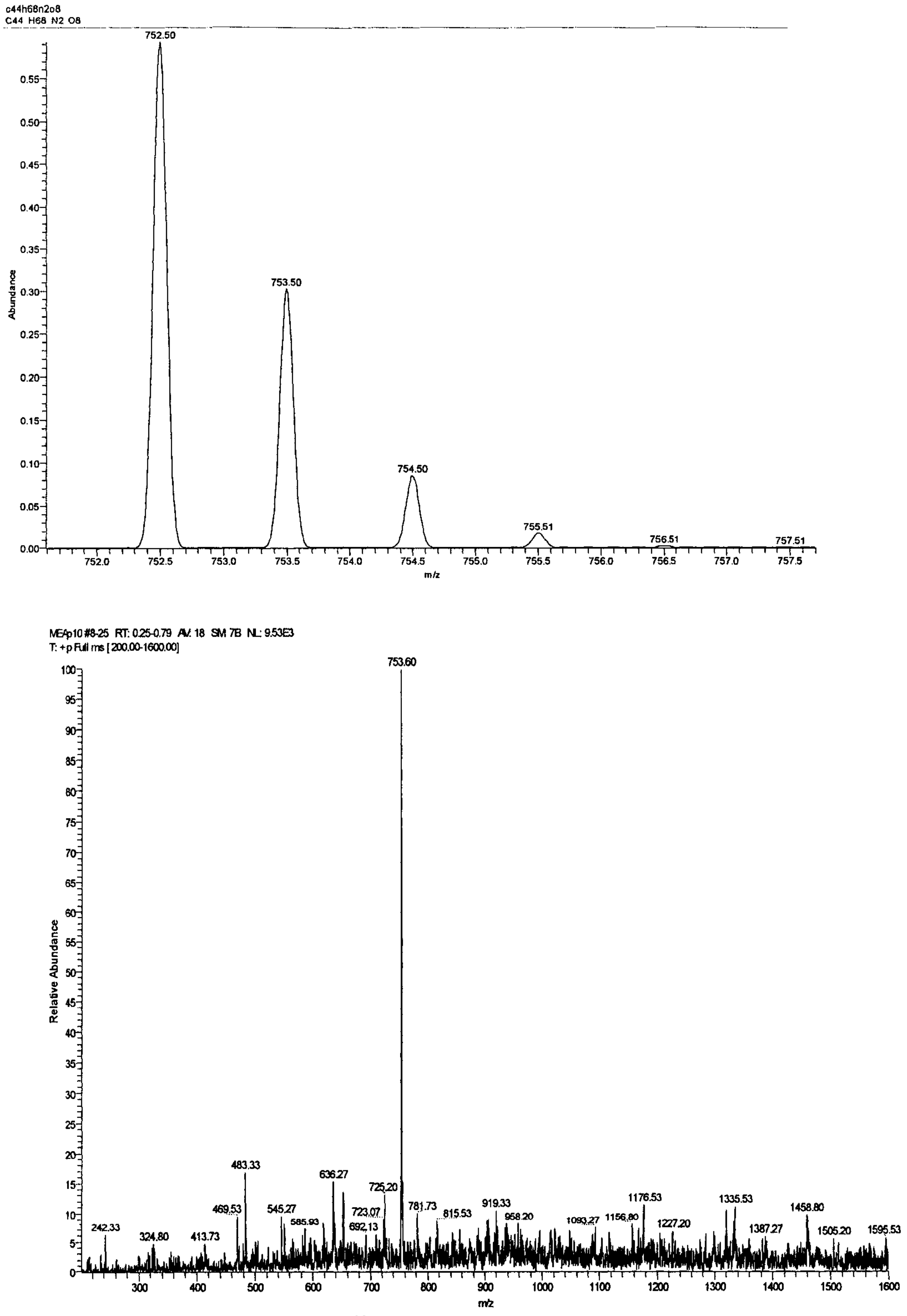

Figure 1. 6. Theoretical (top)[43] and experimental (bottom) positive ion electrospray mass spectra (ESI$^+$) of ligand **11**. The difference in the m/z values is due to protonation during the experimental timescale.

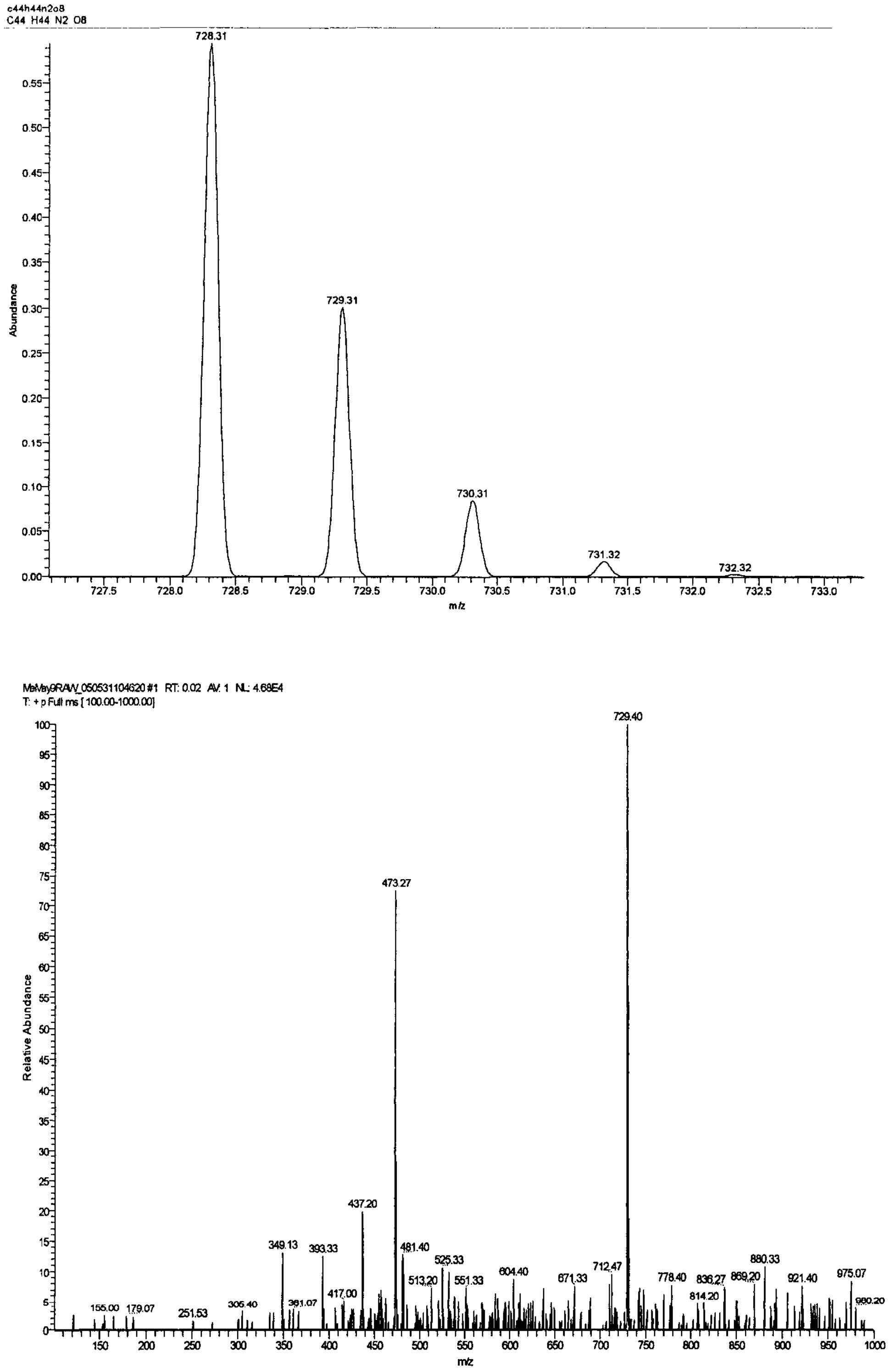

Figure 1. 7. Theoretical (top) [43] and experimental (bottom) positive ion electrospray mass spectra (ESI$^+$) of ligand **2l**. The difference in m/z values is due to protonation during the experimental timescale.

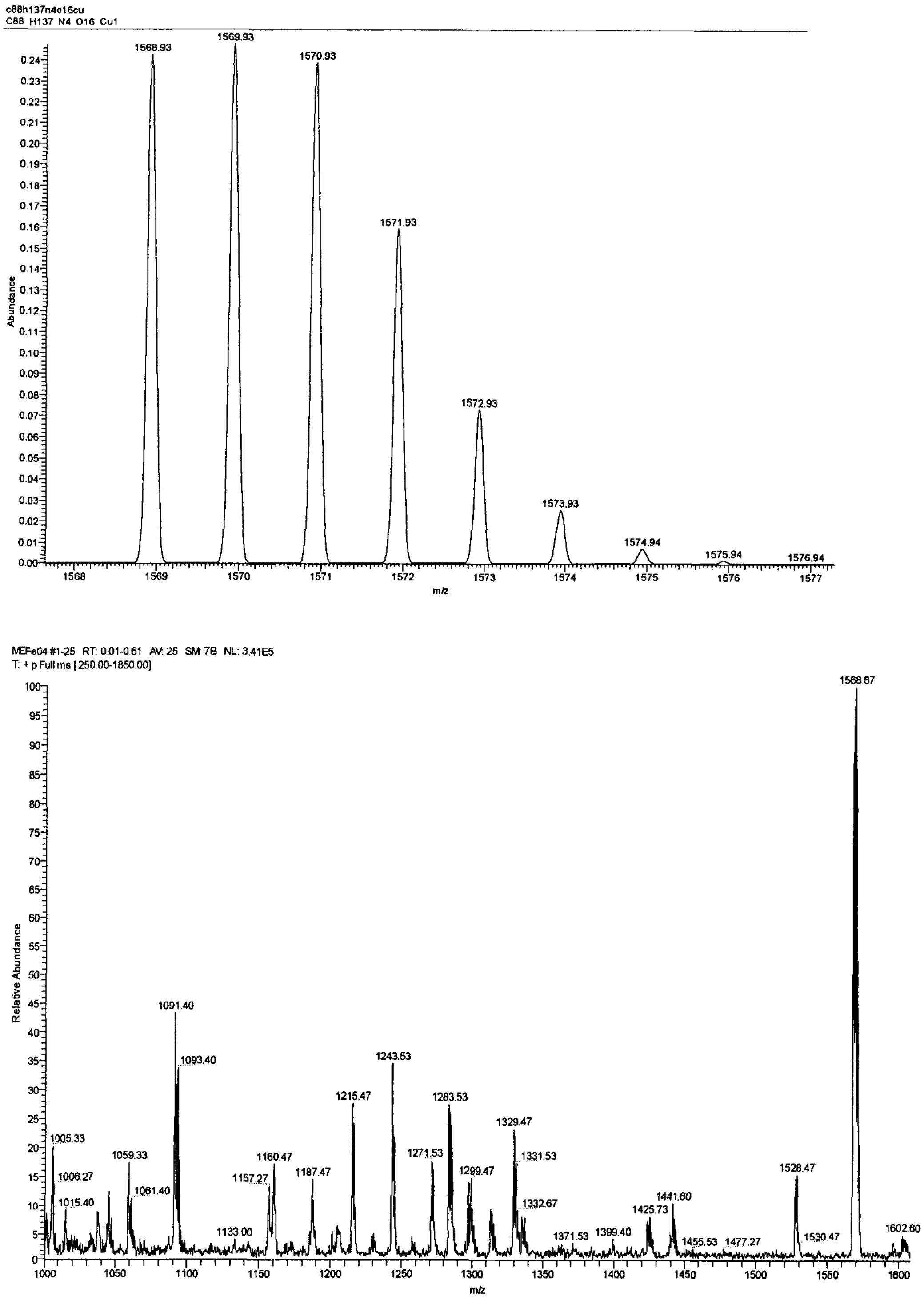

Figure 1. 8. Theoretical (top) [43] and experimental (bottom) positive ion electrospray mass spectra (ESI$^+$) of complex **1u**.

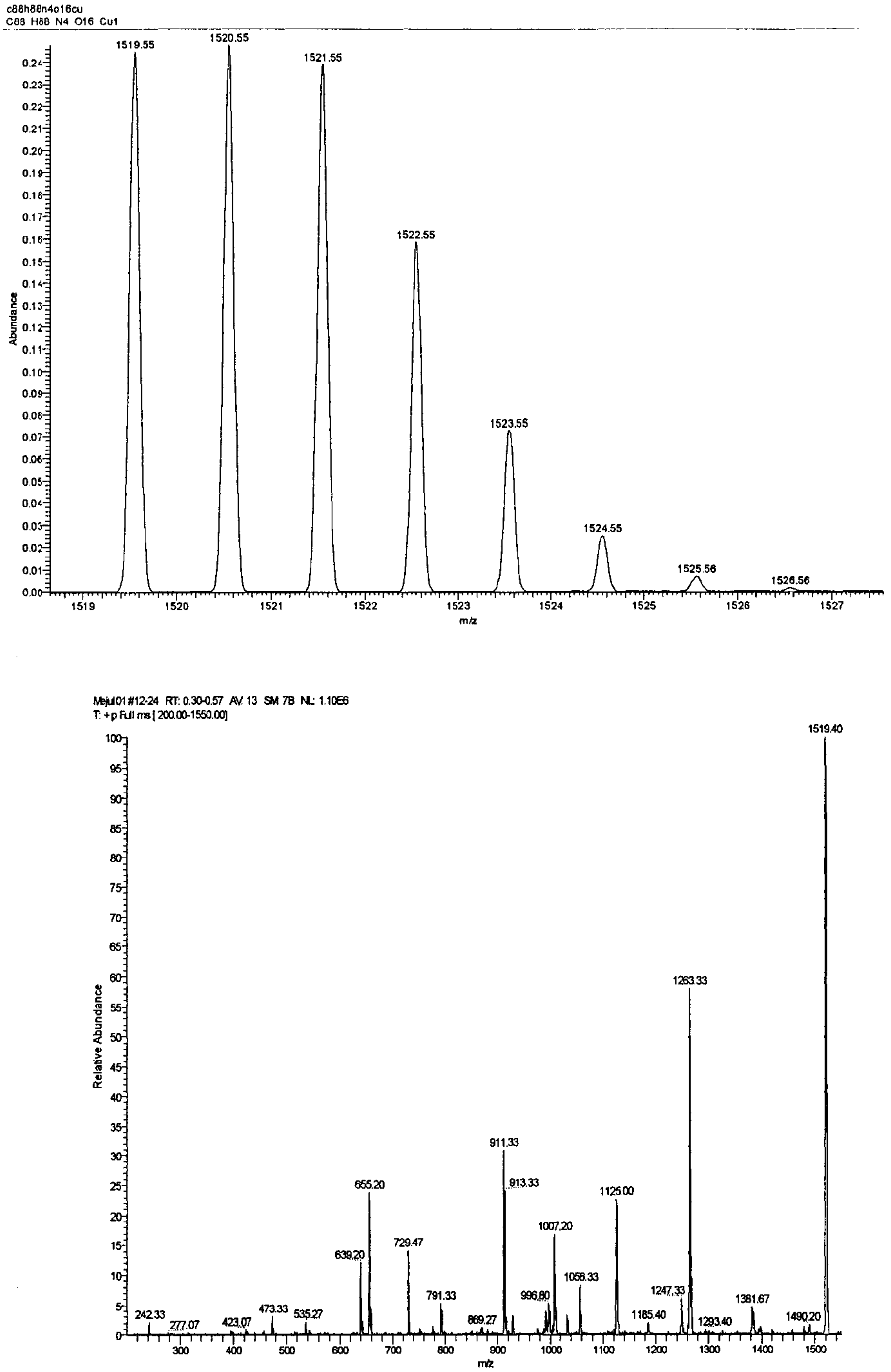

Figure 1. 9. Theoretical (top) [43] and experimental (bottom) positive ion electrospray mass spectra (ESI^+) of complex **2u**.

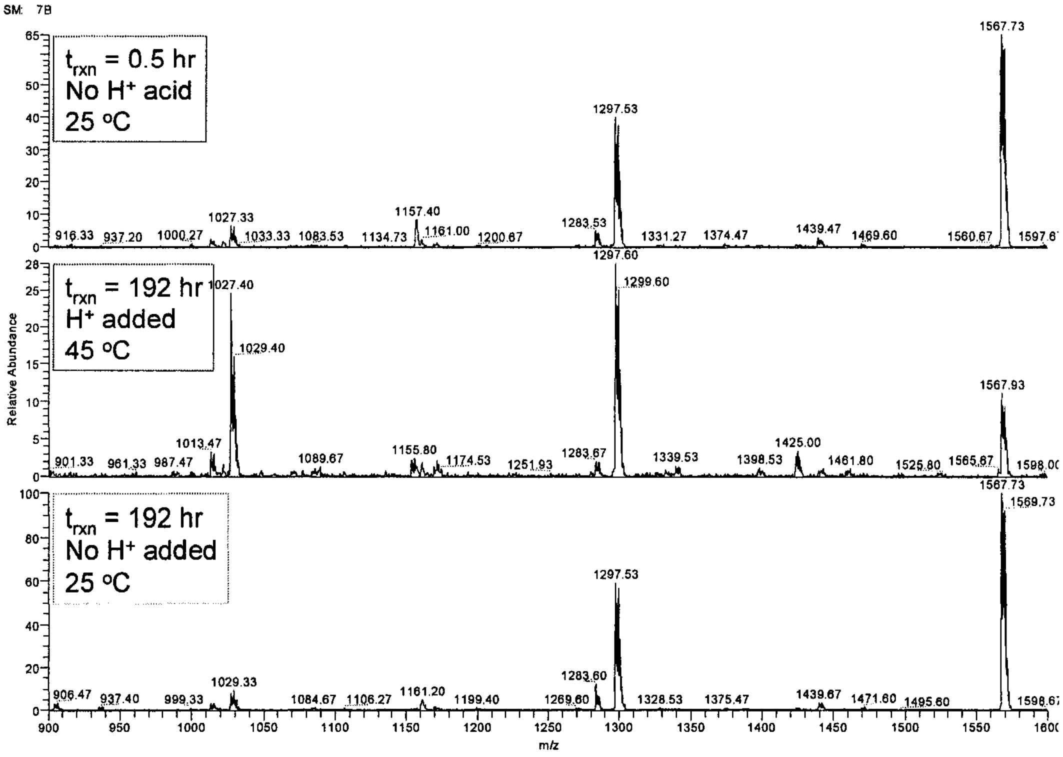

Figure 1. 10. Change in electrospray mass spectrum of **1u** upon acid catalyst addition. Complex **1u** remains intact (upper spectrum) if no ammonium acid catalyst is added. Four alcohol moieties are lost from **1u** to create the **1c** adduct observed (middle spectrum). The alcohol moieties are not lost if no acid catalyst is added (bottom spectrum).

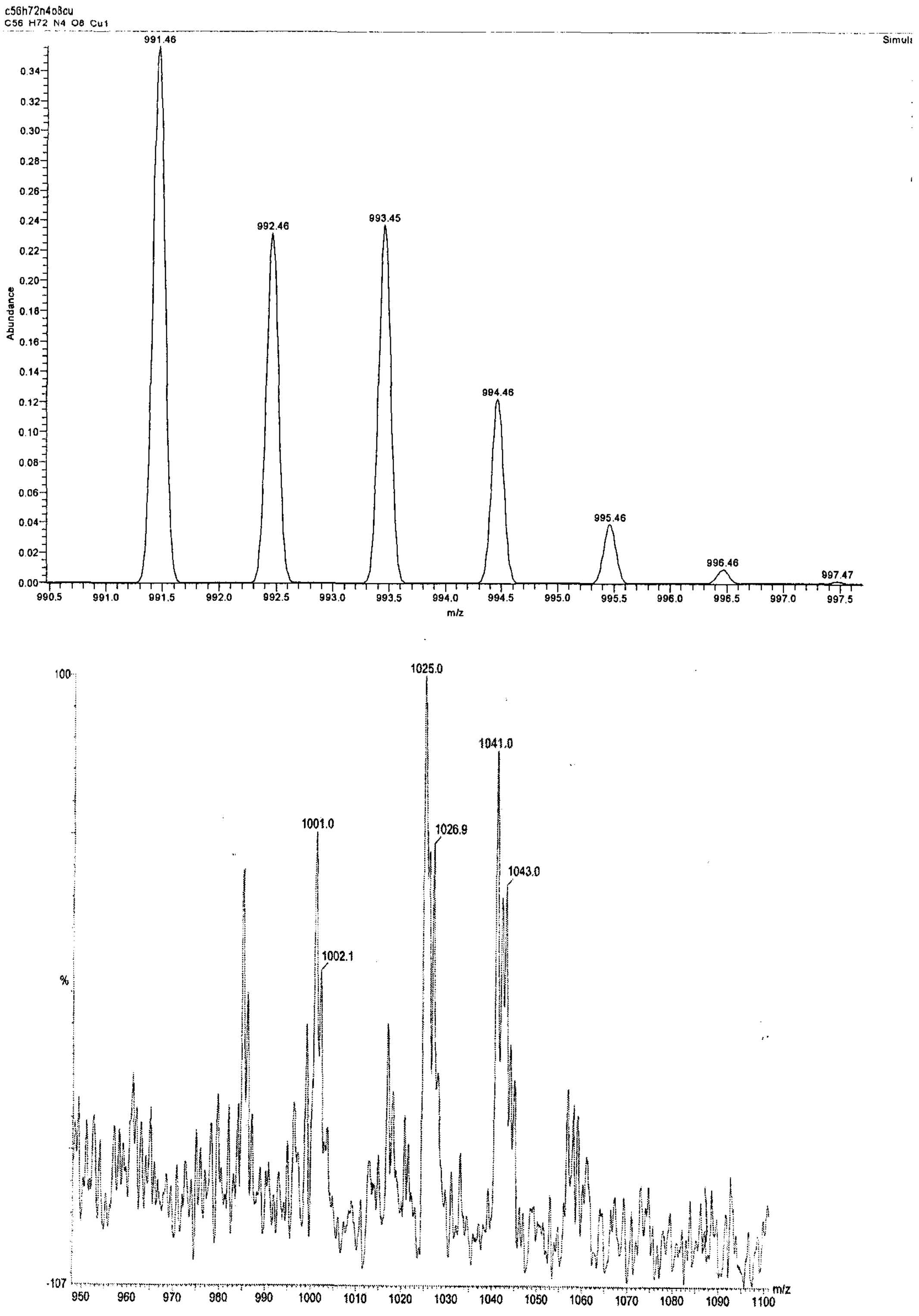

Figure 1. 11. Theoretical (top) [43] and experimental (bottom) positive ion electrospray mass spectra (ESI$^+$) of complex **1c**.

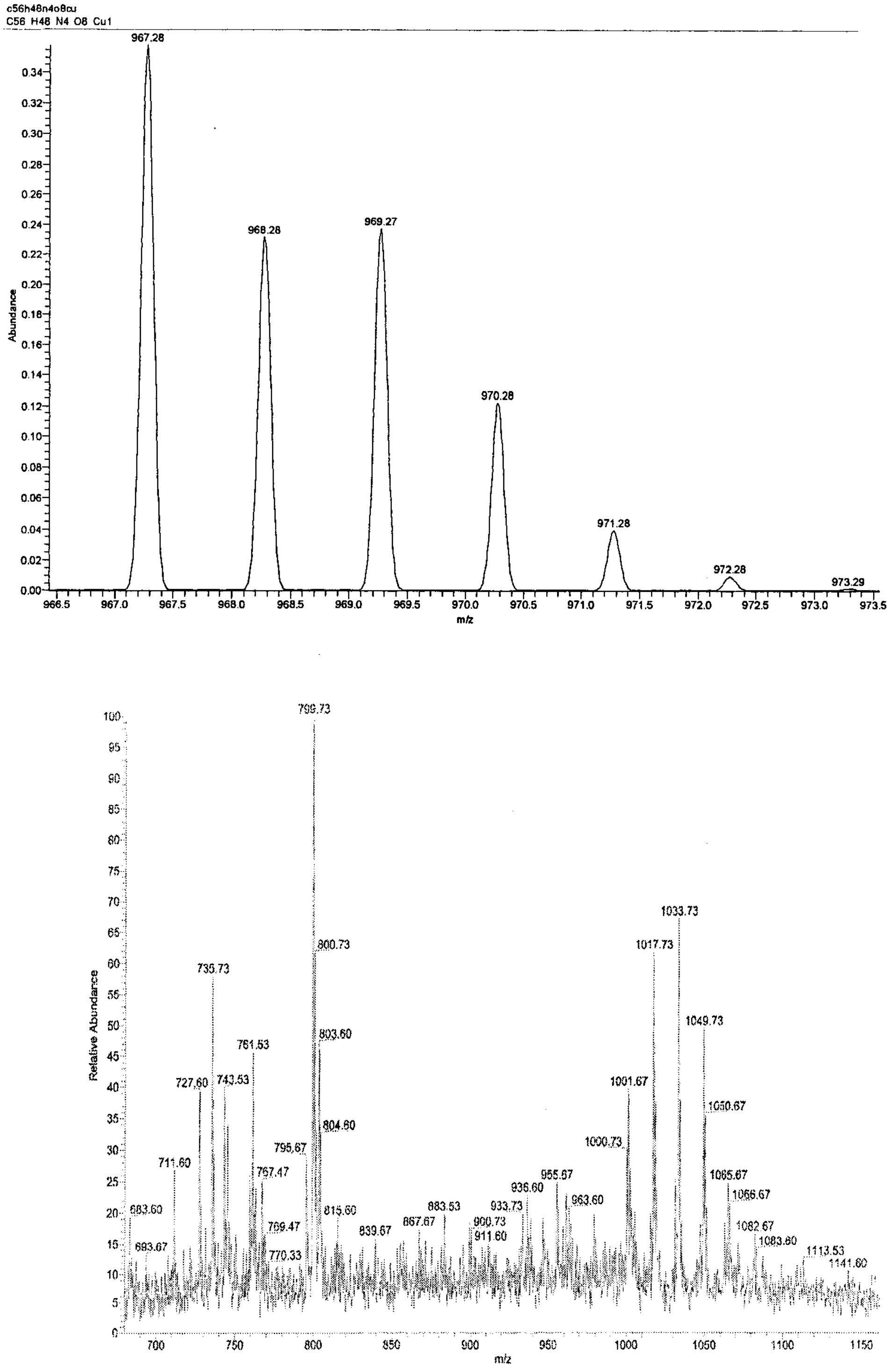

Figure 1. 12. Theoretical (top) [43] and experimental (bottom) positive ion electrospray mass spectra (ESI^+) of complex **2c**.

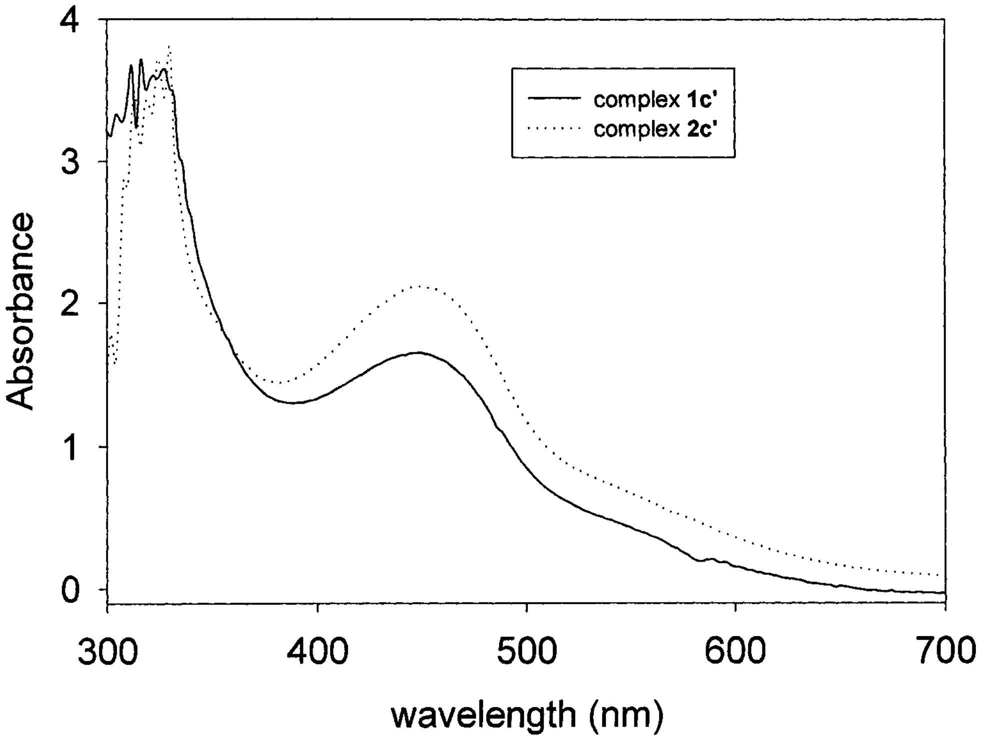

Figure 1. 13. Ultraviolet-visible (UV-vis) absorption spectra of acetal-functionalized encaged bis(bipyridine)copper(I) complexes. The absorption spectra of **1c'** (–) and **2c'**(···) were collected in degassed acetonitrile. The absorption maxima are reported in the text.

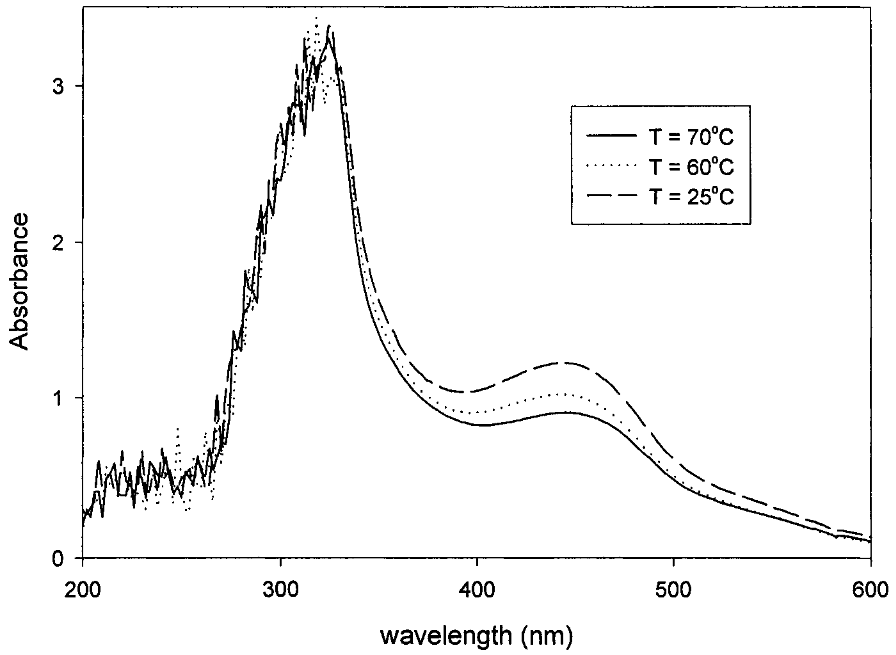

Figure 1. 14. The UV-vis absorption spectra of **1u** in acetonitrile measured at 70 °C (–), 60 °C (···), and 25 °C (--). The MLCT absorption (at ~ 450 nm) of the precursor complex **1u** decreases as temperature increases, because of enhanced ligand lability.[47-48] In contrast, the encaged complex **1c'** does not undergo a change in absorption (at ~ 450 nm) with temperature.

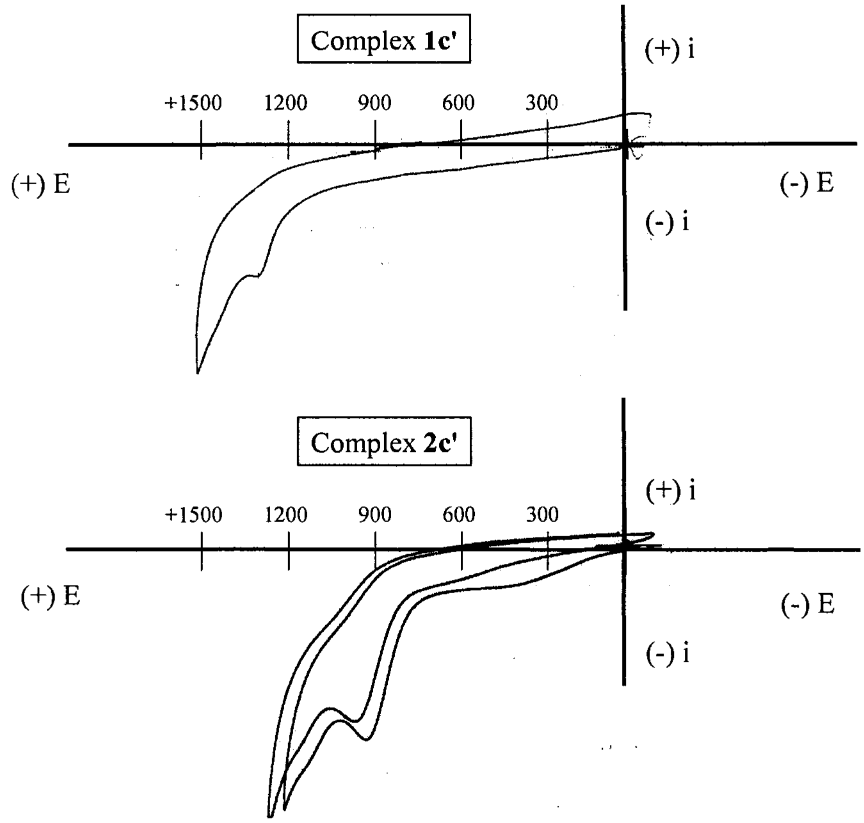

Figure 1. 15. Positive scan cyclic voltammograms of acetal-functionalized encaged bis(bipyridine)copper(I) complexes. Positive scan cyclic voltammograms are presented for complexes **1c'** (top) and **2c'** (bottom). Voltammograms were collected in 0.10 M acetonitrile solutions of tetrabutylammonium hexafluorophosphate ($TBAPF_6$) supporting electrolyte using a glassy carbon working electrode, a platinum coil counterelectrode, and a Saturated Sodium Calomel Electrode (SSCE) reference electrode. Scan rates were 50 mV/s. A coupled Electrochemical oxidation-Chemical reaction (EC) mechanism is postulated to explain the (quasi)irreversible nature of the copper(I)/copper(II) half-wave potential ($E_{1/2}^{(Cu(I)/Cu(II))}$).[51-52] From the electrochemical results, complex **1c'** is less prone to the flattening distortion responsible for emission quenching than **2c'**, because $E_{1/2}^{(Cu(I)/Cu(II))}$ is greater for the former. Contaminant ferrocene is evident at + 450 mV.

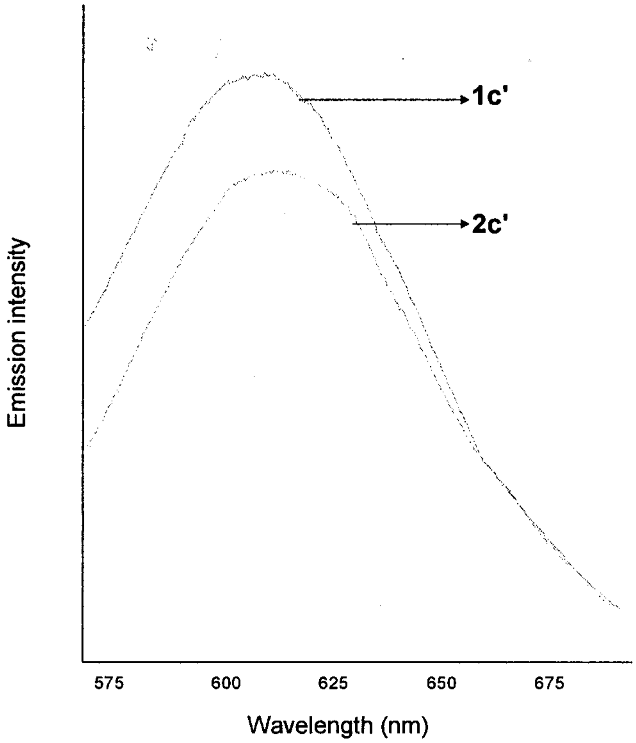

Figure 1. 16. Fluorescence emission spectra of acetal-functionalized encaged bis(bipyridine)copper(I) complexes. Emission spectra of complex **1c'** (A) and complex **2c'** (B) are presented. Neither complex **1u** nor **2u** emits light. The emission maximum (λ_{em}) of **1c'** is centered at a shorter wavelength. Therefore, according to the energy gap law,[54] complex **1c'** should have a longer emission lifetime (τ_{em}) than **2c'**.

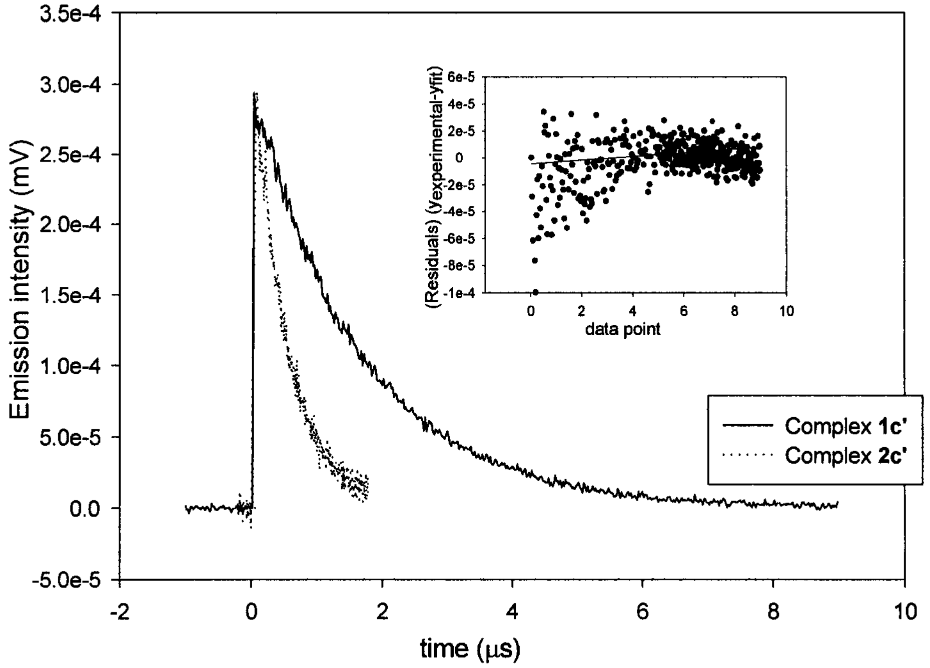

Figure 1. 17. Intensity-normalized fluorescence emission decays of acetal-functionalized encaged bis(bipyridine)copper(I) complexes with plotted residuals (inset). Normalized emission decays for complexes **1c'** and **2c'** exhibit single exponential decay kinetics indicating that one unique species emits light at one unique time constant. The τ_{em} value of **1c'** is longer than **2c'**. For solubility reasons, τ_{em} values were determined only for acetonitrile solutions of the complexes. In general, τ_{em} values for fluorophores in acetonitrile are held to be ten times shorter than those collected in dichloromethane.[55] Accordingly, complexes **1c'** and **2c'** can serve as viable photosensitizers in many different capacities and in many different solvents.

Chapter 1 References:

(1) Kalyanasundaram, K. *Cat. Metal Comp.* **1993**, *14 (Photosensitization and Photocatalysis Using Inorganic and Organometallic Compounds)*, 113-160.

(2) Schmehl, R. *Spectrum* **2000**, *13*, 17-21.

(3) Guldi, D. M.; Imahori, H. *J. Porph. Phthalo.* **2004**, *8*, 976-983.

(4) Wohrle, D.; Suvorova, O.; Kaneko, M.; Trombach, N.; Gerdes, R.; Bartels, O.;Schnurpfeil, G. *Macromolecular Symposia.* **2000**, *156 (IUPAC 8th International Symposium on Macromolecule-Metal Complexes (MMC-8 Tokyo), 1999)*, 109-116.

(5) Sauvage, J. P.; Collin, J. P.; Chambron, J. C.; Guillerez, S.; Coudret, C.; Balzani, V.; Barigelletti, F.; DeCola, L.; Flamigni, L. *Chem. Rev.* **1994**, *94*, 993-1019.

(6) Kalyanasundarum, K. *Photochemistry and Photophysics of Polypyridine and Porphyrin Complexes*; Academic Press: London, 1992.

(7) Costellano, F.; Tyson, D. F.; Juman, C. R.; Zhou, X. *Inorg. Chem.* **2001**, *40*, 4063-4066.

(8) Lippard, S. J.; Berg, J. M. *Principles of Bioinorganic Chemistry*; University Science Books: Mill Valley, CA, 1992.

(9) Ruthkosky, M.; Kelly, C. A.; Zaros, M. C.; Meyer, G. J. *J. Am. Chem. Soc.* **1997**, *119*, 12004-12005.

(10) Scalrito, D. V.; Kelly, C. A.; Ruthkosky, M.; Zaros, M. C.; Meyer, G. J. *Inorg. Chem.* **2000**, *39*, 3765-3770.

(11) Riesgo E. C.; Hu, Y. Z.; Bouvier, F.; Thummel, R. P.; Scaltrito, D. V.; Meyer, G. J. *Inorg. Chem.* **2001**, *40*, 3413-3422.

(12) Schilt, A. A. *Analytical Applications of 1,10-Phenanthroline and Related Compounds*; Pergamon Press: New York, NY, 1969.

(13) Williams, R. J. P. *Eur. J. Biochem.* **1995**, *234*, 363-381.

(14) McMillan, D. R.; Cunningham, C. T.; Cunningham, K. T.; Michalec, J. F. *Inorg. Chem.* **1999**, *38*, 4388-4393.

(15) Armaroli, N. *Chem. Soc. Rev.* **2001**, *30*, 113-118.

(16) Meyer, G. J.; Ruthkosky, M.; Castellano, F. N. *Inorg. Chem.* **1996**, *35*, 6406-6411.

(17) Ruthkosky, M.; Kelly, C. A.; Castellano, F. N.; Meyer, G. J. *Coord. Chem. Rev.* **1998**, *171*, 309-322.

(18) Gushurst, A. K. I.; McMillin, D. R.; Dietrich-Buchecker, C. O.; Sauvage, J.-P. *Inorg. Chem.* **1989**, *28*, 4070-4072.

(19) Livoreil, A.; Sauvage, J.-P.; Armaroli, N.; Balzani, V.; Flamigni, L.; Ventura, B. *J. Am. Chem. Soc.* **1997**, *119*, 12114-12124.

(20) McMillan, D. R.; Cunningham, C. T.; Moore, J. P.; Cunningham, K. T.; Fanwick, P. E. *Inorg. Chem.* **2000**, *39*, 3638-2642.

(21) Hinton, H. D.; Nieuwland, J. A. *J. Am. Chem. Soc.* **1930**, *52*, 2892-2896.

(22) Wade, L. G. Jr. *Organic Chemistry*, 3rd ed.; Prentice Hall: Upper Saddle River, NJ, 1995.

(23) Manahan, S. E. *Can. J. Chem.* **1967**, *45*, 2451-2452.

(24) Barco, A.; Benetti, S.; Pollini, G. P.; Taddia, R. *Synthesis* **1974**, *12*, 877-888.

(25) Brownstein, S.; Miller, R. *J. Org. Chem.* **1959**, *24*, 1886-1887.

(26) Rode, T.; Breitmaier, E. *Synthesis* **1987**, *25*, 574-575.

(27) Baxter, P. N. W.; Connor, J. A. *J. Organomet. Chem.* **1988**, *355*, 193-196.

(28) Uchida, Y.; Onoue, K.; Tada, N.; Nagao, F. *Tet. Lett.* **1988**, *29*, 4445-4452.

(29) Uchida, Y.; Kajita, R.; Kawasaiki, Y.; Oae, S. *Tet. Lett.* **1995**, *36*, 4077-4083.

(30) Schubert, U. S.; Eschbaumer, C.; Heller, M. *Org. Lett.* **2000**, *2*, 3373-3376.

(31) Aida, T.; Akasaka, T.; Furukawa, N.; Oae, S. *Bull. Chem. Soc. Jpn.* **1976**, *49*, 1117-1121.

(32) Katritzky, A. R.; Fan, W.-Q.; Li, Q.-L. *Tet. Let.* **1987**, *28*, 1195-1198.

(33) Madsen, R.; Fraser-Reid, B. *J. Org. Chem.* **1995**, *60*, 772-779.

(34) Cerius$^{2®}$ Molecular Simulations Inc.

(35) Sapp, S. A.; Elliott, C. M. *Chem. Mater.* **2003**, *15*, 1237-1241.

(36) Janiak, C. *J. Chem. Soc. Dalton Trans.* **2000**, *239-241*, 3885-3896.

(37) Lipshultz, F. H.; Harvey, D. F. *Syn. Comm.* **1982**, *12*, 267-277.

(38) Meyer, M.; Albrecht-Gary, A.-M.; Dietrich-Buchecker, C. O.; Sauvage, J.-P. *Inorg. Chem.* **1999**, *38*, 2279-2287.

(39) Pouchert, C. J.; Campbell, J. R. *The Aldrich Library of NMR Spectra*, vol. 1, 2nd ed.; Aldrich Chemical Company Press, Milwaukee, WI, 1983.

(40) Drago, R. S. *Physical Methods for Chemists*, 2nd. ed.; Surfside Scientific Publishers: Gainesville, FL, 1992.

(41) Nelson, J. H. *Nuclear Magnetic Resonance Spectroscopy*; Prentice Hall Publishers: Upper Saddle River, NJ, 2003.

(42) Bakhmutov, V. I. *Practical NMR Relaxation for Chemists*; Wiley Interscience Publishers: Hoboken, NJ, 2004.

(43) The theoretical m/z ratios for the investigated species were experimentally obtained from a modeling program included in the 1992 Fisons VG Quattro-SQ single quadrupole mass spectrometer software.

(44) Yam, U.-W.; Lo, K. K. *Chem. Soc. Rev.* **1992**, *28*, 323-334.

(45) Sauvage, J. P. *Inorg. Chem.* **1987**, *26*, 4290-4294.

(46) Karpishin, T. B.; Miller, M. T.; Gantzel, P. K. *Inorg. Chem.* **1999**, *38*, 3414-3418.

(47) McMillan, D. R.; Kirchoff, J. G.; Gamanche, R. E.; Blaskie, M. W.; del Paggio, A. A. *Inorg. Chem.* **1983**, *22*, 2380-2384.

(48) Barrow, G. M. *Physical Chemistry*, 6th. ed.; McGraw-Hill Companies: New York, NY, 1996.

(49) Karpishin, T. B.; Miller, M. T.; Gantzel, P. K. *Agnew. Chem. Intl. Ed.* **1998**, *37*, 1556-1560.

(50) McMillan, D. R.; Eggleston, M. K.; Koenig, K. S.; Dallenberg, A. J. *Inorg. Chem.* **1997**, *36*, 172-177.

(51) Bard, A. J.; Faulkner, L. R. *Electrochemical Methods: Fundamentals and Applications*, 1st ed.; John Wiley and Sons: New York, NY, 1980.

(52) Datta, D.; Chowdhury, S.; Goutam, K. P.; Drew, M. G.; Chattopadhay, N. *J. Chem. Soc. Dalton Trans.* **2000**, *235-237,* 235-242.

(53) Armaroli, N.; Felder, D.; Nierengarten, J.-F.; Barigelletti, F.; Ventura, B. *J. Am. Chem. Soc.* **2001**, *123*, 6291-6294.

(54) Palmer, C. E.; McMillan, D. R. *Inorg. Chem.* **1987**, *26*, 3837-3840.

(55) Kuang, S.-M.; Cuttell, D. G.; McMillin, D. R.; Fanwich, P. E.; Walton, R. A. *Inorg. Chem.* **2002**, *41*, 3313-3321.

(56) Okano, H.; Harada, N.; Kiji, J. *Bull. Chem. Soc. Jpn.* **1994**, *67*, 2329-2332.

Chapter 2.

Chromophore-sequestered Polymer Encapsulated Aerosol-OT Reverse Micelle Composite Materials of Aqueous and Nonaqueous Polar Phase Constitutions.

Introduction.

Solidified reverse micellar solutions offer researchers the chance to discover phenomenological details about organized assemblies and develop drug carriers. There are several synthetic strategies that have been employed to prepare solidified reverse micellar solutions for participation in such studies. The first strategy devised by Robinson and coworkers used elevated pressures and temperatures to solidify reverse micellar solutions.[1] Another strategy was presented by Costa and coworkers wherein polyethylene oxide-polypropylene oxide was chosen as a component for reverse micellar solution preparation.[2] Muller-Goymann and coworkers developed solidified lecithin reverse micellar solutions composed of either Witepsol™ W 35 (a high monodiglyceride), hardening fats, or triglycerides.[3-5] Menger and coworkers and Zhu and coworkers produced solidified reverse micellar solutions, namely polymer encapsulated reverse micelle composite materials, through polymerizing the nonpolar phase of precursor reverse micellar solutions.[6-10] These two groups even produced a practical application of such technology when they developed chromatographic packing materials throughout the course of their efforts. The resins of different porosity and chemical constitution had corresponding chromatographic properties. These applications were not focused on the optical quality of the materials because the solids were pulverized.[6-10]

Solidified reverse micellar solutions, in the form of polymer encapsulated reverse micelle composite (PERMC) materials, have been studied in the Elliott Research Group from the standpoints of phenomenological chemical environment studies (Chapter 2), and the practical applications thereof (Chapter 3).[11] Generally, a known concentration of a chromophore species in a polar solvent is injected in microliter amounts into a 2:1 styrene:divinylbenzene nonpolar phase Aerosol-OT (AOT) surfactant solution. *[Note, the chromophore also acts as a fluorophore. Such species will be referred to as chromophores in throughout this dissertation.]* The nonpolar phase polymerizations of composite precursor reverse micellar solutions (CPRMSs) proceed in stages through a viscous solution to a gel to a hard PERMC after the addition of a radical polymerization initiator (Figure 2. 1). Initial phenomenological work studied the effects of sequestering the well-characterized tris(bipyridine)ruthenium(II) chloride ($[Ru(bpy)_3]Cl_2$) chromophore within the nanoscopic-sized fluid polar phase domains interspersed inside poly(styrene-*co*-divinylbenzene) encapsulated Aerosol-OT (AOT) reverse micelle composite materials.[11]

Herein, it is shown that the polar phase of the PERMCs can be altered as necessary. Thereby, versatility of the PERMCs to sequester probes and molecular sensors of different solubilities and polarities is achieved. Reverse micelles of nonaqueous polar phases have infact been characterized in previous reports.[12-16] The elevated temperature Dynamic Light Scattering (DLS) particle sizing analysis performed on the CPRMSs, as well as the static and dynamic emission qualities of sequestered $[Ru(bpy)_3]Cl_2$ chromophore in the PERMCs are presented. The results are interpreted with respect to the respective PERMCs' polar phase and W_0 ([polar phase] ÷ [surfactant]). Accounts of the increases in the τ_{em} values of the sequestered chromophores in response to the hardening of the CPRMS nonpolar phases are provided. The reverse micellar imprints in representative PERMCs are imaged by Scanning Electron Microscopy (SEM) and Tapping Mode-Atomic Force Microscopy (TM-AFM). Finally, tensometry (stress-strain) studies were conducted on the PERMCs and these results were compared to poly(styrene-*co*-divinylbenzene).

Experimental Section.

Materials. The synthesis of the tris(bipyridine)ruthenium(II) chloride $[Ru(bpy)_3]Cl_2$ chromophore has been reported previously.[17] Activated neutral alumina, 98 % sodium bis(2-ethylhexyl)sulfosuccinate (AOT), 99 % styrene, and technical grade 80 % divinylbenzene (with the main impurity as 4-ethylstyrene) were purchased from Aldrich. Doubly deionized water was used. The A. C. S. Certified 99.9 % acetonitrile optima and 99.9 % methanol polar phase solvents were purchased from Aldrich and used as received. Dehibit 200® was purchased from Polysciences Inc. and used as received. The radical polymerization initiator 2,2′-azobis(2,4-dimethylpentanenitrile) (ADPN) was kindly provided by Professor Marc M. Greenberg (Johns Hopkins University, JHU).

Chromophore-sequestered Polymer Encapsulated Reverse Micelle Composite Material Preparation Preliminaries. Styrene and divinylbenzene were mixed in a 2:1 ratio to constitute the nonpolar phase of the composite precursor reverse micellar solutions (CPRMSs). Immediately before polymer encapsulated reverse micelle composite (PERMC) material preparations, the nonpolar phase was de-inhibited by sequentially eluting the mixture through separate columns of Dehibit-200 and alumina. To prepare a 50.00 mM AOT stock solution, 1.132 g of wet AOT (0.46 % H_2O by ^1H NMR) was added to a 50.00 mL volumetric flask, which was then filled with the de-inhibited 2:1 styrene:divinylbenzene mixture. The CPRMS polar phases consisted of 20.00 mM $[Ru(bpy)_3]Cl_2$ stock solutions prepared using DDI, acetonitrile, and methanol solvents (**Stock1**, **Stock2**, and **Stock3,** respectively).

Preparation of Chromophore-sequestered Polymer Encapsulated Reverse Micelle Composites (PERMCs) of Water Polar Phases (C1 Series). Using a glass syringe, five 2.00 mL aliquots of the 50.00 mM AOT solution were dispensed into five (15 x 45) mm^2 4.0 mL Fisherbrand cylindrical screw-cap vials (Figure 2. 2). Then, 1.8, 9.0, 18.0, 27.0, 36.0 μL volumes of **Stock1** were injected into these respective vials using a Gastight® 1710 glass microliter syringe. This constituted the **S1** CPRMS series (**S1-1.00** through **S1-20.00**) with corresponding W_0 values of 1.00, 5.00, 10.00, 15.00, and 20.00 (Table II. 1). The tightly-capped samples were sonicated and then agitated on a Vari-Whirl® mixer for five minutes. Aliquots of 0.20 mL taken from each CPRMS were stored for future Dynamic Light Scattering (DLS) particle sizing analysis. Then, ca. 1.0 wt. % ADPN nonpolar phase radical polymerization initiator (0.010 g, 5.84×10^{-5} mol) was dissolved in each CPRMS. The screw caps were replaced with 11 x 17 mm rubber septa. The CPRMSs were purged with nitrogen and then placed in a 37.0 °C sand bath to effect the nonpolar phase polymerization to yield the **C1** PERMC series, consisting of **C1-1.00** through **C1-20.00**, respectively (Table II. 1).

Preparation of Chromophore-sequestered Polymer Encapsulated Reverse Micelle Composites (PERMC) of Acetonitrile Polar Phases (C2 Series). Using a glass syringe, a total of five 2.00 mL aliquots of the 50.00 mM AOT solution were dispensed into respective (15 x 45) mm^2 4.0 mL Fisherbrand cylindrical screw-cap vials. Then, 1.8, 9.0, 18.0, 27.0, and 36.0 μL volumes of **Stock2** were injected using a 100 μL Gastight® 1710 glass syringe. This constituted the **S2** series CPRMSs (**S2-0.34** through **S2-6.88**) with corresponding W_0 values of 0.34, 1.72, 3.44, 5.16, and 6.88, respectively (Table II. 1). The remaining procedure follows **C1** PERMC preparations (Figure 2. 2).

Preparation of Chromophore-sequestered Polymer Encapsulated Reverse Micelle Composites (PERMCs) of Methanol Polar Phases (C3 Series). Using a glass syringe, five 2.00 mL aliquots of the 50.00 mM AOT solution were dispensed into respective (15 x 45) mm^2 4.0 mL Fisherbrand cylindrical screw-cap vials. Then, 1.8, 9.0, 18.0, 27.0, 36.0 μL volumes of **Stock3** were injected using a 100 μL Gastight® 1710 glass microliter syringe. This constituted the **S3** series CPRMS (**S3-0.56** through **S3-11.72**) with corresponding W_0 values of 0.56, 2.81, 5.63, 8.44, and 11.72, respectively (Table II. 1). The remaining procedure follows **C1** PERMC preparations.

Composite Precursor Reverse Micellar Solution (CPRMS) Dynamic Light Scattering (DLS) Particle Sizing. Dynamic Light Scattering (DLS) particle sizing was performed on CPRMSs using a Dyna-Pro® MSTC operated at 25.0 °C. The difference in the refractive indices of the nonpolar phases (at 1.5470 and 1.5740 for styrene and divinylbenzene, respectively) and polar phases (at 1.000, 1.3440, and 1.3290 for water, acetonitrile, and methanol, respectively) confirms the viability of using DLS to determine micellar radii.[18] A styrene blank was chosen in place of the actual 2:1 styrene:divinylbenzene nonpolar phase, because the refractive indices are very similar at 1.5470 and 1.5740, respectively.[18] Particulate matter was removed by filtering the 0.20

mL CPRMSs volumes through a Teflon®-construct 0.02 μm Whatman® Anodisc 13 membrane filter four times. For each CPRMS, ten particle size readings were collected which were then averaged and reported as mean values with error bars representative of one standard deviation. No incident polymerization occurred during the DLS experimental time frame. Elevated temperature DLS studies were done on representative CPRMSs **S1-5.00**, **S2-1.72**, and **S3-2.80**. After collecting five size measurements at 25.0 °C, the temperature of the cuvette containing the CPRMSs was increased at a rate of 1 degree per 30 seconds up to a final temperature of 42.0 °C.

Polymer Encapsulated Reverse Micelle Composite (PERMC) Finishing. After scoring, the vials were broken to retrieve their resulting cylindrical PERMC series **C1**, **C2**, and **C3**. A Buehler® Variable Speed polishing wheel equipped with progressively finer grit sandpaper was used to refine the PERMCs into orthogonal dimensions on the order of (0.25 x 0.75 x 1.0)cm^3. The PERMC series were polished using 0.3 micron Buehler® Micropolish II polishing materials. The polishing action provided smooth, homogeneous, non-light scattering monolith surfaces suitable for optical studies.

Static Emission Spectroscopy of Chromophore-sequestered Polymer Encapsulated Reverse Micelle Composite (PERMC) Series. The emission spectra of the sequestered $[Ru(bpy)_3]Cl_2$ probe were collected over the range of 550.0 nm to 650.0 nm and were recorded by 0.5 nm increments under 1.0 second integration times using a Fluorolog-3 Hosuni® spectrofluorimeter in perpendicular geometry. The excitation wavelength was 450 nm. Excitation and emission slit widths were set to 5.00 nm. Three series of emission spectra (**C1** through **C3**) are presented with intensity normalizations. The static spectra of PERMCs with like polar phases but unlike W_0 values (**C1-1.00**, **C1-**

5.00, **C1-10.00**, **C1-15.00**, and **C1-20.00** for example) are plotted on the same I vs. λ(nm) graph. Irreproducible composite dimensions and placement in the fluorimeter precluded any strict analysis of the emission intensity with polar phase or W_0. Emission maxima (λ_{em}) are reported.

Emission Lifetime (τ_{em}) Determinations of Chromophore-sequestered Polymer Encapsulated Reverse Micelle Composite (PERMC) Series. The laser system used for time-resolved spectroscopy is similar to that which is described in previous reports and is as follows (Figure 2. 3).[11] All emission lifetimes were taken ca.104 hours after the addition of ADPN. The composites were mounted on a Thorlabs® aluminum post with an adhesive. The frequency-tripled output of a Spectra-Physics® LAB-190 Nd:YAG laser operating at 30.00 Hz produced a train of 8.0 ns pulses of 355 nm light at 1.50 W power. This pumped a Coumarin 450 (Exciton) dye in a Spectra-Physics® PDL-3 dye laser to provide the 450 nm pump beam which approximated the wavelength of the chromophore's absorption maximum. Dye laser powers were typically 45 ± 5 mW. The 450 nm excitation wavelength was incident surface-normal upon the (0.2 x 1.0)cm^2 face of the monolith. The emission emanating from one of the (0.75 x 1.0)cm^2 perpendicular monolith faces was first collimated then focused through a Melles-Griot® 480 nm high band pass filter onto a Jarrell Ash® model 82-410 monochromator that selected 600 nm light. Light of this wavelength corresponds to the emission maximum wavelength of the chromophore. The emitted light was collected using a Hamamatsu® model R2496 photomultiplier tube commonly set to a bias 500 V. The current output of the photomultiplier tube was recorded and displayed electronically on a Tektronix® TDS602B digital oscilloscope. A Thorlabs® DET310 photodiode was used to trigger and synchronize the oscilloscope with the dye laser pulse. Averaging 1000 decay curves yielded signal-to-noise (S:N) values greater than ten over the 33 second experimental timeframe. The averaged data was transported to LabView® 5.1 and imported as ASCII x-y pairs into Microsoft Excel® whereupon baseline corrections and intensity normalizations were completed. Monoexponential decay regression fits were completed using SigmaPlot® 2000 to obtain the emission lifetime (τ_{em}) for each chromophore-sequestered PERMC. Monoexponential decay fits linear regressions are reported.

Nonpolar Phase Polymerization Time (t_p)-dependent Emission Lifetime Study on Representative Chromophore-sequestered Polymer Encapsulated Reverse Micelle Composites (PERMCs). The τ_{em} values of the **S1-5.00** and **S2-1.72** CPRMSs were determined before the addition of ca. 1.0 wt. % ADPN. The CPRMSs were then placed in the 37.0 °C heated sand bath to complete the nonpolar phase polymerization. Over time, the fluid CPRMSs turned viscous, then transformed into gels, then tacky polymers, until finally hardened into PERMCs. The curing CPRMSs were retrieved from the sand bath at specific polymerization times (t_p) of 0.5, 1.0, 1.5, 3.0, 4.0, 5.0, 6.0, 7.0, 10.0, 20.0, 22.5, 31.5, 48.0, 96.0, 194.0, and 400.0 hours to measure the τ_{em} of the sequestered $[Ru(bpy)_3]Cl_2$ as a function of the physical state of the curing CPRMS nonpolar phase. After each determination, the curing CPRMSs were replaced into the heated sand bath.

Proton Nuclear Magnetic Resonance Spectroscopy Study on the Effect of Purging CPRMSs with Dry Nitrogen. A CPRMS was prepared which was similar to **S1-15.00** in every way except that it had a nonpolar phase of divinylbenzene only—not 2:1 styrene:divinylbenzene. The nonpolar phase substitution was made to obtain one set of resonances from the nonpolar phase instead of two. The prepared CPRMS was sealed with a septum. A 0.5 mL aliquot was extracted from the CPRMS and placed in an NMR tube. The NMR tube contents were capped with a septum and sealed with Parafilm®. Under stopwatch timing, the CPRMS was purged for one minute. Another 0.5 mL of the CPRMS was extracted with a syringe and placed into a different NMR tube. The process was iterated two more times following total purge times of four and eight minutes. A 500 MHz Varian® NMR was used to collect spectra over periods of eight minutes. The area of the peak corresponding to water (at 4.80 ppm) was integrated with respect to a surfactant-based alkane stretch centered at 2.7 ppm whose area was set to unity.

Scanning Electron Microscopy (SEM). All scanning electron microscopy images were taken using a JEOL JEM-2000 LX-II® microscope. A polymer encapsulated reverse micelle composite material for imaging was made from the radical-initiated nonpolar phase polymerization of a composite precursor reverse micellar solution consisting of 2.00 mL of a 2:1 styrene:divinylbenzene 50.00 mM Aerosol-OT stock solution to which 9.0 μL of $[Ru(bpy)_3]Cl_2$ in water was added. After four days of exposure to a 37.0 °C sand bath, the resulting PERMC was ground into a $(0.75 \times 0.75 \times 0.10)cm^3$ tile. The hardened meniscus of the resulting PERMC (due to the surface tension effects of the CPRMS in the vial) remained intact on one 0.75 x 0.75 cm^2 face. The same was done for a poly(styrene-*co*-divinylbenzene) sample for imaging. The curved hardened meniscus 0.75 x 0.75 cm^2 tile faces for both samples were placed face-up on an Aluminum stub of 1 cm thickness and 1.25 cm diameter. The tile-shaped composite was then mounted on the stub using Colloidal graphite with an *iso*-propanol base (Energy Beam Sciences®). The paste hardened in the absence of any applied heat over a period of 16 hours. No gold sputtering of the samples was undertaken to ensure that any detectable reverse micellar imprint features would not be occluded. The specific parameters used in the imaging process are given in the SEM images themselves, as well as their respective magnifications and scale bars. Images were imported as TIFF files into Photoshop Adobe 6.0®. The only alteration performed on the presented images was that of the Adjust levels command.

Tapping Mode-Atomic Force Microscopy (TM-AFM). Cryo-cut fractography was employed to expose an interior poly(styrene-*co*-divinylbenzene) or PERMC surface for AFM analysis. A blank of poly(styrene-*co*-divinylbenzene) **(Cut I)** was radically-polymerized with ADPN at 37.0 °C and ground to rectangular dimensions. A tris(bipyridine)ruthenium(II) chloride $[Ru(bpy)_3]Cl_2$ **(C)** chromophore-sequestered composite **(Cut II)** was also analyzed. First, **Cut I-II** were cooled in an ice bath to 0 °C, then slowly introduced into a dry ice/acetone bath (-72 °C). Following, **Cut I-II** were carefully introduced into a dewer containing liquid nitrogen (-196 °C) for one minute before being transferred to a Styrofoam© cup containing a smaller volume liquid nitrogen sufficient to immerse each. **Cut I-II** were each fractured by striking an Exacto-Knife® blade which was already in contact with the liquid nitrogen. The fractured surface of each sample was then covered with Parafilm®, and the opposing surface was ground flat. The Parafilm® was removed and the samples were placed in a Branson® ultrasonic cleaner containing methanol for ten minutes. Samples were dried with compressed air.

Both samples were imaged under ambient air conditions. Samples were mounted on a stainless steel stub using double-sided tape. All samples were featureless to examination by a one thousand magnification optical microscope. Height and Phase Imaging was performed using a commercial atomic force microscope (Nanoscope IIIa, Digital Instruments®) operated in 'tip-sample' repulsive mode. A commercial uncoated square-pyramidal-shaped silicon tip, with a radius of curvature of less than 10 nm, adjunct to a 230 ± 5 μm long silicon cantilever of reported spring constant 40 ± 15 N/m (NSC-16 Ultrasharp® Cantilevers and Gratings) was used to image cryo-cut samples at low amplitudes (A_o) in constant amplitude mode. The cantilever oscillated at a drive frequency of 170.00 ± 10.00 kHz with an amplitude set-point of 1.8 ± 0.2 V. Such settings ensured that no sample degradation occurred during the imaging process. Scans were repeated at lower frequencies to ensure the image reproducibility. Obtained image scan sizes on the order of (256 x 256) pixels ranged from (4.00 x 4.00) μm^2 to (300 x 300) nm^2 dimensions. The latter domain was achieved by preferentially scanning ridge-like hillock features exhibited by the cryo-cut surfaces that were visualized on a (1.00 x 1.00) μm^2 scale. A scan of one sheet of mica was collected for comparison to **Cut I-II**. All images shown are the raw experimental data without any image processing except flattening. Image Histograms were examined along the vertical axis where no in-plane shearing effects occur.

Stress-strain Analysis. Every attempt was made to conform to American Society of Testing and Materials (ASTM) standard D.683 with respect to the dimensions of the samples subjected to stress-strain tests.[19] A Teflon® construct mold was prepared according to ASTM D 683 Type V (limited material) specifications. However, all of the resulting composites polymerized in the mold were already crazed at the junction points of the mold. Therefore, the reported stress-strain curves herein regrettably do not strictly conform to ASTM standards. Instead, slabs of samples with the same dimensions were examined. To do so, a volume of 27.5 mL of 2:1 styrene:divinylbenzene mixture was injected into a screw-threaded (25 x 95) mm 8 dram glass vial (Fisher Scientific) using a 10 mL glass syringe. Then, ca. 1.0 wt. % ADPN (0.010 g, 7.25×10^{-5} mol) was dissolved in the mixture. A 14 x 18 mm septum sealed the vial's contents. The vial was placed in a mineral oil bath set to 37.0 °C to facilitate polymerization over a period of four days. The result was a hardened cylindrical-shaped sample of poly(styrene-*co*-divinylbenzene), **I**. Then, 27.5 mL of a 50.00 mM AOT solution was injected into two screw-threaded (25 x 95) mm 8 dram glass vials. Using a 100 μL 1710 Gastight® syringe, volumes of 0.0 and 123.8 μL of 20.00 mM $[Ru(bpy)_3]Cl_2$ water stock solution were injected into the solutions to effect CPRMSs with W_0 values of 0.00 and 5.00, respectively. The CPRMSs were polymerized as before into cylindrical-shaped samples **II** and **III**, respectively.

The glass vials containing the samples were scored with a carbide file, then retrieved to obtain clear cylindrical composites with lengthwise dimensions and diameters on the order of 270 and 90 mm, respectively. Samples **I**, **II**, and **III** were ground into rectangular slabs using a Buehler variable speed polishing wheel equipped with progressively finer (120 →600) grit sandpaper. The samples were then polished with Microcloth® polishing pads (Buehler) and Mastermet® 2 non-crystallizing polish (Buehler). The dimension of each of the composites was measured to be (65.0 x 17.5 x. 4.0) mm^3 by using electronic calipers. The measurements were made at three different sections along each specified dimension to ensure 'thinning' or 'thickening' of the samples did not result during the grinding process.

All stress-strain analyses were made on an Instron® IX interface 4442 tensometer (Instron Corporation) in a 27 °C room with 50 % humidity.[20] To partially conform to ASTM D 683 Type V specifications for the mechanical testing of rigid plastic materials, the crosshead speed was set to one mm/minute. The gauge length was set to 25 mm. The length of the composite in contact with the mechanical gripping crossheads on either side of the gauge length was 20 mm. The samples were placed in the hydraulic grippers such that they were perfectly erect. The maximum load able to be exerted by the Instron® was 500 N. The sustainable small load limit (the load at which the samples are considered broken and the test ends) is 20 N. The sampling rate for the presented stress-strain curve was 6.6 points per second. Once a test was completed, the crosshead returned to the original gauge length of 25 mm. Data was exported in ASCII x-y pair format into Sigmaplot® 2000 plotting program. The Young's moduli of **I, II,** and **III** were determined at different load levels by calculating the slope of the line at that load level. Sample toughness was determined by calculating the area under the stress-strain curves.

Results and Discussion.

Compositions of Chromophore-sequestered PERMC Series C1-C3. The constitutions of the chromophore-sequestered polymer encapsulated reverse micelle composite materials (PERMCs) are given (Table II. 1). The general synthetic scheme used to prepare the PERMCs is presented (Figure 2. 1). The **C1**, **C2**, and **C3** composite series were prepared with 20.00 mM tris(bipyridine)ruthenium(II) chloride ($[Ru(bpy)_3]Cl_2$) water, acetonitrile, and methanol polar phase stock solutions, respectively. For the each PERMC series, five different volumes (1.8, 9.0, 18.0, 27.0, and 36.0 μL) of the respective 20.00 mM $[Ru(bpy)_3]Cl_2$ polar phase stock solution were injected into separate vials containing 2.00 mL of the 2:1 styrene:divinylbenzene nonpolar phase. These volumes corresponded to each series' different W_0 values. The W_0 value of a PERMC is calculated from the following expression, where V_{plr} is the chromophore solution volume, c_{plr} is the polar phase concentration, V_{tot} is the CPRMS total volume, and c_{AOT} is the surfactant concentration:[21]

$$W_0 = V_{plr}(c_{plr}) \div V_{tot}(c_{surf}) \qquad (1.)$$

The W_0 values are (1.00, 5.00, 10.00, 15.00, and 20.00), (0.34, 1.70, 3.44, 5.16, and 6.88), and (0.56, 2.81, 5.63, 8.44, and 11.52) for series **C1**, **C2**, and **C3**, respectively. In spite of the equivolume polar phase injections for each series, the W_0 values are different because the concentrations of bulk water, acetonitrile, and methanol, are 55.5 mM, 19.1 mM, and 31.2 mM, respectively.

A surfactant concentration of 50.00 mM was chosen for all composites characterized herein. The 50.00 mM AOT concentration is greater than the cmc below which no reverse micelles form.[22] In general, the cmc is indirectly proportional to the polar phase solvent dielectric constant. The optical quality of the PERMCs decreases at surfactant concentrations larger than 50.00 mM. This phenomenon is due to the corresponding greater number of intermicellar collisions between micelles.[23-24] Such intermicellar collisions and the exchange of polar phase media therefrom can terminate polymerizing chains in the nonpolar phase to ultimately produce shorter polymer chains constituting microcrystalline regions which scatter light.[25] Alternatively, at higher surfactant concentrations, micelles form aggregates with diameters above the that of the light scattering limit. Such aggregation has been exhibited in previous work.[26]

There is more than one way to polymerize the CPRMS nonpolar phases and still obtain optically clear PERMCs. For instance, the addition of ca. 1.0 wt. % 2,2'-

azobis(2,4-isobutyronitrile) (AIBN) to the CPRMSs and subsequent exposure to long wave ultraviolet (UV) light polymerization for two days yields optically clear PERMCs. The UV-initiated nonpolar phase CPRMS polymerization method serves to decrease the evaporation of the CPRMS constituents, thereby preserving the CPRMS W_0 in the corresponding PERMCs. Moreover, ca. 1.0 wt. % of the less expensive benzoyl peroxide (BPO) initiator also facilitates thermally assisted radically induced CPRMS nonpolar phase polymerizations at 37.0 °C. Even so, the decay kinetics of ADPN are faster than that of AIBN and BPO.[27] Accordingly, all PERMCs presented herein were prepared using 37.0 °C thermally assisted radical-induced CPRMS nonpolar phase polymerizations with 1.0 wt. % 2,2′-azobis(2,4-dimethylpentanenitrile) (ADPN).

Characterization of the C1 Series. Dynamic Light Scattering studies showed that the water-based polar phase is sequestered inside reverse micelles. According to the documented solubility of water in styrene, only 0.065 wt. % of water partitions into the nonpolar phase (Table II. 2). Dynamic Light Scattering (DLS) measurements on CPRMSs show that micelles are still intact at room temperature for all W_0 ([polar phase]/[surfactant]) values examined (Table II. 3). The CPRMSs of smallest fluid phase component (**C1-1.00**) and largest fluid phase component (**C1-20.00**) have polydisperse micellar radii that are within one standard deviation of each other (Table II. 3).

The polydispersities are ca. half as large as the measured mean micellar radii for one main reason. The radii measured by DLS describe both solvent-sequestered (empty) and solvated chromophore-sequestered (filled) reverse micelles, according to Poisson statistical calculations.[28-30] About 10 % of the micelles sequester one chromophore and water polar phase with the remaining 90 % sequestering only water. Such micellar occupancy polydispersity causes larger micellar radii polydispersities

A series of Dynamic Light Scattering particle sizing experiments were also conducted to establish the effect of the $[Ru(bpy)_3]Cl_2$ chromophore concentration on micelle size and polydispersity. The examined CPRMSs all had 2:1 styrene:divinylbenzene nonpolar phases, water polar phases, and W_0 values of 10.00, but had different $[Ru(bpy)_3]Cl_2$ concentrations of 1.00, 3.00, 5.00, 10.00, and 40.00 mM (Figure 2. 4). The size and the polydispersity of the reverse micelles both increase as the $[Ru(bpy)_3]Cl_2$ concentration increases. Particles of radius > 50 nm are polymeric species. Electrostatic and hydrophobic interactions between the chromophore and anionic wall of the polymer encapsulated AOT reverse micelles have been documented.[31-34] Such interactions can induce spherical micellar morphology deformations consequently giving rise to exacerbated polydispersities.

Elevated temperature DLS on CPRMS **S1-15.00** shows that micelles are still intact at the nonpolar phase polymerization temperature (Figure 2. 5A). The micellar structural stability at these temperatures can be attributed to the strong electrostatic interactions between the cationic chromophore and the anionic micelle wall which lower the induced critical micelle concentration (i_{cmc}). Micellar collisions, which become more frequent at elevated temperature, therefore do not result in as many free surfactant or polar phase species which can prematurely terminate the nonpolar phase polymerization.

The static emission spectra of all **C1** series PERMCs exhibit single broad bands, and have emission maxima (λ_{em}) that are dependent on W_0 (Figure 2. 6A, Table II. 3). The broadness of the emission maximum indicates that the sequestered chromophore is subject to one averaged chemical environment due to the sequestered chromophores' emission from different vibrational energy states afforded by solution.[35] The static emission spectra maxima of sequestered $[Ru(bpy)_3]Cl_2$ in the **C1** series PERMCs red-shift by 14 nm across the investigated W_0 range of 1.00 to 20.00. This increase in λ_{em} corresponds to a chemical environment polarity increase about the chromophore.[36-37]

The emission lifetimes (τ_{em}) of the sequestered chromophores in the **C1** series PERMCs decreases by ca. 550 ns as the W_0 increases from 1.00 to 20.00. The τ_{em} values asymptotically approach the chromophore's documented 600 ns emission lifetime in degassed bulk water at higher W_0 values (Figure 2. 7, Table II. 3).[38] Even the PERMC of smallest W_0, **C1-1.00**, with a τ_{em} of 1.2 μs, better approximates lifetimes consistent with bulk solution-like environments.[38]

The spectroscopic results of the **C1** series contained in this report are different than those previously disseminated for water-based PERMCs in two respects.[11] First, in the previous study, the sequestered chromophores' emission maxima shift by only 6 nm across the investigated W_0 range of 1.00 to 20.00.[11] Second, the PERMC τ_{em} values do not attain the smaller bulk solution-scale chromophore emission lifetimes of 600 ns at higher W_0 values.[11] To explain, there was one key difference between the previous experimenter's (S. A. Sapp) and the current author's (J. Kremer) experimental procedure. The previous experimenter purged the CPRMSs with dry nitrogen for a longer time than the author did. Extensive dry nitrogen purging will decrease the W_0 of the resulting CPRMSs, because the liquid↔vapor water equilibrium shifts towards vapor. Consequently, the observed τ_{em} values will increase. An ^1H NMR experiment was devised to determine the extent of water loss upon CPRMS dry nitrogen purging. The water content is substantially decreased upon dry nitrogen purging for greater than four minutes (Figure 2. 8) In all, the **C1** PERMC series reported herein most accurately reflects the true nature of the chemical environment about the sequestered chromophores.

Characterization of the C2 Series. There are key differences in the dielectric constants and W_0 values of PERMC series **C1** and **C2** employing water and acetonitrile polar phases, respectively. Acetonitrile has a dielectric constant of 37.5 which is approximately half that of water.[18] Therefore, the electrostatic interactions between the sequestered chromophore and the anionic wall will be stronger in the **C2** PERMC series. Despite being equivolume in polar phase to **C1**, the **C2** PERMC series only has a W_0 range of 0.34 to 6.88 (Table II. 3). No **C2** series PERMCs with W_0 values greater than of 6.88 can be reproducibly made because of the poor PERMC optical quality. There is either incomplete micellar formation or micellar aggregation at such large W_0 values.

Micellar radii for the **S2** CPRMS series are independent of W_0 and dependent on polar phase (between acetonitrile and water) (Table II. 3). The radii of the **C2** reverse micelles should be larger than the **C1** reverse micelles since acetonitrile is larger than water. Yet, the average radii of **C2** series at 25.0 °C are ca. 0.6 nm less than the **C1** series micellar radii at like polar phase volumes (i.e. **C1-3.44** and **C2-6.88**). In conclusion, the AOT micelles sequester the chromophore and only a fraction of the acetonitrile polar phase. According to Ritzoulis and coworkers, acetonitrile and toluene form binary mixtures of any molar ratio.[39] Thus, a portion of the acetonitrile polar phase is partitioned into the styrene:divinylbenzene nonpolar phase. Consequently, the DLS readings are smaller for the **S2** series than the **S1** series. Even so, the obtained micellar sizes from DLS studies on the **C2** CPRMSs series are larger than those of empty AOT micelles in isooctane nonpolar phases which have radii of 1.8 to 2.0 nm.[40] Polydispersities on the order of 65 % of the measured radii are explained by the non-double occupancy of sequestered chromophores within micelles and micellar spherical deformation arising from the interactions between the chromophore and surfactant species, vide supra. The micelles are still intact (i.e. micellar radii are able to be measured) in the **S2-5.00** CPRMS at the polymerization temperature of 37.0 °C (Figure 2. 5B).

In brief, there is an alternate explanation which can explain the DLS data. The amount of acetonitrile that partitions into the reverse micelles might simply be a function of how much water is present in the wet AOT and whether there is a chromophore sequestered in that particular micelle to facilitate solvent partitioning.

Differing opinions have been offered regarding AOT reverse micellar solutions of acetonitrile polar phases. Levinger and coworkers characterized isooctane/AOT/ acetonitrile reverse micellar systems.[41] Yet, Wallen and coworkers have concluded that acetonitrile partitions into the nonpolar isooctane phase of AOT reverse micelles from nuclear magnetic resonance studies.[42] In this work, at least those micelles containing a chromophore in the **C2** PERMC series are postulated to sequester acetonitrile to a greater degree than in the systems studied by Levinger and coworkers and Wallen and coworkers. The chromophore and its solvation sphere were not components in the systems studied by Levinger and coworkers and Wallen and coworkers

The static emission characterizations of the chromophores sequestered in the fluid nanoscopic domains of the **C2** PERMC series are somewhat different than those of **C1**. The only similarity that holds is that broad emission maxima are present for all **C2** series PERMCs (Figure 2. 6B, Table II. 3). The first difference in emission behavior between the **C1** and **C2** series lies in the λ_{em} values of the **C2** series only showing a bathochromic shift of 6.0 nm over the same polar phase volume injection range of 1.0 to 36.0 μL. Acetonitrile cannot solvate the chromophores' bipyridine ligands out of the hydrophobic Stern layer to the extent that water can. Therefore, the chromophore structures acetonitrile to a lesser extent (i.e. the bathochromic shift is smaller), because the chromophore is embedded in the micelle to a greater extent. Alternatively, the smaller bathochromic shift may be due to the W_0 range is smaller for the **C2** series.

The $[Ru(bpy)_3]Cl_2$ τ_{em} values in the **C2** series underpin the above static emission studies. The τ_{em} values of the sequestered chromophores are 1.2 μs across the same polar phase injection range, albeit ca. 25 % of the **C1** series W_0 range. (Figure 2. 7, Table II. 3). A compromised bulk solution-like chemical environment is present about the sequestered chromophore irrespective of the W_0 value. Still, the experimentally-obtained τ_{em} values are only two times greater than that of the dye in bulk acetonitrile, as compared to five times less than that of the chromophore's emission lifetime when frozen in a glass. The results of the time-resolved emission studies on the **C2** series agree with previous characterizations performed by Sakhar and coworkers[13-16] In these accounts, AOT reverse micelles of acetonitrile polar phases have much slower solvent dynamics with respect to micelles of aqueous polar phases and bulk acetonitrile. In general, there is no W_0 dependence for reverse micelles of acetonitrile polar phases, because of the lack of hydrogen bonding between the solvent and the AOT sulfonate head groups.[13-16]

In conclusion, only a compromised fluid environment can be achieved upon using PERMC polar phases of lower dielectric constants. The electrostatic and hydrophobic interactions of the chromophore take precedence in polar phases of lower dielectric constants. Another difficulty encountered is the incomplete sequestration of nonaqueous polar phases into the reverse micelle (DLS results). Even worse, acetonitrile is a common solvent for radical reactions. Even so, such lower dielectric constants can facilitate the partitioning of slightly polar species such as coumarin dyes. Thus, acetonitrile polar phase PERMCs are not entirely without merit.

Characterization of the C3 Series. As with the **C2** composite series, there are differences in the dielectric constants and W_0 values of composites series **C1** and **C3** which employ water and methanol polar phases, respectively. Methanol has a dielectric constant of 32.5.[18] In a similar fashion to the **C2** series, the electrostatic interactions between the cationic chromophore and the anionic micellar wall will be greater in the **C3** than in the **C1** PERMC series. The W_0 values of the **C3** series composites, although corresponding to the equivolume polar phases of 1.8, 9.0, 18.0, 27.0, and 36.0 μL, are not the same as the W_0 values of either the **C1** or **C2** series (Table II. 3). No **C3** series PERMCs with W_0 values greater than 12 are optically clear. Micellar radii for the CPRMS **S3** series are dependent on polar phase and independent of W_0 (Figure 2. 5C). Arguments offered for the **C2** series apply to the **C3** series.

The emission of the **C3** PERMC series follows that of the **C2** composite series, given the similar dielectric constants of the respective methanol and acetonitrile polar phases. The emission maxima of the **C3** series show a single broad band which is indicative of a solution environment about the sequestered chromophore (Figure 2. 6C, Table II. 3).[35] The collective λ_{em} values of the sequestered chromophores in the **C3** composite series show a bathochromic shift of 7.0 nm. Methanol is structured to a lesser degree by the chromophore and AOT species than water.

The $[Ru(bpy)_3]Cl_2$ τ_{em} values in the **C3** series corroborate the above static emission studies. The τ_{em} values of the sequestered chromophores within the nanoscopic-sized fluid methanol domains hold constant at ca. 1.20 μs across W_0 range (Figure 2. 7, Table II. 3). Note, the sequestered chromophores' emission lifetimes are still only ca. two times greater than that of the chromophore's emission lifetime in bulk methanol. In conclusion, methanol can be employed out of necessity as the PERMC of polar phase choice to counter polar probe solubility problems.

Characterization of the Increase in Sequestered Chromophore Emission Lifetime Throughout the CPRMS Nonpolar Phase Polymerization. During the CPRMS polymerizations of **S1-1.00** and **S2-0.34**, the increase in the $[Ru(bpy)_3]Cl_2$ τ_{em} values was determined as a function of the nonpolar phase physical state (i.e. viscous solution, gel). Such changes are ultimately dependent on the CPRMS nonpolar phase polymerization time (t_p). The **S1-1.00** and **S2-0.34** CPRMSs were chosen for this study because the corresponding PERMCs exhibited the largest increase in the respective sequestered chromophore τ_{em} values. Starting from τ_{em} values of 534 and 683 ns for chromophore-sequestered CPRMSs **S1-1.00** and **S2-0.34**, the lifetimes nearly double before asymptotically approaching values of 1.26 and 1.20 μs, respectively (Figure 2. 9).

The most marked increase in τ_{em} values occurs once a stiff gel is formed. This experimental observation arises from the loss of micellar translation which decreases the degrees of freedom of the sequestered chromophores. The magnitude of the electrostatic and hydrophobic interactions between the chromophore and the surfactant wall are less substantial for a CPRMS than for those where the micelle and its component surfactants are permanently immobilized in a polymer. Micellar translation slows once the CPRMS nonpolar phase hardens thereby locking the chromophore into such motion-restricting electrostatic and hydrophobic interactions. The efficiency of the MLCT's solvent-induced relaxation mechanism decreases, and consequently the τ_{em} increases. Such emission lifetime dependencies on the physical state of the chemical environment have been demonstrated for many other systems, as well. Demas and coworkers have determined that both the decrease in the ^{3}MLCT excited state deactivation rate and the decrease in the nonradiative pathway rate consequently cause emission lifetimes of tris(bipyridyl)ruthenium(II) species to increase upon micellization.[43]

Scanning Electron Microscopy (SEM). Efforts were made to image the reverse micellar imprints to ensure that reverse micelles are intact within the PERMCs. One hundred nanometer-thick microtomed PERMCs were examined by SEM in an effort to reproduce the surface features reported by Menger and coworkers,[6] Unfortunately, no pore structure, on the order of 10 nm diameters (as indicated by DLS studies of CPRMSs) (Figure 2. 10A) was resolved. Moreover, SEM techniques provide information over the entire sample thickness, instead of just the surface.[44] In addition, the technique gives no information on pore connectivity.[45] Regardless, the PERMCs were likely damaged by the vacuum and the 1.2 kV accelerating electron gun voltage.

Tapping-Mode Atomic Force Microscopy (TM-AFM). Surface analysis TM-AFM was used to image two samples: poly(styrene-*co*-divinylbenzene) (**Cut I**) and a composite made from the nonpolar phase polymerization of 50.00 mM AOT in 2.00 mL styrene:divinylbenzene to which 18.0 μL of 20.00 mM tris(bipyridine)ruthenium(II) chloride ($[Ru(bpy)_3]Cl_2$) chromophore was added corresponding to a W_0 of ten (**Cut II**). The TM-AFM method causes less sample damage and only images surface features.

Both **Cut I** and **Cut II** were prepared for TM-AFM analysis by established cryo-cutting techniques.[46-47] A photograph of the cryo-cut samples is presented showing the surface features of the samples (Figure 2. 11). This work is the first to report TM-AFM imaging of polymer encapsulated reverse micellar composites retaining micellar imprints.

The TM-AFM height and phase images of **Cut I** reflect the polymer morphology. The 30 nm relief exhibited by the corresponding cryo-cut **Cut I** is on the order of previously reported samples (Figure 2. 12A).[48] The highly-crosslinked regions of the copolymer are also of higher relief than the polystyrene-rich domains because the former have more crosslinks (bonds) into the sample base. It is harder to force the mechanical cleavage of these branch points. Moreover, the thermosets are spaced on average 30 nm apart in the phase image. This distance directly corresponds to reported height relief scale of **Cut I**.

A phase image, which measures oscillating tip energy dissipation, $\Delta\phi$, was collected on **Cut I**. The variation in $\Delta\phi$ is indicates differences in polymer morphology over a sample surface.[49] In **Cut I**, such morphology disparities are due to the preferential polymerization of divinylbenzene from the nonpolar phase before that of styrene, according to the respective 2.60 and 1.18 reactivity ratios.[50-51] Such preferential copolymerization generates harder, thermoset branch points attributable to highly-crosslinked regions that appear as darker regions in the phase image. These regions dissipate less oscillating tip energy. The branch point image regions contrast with the softer, more energy-dissipating, polystyrene-rich domains that appear lighter in color.[52] It is unlikely that surface tension effects are responsible for the phase image patterns observed, because there is no substantial difference in surface tension between liquid styrene and divinylbenzene (they are miscible).[53]

Successive TM-AFM images were obtained at different scan rates and at different areas of **Cut I** as well as on duplicates. All images had consistent features. The height and phase images are also provided for a 1 x 1 μm dimension for **Cut I** to demonstrate that the image qualities hold throughout a larger scanned area (Figure 2. 13).

The height TM-AFM image of **Cut II** is markedly than **Cut I**. The former has a height relief scale of only 5.0 nm (Figure 2. 12B). The height image of **Cut II** exhibits imprints of reverse micelles that appear as dark holes randomly spaced throughout the image. The presence of polymer encapsulated reverse micelles is responsible for the markedly different height relief scales. The applied cryo-cut force causes fractures along a so-called micellar plane, or a 'micelle-to-micelle' cleavage plane, wherein encapsulated micelles hemispherically rupture upon impact giving rise to the height scales of **Cut II** (Figure 2. 14). There are two reasons why such fracture dynamics hold. First, the frozen fluid sequestered inside reverse micelles is anticipated to be of lower mechanical strength than the nonpolar phase network polymer. Second, to the extent that water within the micelles behaves as bulk water, it should expand upon freezing and stress of the surrounding polymeric nonpolar phase. Consequently, the micelles should be the first to fracture upon cryo-cut impact. Imprint depressions on the order of 0.5 nm are reported, rather than median expected depression depth of 2.0 nm, according to DLS measurements performed at 37.0 °C. This discrepancy is due to the large curvature radius of the tapping silicon tip (on the order of 15 nm); it is not possible to entirely fit the tip into any one imprint to record larger hole depths. The nature of the polymer-surfactant interface may also be responsible for the aspherical shape of the indentations in addition to micellar polydispersity contributions, tip artifacts, non-hemispherical cleavage of encapsulated micelles.[45] Finally, the imprints are not likely derived from shards of polymer that were shattered and ejected during the cryo-cut impact, since such types of indentations would be more irregularly-shaped. The height and phase images are also provided for a 1 x 1 μm dimension for **Cut II** to demonstrate that the image qualities hold throughout a larger scanned area (Figure 2. 13).

The phase TM-AFM image of **Cut II** is also markedly different from that observed for the cryo-cut image of PERMC **Cut I**. The phase image of **Cut II** shows only a one degree difference over the entire surface area (Figure 2. 12B) indicating that the entire surface dissipates tip energy uniformly. The exposed surface has the same surface morphology throughout the entire scanned area because the cryo-cut plane in **Cut I** is determined by the cleaved micelles and not by differences in polymer morphology, Such uniform morphologies correlate to negligible phase differences in TM-AFM. Quantitative root mean square analysis of depression depths is provided (Figure 2. 15).

Stress-strain Tensometry. Tensometry experiments were performed on three different samples. Sample **I** is poly(styrene-*co*-divinylbenzene) made from a 25 % divinylbenzene solution. Sample **II** consists of the same polymer, but with 50.00 mM of wet AOT dispersed in it. Sample **III** is a PERMC composed of 9.0 μL of a 20.00 mM water stock solution of $[Ru(bpy)_3]Cl_2$ sequestered in the AOT reverse micellar polar phase with a W_0 of five. The tests do not conform to the ASTM D.683 specifications for plastics given the problems of the molded samples crazing during polymerization.[19]

Sample **I** behaves as a hard brittle plastic. A modest yield point is present upon the application of a 100 N load (Figure 2. 16). Beyond 100 N, the mechanical deformation is permanent as polymer chains disentangle and flow past each other. Further application of stress on amorphous copolymers will increase crystallinity by causing polymer chains to align with each other; therefore, the Young's modulus will increase upon stress application.[25] Such behavior is observed in the stress-strain curve of **I**, in that the slope is greater at load levels greater than the yield point load level.

Sample **II** is more susceptible to mechanical stress than sample **I**. At 410 N, the load exerted on **II** is sufficient to craze, or internally crack, it (Figure 2. 16). This crazing then deteriorates into more extensive cracking which ultimately breaks **II** at higher applied loads. The cracking occurs for **II** where it did not for **I** because the AOT used is wet. As such, the W_0 of **II** is not zero even though no polar phase was injected into the corresponding CPRMS. Thus, the micellar fluid regions inside the otherwise solid composite will stress in a different manner than atactic copolymer chains. The difference in the rates and mechanisms of mechanical expansion between the atactic chains and the micelles causes stresses inside the composite material. Yet, while the micelles cause premature fracturing of **II** compared to **I**, they also increase the Young's Modulus of **II** with respect to that of **I**. To explain, the change in sample length for the same force applied is smaller in **II** than in **I**. The micelles interfere in the disentangling of polymer chains after the yield point of 80 N has been attained.

The mechanical stress exhibited in **II** is amplified for **III**. There are several fracture points throughout the 500 N load range exerted on **III** at the following load levels: 115 N, 260 N, and 370 N (Figure 2. 16). Recall, the micelles in **III** were determined by elevated temperature DLS to have radii on the order of 4.0 nm, compared with 2.0 nm for empty micelles from wet surfactant molecules like those in **II**. The larger micelles in **III** cause more extensive mechanical stress. The maximum load of 500 N can never be exerted on **III** because it completely broke at 370 N.

The toughness of a composite is the area under the stress-strain curve. Although exact areas are not calculated, **III** has the greatest toughness. Thus, **III** is the one composite herein which can be bent and twist the most without breaking or tearing. Upon no applied load, the fluid micelles provide a cushioning device with respect to applied stress over finite periods of time. Those same stresses can quickly fracture such PERMCs like **III** if the load is not removed (Figure 2. 16). Thus, the material has a low fracture point but is still tough.

Conclusions.

Three series of tris(bipyridine)ruthenium(II) chloride $[Ru(bpy)_3]Cl_2$ chromophore-sequestered poly(styrene-*co*-divinylbenzene) encapsulated Aerosol-OT (AOT) reverse micelle composite materials were prepared. Such composites sequestering $[Ru(bpy)_3]Cl_2$ in water, acetonitrile, and methanol polar phases had variable W_0 values. These polar phases were used for the preparation of composite series **C1**, **C2**, and **C3**, respectively. Micelles for all composite series **C1**, **C2**, and **C3** were detected by DLS at the CPRMS nonpolar phase polymerization temperature. Emission spectroscopy results follow from the dielectric constants of the sequestered polar phases. Imaging of cryo-cut composites using TM-AFM analysis showed a micellar pore structure. Tensometry tests showed that PERMCs fracture at lower loads than polymers.

Chapter 2.

Tables

Table II. 1. Compositions of chromophore-sequestered PERMCs of aqueous and nonaqueous polar phases.

CPRMS[a]	Polar Phase[a]	$V_{\text{plr phase}}$ (μL)[a]	W_0[a]	PERMC[b]
S1-1.00	20.00 mM $Ru(bpy)_3Cl_2$ in H_2O	1.80	1.00	**C1-1.00**
S1-5.00	20.00 mM $Ru(bpy)_3Cl_2$ in H_2O	9.00	5.00	**C1-5.00**
S1-10.00	20.00 mM $Ru(bpy)_3Cl_2$ in H_2O	18.00	10.00	**C1-10.00**
S1-15.00	20.00 mM $Ru(bpy)_3Cl_2$ in H_2O	27.00	15.00	**C1-15.00**
S1-20.00	20.00 mM $Ru(bpy)_3Cl_2$ in H_2O	36.00	20.00	**C1-20.00**
S2-0.34	20.00 mM $Ru(bpy)_3Cl_2$ in CH_3CN	1.80	0.34	**C2-0.34**
S2-1.72	20.00 mM $Ru(bpy)_3Cl_2$ in CH_3CN	9.00	1.72	**C2-1.72**
S2-3.44	20.00 mM $Ru(bpy)_3Cl_2$ in CH_3CN	18.00	3.44	**C2-3.44**
S2-5.16	20.00 mM $Ru(bpy)_3Cl_2$ in CH_3CN	27.00	5.16	**C2-5.16**
S2-6.88	20.00 mM $Ru(bpy)_3Cl_2$ in CH_3CN	36.00	6.88	**C2-6.88**
S3-0.56	20.00 mM $Ru(bpy)_3Cl_2$ in CH_3OH	1.80	0.56	**C3-0.56**
S3-2.81	20.00 mM $Ru(bpy)_3Cl_2$ in CH_3OH	9.00	2.81	**C3-2.81**
S3-5.63	20.00 mM $Ru(bpy)_3Cl_2$ in CH_3OH	18.00	5.63	**C3-5.63**
S3-8.44	20.00 mM $Ru(bpy)_3Cl_2$ in CH_3OH	27.00	8.44	**C3-8.44**
S3-11.26	20.00 mM $Ru(bpy)_3Cl_2$ in CH_3OH	36.00	11.26	**C3-11.26**

(a) The W_0 varies for each PERMC of identical polar phase volume injection, because of the different 55.5, 19.1, and 24.7 mM concentrations of water, acetonitrile, and methanol, respectively. The corresponding expression used to obtain the polar phase solvent molarities is as follows: (ρ x 1000)/f.w.

(b) The surfactant concentration is 50.00 mM AOT. The initial (CPRMS) nonpolar phase is 2:1 styrene:divinylbenzene; the final (PERMC) nonpolar phase is poly(styrene-*co*-divinylbenzene). Such PERMCs were prepared by the addition of 1.0 wt. % ADPN radical initiator to the CPRMSs and the subsequent heating of the CPRMSs at 37.0 °C for ca. 96 hours.

Table II. 2. The calculated solubility of water in the nonpolar phase of the CPRMSs.

(a)

V_{plr} (μL)^{c}	m_{plr} (g)^{d}	$m_{(plr\ in\ nplr)}$ (g)^{e}	$V_{(plr\ in\ nplr)}$ (mL)^{d}	$V_{(plr\ in\ nplr)}$ (μL)	$V_{(plr\ remaining)}$ (μL)	W_0 corrected
1.8	1.8E-03	1.2E-06	1.2E-06	0.0012	1.8E+00	1.0
9.0	9.0E-03	5.9E-06	5.9E-06	0.0059	9.0E+00	5.0
18.0	1.80E-02	1.19E-05	1.19E-05	0.0119	1.80E+01	9.98
27.0	2.70E-02	1.78E-05	1.78E-05	0.0178	2.70E+01	15.0
36.0	3.60E-02	2.38E-05	2.38E-05	0.0238	3.60E+01	20.0

(b)

V_{plr} (μL)^{c}	m_{plr} (g)^{d}	$m_{(plr\ in\ nplr)}$ (g)^{e}	$V_{(plr\ in\ nplr)}$ (mL)^{d}	$V_{(plr\ in\ nplr)}$ (μL)	$V_{(plr\ remaining)}$ (μL)	W_0 corrected
1.8	1.800E-03	1.188E-06	1.188E-06	0.001188	1.799	0.9983
9.0	9.000E-03	5.940E-06	5.940E-06	0.005940	8.994	4.992
18.0	1.800E-02	1.188E-05	1.188E-05	0.01188	17.99	9.983
27.0	2.700E-02	1.782E-05	1.782E-05	0.01782	26.98	14.98
36.0	3.600E-02	2.376E-05	2.376E-05	0.02376	35.98	19.97

(a) Calculations performed with the correct number of significant figures.

(b) Calculations performed with an extra number of significant figures to show perturbations in W_0.

(c) Volumes correspond to the actual volumes of polar phase used to prepare CPRMSs corresponding to PERMCs **C1-1.00** through **C1-20.00** in the text (Table II. 1).

(d) Assuming that ρ_{H2O} is 1.0 g/mL.

(e) Assuming a 0.065 % solubility of water in styrene.[18] Acetonitrile and methanol are completely miscible with styrene.[43] Therefore, no such calculations are warranted.

Table II. 3. Characterizations of chromophore-sequestered PERMCs of aqueous and nonaqueous polar phases.

PERMC	Polar Phase	radius (nm)^a	σ (nm)^b	I_{em}(arb. units)^c	λ_{em} (nm)	τ_{em} (ns)
C1-1.00	H_2O	2.7	1.4	4.29E+06	592.0	1.15
C1-5.00	H_2O	2.8	0.9	1.16E+07	59605.0	0.78
C1-10.00	H_2O	3.4	0.6	1.37E+07	598.0	0.61
C1-15.00	H_2O	3.6	0.5	1.00E+07	599.0	0.60
C1-20.00	H_2O	3.6	2.1	9.36E+06	606.0	0.63
C2-0.34	CH_3CN	2.7	1.4	5.07E+07	591.0	1.24
C2-1.72	CH_3CN	2.6	1.1	1.26E+07	593.5	1.25
C2-3.44	CH_3CN	2.7	1.8	1.32E+07	596.5	1.15
C2-5.16	CH_3CN	3.1	0.6	1.70E+07	595.5	1.20
C2-6.88	CH_3CN	2.4	1.0	1.44E+07	597.0	1.15
C3-0.56	CH_3OH	2.3	1.0	3.91E+06	592.5	1.09
C3-2.81	CH_3OH	2.4	0.8	9.45E+06	591.5	1.30
C3-5.63	CH_3OH	2.6	1.2	1.40E+07	593.5	1.27
C3-8.44	CH_3OH	2.4	0.9	1.55E+07	594.0	1.20
C3-11.72	CH_3OH	2.6	0.7	1.25E+07	596.5	1.15

(a) Determined from DLS particle sizing measurements on corresponding CPRMSs at 25.0 °C. The values presented have been averaged over ten (or more) readings.

(b) One standard deviation unit of the reverse micellar radius. These values correspond to vertical error bars. The reported standard deviations have also been averaged over ten (or more) readings.

(c) Values are not absolute insomuch as the fluorescence intensities are dependent upon sample pathlength (thickness) which is irreproducible due to irreproducible PERMC placement in the fluorimeter.

(d) The linear regression factor corresponds to monoexponential decay fits of the time-resolved emission profiles.

Chapter 2.

Figures

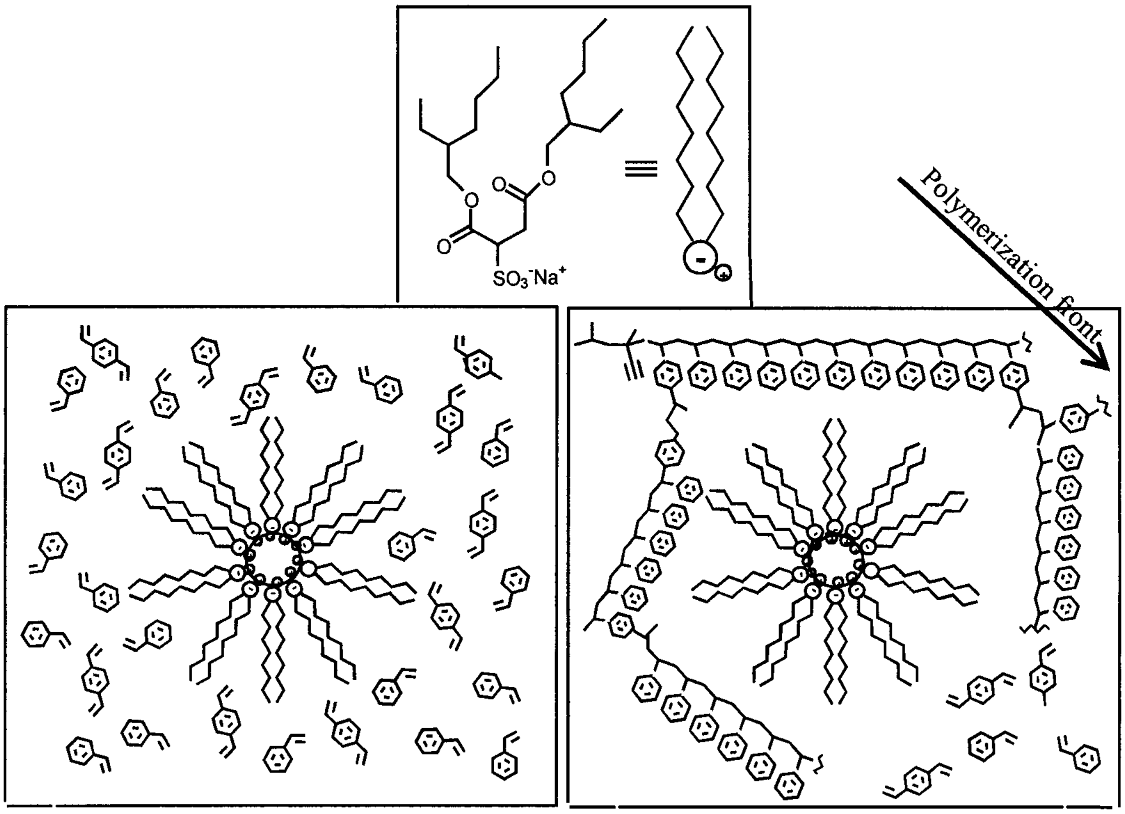

Figure 2. 1. Schematic cross-sectional representations of a composite precursor reverse micellar solution (CPRMS) at the bottom left and a polymer encapsulated reverse micelle composite material (PERMC) at the bottom right. The chemical structure of the Aerosol-OT (AOT) surfactant molecules composing the micelles in the CPRMSs and PERMCs is represented by the crosshatched drawing (upper center). The 2:1 styrene:divinylbenzene nonpolar phase of the CPRMS (bottom left) is polymerized after the addition of 2,2'-azobis(2,4-dimethylpentanenitrile) (ADPN) and subsequent sample heating to 37.0 °C for ca. 96 hrs. The polymerization front proceeds from northwest to southeast leaving the micelle(s) and the spherical (core) polar phases intact inside the PERMC (bottom right).

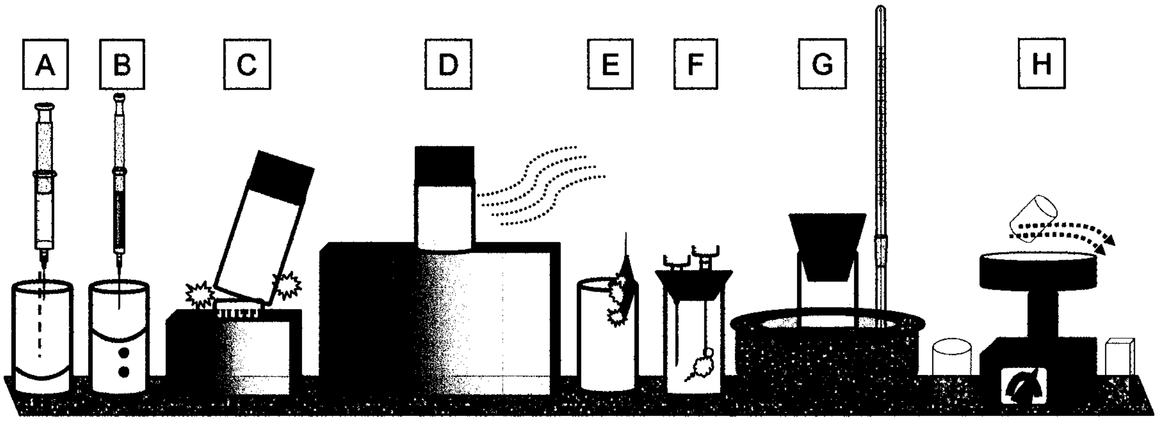

[Surfactant]	50.00 m$\underline{M}$ AOT
Nonpolar Phase	2.00 mL 2:1 styrene:divinylbenzene
[Molecular Sensor]	$\in$(1.0, 36.0) μL 20.00 m$\underline{M}$ $[Ru(bpy)_3]Cl_2$
Polar Phase	H_2O, CH_3CN, or CH_3OH
Mixing	Mechanical Agitation and Sonication
Polymerization Initiation	1 wt. % ADPN
Gas purging	N_2 for 5 minutes
Polymerization Conditions	$T_p = 37$ °C; $t_p = 96$ hrs
Nonpolar Phase Polymer	poly(styrene-*co* -divinylbenzene)

Figure 2. 2. A schematic diagram showing the steps necessary to prepare PERMC materials of Aerosol-OT surfactant systems. A 50.00 mM AOT solution in styrene:divinylbenzene nonpolar phase is charged into a glass vial (A). Microliter amounts of the polar phase (which can contain a polar dye such as $[Ru(bpy)_3]Cl_2$) are charged into the same glass vial (B). The CPRMS is agitated (C) and sonicated (D) to obtain an optically clear solution which is an indication of micellar formation. Approximately 1.0 wt. % of a solid radical initiator is added to the CPRMS (E). The CPRMS is sealed and purged with nitrogen (F). The CPRMS is placed in a 37.0 °C sand bath for 96 hours to prepare the corresponding PERMC (G). The PERMC is ground and polished into orthogonal dimensions amenable to spectroscopic analyses (H). The accompanying table recapitulates the amounts of each constituent and the preparation conditions.

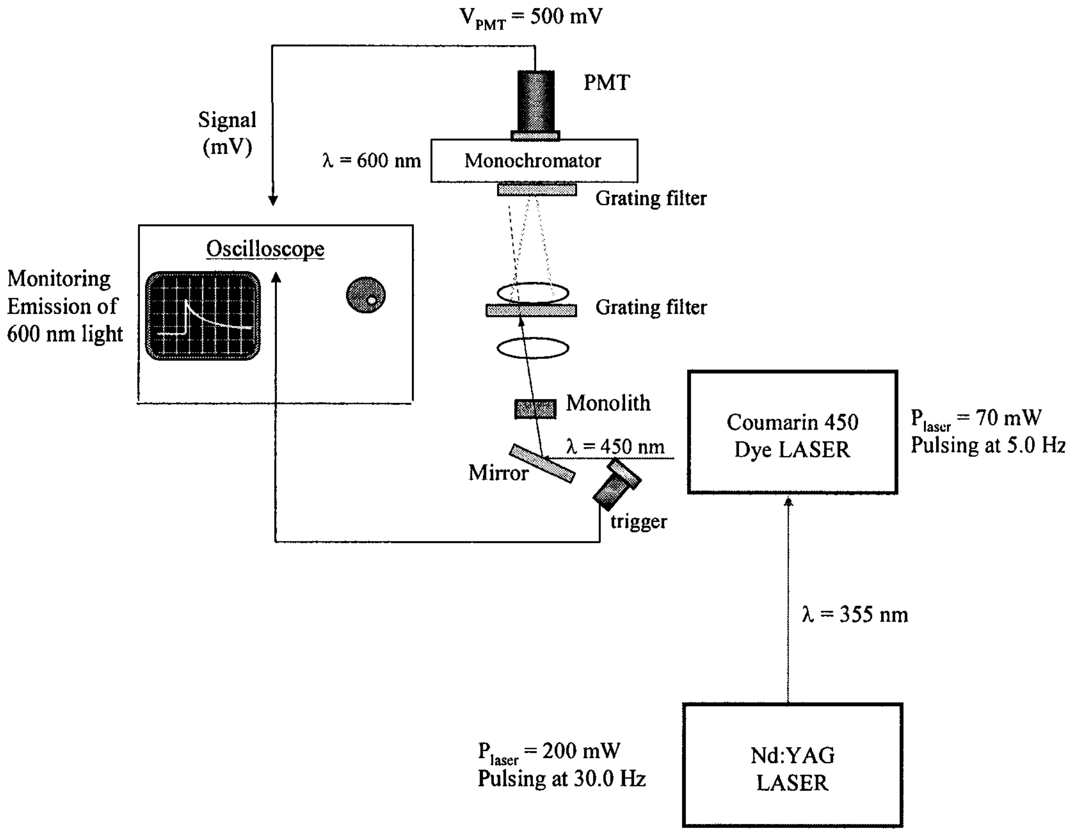

Figure 2. 3. Schematic diagram of the instrumental set-up for measuring fluorescence lifetimes using an Nd:YAG pumped dye laser for 450 nm $[Ru(bpy)_3]Cl_2$ MLCT excitation.

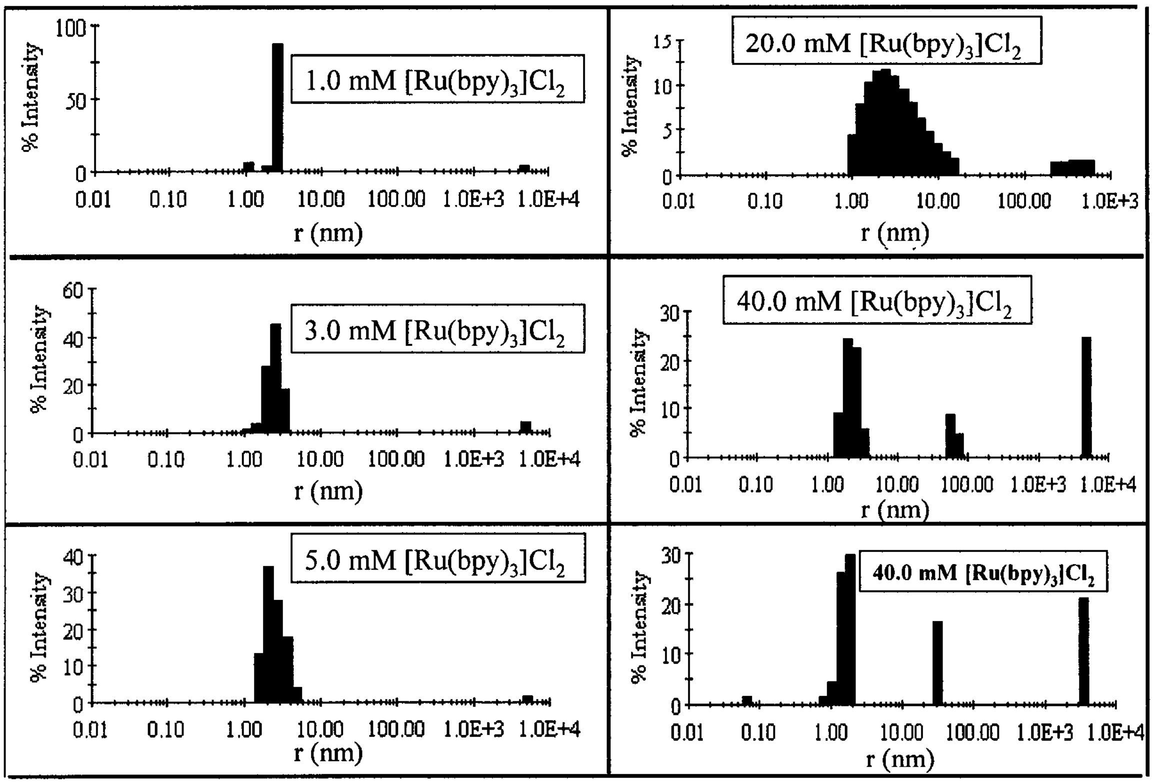

Figure 2. 4. The DLS measurements of tris(bipyridine)ruthenium(II) chloride ($[Ru(bpy)_3]Cl_2$) chromophore-sequestered CPRMSs of water polar phases and variable chromophore concentrations ([chromophore]). Both the reverse micellar size and polydispersity increase as [chromophore] increases. The results demonstrate the interdependence of micellar size polydispersity on the percent occupancy of the chromophore in the reverse micelles.

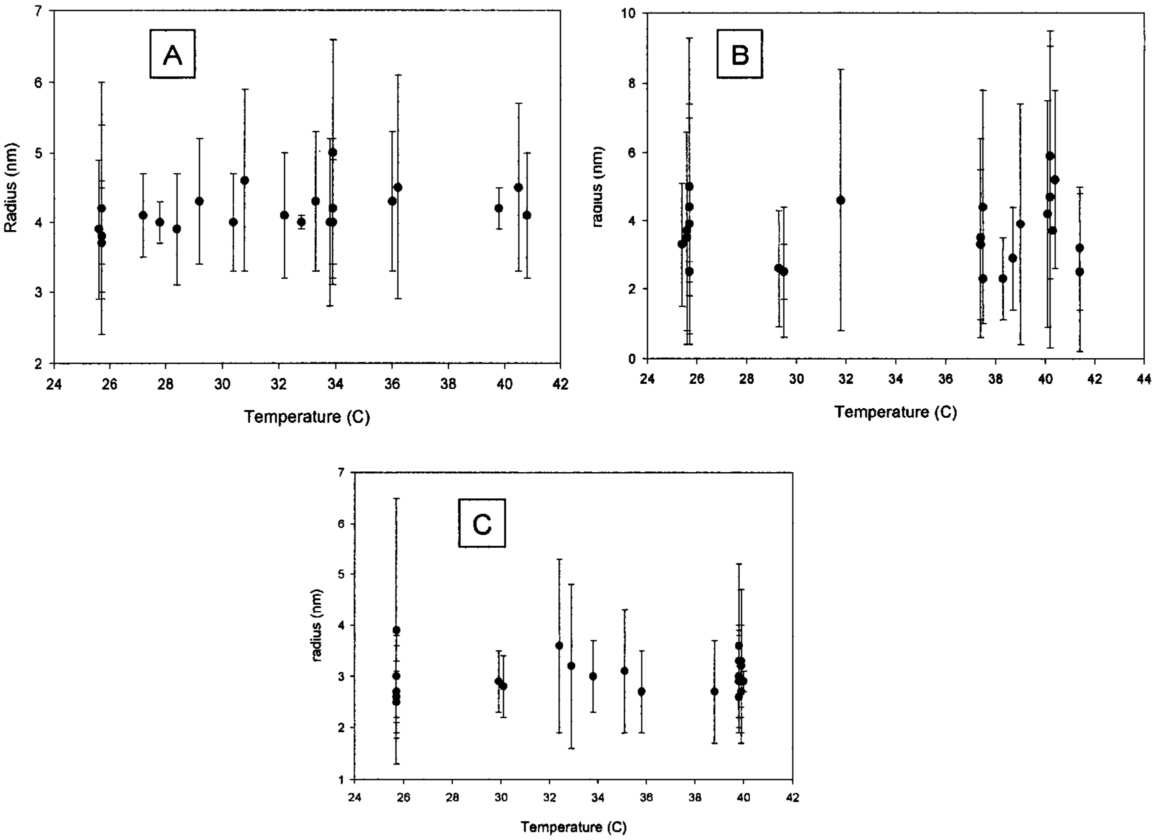

Figure 2. 5. Temperature-dependent DLS particle sizing analysis on tris(bipyridine)ruthenium(II) chloride ([Ru(bpy)$_3$]Cl$_2$) chromophore-sequestered CPRMSs with different polar phases. Particle sizing results from the following CPRMS constitutions are presented: a water polar phase with a W$_0$ of 15.00 (A), an acetonitrile polar phase with a W$_0$ of 5.16 (B), and a methanol polar phase with a W$_0$ of 8.44 (C). Micelles remain intact at the CPRMS nonpolar phase polymerization temperature for all systems studied. This study is valuable because it is not sufficient just to minimally perform particle sizing measurements at 25 °C only and simply assume that the results obtained are applicable to all temperatures.

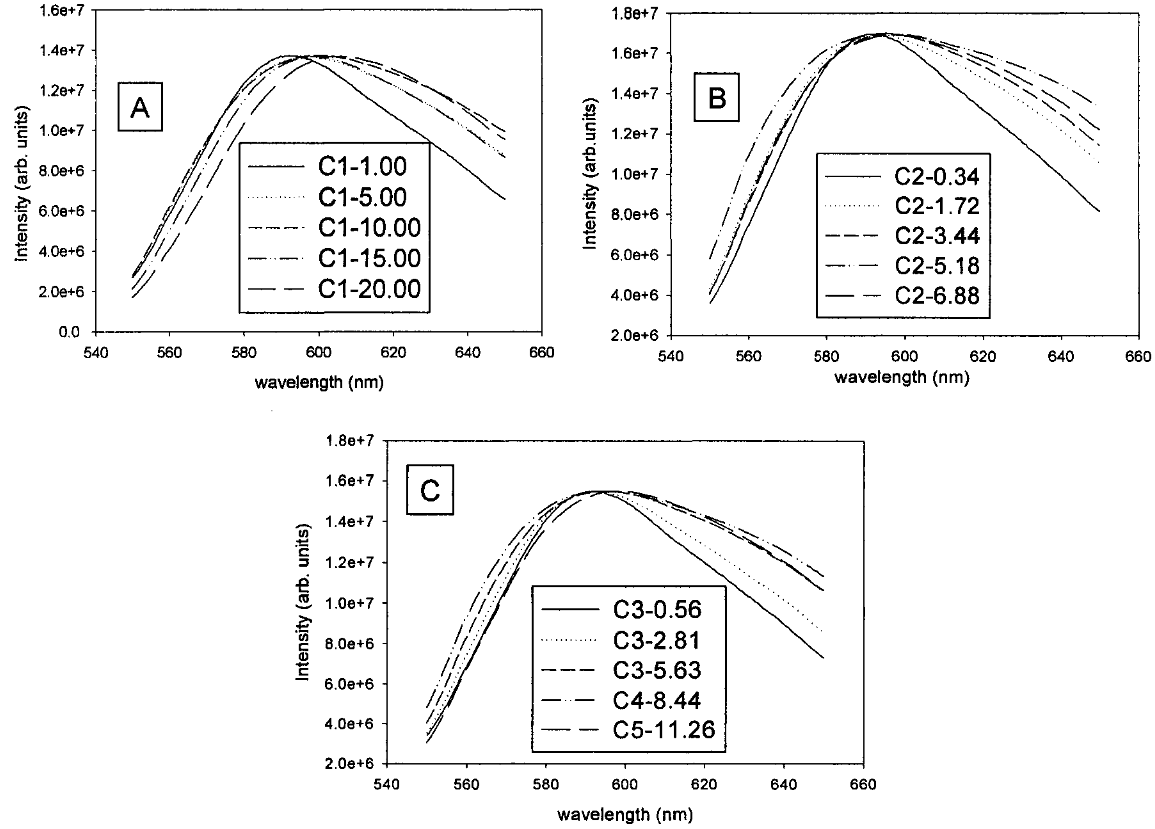

Figure 2. 6. Intensity-normalized static emission spectra of ($[Ru(bpy)_3]Cl_2$) chromophore-sequestered PERMCs of variable polar phases and W_0 values. Emission spectra of the following variable-W_0 PERMC series are presented: PERMCs of water polar phase (A), PERMCs of acetonitrile polar phase (B), and PERMCs of methanol polar phase (C). The emission spectra of PERMCs exhibit broad bands which indicate that the chromophore presides in a solution-like chemical environment.[35]

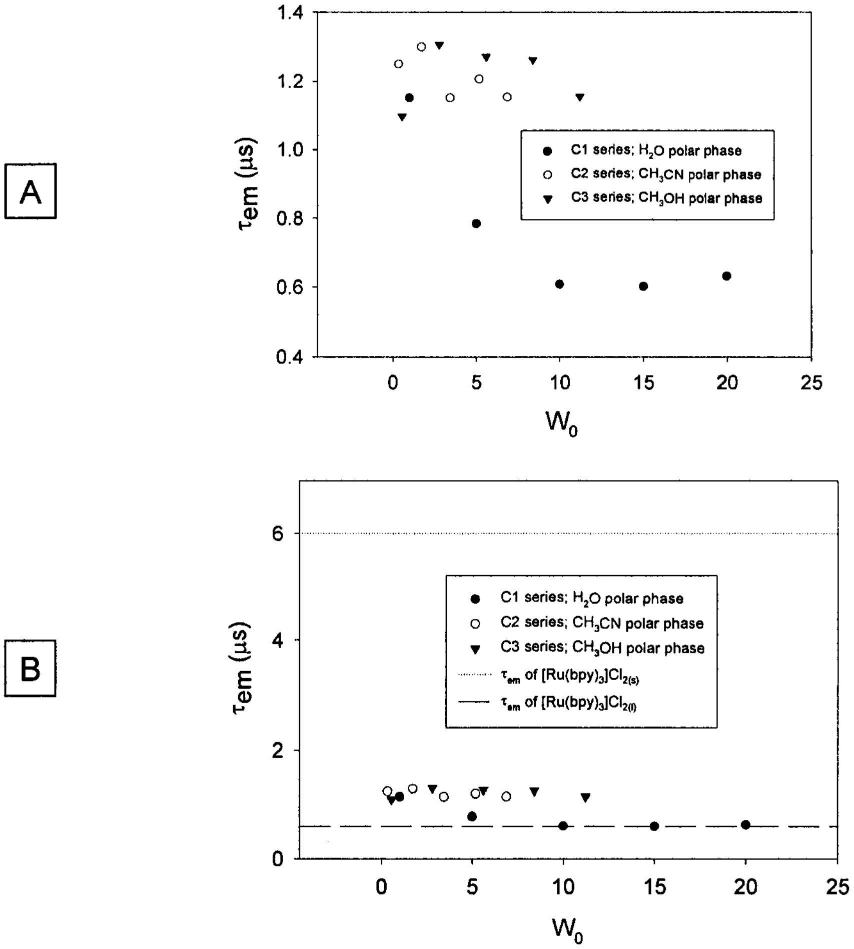

Figure 2. 7. Emission lifetimes (τ_{em}) of ($[Ru(bpy)_3]Cl_2$) chromophore-sequestered PERMCs of variable polar phases and W_0 values plotted versus W_0 (A). The same τ_{em} versus W_0 plotted data in (A) is represented in (B) with respect to the literature τ_{em} values of the $[Ru(bpy)_3]Cl_2$ chromophore in a degassed water solution (--- at 0.60 μs) and frozen in a glass (··· at 6.00 μs) (B).[38] Only **C1** series composites of large W_0 achieve $[Ru(bpy)_3]Cl_2$ τ_{em} values on the order of bulk degassed solutions. The $[Ru(bpy)_3]Cl_2$ chromophore-sequestered **C2** and **C3** composites maintain ca. 1.20 μs τ_{em} values irrespective of W_0. The lower dielectric acetonitrile and methanol polar phases are unable to solvate the sequestered chromophore out of the palisade layer of the reverse micelle in lieu of electrostatic and hydrophobic interactions between the cationic chromophore and the micellar anionic headgroups.

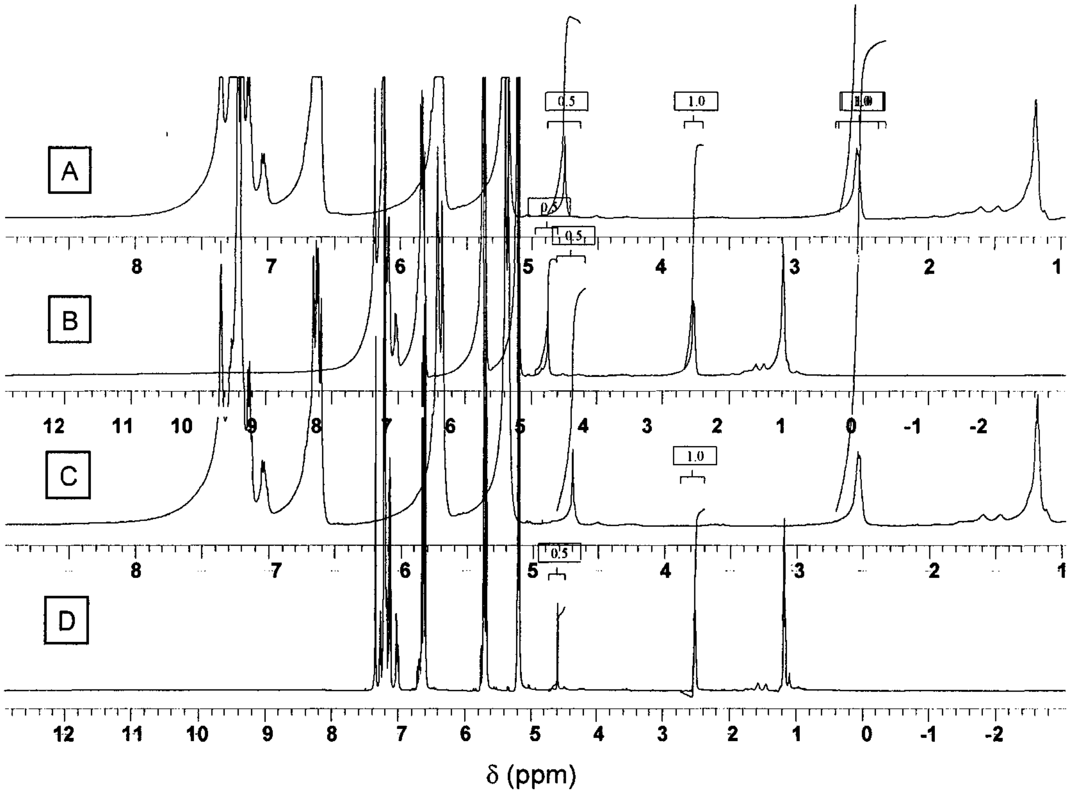

Figure 2. 8. X-axis staggered ^{1}H NMR spectra of a CPRMS composed of 2.00 mL of a 50.00 mM AOT solution in divinylbenzene and 27.0 μL of a 20.00 mM $[Ru(bpy)_3]Cl_2$ solution in water which was purged for 0 (A), 1 (B), 4 (C), and 8 (D) minutes with dry nitrogen. The water resonance at 4.8 ppm was integrated and compared against the surfactant at 2.5 ppm. No water is detected in the CPRMS that has been purged for eight minutes with dry nitrogen. The experiment demonstrates that purging CPRMSs with dry nitrogen lowers the effective W_0 of the resulting PERMCs. Such lower W_0 PERMCs of water polar phases are consistent with larger τ_{em} values (Figure 2. 7). Early samples (Sapp, S. A.; Elliott, C. M. *Chem. Mater.* **2003**, *15*, 1237-1241.) were purged for eight minutes. In stark contrast, the samples reported in this chapter were each purged for two minutes. The ^{1}H NMR spectra serve to explain the discrepancy between the emission data from the two sets of independent experiments. The data presented in this chapter more accurately describes the true τ_{em} trend with respect to W_0, because there is actually water present in the corresponding samples. The integrations are difficult to see because of the MestReC© fitting program which does not allow font changes.

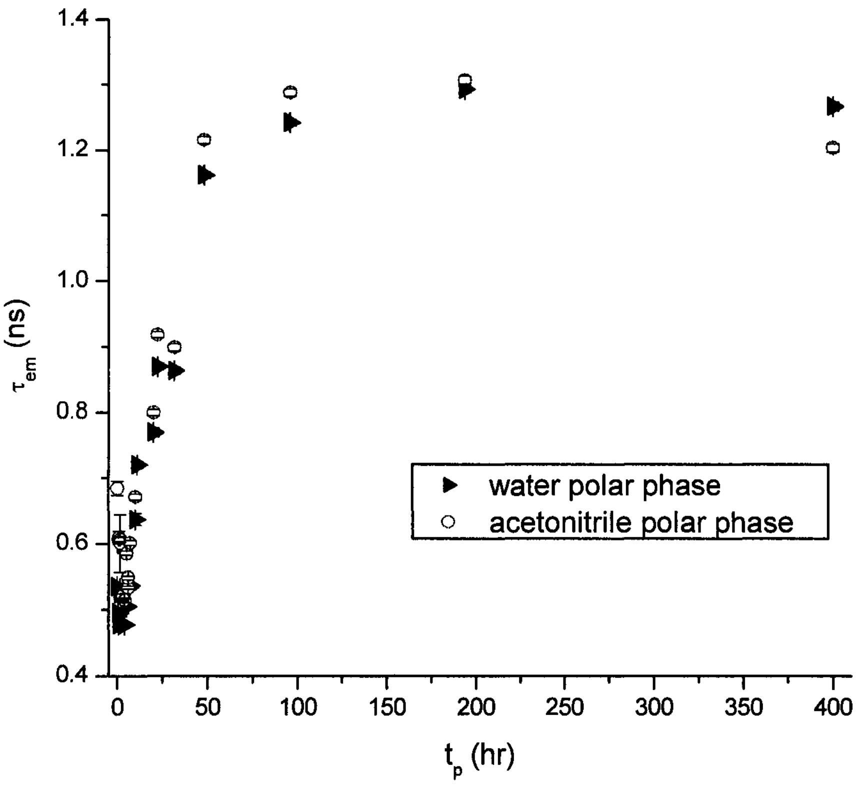

Figure 2. 9. Emission lifetimes of ([Ru(bpy)$_3$]Cl$_2$) chromophore-sequestered PERMCs **C1-1.00** and **C2-0.34** of water (►) and acetonitrile (○) polar phases, respectively, plotted versus the CPRMS nonpolar phase polymerization time (t_p). The increases in the τ_{em} values correspond to the hardening physical states of the nonpolar phase-polymerizing CPRMSs. The τ_{em} values markedly increase once a stiff gel is produced as a result of the ongoing CPRMS polymerization (at t_p ~ 7 hours) for reasons explained in the text.

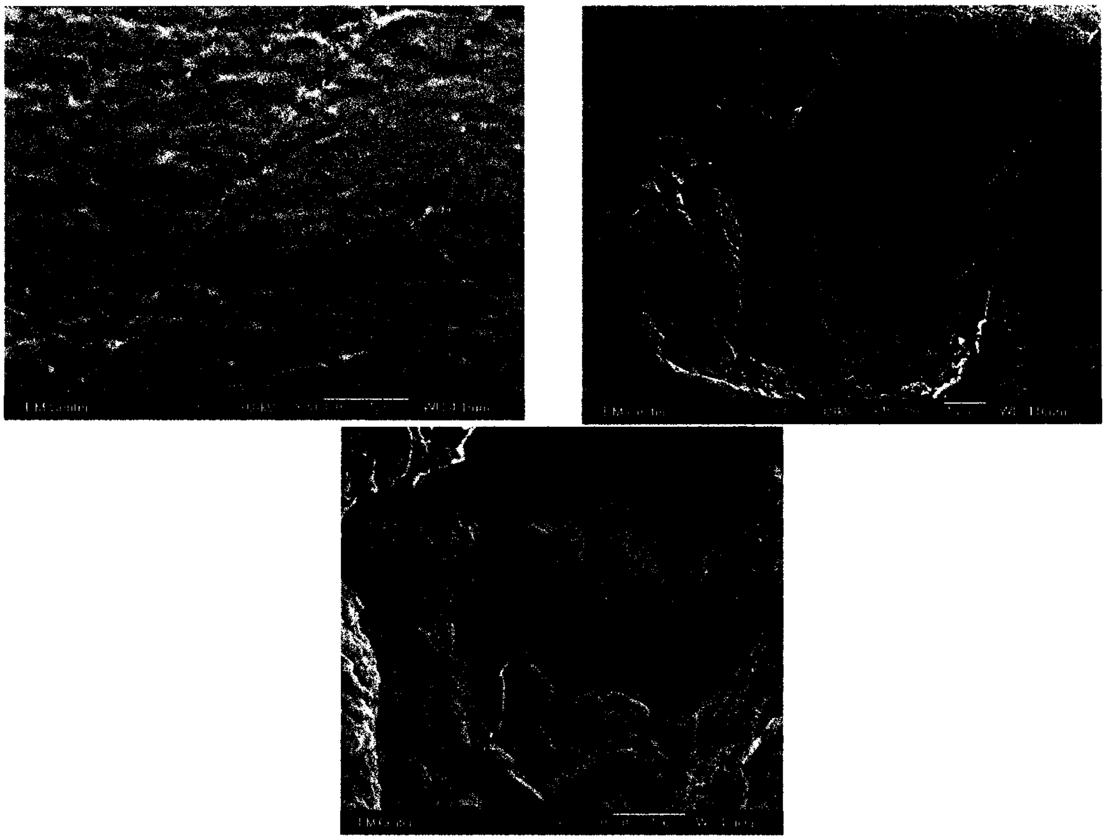

Figure 2. 10. Scanning Electron Microscopy (SEM) images of the unphysically-altered polymerization-hardened CPRMS menisci surfaces of poly(styrene-*co*-divinylbenzene) and a chromophore-sequestered PERMC. The Scanning Electron Microscopy images presented are as follows: poly(styrene-*co*-divinylbenzene) (A), a PERMC composed of poly(styrene-*co*-divinylbenzene)/50.00 mM AOT/9.0 μL of 20.00 mM $[Ru(bpy)_3]Cl_2$ with a W_0 of 1.72 (B), and an enlarged image of the 'burst bubble feature' on (B) which shows a porous morphology (C).

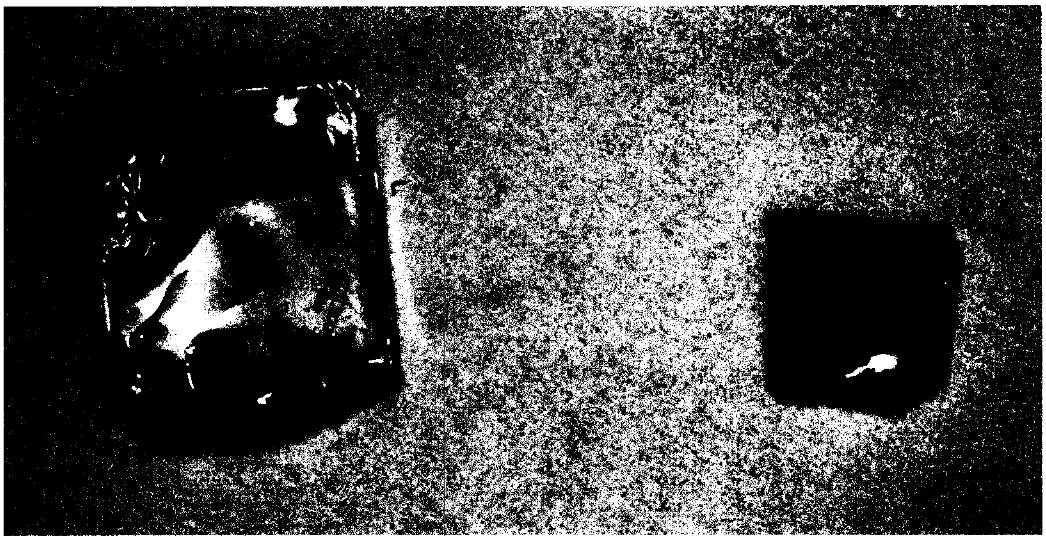

Sample	Nonpolar Phase	Polar Phase	[Surfactant]	W_0
Cut I	poly(styrene-co-divinylbenzene)	None	None	None
Cut II	poly(styrene-co-divinylbenzene)	9.0 µL $[Ru(bpy)_3]Cl_2$	50.0 mM AOT	5.0

Figure 2. 11. A digital picture of cryo-cut poly(styrene-*co*-divinylbenzene) (**Cut I**, left) and chromophore-sequestered PERMC (**Cut II**, right) analyzed by Tapping Mode-Atomic Force Microscopy (TM-AFM) surface analysis. The PERMC is orange because of the $[Ru(bpy)_3]Cl_2$ chromophores sequestered in the polar phase domains. The accompanying table recapitulates the difference between the two samples.

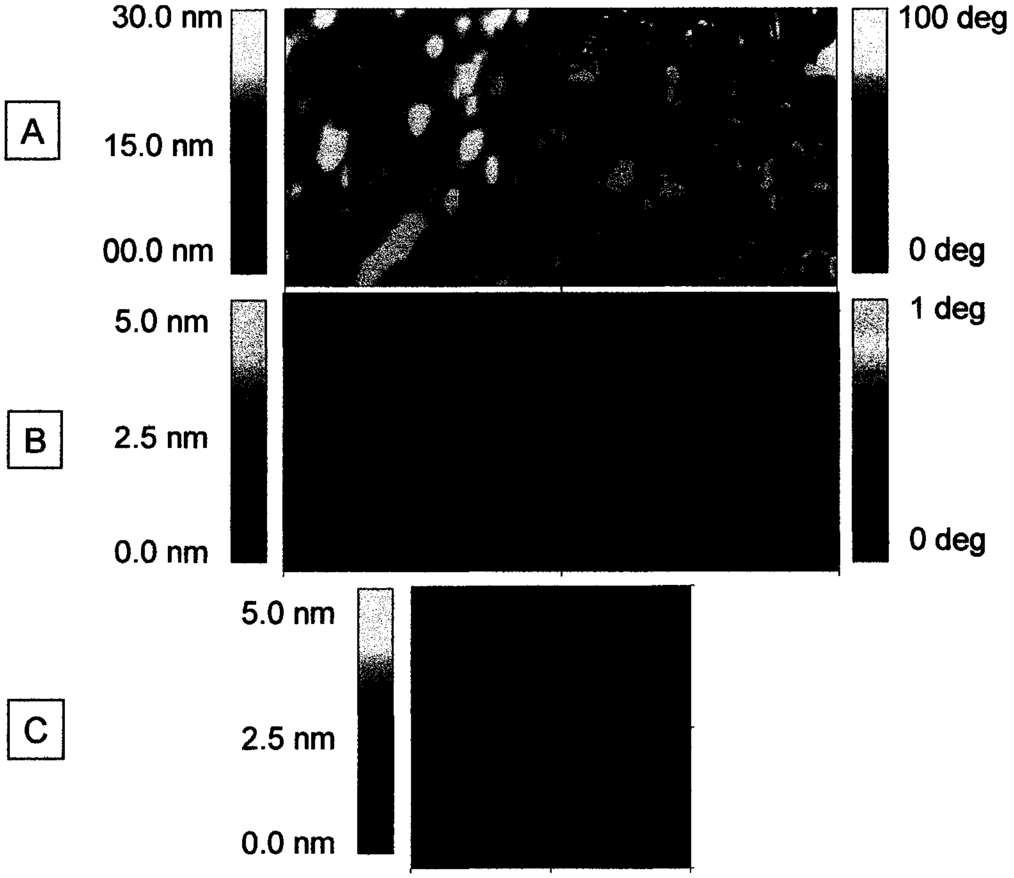

Figure 2. 12. Height and Phase TM-AFM images of cryo-cut poly(styrene-*co*-divinylbenzene) (**Cut I**) and a chromophore-sequestered PERMC (**Cut II**). The TM-AFM images presented are as follows: height (A-left) and phase (A-right) images of cryo-cut poly(styrene-*co*-divinylbenzene) **Cut I** over a (1000 x 1000)nm^2 area; height (B-left) and phase (B-right) images of a chromophore-sequestered PERMC over a (300 x 300)nm^2 area; and a height image of a sheet of mica with the exact same scale bar used for B. Regions of higher relief (and larger $\Delta\Phi$) are lighter in color (analogous to topographical map presentational conventions). The cryo-cut cleavage of **Cut I** is rougher than **Cut II** on both the height and phase images for reasons explained in the text.

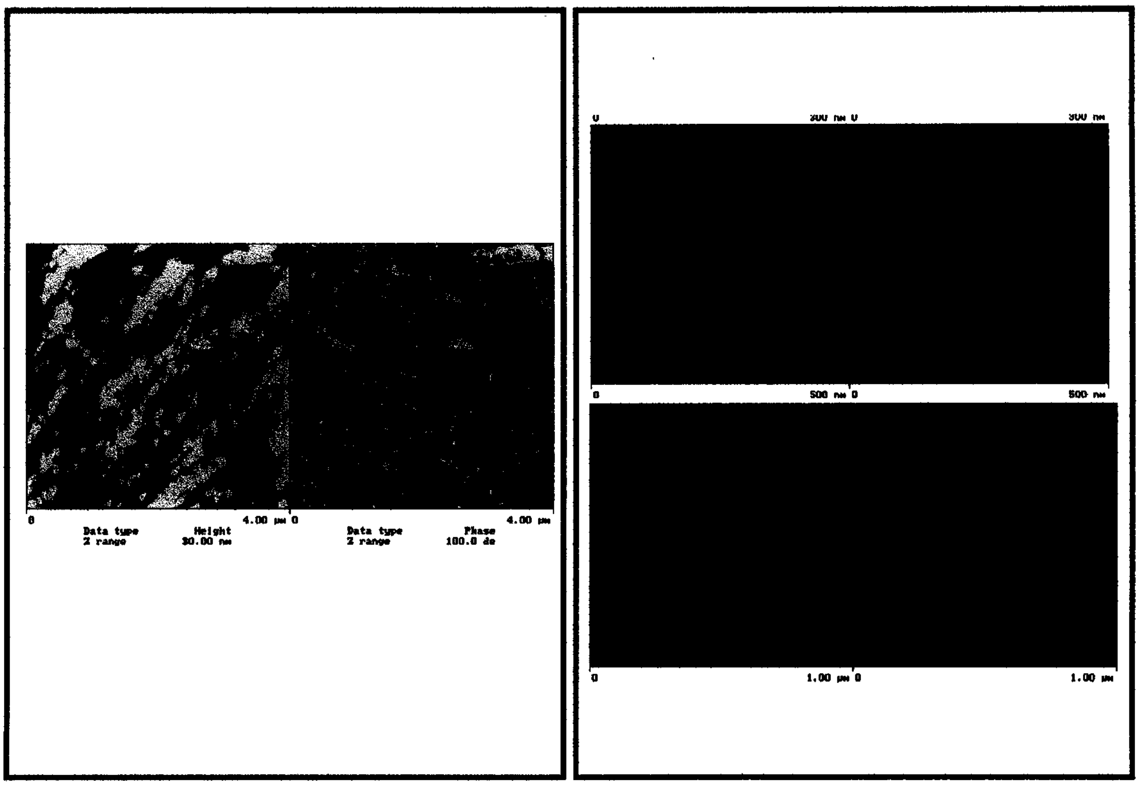

Figure 2. 13. Height and Phase TM-AFM images of cryo-cut poly(styrene-*co*-divinylbenzene) (**Cut I**) and a chromophore-sequestered PERMC (**Cut II**) scanned over larger areas to demonstrate sample uniformity. The TM-AFM images presented are as follows. On the left portal, height (left half) and phase (right half) image of **Cut I** over a (4000 x 4000)nm^2 area. On the right portal, height (left half) and phase (right half) images of **Cut II** over a (500 x 500)nm^2 (top), and a (1000 x 1000)nm^2 area (bottom).

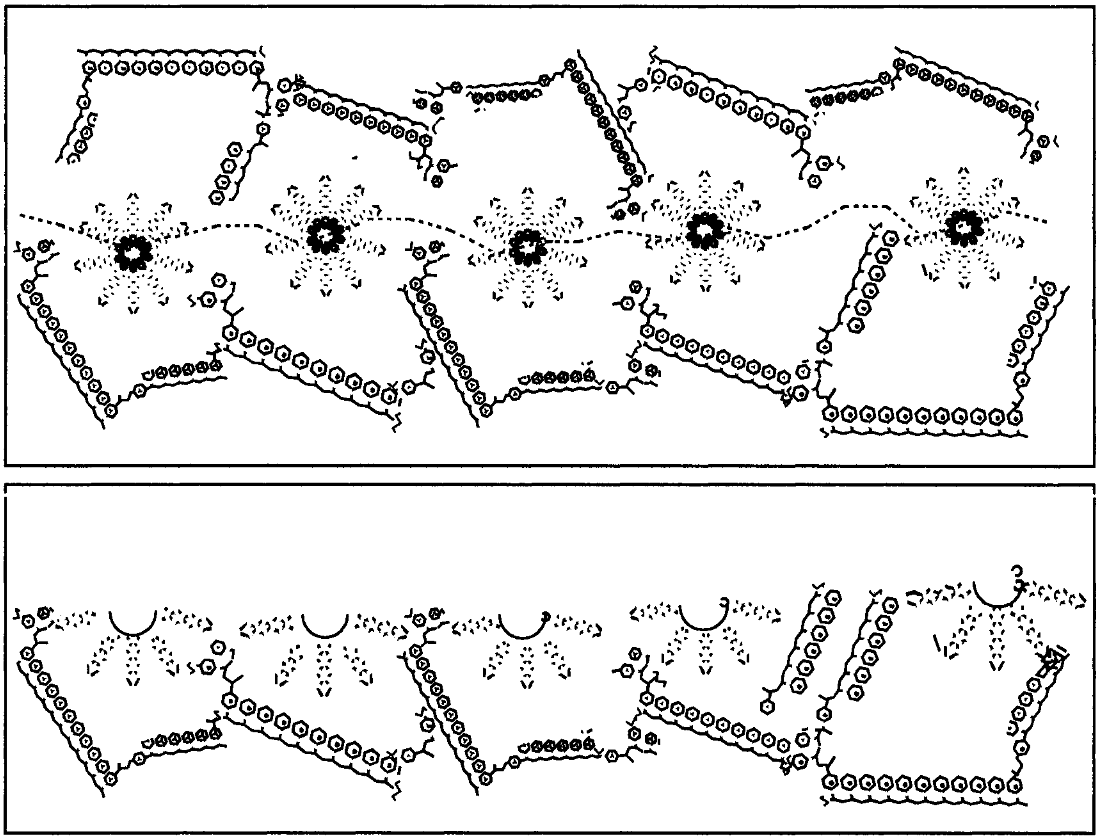

Figure 2. 14. Schematic representation of the postulated cryo-cut cleavage action in a PERMC material. In the top portal, a PERMC cross-section is presented (as in Figure 2. 1). In the bottom portal, a cross-section of the hypothesized cryo-cut surface is presented. The cyro-cut cleavage is believed to originate and fracture along the fluid micellar cores which are of lower mechanical strength than the surrounding polymer.

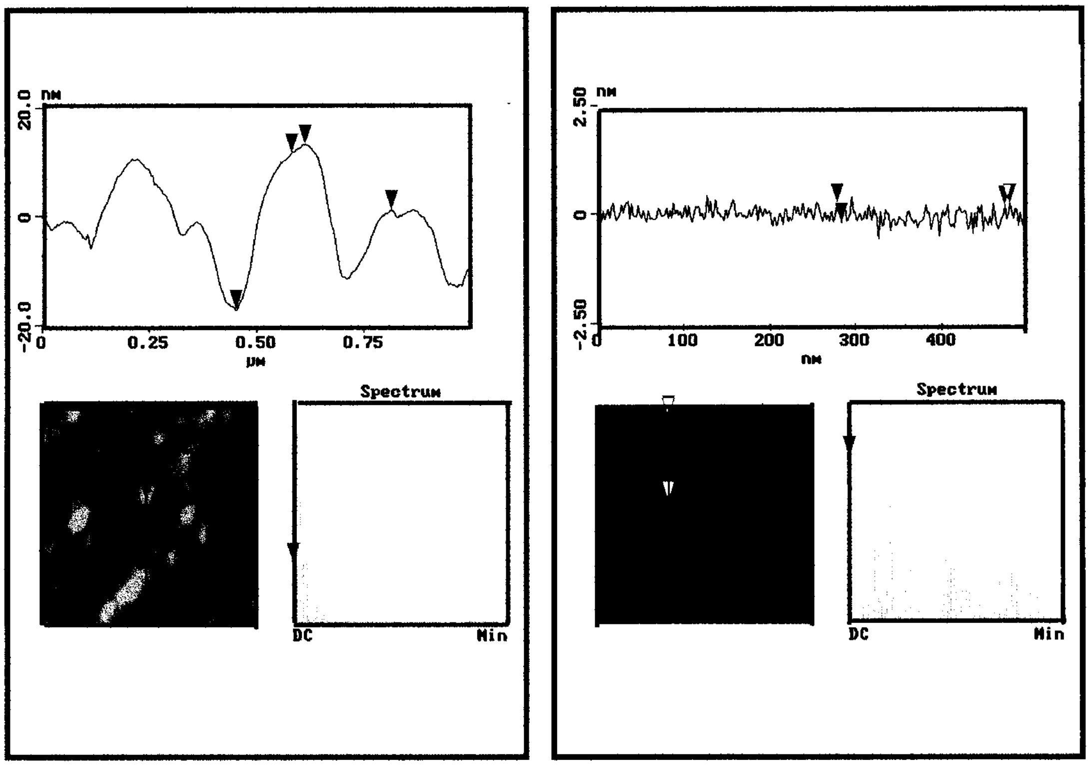

Figure 2. 15. Topographical traces (upper plot) and histograms (lower right plot) taken along a black line-vertical axis (to eliminate shearing effects) of cryo-cut poly(styrene-*co*-divinylbenzene) (**Cut I**) (left portal) and chromophore-sequestered PERMC (**Cut II**) (right portal) surface analysis samples. The original TM-AFM images are in the bottom left corner. The polymer has a rougher surface than the PERMC for reasons given in the text. The topographical traces plot height on the y-axis and the vertical length dimension on the x-axis.

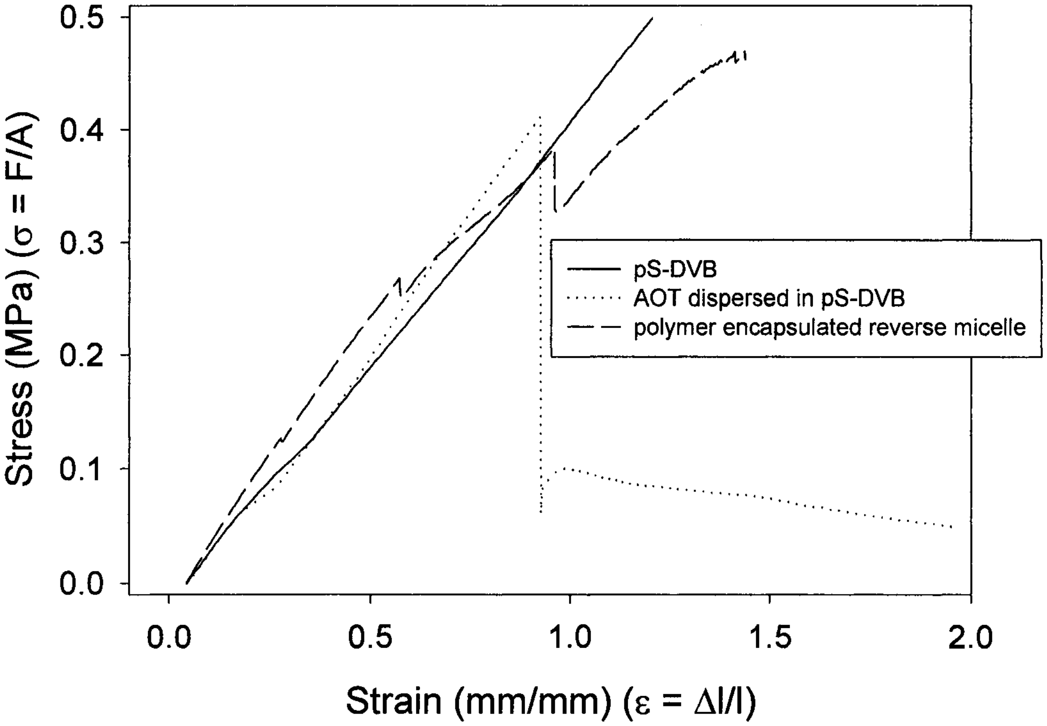

Sample	Nonpolar Phase	Polar Phase	[Surfactant]	W_0
I	poly(styrene-co-divinylbenzene)	None	None	None
II	poly(styrene-co-divinylbenzene)	0.0 μL $[Ru(bpy)_3]Cl_2$	50.0 mM AOT	0
III	poly(styrene-co-divinylbenzene)	9.0 μL $[Ru(bpy)_3]Cl_2$	50.0 mM AOT	5.0

Figure 2. 16. Stress-strain curves of poly(styrene-*co*-divinylbenzene) (**I**) (–), 50.00 mM AOT dispersed in poly(styrene-*co*-divinylbenzene) (**II**) (···), and a chromophore-sequestered PERMC (**III**) (---). The PERMC mechanically fractures at lower load levels for reasons explained in the text. The accompanying table recapitulates the differences among the samples.

Chapter 2 References:

(1) Eastoe, J.; Robinson, B. H.; Visser, A. J. W. G.; Steytler, D. C. *J. Chem. Soc. Faraday Trans.* **1991**, *87*, 1899-1903.

(2) Laia, C. A. T.; Brown, W.; Almgren, M.; Costa, S. M. B. *Langmuir* **2000**, *16*, 465-470.

(3) Schneeweis, A.; Muller-Goymann, C. C. *Int. J. Phar.* **2000**, *196*, 193-196.

(4) Freidrich, I.; Muller-Goymann, C. C. *Eur. J. Phar. Biophar.* **2003**, *56*, 111- 119.

(5) Freidrich, I.; Reichl, S.; Muller-Goymann, C. C. *Int. J. Phar.* **2005**, *305*, 167-175.

(6) Menger, F. M.; Tsuno, T. *J. Am. Chem. Soc.* **1990**, *112*, 6723-6724.

(7) Menger, F. M.; Tsuno, T.; Hammond, G. S. *J. Am. Chem. Soc.* **1990**, *112*, 1264-1265.

(8) Zhu, X. X.; Banana, K.; Yen, R. *Macromolecules* **1997**, *30*, 3031-3035.

(9) Zhu, X. X.; Banana, K.; Liu, H. Y.; Krause, M.; Yang, M. *Macromolecules* **1999**, *32*, 277-281.

(10) Leporini, D.; Zhu, X. X.; Krause, M.; Jeschke, G.; Spiess, H. W. *Macromolecules* **2002**, *35*, 3977-3983.

(11) Sapp, S. A.; Elliott, C. M. *Chem. Mater.* **2003**, *15*, 1237-1241.

(12) Shirota, H.; Horie, K. *J. Phys. Chem. B* **1999**, *103*, 1437-1443.

(13) Hazra, P.; Sakhar, N. *Phys. Chem. Chem. Phys.* **2002**, *4*, 1040-1045.

(14) Hazra, P.; Chakrabarty, D.; Sarkar, N. *Langmuir* **2002**, *18*, 7872-7879.

(15) Hazra, P.; Chakrabarty, D.; Sarkar, N. *Chem. Phys. Lett.* **2003**, *371*, 553-562.

(16) Hazra, P.; Chakrabarty, D.; Chakrabarty, A.; Sarkar, N. *J. Photochem. Photobiol. A* **2004**, *167*, 23-30.

(17) Burstall, F. H. *J. Chem. Soc.* **1936**, 173-177.

(18) Lide, D. R. ed. *Chemical Rubber Company Handbook of Chemistry and Physics*, 76th ed.; CRC Press: Boca Raton, FL, 1995.

(19) American Society for Testing and Materials. *Annual Book of ASTM Standards*; Section D.683, Philadelphia, PA, 1998.

(20) Accessed www.instron.com (June 2004).

(21) Riter, R. E.; Undiks, E. P.; Levinger, N. E. *J. Am. Chem. Soc.* **1998**, *120*, 6062-6067.

(22) Zheng, L.; Li, F.; Hao, J. *Coll. Surf. A: Phys. Eng. Asp.* **1995**, *98*, 14-18.

(23) Lang, J.; Jada, A.; Malliaris, A. *J. Phys. Chem.* **1988**, *92*, 1946-1953.

(24) Lang, J.; Lalem, N.; Zana, R. *J. Phys. Chem.* **1992**, *96*, 4667-4671.

(25) Allcock, H. R.; Lampe, F. W. *Contemporary Polymer Chemistry*, 2nd ed.; Prentice Hall Publishing: Englewood Cliffs, NJ, 1990.

(26) Sapp, S. A. Materials synthesis strategies for: microstructure self-assembly, polymer-encapsulated reverse micelles, ionic donors in bimolecular photosystems, and efficient mediators in dye-sensitized solar cells; Ph. D. Thesis, Colorado State University, 2002.

(27) Wolf, R. A. *Polym. Mater. Sci. Eng.* **1988**, *58*, 586-589.

(28) Infelta, P. P.; Graetzel, M. *J. Chem. Phys.* **1979**, *70*, 1791-1796.

(29) Joselevich, E.; Willner, I. *J. Phys. Chem.* **1994**, *98*, 7628-7635.

(30) Atik, S. S.; Thomas, J. K. *J. Am. Chem. Soc.* **1981**, *103*, 4367-4371.

(31) Arkin, M. R.; Stemp, E. D. A.; Turro, C.; Turro, N. J.; Barton, J. K. *J. Am. Chem. Soc.* **1996**, *118*, 2267-2274.

(32) Hauenstein, B. L.; Dressick, W. J.; Buell, S. L.; Demas, J. N.; DeGraff, B. A. *J. Am. Chem. Soc.* **1983**, *105*, 4251-4255.

(33) Hauenstein, B. L. Jr.; Dressick, W. J.; Gilbert, T. J.; Demas, J. N.; DeGraff, B. A. *J. Phys. Chem.* **1984**, *88*, 1902-1905.

(34) Snyder, S. W.; Buell, S. L.; Demas, J. N.; DeGraff, B. A. *J. Phys. Chem.* **1989**, *93*, 5265-5271.

(35) Drago, R. S. *Physical Methods for Chemists*, 2nd ed.; Surfside Scientific Publishers: Gainesville, FL, 1992.

(36) Shirota, H.; Horie, K. *J. Phys. Chem. B* **1999**, *103*, 1437-1443.

(37) Pant, D.; Levinger, N. E. *Langmuir* **2000,** *16*, 10123-10130.

(38) Kalyanasundarum, K. *Photochemistry and Photophysics of Polypyridine and Porphyrin Complexes*; Academic Press: London, 1992.

(39) Ritzoulis, G.; Papadopoulos, N.; Jannakoudakis, J. *J. Chem. Eng. Data* **1986,** *31*, 146-148.

(40) Derecskei, B.; Derecskei-Kovacs, A.; Schelly, Z. A. *Langmuir* **1999**, 15, 1981-1992.

(41) Riter, R. E.; Kimmel, J. R.; Unkiks, E. P.; Levinger, N. E. *J. Phys. Chem. B* **1997**, *101*, 8292-8297.

(42) Wallen, S. L. personal communication.

(43) Dressick, W. J.; Cline III, J.; Demas, J. N.; DeGraff, B. A. *J. Am. Chem. Soc.* **1986**, *108*, 7567-7574.

(44) Eppell, S. J.; Zypman, F. R.; Marchant, R. E. *Langmuir* **1993**, *9*, 2281- 2288.

(45) Marcus, M. M.; Eriksson, M. A.; Sasaki, D. Y.; Carpick, R. W. *Ultramicroscopy* **2003**, *97*, 145-150.

(46) Guerrero, C.; Reyes, E.; Gonzalez, V. *Polymer* **2002,** *43*, 6683-6693.

(47) Pfau, A.; Janke, A.; Heckmann, W. *Surf. Interface Anal.* **1999**, *27*, 410-417.

(48) Liaw, J.; Aoyagi, T.; Kataoka, K.; Sakurai, Y.; Okano, T. *Phar. Res.* **1998,** *15*, 1721-1726.

(49) Neves, M. A. F. S.; Coutinho, F. M. B.; Dias, M. L.; Simao, R. A.; Achete, C. A. *J. App. Pol. Sci.* **2002,** *84*, 541-551.

(50) Ambler, M. R.; McIntyre, D. *J. App. Pol. Sci.* **1977,** *21*, 2269-2282.

(51) Stevens, M. *Polymer Chemistry: An Introduction*, 3rd ed.; Oxford Press, 1999.

(52) Tsukruk, V. V.; Wahl, K. J. *ACS Symposium Series 741: Microstructure and Microtribology of Polymer Surfaces*; Oxford University Press: Washington, DC, 2000.

(53) Motomatsu, M.; Nie, H.-Y.; Mizutani, W.; Tokumato, H. *Jpn. J. App. Phys.* **1994,** *33*, 3475-3478.

Chapter 3.

Triad-sequestered Polymer Encapsulated Reverse Micelle Composite Materials as Optical Magnetic Field Sensors.

Introduction.

Donor-Chromophore-Acceptor ($D-C^{2+}-A^{2+}$), or triad, electron transfer species were developed to study the initial steps of photosynthesis (Figure 3. 1).[1-6] Fortuitously, the relaxation processes of the triad photoexcited states are spin-dependent; therefore, their rates can be controlled by magnetic fields.[7] These $D-C^{2+}-A^{2+}$ supramolecular assemblies can thus, in principle, be used to optically detect magnetic fields by monitoring the triad's change in absorbance (ΔA) over time. Unfortunately, some restrictions are imposed upon the sensing system. First, the triad must be in solution to generate the magnetic field-sensitive photoexcited states.[8] Second, the triad cannot simultaneously be exposed to both light and oxygen or else it will decompose.

The general $D-C^{2+}-A^{2+}$ triad structure is presented along with its electron transfer processes (Figure 3. 1). The tris(bipyridine)ruthenium(II) moiety is the triad's chromophore given its intense optical transitions and its inertness to ligand substitution. The chromophore (C^{2+}) is photoexcited by 450 nm light to a singlet metal-to-ligand-charge-transfer state (^{1}MLCT). The ^{1}MLCT intersystem crosses (isc) to a triplet metal-to-ligand-charge-transfer state (^{3}MLCT) in less than one picosecond.[6] The chromophore has an efficient emission quantum yield and a long-lived ^{3}MLCT excited state; therefore, it can undergo electron-transfer reactions in the excited state. The N,N'-diquaternary-

2,2′-bipyridine electron acceptor (A^{2+}) moiety, covalently attached to one of the chromophore's bipyridine ligands, is reduced by this photoexcited ^{3}MLCT electron (k_1) consequently generating a triplet charge transfer state (^{3}CTS, $D\text{-}C^{3+}\text{-}A^{+\bullet}$).[1-6] An azine electron donor moiety then reduces the oxidized chromophore in the CTS (k_2) to yield an optically detectable triplet Charge Separated State (^{3}CSS, $D^{+\bullet}\text{-}C^{2+}\text{-}A^{+\bullet}$). The CSS quantum yields are on the order of 90 %.[6] The normal CSS lifetime (τ_{CSS}) in bulk solution ranges from 100 to 300 ns depending on the solvent. The τ_{CSS} values are larger for solvents of lower dielectric constants.

The magnetic field sensing behavior of the triad is a direct result of the Zeeman splitting of the CSS. In the absence of a magnetic field, the ^{3}CSS and ^{1}CSS states are essentially degenerate; consequently, hyperfine coupling mixes the states. Upon the application of a magnetic field, the degeneracy of the $T_\pm$ and T_0 ^{3}CSS energy levels is lost. The ^{1}CSS and ^{3}CSS state mixing then becomes progressively less efficient as the field strengthens. Therefore, the relaxation of the ^{3}CSS $T_\pm$ components back to the singlet ground state via isc (k_3) to ^{1}CSS becomes progressively slower, while the isc of the ^{3}CSS T_0 level is not affected. Therefore, this two-component (T_0 and $T_\pm$) ^{3}CSS relaxation pathway corresponds to a biexponential decay of the optically detectable ^{3}CSS under applied magnetic fields and in doing so constitutes a magnetic field effect (MFE). This MFE can be quantified by fitting the change in absorbance (ΔA) of the time-resolved CSS profile at either 388 nm (the absorption maximum of the reduced acceptor $A^{+\bullet}$ in the CSS) or at 520 nm (the absorption maximum of the oxidized donor $D^{+\bullet}$ in the CSS) to a biexponential decay.[7] An MFE is observed for the triads in bulk solution even at 5 mT. The long component of the τ_{CSS} ($T_\pm$) increases by an order of magnitude for degassed bulk solutions of triads exposed to modest external magnetic fields[7] (~ 300 mT which is approximately the field strength experienced at the read head of a standard computer drive).[9] The MFE saturates at fields of > 500 mT, because the field independent pathway k_4 (which induces spin-orbit coupling) becomes rate limiting.[7] Shorter τ_{CSS} values at 0 mT correspond to larger MFEs.

It would be useful to incorporate such magnetic field-sensitive triads into sensors. Several problems are coincident with this undertaking. The formation and the relaxation of the ^{3}CSS requires a fluid medium that allows motion in the $D^{+\bullet}$ and $A^{+\bullet}$ moieties. The desired MFEs will not be observed for the triad suspended in a glassy polymer while fluid solutions are not ideal candidates for general sensor applications.

A composite sensor material that would maintain a nanoscopic domain-sized solution environment about the triad so that the ^{3}CSS can form in a macroscopic oxygen-impermeable solid matrix was sought. The refinement of polymer encapsulated reverse micelle synthesis was undertaken to create an organic solid state sensor for the optical detection of magnetic fields. Such materials were first pioneered by Menger and coworkers and Zhu and coworkers[10-12] In this chapter, materials synthesis strategies were devised which produced triad-sequestered polymer encapsulated reverse micelle composite (PERMC) materials. The triad-sequestered PERMCs are amenable to spectroscopic CSS decay detection because they are transparent.[13-14]

The work described herein has three aims. The first is to demonstrate the formation and stability of reverse micelles in the room temperature composite precursor reverse micellar solutions (CPRMSs), as well as during the CPRMS nonpolar phase polymerization. The second objective is to demonstrate ^{3}CSS formation within these materials, and thus to confirm triad sequestration. The last objective is to investigate the optical responses of the triad-sequestered PERMCs to externally applied magnetic fields.

Developing such novel sensing materials designed to detect weak magnetic fields (< 100 mT) can impact magnetic data storage processes.[15-19] Substantial improvements in data storage capacity require new stratagem such as changing from giant magnetoresistive- (GMR) to magnetooptical (MO)-based magnetized domain sensing.[20-22] Triad-sequestered PERMCs partially function as MO materials. Maxwell®, Nikon®, Sony®, and Verbatim® all sell MO technology (Figure 3. 2).[23-24]

It is instructive to review the constitution and underpinnings of GMR and MO read head drives. The read heads consist of several layers (Figure 3. 3). The most important layer is the magnetizable film, commonly a rare earth (RE') oxide. Examples include $CoFeMn_{0.9}RE'_{0.1}O_4$[25], GdFeCo[26], and TbFeCo.[27] This film determines the specifications of the drivehead and in particular the maximum data storage capacity. Any such magnetizable domain material must satisfy the following conditions to serve as a GMR or MO disk: low thermal conduction, high melting point, amorphous structure, and retain a pronounced drop in the magnetic coercivity temperature (T_c).

The GMR and MO data writing processes are both based on thermomagnetic phenomena (Figure 3. 4).[28] The temperature of the read head material is heated to above T_c. Old data is erased at this point. Then, the heated film area is subjected to a strong magnetic field to induce a change in magnetization, M. Data is written at this point. The coercivity of the read head material drops once the magnetic field is removed. The written data is preserved once the film cools.

The GMR and MO data reading processes differ.[28] The former measures a change in M via an electrical current transducer; the latter operates according to the Optical Kerr Effect. The Optical Kerr Effect states that a change in magnetization is a function of the angle of reflected polarized light (Θ_K).

The potential advantages of the MO systems are high storage capacity and high speed data writing.[20-23] Yet, MO is currently experiencing reduced sales because of competing CD-ROM/R/RW and DVD-ROM/RAM data storage systems. Resolutely, researchers continue to develop organic-based materials that optically detect weak magnetic fields. Two main branches of this work are the biological sensing of magnetic fields and single molecule magnets.[30]

Experimental Section.

Materials. The preparation, purification, and isolation of the D-C^{2+}-A^{2+} [Ru(4-POZ)$_2$(4-DQ^{2+})](NO_3^-)$_4$ triad (**T1**) (where n = 4, X = oxygen atom, and Anion = NO_3^-), as well as the 4-POZ and the 4-DQ^{2+} ligands are similar to the preparation of the X = S analog.[31] Activated neutral alumina, 98 % sodium bis(2-ethylhexyl)sulfosuccinate (Aerosol-OT, or AOT), 99 % styrene and technical grade 80 % divinylbenzene (with 4-ethylstyrene as the major contaminant) were purchased from Aldrich. Dehibit 200® was purchased from Polysciences Inc. and was used as received. Radical initiator 2,2′-azobis(2,4-dimethylpentane)nitrile (ADPN) was kindly provided by Professor Marc M. Greenberg (JHU).

Synthesis of the $[Ru(II)(4\text{-}POZ)_2(4\text{-}DQ^{2+})](NO_3)_4$ T1 Triad. The synthesis was done in an inert atmosphere glovebox. The donor moiety ligand, $(4\text{-}DQ^{2+})(PF_6)_2$, (0.020 g, 2.86 x 10^{-5} mol) was placed in a 50 mL round bottom flask containing 20 mL of ethylene glycol and 5 mL of acetone (Aldrich). Acetone was added to assist dissolution of the reactants. It was later evaporated during the reaction. The $[Ru(II)(Cl)_n(OH)_{n-1}(4\text{-}POZ)_2]$ (where n can range from one to four) (0.026 g, 3.90 x 10^{-5} mol) precursor complex (graciously provided by Matthew Rawls) was added to the ligand solution. The reaction mixture was sealed and heated to 50 °C to ensure total dissolution of reactants. The orange-brown reaction mixture turned blood-red after one hour of heating at 120 °C. The reaction mixture was allowed to cool, retrieved from the glovebox, and taken into a dark room. The reaction mixture was diluted with 40 mL of doubly deionized water. A 2.0 g excess of ammonium hexafluorophosphate (NH_4PF_6) (Alfa Aesar) was added as a solid to induce precipitation of $[Ru(II)(4\text{-}POZ)_2(4\text{-}DQ^{2+})](PF_6)_4$. Red cirrus-like clouds of solid were observed floating in the ethylene glycol solution. Centrifugation at high speeds isolated the red product at the bottom allowing for the removal of the ethylene glycol phase by decantation. The product was redissolved with 60 mL of 1:1 acetonitrile:water to repeat the centrifugation process two more times. A one inch diameter column was packed well with 10 cm of 1:1 acetonitrile:water packed Flash Silica for liquid chromatographic resolution of the triad. The hexafluorophosphate salts were redissolved in 2 mL of acetonitrile:water and eluted with (50 % acetonitrile, 40 % water, 10 % saturated potassium nitrate) under 30 psi of nitrogen pressure. It is important that elution start immediately after the introduction of the complex onto the column to its avoid irreversible adsorption to the stationary phase. It is crucial to pack the column's stationary phase very tightly to avoid band diffusion. The column converted all hexafluorophosphate salts into nitrate salts. Twenty fractions were collected and recombined according to thin layer chromatography plates run on each fraction. ESI^+: 1505 ($M+-(NO_3)_3$), 1446 ($M+-(NO_3)_2$).

Preparation of Triad-sequestered Polymer Encapsulated Reverse Micelle Composite (PERMC) Material Magnetic Field Sensors. All PERMC materials synthesis was done at room temperature in a darkroom to avoid triad decomposition in the simultaneous presence of both light and air. Consult Table III. 1. to access CPRMS and PERMC constitutions. Consult Chapter 2 to review the PERMC preparation method.

Two different solutions of **T1** were prepared to determine the respective τ_{CSS} values for comparison to those of the PERMCs **C1-3**. A water solution of **T1** was prepared whose absorbance at 450 nm was adjusted by dilution to be 0.225 (**Soln I**). A CPRMS consisting of 2.00 mL of 50.00 mM solution of AOT in benzene as the nonpolar phase and 27.0 μL of 20.00 mM **T1** with doubly deionized water ($W_0 = 15.00$) as the polar phase was also prepared (**Soln II**). A typical cell assembly consists of an optical measurement chamber that has an attached sidearm for freeze-pump-thaw degassing. The cells are sealable under nitrogen after freeze-pump-thaw cycles using a Kontes Teflon® glass valve. The optical portion of the cell consists of a $(0.4 \times 1.0 \times 1.0)cm^3$ rectangular optical quality fused silica glass compartment. Once the solutions were transferred into their respective cells, the cells were tilted to collect all of the liquid in the sidearm for freezing. Each solution sample was subjected to four freeze-pump-thaw cycles. After these cycles, the solutions no longer needed protection from ambient light exposure. Both solution cells were freeze-pump-thawed (FPT) degassed four times then backfilled with nitrogen.

Polymer Encapsulated Reverse Micelle Composite (PERMC) Finishing. A heating mantle filled with sand and set to 37.0 °C using a Variac was used to cure the nonpolar phases of the CPRMSs **S1-3** for 96 hours. The PERMCs were ground and polished in similar fashion to the PERMCs described in Chapter 2. Smooth, homogeneous, non-light scattering monolith surfaces suitable for optical studies were obtained by polishing composites with a slurry of 0.3 micron Micropolish® II (Buehler).[32] Finer PERMC surfaces were obtained by using MasterMet 2® polish (Buehler) in tandem with Microcloth® polishing pads (Buehler).[33]

Composite Precursor Reverse Micellar Solution (CPRMS) Dynamic Light Scattering (DLS) Particle Sizing. The CPRMSs were particle sized in similar fashion to the CPRMSs described in Chapter 2. As in Chapter 2, the refractive indices of styrene and divinylbenzene are sufficiently different from that of water.[34]

Time-resolved Transient Absorption Spectroscopy Determinations of the Polymer Encapsulated Reverse Micelle Composite (PERMC) Sensor Magnetic Field Effects. The laser system used for time-resolved transient absorption spectroscopy is the same as in previous reports and is as follows (Figure 3. 5).[7,14] The composites were mounted on a stainless steel Thorlabs® post using an adhesive. The output of a 30.0 Hz Quanta Ray® 150-5 Nd:YAG laser was operated at its third harmonics (355 nm) as the pump laser. The laser pulse width was 5.0 to 7.0 ns. This source was coupled to a methanolic Coumarin 47 dye laser operated at 1.0 Hz which provided a 460 nm excitation pump beam. The dye laser's pulse energy was adjusted to be between three to five millijoules by controlling the power source and by using a 30 cm focal length defocusing lens. Composite degradation and charring from surface heating at the pump beam incident spot did not occur at such low pump beam powers. A pulsed Oriel® 75 W Xenon arc lamp served as the probe beam. The probe beam was focused by a 20.0 cm focal length lens. The probe beam approached mounted PERMCs at an angle of ca. 2 degrees with respect to the pump beam (approximately collinear). Both pump and probe beam paths were incident surface-normal upon the (0.5 x 1.0)cm^2 face of the monolith. The pump and probe beams eventually intersected in the interior of the mounted PERMC. At the point of intersection, the probe beam had a cross-section of ca. 5 mm^2. The intersection of the beams was optimized to enhance the signal-to-noise of the CSS decays. The pump beam excited the sequestered triads in the PERMCs and the probe beam monitored the triads' absorption of that light over time. The decay of the transient absorption coming from the opposite PERMC face was first collimated then focused through a Melles-Griot® 370 nm high band pass filter onto a Jarrell Ash® model 82-410 monochromator which selected 388 nm light. This wavelength of light corresponded to the absorption maximum of the $A^{+\bullet}$ in the CSS. Light was collected using a Hamamatsu® model R2496 photomultiplier tube set to 500 V. The current output of the photomultiplier tube was displayed electronically on a Tektronix® TDS602B digital oscilloscope. A Thorlabs® DET310 photodiode was used to trigger and synchronize the oscilloscope with the pump beam pulses.

For magnetic field dependent measurements, PERMCs (**C1-3**) and solutions (**Soln I-II**) were placed between the poles of a Bruker® B-E 15 electromagnet fitted with tapered pole caps and having a 1.2 cm air gap. The external magnetic field was applied perpendicular to the optical path along the 0.5 x 1.0 cm axis of the PERMCs. The magnetic field strength was measured by an F.W. Bell® STB1-0404 transverse Hall Probe. For experiments conducted at 0 mT, the residual field was cancelled by reversing the current through the electromagnet.

The experimentally-obtained time-resolved transient absorption CSS decays were collected first at 0 mT and then at progressively increasing field strengths before a second collection at 0 mT was redone. Baseline corrections and transient absorption decay fits to single exponential and double exponential decay functions with plotted residuals were completed. For presentational purposes, some of the data has been smoothed using SigmaPlot® 2000. All transient absorption decays are presented as Delta Absorbance (ΔA) versus time and normalized to $\Delta A_{(t=0)}$.

Results and Discussion.

Preparation of Triad-sequestered PERMC Material Magnetic Field Sensors. The nonpolar and polar phase components used to prepare magnetic field sensing PERMC materials are relevant. Styrene:divinylbenzene is the polymerizable CPRMS nonpolar phase. The 25 vol. % of divinylbenzene concentration in the CPRMS nonpolar phase ensures the formation of a highly crosslinked network polymer capable of excluding oxygen. This is necessary to avoid the decomposition of the triad under simultaneous light and oxygen exposure.[7] Water was chosen for the polar phase, because it is immiscible with the nonpolar phase and it solvates the nitrate salt of the triad.

The surfactant, radical initiator, and the triad, as well as their respective concentrations, are also relevant to PERMC materials synthesis (Table III. 1). Aerosol-

OT (AOT) is the surfactant. Aerosol-OT forms especially stable reverse micelles because of its efficient hydrophobic packing structure.[35-36] The 50.00 mM AOT concentration is greater than its reported cmc.[36] The PERMC optical quality decreases at surfactant concentrations larger than 50.00 mM. At such elevated surfactant concentrations, micelles can form aggregates with diameters above that of the light scattering limit.[37] Moreover, there is a greater chance for CPRMS nonpolar phase polymer chain termination due to the presence of highly-concentrated surfactant and polar phase species. Such premature polymerization termination produces microcrystalline regions which scatter light.[38] The specific triad used in these studies is in Figure 3. 1 where n = 4, X= oxygen, and the anion is nitrate (**T1**). The 20.00 mM triad concentration employed herein follows from the previous report.[14] According to Poisson statistics, no reverse micelles contain more than one triad thereby preventing interspecies electron transfer processes (Table III. 2).[39-41] Such calculations confirm that 'bulk solution concentration conditions' are simulated within PERMCs. The three different 20.00 mM **T1** polar phase volumes of (9.0, 18.0, and 27.0 μL) correspond to W_0 values of 10.00, 15.00, and 20.00 (Table III. 1).[42]

The **S1-3** CPRMS nonpolar phases radically polymerize after heating to 37.0 °C for 96 hours producing the corresponding PERMCs **C1-3**. It is crucial to control the polymerization temperature. Too high of a polymerization temperature will increase the CPRMS component species vapor pressures and thus lower the PERMC W_0. Moreover, the exchange rate of micellar material occurs is proportional to temperature.[43-44] As a result, PERMCs polymerized at higher polymerization temperatures are poorer in optical quality. The triad-sequestered PERMCs are of high optical quality (Figure 3. 6).

Dynamic Light Scattering (DLS) Particle Sizing Analysis of CPRMSs. Dynamic Light Scattering (DLS) particle sizing analysis was performed on CPRMSs **S1-3** before the addition of ADPN to confirm both that micelles were intact in the relatively higher dielectric nonpolar phase, and that these micelles sequestered triads (Figure 3. 7). Moreover, DLS particle sizing of CPRMSs was conducted at 25.0 °C and at 37.0 °C CPRMS polymerization temperature. The elevated temperature experiments were established that the micelles remain intact at the CPRMS polymerization temperature. Ten micellar radius readings were collected for reverse micellar solutions **S1-3.** These readings were averaged for each CPRMS to report a mean micellar radius. The error bars for these individual W_0-dependent measurements represent one standard deviation from the mean. Consult the Dynamic Light Scattering Particle Sizing section in Chapter 2 for an explanation of the data.[45-55]

Time-Resolved Charge Separated State (CSS) Transient Absorption Studies on CPRMSs and PERMCs Under No Applied Magnetic Field. The triad's degrees of freedom were expected to decrease as follows: bulk solution > CPRMS > PERMC. The collisional frequency between the CSS $D^{+\bullet}$ and $A^{+\bullet}$ moieties (necessary for CSS relaxation) decreases as the triad increasingly interacts with the surfactants composing the micelle. Such electrostatic and hydrophobic interactions can entail the embedment of components of the triad into the micellar wall. The experimentally-observed ^{3}CSS lifetimes (τ_{CSS}) at an applied field of 0 mT decrease in the following order: PERMC > CPRMS > bulk solution indicating a progressively less restrictive environment about the triad (Figure 3. 8). It is important to recognize that the τ_{CSS} represents a distribution of chemical environments and thus a distribution of rates of $D^{+\bullet}$ and $A^{+\bullet}$ collisional encounters.

Most importantly, the triads are in a fluid environment because the CSS is detected for **T1** in PERMCs. Transient absorption spectra were recorded for **C2** at six distinct times after the 450 nm photoexcitation of the PERMC. The presence of an absorption peak centered at 388 nm shows that a CSS forms and decays (Figure 3. 9).

The τ_{CSS} for the PERMC under no applied magnetic field is a factor of ca. 15 times greater than that of the τ_{CSS} for **Solns I-II**. In general, the lifetimes of intramolecular charge transfer states are known to increase in micellar media with respect to bulk solution.[56-58] The PERMC chemical environment affords fewer degrees of freedom to the sequestered triad, because fast CSS decay requires fast motion of the $D^{+\bullet}$ and $A^{+\bullet}$ moieties, (Figure 3. 10). As the nonpolar phase of a CPRMS hardens, the surfactants presumably become immobilized. Therefore, the contents of the entire micelle become less fluid; such dynamics correspond to less frequent $D^{+\bullet}$ and $A^{+\bullet}$ encounters. Any PERMC-based MFE must produce a τ_{CSS} which is longer than ca. one microsecond.

Precision of Time-resolved Transient Absorption Measurements on PERMCs. A reproducible CSS is observed over successive laser pulses. This behavior holds because the τ_{CSS}, after background subtractions which are independent of relaxation processes, is the same to within one standard deviation (Figure 3. 11).

Ruggedness of PERMCs. In addition to being resistant to triplet oxygen gas permeation, which would shorten the τ_{CSS}, the PERMC sensor is also resistant to swelling after being immersed in aromatic and halogenated solvents that commonly dissolve polystyrene.[59] In a simple test, a triad-sequestered PERMC was immersed in toluene for two days at room temperature. The PERMC was still impenetrable after attempting to impale it with a syringe needle. It is difficult to dissolve the composite in any solvent, because of the large degree of chemical crosslinking in the poly(styrene-*co*-divinylbenzene) nonpolar phase. Accordingly, the nonpolar phase cannot be characterized by molecular weight via standard colligative experiments, size exclusion chromatography, or MALDI-TOF spectrometry.

The major drawback of the solid state PERMC is the poor signal-to-noise (S:N) of the CSS decays. The S:N is sacrificed to prevent sample charring, or burning, over the course of time-resolved transient absorption spectroscopy experiments (Figure 3. 12A). The PERMC is prone to such thermal degradation because it is an insulator. The charring phenomenon is not exclusive to PERMCs. Infact, a polystyrene cuvette also chars in the 450 nm excitation laser beam. In direct contrast, freeze-pump-thawed degassed solutions of triads in bulk solution at room temperature can efficiently act as magnetic field sensors without charring due to convection in the bulk solvent which dissipates heat.[60] According to known depolymerization phenomena, the charring is caused by nonchain scission, random chain scission, or depropagation processes which yield oligomers of smaller molecular weight and combustible gases such as hydrogen.[61] The combustibles are self-sustaining providing oxygen is present. Char formation actually reduces the flammability of the sensor by acting as a carbonaceous barrier that can further inhibit combustible gases from diffusing to the pyrolysis zone.

The degree of PERMC charring is dependent upon the laser power. Lower laser powers cause charring throughout the interior of the sample; larger laser powers cause charring on the surface only. Hence, lower laser powers are highly destructive to the chemical integrity of the PERMC interior (Figure 3. 12B). This is problematic because the spectroscopic determinations are performed on the interior of the PERMC sensors.

Accordingly, several approaches have been taken to mitigate PERMC sensor charring during spectroscopic experiments. The approaches can be broadly classified as either sample-oriented or optical train-oriented. The most successful sample-oriented approach entailed PERMC mechanical agitation (Figure 3. 12C). The PERMC mechanical oscillation rate is the same rate at which the PERMC can convectionally cool in air before being re-impinged by the laser beam. Charring is not completely mitigated by this strategy. An unexplored sample-oriented strategy is to coat the sensor with a char-resistant film. With respect to optical train-oriented adjustments towards reducing PERMC charring, the laser can be defocused with a lens (Figure 3. 5). Such optical adjustments defocus the pump over a larger area of the sample thereby reducing charring propensity. In the end, the most effective techniques that reduce PERMC charring during optical experiments entail both laser beam defocusing and pulsing at frequencies slower than 30 Hz. Light source intensities increase upon pulsing. The transient absorption intensity of the triad-sequestered PERMCs increases as a direct result. Finally, composite sensors must be made with a W_0 value $\geq$ ten to obtain acceptable S:N values.

Magnetic Field Sensing Capabilities of PERMCs. The raw MFE data of **C2** is presented (Figure 3. 13, Table III. 3). The corresponding smoothed MFE data is presented as well (Figure 3. 13). Composites **C1-C3** showed analogous MFEs (Figure 3. 14). In a qualitative MFE display of **C2**, three low field (< 300 mT) and two high field (> 300 mT) CSS decays are plotted as the change in 388 nm absorbance (ΔA) versus time after the 450 nm photoexcitation pulse (Figure 3. 13). The MFE is confirmed as τ_{CSS} elongates with increasing magnetic field strengths.

There are two main features of the MFE that warrant discussion. First, the MFE is reversible; the τ_{CSS} at 0 mT is the same both before and after the external magnetic field is applied and removed, respectively. Second, the CSS decay becomes modestly biexponential as the magnetic field strength increases above 300 mT.

The MFE following from the raw data are quantitatively represented by fitting the time-resolved CSS profiles to exponential decay functions and plotting the experimentally-obtained time constants as a function of magnetic field strength. A biexponential decay is expected according to the ^{3}CSS Zeeman splitting. Unfortunately, the poor S:N makes fitting to biexponential functions of questionable value. Consequently, the same CSS profiles were also fit to single exponential decay functions to obtain one unique constant incorporating all time-related information. Yet, the plotted residuals obtained from monoexponential CSS decay fits were harmonic in nature clearly indicating the multiexponential nature of the CSS decays. In contrast, residuals obtained from biexponential CSS decay fits were nonharmonic in nature. Accordingly, results from both monoexponential and biexponential fits are presented (Table III. 3).

For CSS profile monoexponential decay fits, the MFE of **C2** is consistent with a three-fold increase in the τ_{CSS} before saturating, or asymptotically approaching at a maximum τ_{CSS}, of ca. 5 μs near 500 mT (Figure 3. 15). For CSS profile biexponential decay fits, the MFE of **C2** is consistent with a twelve-fold increase in the τ_{CSS} long component before saturating at a maximum τ_{CSS} of ca. 15.4 μs near 2700 mT (Table III.

1). The increase in the slow component of the τ_{CSS} from 0 to 500 mT is similar to observations made for the same triad in bulk solution.[14]

The closest related fields of study to triad-sequestered PERMC-based MFEs described herein encompass intermolecular electron transfers in glasses or temperature-frozen reverse micellar solutions.[62-64] The magnetic field behavior of triad-sequestered PERMC systems differ greatly from those in fluid reverse micellar solution, wherein the 'cage effect' largely determines the photogenerated radical relaxation rates.[65-69] In contrast, there is no such 'cage effect' for triad-sequestered PERMCs, because the triplet biradical CSS of the triad is formed intramolecularly. Moreover, the triplet biradical CSS cannot escape the micellar cage due to its high polarity and the solid state of the nonpolar phase. As such, the MFEs of PERMCs, on the whole, represent a unique class of photogenerated biradical relaxation pathways in the presence of magnetic fields. Upon further refinement, the PERMC composites can serve as a novel class of optical magnetic field sensors and can be considered in kind with optical sensors on the market.[70-72]

The PERMCs as Writable Media for MO Discs. From a theoretical standpoint, data can be written using PERMCs as the MO media through applying an externally applied magnetic field. The triad-sequestered PERMC field response is lost once the magnetic field is removed. Unfortunately, the CSS response to an external magnetic field does not persist upon cooling. Therefore, there is currently no means to save or retrieve any written data (i.e. the increase in τ_{CSS} under externally applied magnetic fields). A comparison between the writing, reading and data storage techniques of GMR, MO and composite sensors is given (Table III. 4).

Conclusions.

Donor-Chromophore-Acceptor (triad)-sequestered poly(styrene-*co*-divinylbenzene) encapsulated reverse micelle composite (PERMC)materials were prepared containing magnetic field-sensitive triad molecular sensors sequestered in anionic AOT micelles. The chemical environment subjected on the PERMC-sequestered triad caused a lengthening of τ_{CSS} under no applied field relative to bulk solution, because the frequency of encounters between the $D^{+\bullet}$ and $A^{+\bullet}$ moieties is lessened. An MFE which increased the τ_{CSS} by greater than or equal to three times depending on the particular CSS profile fit used.

Chapter 3.

Tables

Table III. 1. Constitutions of Donor-Chromophore-Acceptor ($D\text{-}C^{2+}\text{-}A^{2+}$) triad-sequestered CPRMSs and PERMCs.

CPRMS	Nonpolar Phase	Polar Phase[a]	[Surfactant]	W_0	Polymerization[b]	PERMC
S1	2:1 styrene:divinylbenzene	20.00 mM **T1** in H_2O	50.00 mM AOT	10	radical	**C1**
S2	2:1 styrene:divinylbenzene	20.00 mM **T1** in H_2O	50.00 mM AOT	15	radical	**C2**
S3	2:1 styrene:divinylbenzene	20.00 mM **T1** in H_2O	50.00 mM AOT	20	radical	**C3**
Std1	(c)	20.00 mM **T1** in H_2O	(c)	(c)	(c)	(c)
Std2	benzene	20.00 mM **T1** in H_2O	50.00 mM AOT	15	(d)	(d)

(a) Triad **T1** is $[Ru(II)(4\text{-}POZ)_2(4\text{-}DQ^{2+})](NO_3^-)_4$.

(b) Polymerizations were completed by adding ca. 1.0 wt. % ADPN radical initiator to CPRMSs and then exposing the CPRMSs to 37.0 ^{o}C for ca. 96 hours. The final nonpolar phase was poly(styrene-*co*-divinylbenzene).

(c) **Std1** is neither a CPRMS nor a PERMC.

(d) The nonpolar phase of CPRMS **Std2** was not polymerized.

Table III. 2. Poisson statistical calculations of the occupancy of triads in reverse micelles.

PERMC	W_0	Radius (nm)[a]		Volume/R.M. (nm^3)[b]	mass H_2O (g)/R.M.[c]	mol H_2O/R.M.[d]	molec. H_2O/R.M.[e]
C1	10	average	4.1	288.7	2.887E-19	1.603E-20	9.650E+03
		upper PDI	5.6	735.6	7.356E-19	4.084E-20	2.459E+04
		lower PDI	2.6	57.9	5.790E-20	3.215E-21	1.935E+03
C2	15	average	4.2	310.3	3.103E-19	1.723E-20	1.037E+04
		upper PDI	5.9	860.3	8.603E-19	4.777E-20	2.875E+04
		lower PDI	2.5	64.5	6.445E-20	3.579E-21	2.154E+03
C3	20	average	4.5	381.7	3.817E-19	2.119E-20	1.276E+04
		upper PDI	6.1	950.8	9.508E-19	5.279E-20	3.178E+04
		lower PDI	2.9	102.2	1.022E-19	5.672E-21	3.415E+03

(a) Reverse micelle average radii and polydispersities (over ten successive measurements) obtained from DLS particle sizing experiments.

(b) Obtained from the volume expression: $V = (4/3)\pi r^3$, where r is the reverse micellar radius and V is the volume of the reverse micellar interior. Here, the fluid reverse micellar core (interior) is taken to be spherical.

(c) Obtained from the expression: density H_2O x V, where density is taken as 1 g/mL.

(d) Obtained from the expression: mass H_2O / f. w.

(e) Obtained from the expression: mol H_2O x N_A.

(f) According to random statistical analysis: (55.5 M H_2O ÷ 0.020 M **T1**) = 2775 H_2O molecules: 1 **T1** molecule.

Table III. 3. The Magnetic Field Effect of triad-sequestered PERMC **C2**.

$\Delta A = A\exp(-tx)$						$\Delta A = A_{fast}\exp(-xt_{fast}) + A_{slow}\exp(-xt_{slow})$							
B_{app} (mT)[a]	R^2	t (μs)	$(\pm\sigma)$[b]			B_{app} (mT)[a]	R^2	A_{fast}	τ_{fast} (μs)	$(\pm\sigma)$[b]	A_{slow}	τ_{slow} (μs)	$(\pm\sigma)$[b]
0	0.8531	1.3471	0.0131			0	0.9236	0.0150	0.5527	0.0115	0.0050	4.3101	0.1203
50	0.8295	3.1492	0.0253			50	0.9331	0.0128	0.5968	0.0131	0.0081	6.0074	0.1031
100	0.7758	4.2447	0.0367			100	0.9297	0.0137	0.7933	0.0149	0.0073	11.1189	0.7092
200	0.7810	4.4782	0.0379			200	0.9305	0.0135	0.7258	0.0140	0.0082	10.1136	0.2237
400	0.7571	4.7964	0.0427			400	0.931	0.0137	0.7026	0.0126	0.0082	11.2597	0.2493
700	0.7420	4.8217	0.0509			700	0.9279	0.0158	0.5738	0.0147	0.0059	7.1083	0.2059
1000	0.7997	5.7339	0.0449			1000	0.9296	0.0116	0.5754	0.0125	0.0110	9.4830	0.1284
2000	0.7785	4.8012	0.0401			2000	0.9368	0.0146	0.9654	0.0173	0.0076	15.6750	0.6087
2800	0.7829	5.3906	0.0440			2800	0.9366	0.0113	0.8553	0.0160	0.0090	13.1910	0.3378

(a) The 'round number' magnetic field strengths were generated by adjusting the direct current power source in circuit with the electromagnet.

(b) The standard deviations reported were obtained from the corresponding fit functions (located at the top of the table) run in Origin 7.0®.

Table III. 4. Summary of the writing, saving, and reading data manipulation processes for giant magnetoresistive, magneto-optical, and polymer encapsulated reverse micelle composite material media.

Process	GMR media	MO media	PERMC media
Write	(i). Increase T (decrease coercivity)	(i). Increase T (decrease coercivity)	(i). Transient-absorption spectroscopy
	(ii). ΔM by approach of permanent magnet	(ii). ΔM by approach of permanent magnet	(ii). $\Delta \tau css$ by approach of permanent magnet to molecular-level sensor
Save	Decrease T (increase coercivity)	Decrease T (increase coercivity)	No capability
Read	Electrical current	Reflection of plane polarized light at dift. θ_K	A longer τcss correspond to larger B_{app}

Chapter 3.

Figures

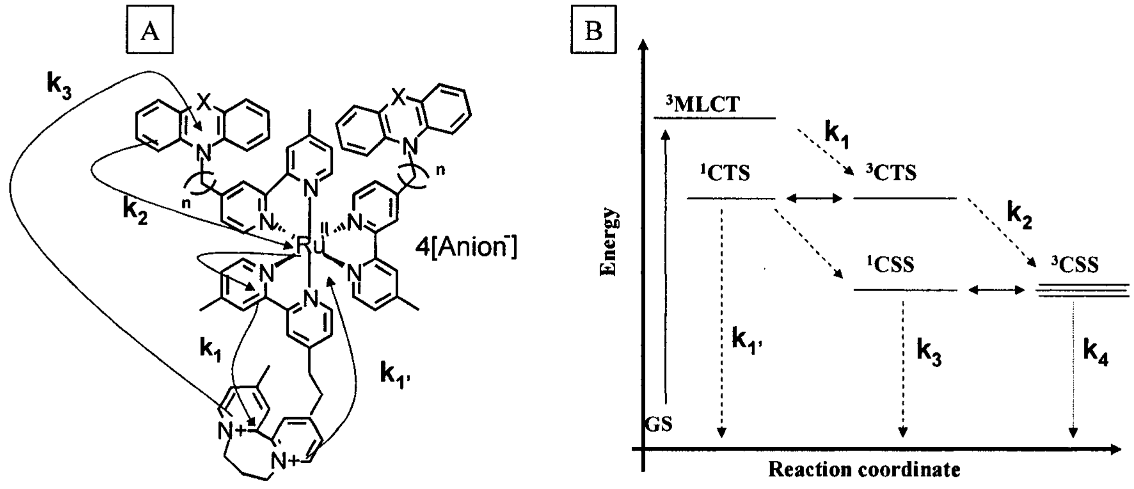

C

Electron Transfer Step	Triad State	Triad Formula
Initially	GS	$D\text{-}C^{2+}\text{-}A^{2+}$
After MLCT	$Ru^{III}(bpy)_2(bpy^{-\bullet})$	$D\text{-}C^{2+}\text{-}A^{2+}$
After k_1	CTS	$D\text{-}C^{3+}\text{-}A^{+\bullet}$
After k_2	CSS	$D^{+\bullet}\text{-}C^{2+}\text{-}A^{+\bullet}$
After k_3	GS	$D\text{-}C^{2+}\text{-}A^{2+}$

Figure 3. 1. General electron transfer steps of a Donor-Chromophore-Acceptor ($D\text{-}C^{2+}\text{-}A^{2+}$) $[Ru(II)(n\text{-}PXZ)_2(4\text{-}DQ^{2+})](Anion^-)_4$ supramolecular triad assembly (A) including an abridged energy diagram of its corresponding photoexcited states (B and C). The **T1** triad is composed of two pendant phenoxazine moieties (where X is oxygen) which both serve as electron donors, a tris(bipyridine)ruthenium(II) core chromophore, and a diquaternary bipyridine (termed a 'diquat') electron acceptor. Upon irradiation with 450 nm light (the wavelength of the corresponding MLCT), the $D\text{-}C^{2+}\text{-}A^{2+}$ species is eventually photoexcited into a Charge Separated State ($D^{+\bullet}\text{-}C^{2+}\text{-}A^{+\bullet}$, CSS) which can only be formed in fluid solution.[1-8] The fluid within the encapsulated micelles provides this medium in the PERMC. Meanwhile, the PERMC network polymer nonpolar phase protects the photogenerated CSS from reaction with ambient oxygen and serves as a rugged housing for the solid state optical magnetic field transducer.

©

Figure 3. 2. A digital picture of magnetooptical (MO) disks (front) and drives (back). Medgrade®, Maxwell®, Nikon®, Sony®, and Verbatim® merchandise MO discs. This picture is copyrighted and is reproduced by permission from Medgrade©.

http://www.medgrade.com/Media.asp?Category=Media
Accessed July 2005.

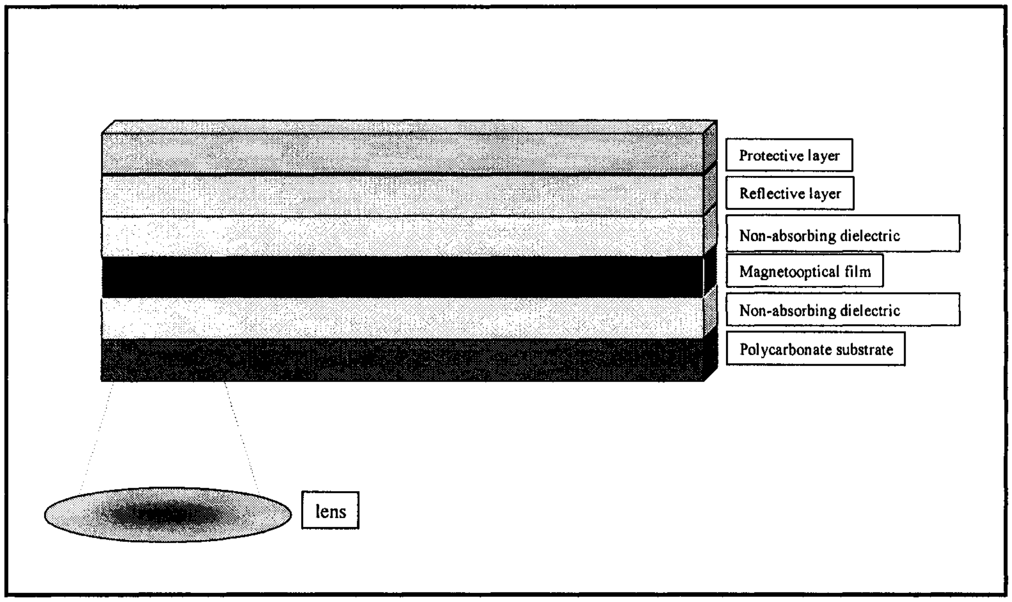

Figure 3. 3. A reproduced schematic representation of a generalized magnetooptical computer disk and how such disks are read by computers. In general, the MO media data writing and saving procedures are the same as giant magnetoresistive (GMR) media. However, the reading processes are different between MO and GMR media. In particular, the angle of the reflection of plane polarized light emanating from the MO film through the lens is the transducer, instead of an electrical current as in GMR materials.

Schematic adapted from: Khurshedov, D. *The Essential Guide to Computer Data Storage: From Floppy to DVD*; Prentice Hall: Upper Saddle River, NJ, 2001.

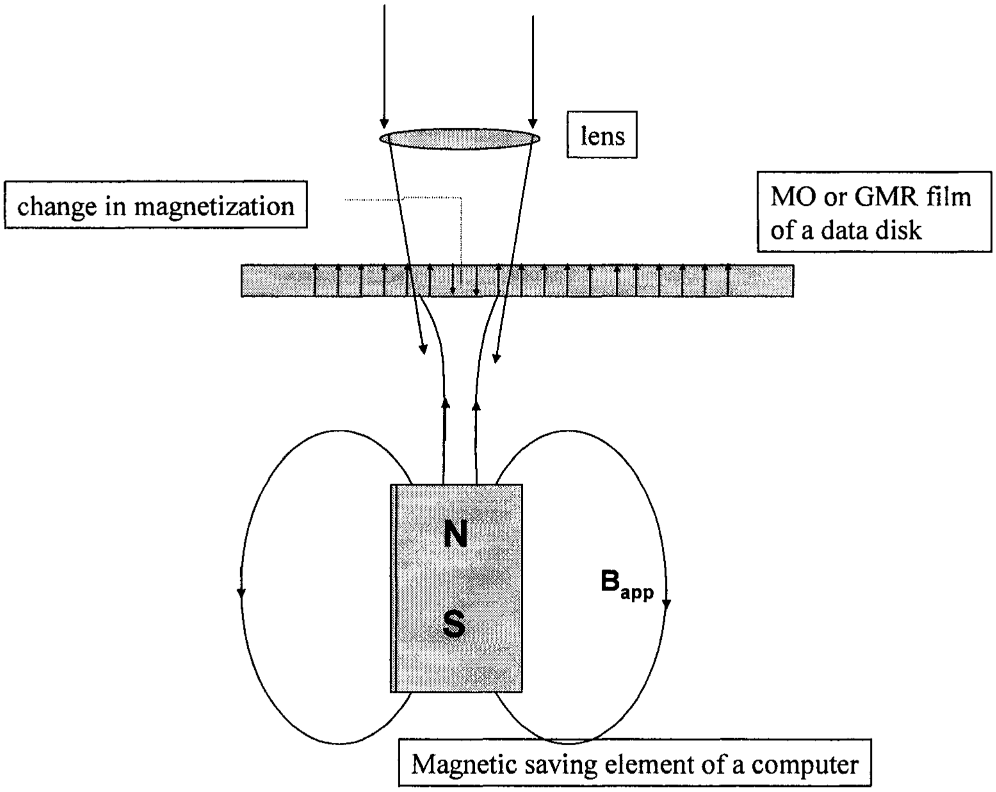

Figure 3. 4. A reproduced schematic representation of the giant magnetoresistive (GMR) and magnetooptical (MO) computer disk drive thermomagneto writing process. Magnetic coercivity is decreased by an increase in temperature, but only over a selected portion of the GMR or MO film. The approach of a magnet to the heated portion film changes the magnetization (↓). Cooling saves the changes in the film magnetization, and thus saves the written data.

Schematic adapted from: Khurshedov, D. *The Essential Guide to Computer Data Storage: From Floppy to DVD*; Prentice Hall: Upper Saddle River, NJ, 2001.

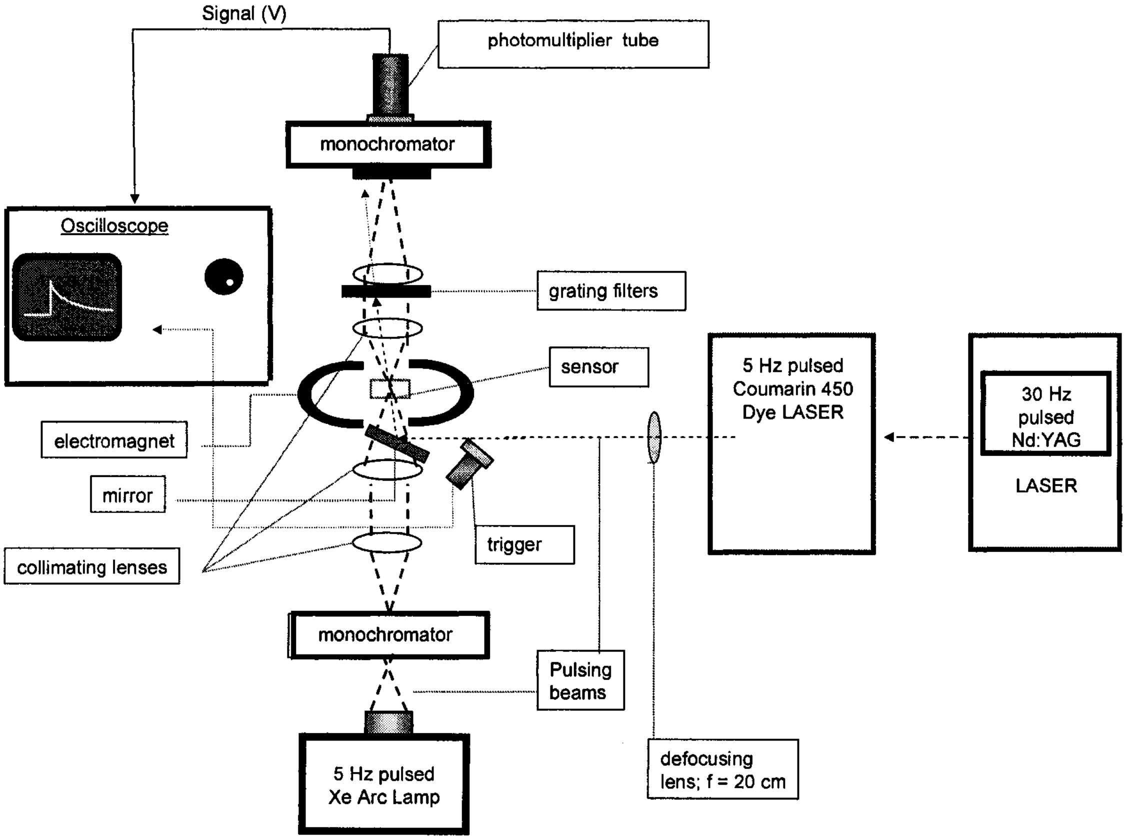

Figure 3. 5. A schematic diagram of the instrumental set-up for measuring Charge Separated State (CSS) time-resolved transient absorption signals in the presence of an externally applied magnetic field using a pulsed Nd:YAG pumped dye laser for 450 nm photoexcitation and a pulsed monochromated xenon arc lamp as an absorbance probe. The following mathematical operations are performed to convert the millivolt-scale intensity signal into a ΔA-scale intensity signal:
$\Delta A = -\log (I \div I_o) = -\log((I_o - \Delta I) \div I_o)$, where I is $|I-I_o|$

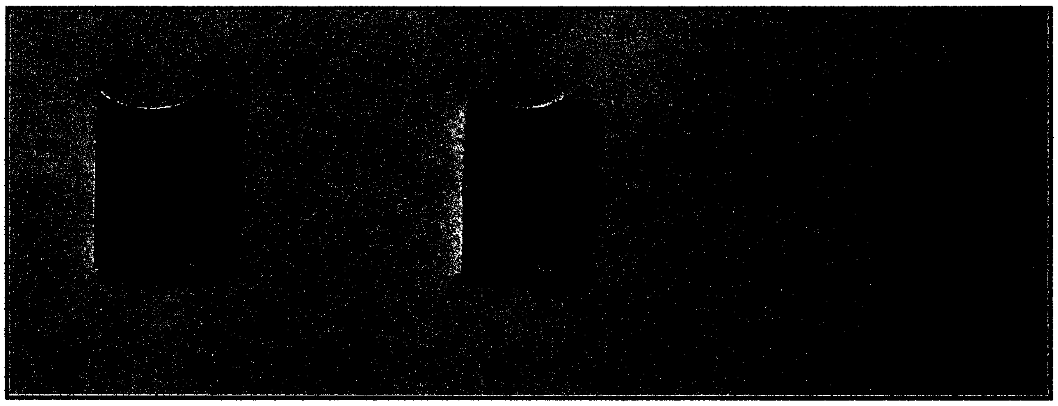

Figure 3. 6. A digital picture exhibiting the optical quality of the analyzed $[Ru(II)(4\text{-}POZ)_2(4\text{-}DQ^{2+})](NO_3)_4$ **T1** triad-sequestered polymer encapsulated AOT reverse micelle composite material magnetic field sensors of water polar phases. From left to right, PERMCs **C1-C3** have W_0 values of 10.00, 15.00, and 20.00, respectively. The transparent nature the PERMCs is necessary in order for them to fully function as optical transducers for the detection of external magnetic fields. The triad's (**T1**'s) MLCT absorption of visible light (centered at 450 nm) is the reason why the PERMCs are orange in color.

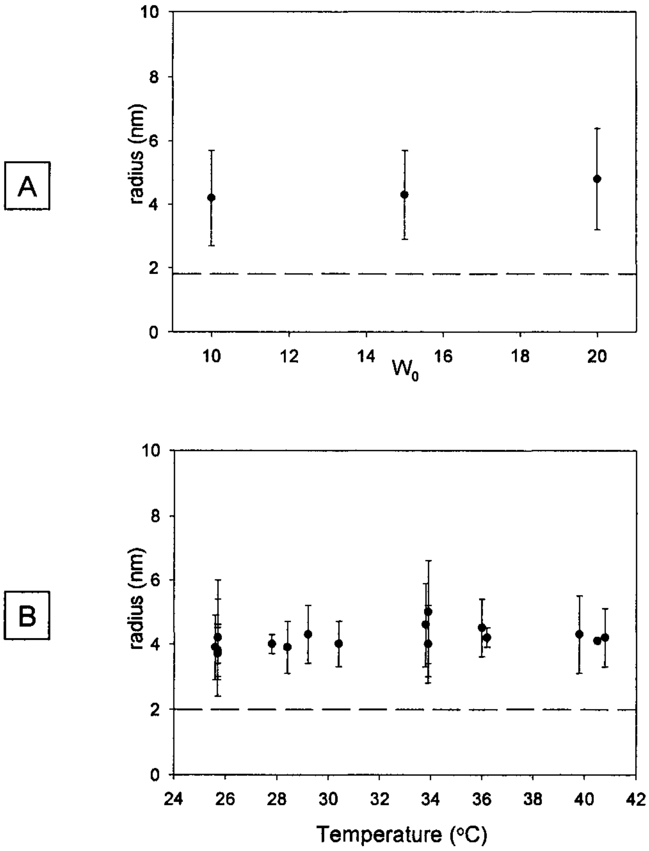

Figure 3. 7. Variable-W_0 and -temperature DLS measurements taken on $[Ru(II)(4\text{-}POZ)_2(4\text{-}DQ^{2+})](NO_3)_4$ **T1** triad-sequestered CPRMSs. The averaged micellar radii are plotted against W_0 (A). The W_0 value has no effect on the averaged radius, but the extent of the fluid polar phase chemical environment increases as the W_0 increases (i. e. the reverse micellar interior becomes more fluid in nature as W_0 increases). The measured radii and polydispersities are larger than that of an AOT reverse micellar solution prepared to a W_0 value of zero (--- at 2.0 nm),[35,47-48] indicating that the triads are sequestered inside the reverse micelles. The large polydispersities are due to the bimodal micellar population (the two different populations of micelles which either contain or do not contain triads) and the asphericalness induced in the reverse micelles because of the electrostatic and hydrophobic interactions between the sequestered cationic triads and the anionic surfactant species. The accompanying plot shows the effect of polymerization temperature on the micellar radii of CPRMS **S2** (B). As in Chapter 2 for chromophore-sequestered CPRMSs, the micelles remain intact at the CPRMS nonpolar phase polymerization temperature.

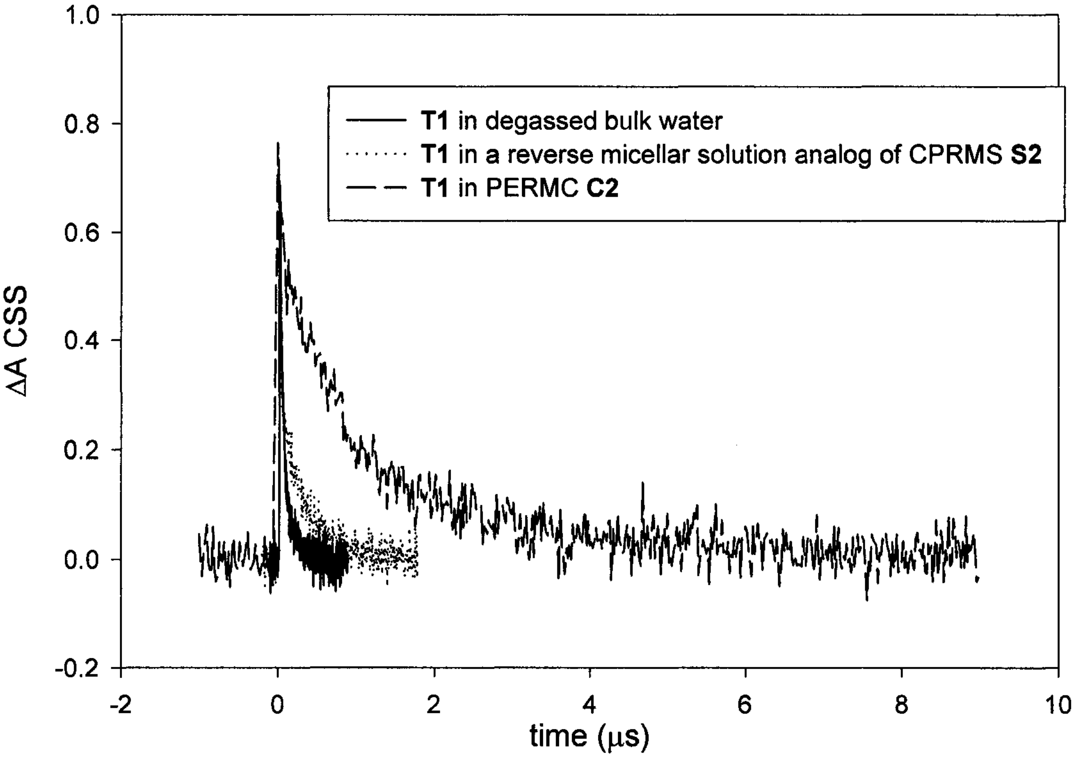

Figure 3. 8. The environmental effect on τ_{CSS} under no applied magnetic field for the $[Ru(II)(4\text{-}POZ)_2(4\text{-}DQ^{2+})](NO_3)_4$ **T1** triad in bulk water (–), sequestered in a CPRMS (···), and finally sequestered inside a PERMC (---). The CPRMS and the PERMC have the same W_0 value. The τ_{CSS} increases as the chemical environment about the triad becomes more restrictive. Such restrictive chemical environments limit the molecular motions of pendant $D^{+\bullet}$ and $A^{+\bullet}$ moieties which are necessary for CSS relaxation.

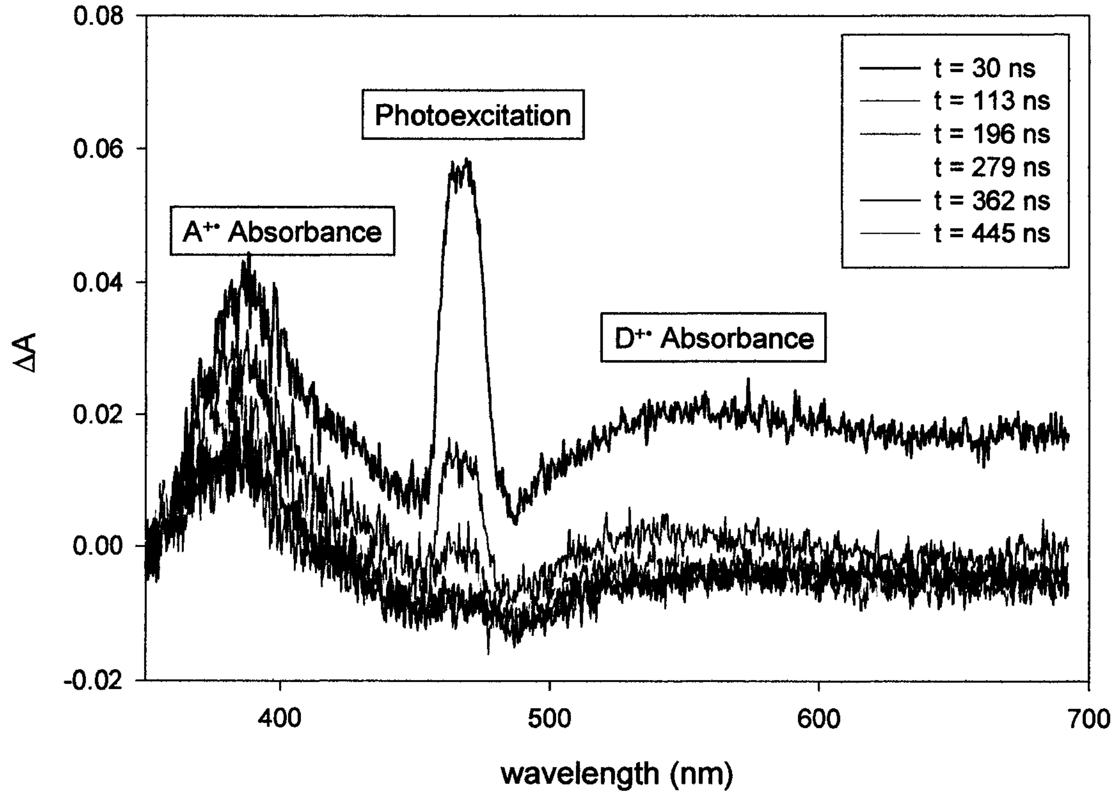

Figure 3. 9. The transient absorption spectra (ΔA vs. wavelength) of [Ru(II)(4-POZ)$_2$(4-DQ^{2+})](NO$_3$)$_4$ **T1** triads sequestered in the **C2** PERMC. The spectra were collected at different times after the initial 450 nm photoexcitation (t = 0 seconds). Upon photoexcitation, the absorption of the A$^{+\bullet}$ moiety in the CSS appears at 390 nm and then decays over time. The absorption of the D$^{+\bullet}$ moiety at 520 nm in the CSS is partially obscured by the matrix (i.e. there is no resolved absorption band). This phenomenon is not completely understood; yet, it poses no interferences in the course of CSS detection providing that A$^{+\bullet}$ absorbance is probed instead of D$^{+\bullet}$ absorbance.

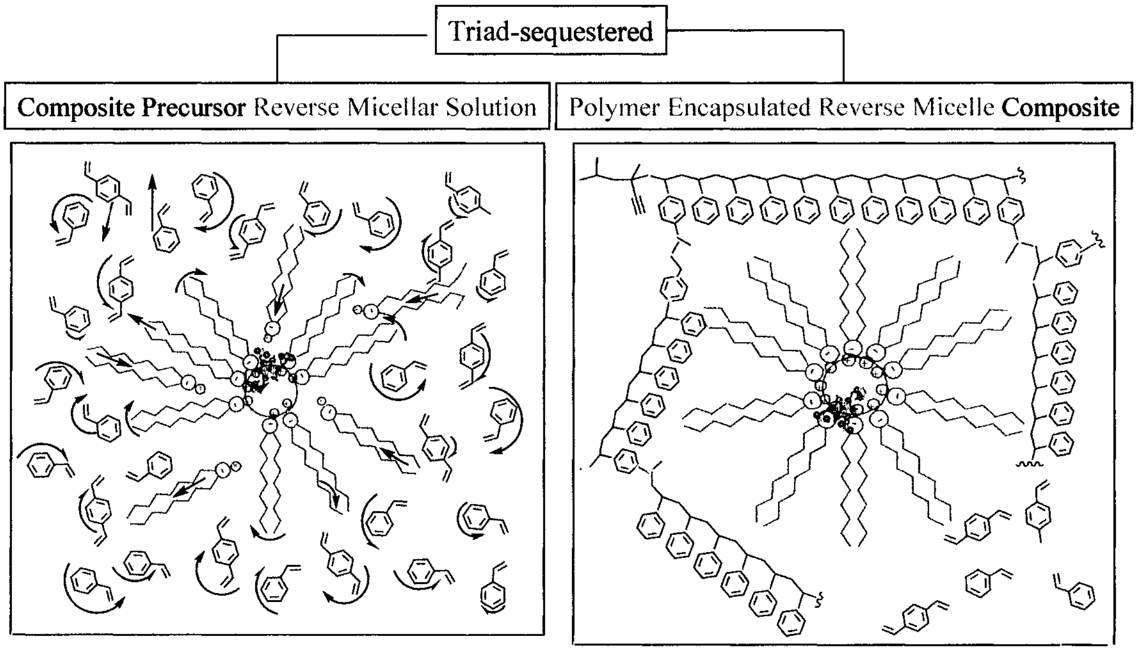

Figure 3. 10. (Species are not drawn to scale). Molecular motion (delineated by arrows) provides the sequestered triad (in dark blue) with more degrees of freedom in the CPRMS. The molecular motions include, but are not limited to, surfactant aggregation (arrows towards micelle) and deaggregation (arrows away from micelle), as well as nonpolar phase species rotation (curved arrows) and translation (straight arrows). Upon nonpolar phase polymerization of the CPRMS into a PERMC, most, if not all, molecular translation and rotation of the surfactant and nonpolar phase species are lost at room temperature. As a consequence, the triad is subject to less degrees of freedom in a PERMC as compared to a CPRMS. Accordingly, the τ_{CSS} lifetime of the triad increases dramatically upon CPRMS conversion into a PERMC. The triad's structure (in blue) was represented in Figure 3. 1. It is important to note that the triad's orientation in the above cross-sectional schematic diagrams is correct in that the more lipophilic donor groups are postulated to embed in the surfactant palisade layer.

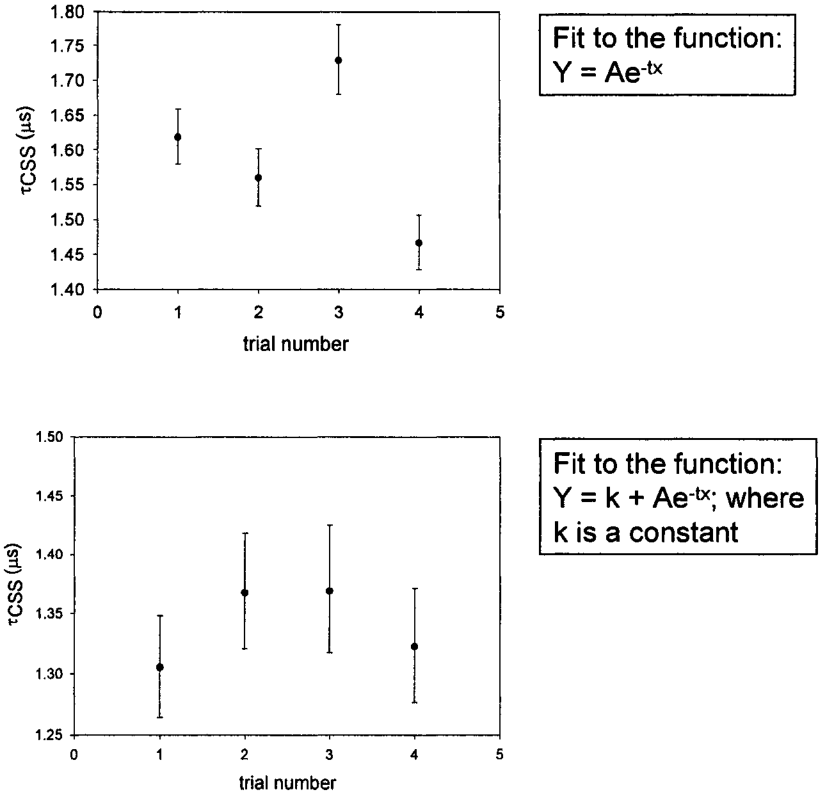

Fit to the function:
$Y = Ae^{-tx}$

Fit to the function:
$Y = k + Ae^{-tx}$; where k is a constant

Figure 3. 11. Reproducibility of the optically measurable τ_{CSS} under no externally applied magnetic field for four consecutive measurements on the **T1** triad-sequestered PERMC **C2**. The upper plot represents the time constants obtained from fits of the CSS decays to a two parameter monoexponential decay ($y = ae^{-tx}$). The lower plot represents the time constants obtained from fits of the CSS decays to a three parameter monoexponential decay ($y = k + ae^{-tx}$, where k is a constant value which corrects for the baseline). The four successive time constants obtained (following from four successive experiments) from the three parameter fits to the CSS decays are within one standard deviation of each other. The CSS decays were monitored at 388 nm which is the absorption maximum of the reduced acceptor ($A^{+\bullet}$).

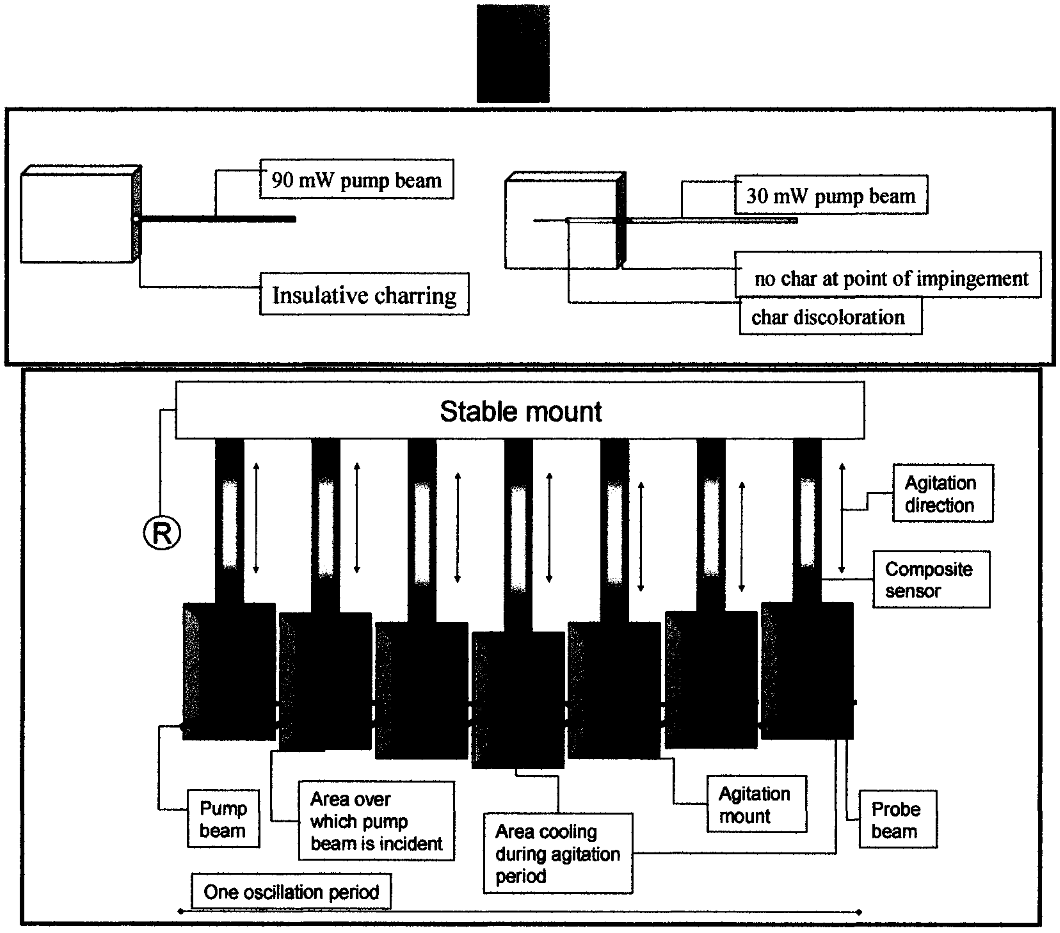

Figure 3. 12. A digital photograph of an unmitigated char mark on a PERMC sensor (top portal). A schematic diagram showing the general effect of triad-sequestered PERMC charring in the 450 nm photoexcitation pump beam (middle portal), and a schematic diagram demonstrating the mechanical agitation of the PERMCs which attenuated charring (bottom portal). In higher power 450 nm photoexcitation pump beams, the composites char on the surface to a greater degree than in the internal regions (middle portal). The opposite is true for low power pump beam charring phenomena. Composite sensor mechanical agitation decreases the overall exposure time of the same area on the PERMC to the pump beam and therefore attenuates charring (bottom portal). In the end, optical train-oriented strategies proved to attenuate charring most efficiently (Figure 3. 5.).

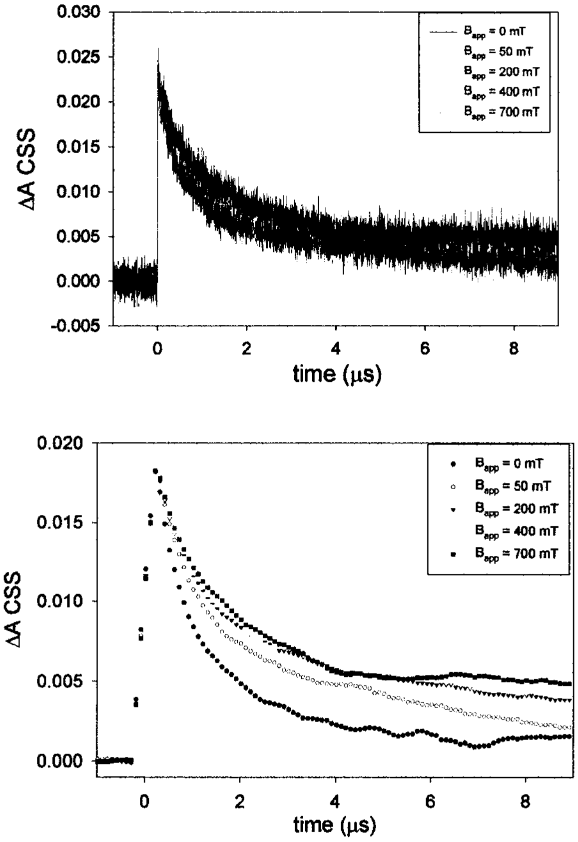

Figure 3. 13. Raw (top) and smoothed (bottom) CSS transient absorption decays of **T1** triad-sequestered PERMC sensor **C2** demonstrating an MFE. Smoothed data was obtained from boxcar averaging. The CSS lifetimes increase and become more bi-exponential in quality as the magnetic field strength increases. The MFE saturates at 300 mT, whereupon the τ_{CSS} stops increasing with increasing field strength. This series of time-resolved transient absorption decays attests to the practical nature of the PERMC systems as optical magnetic field sensors. The CSS decays were monitored at 388 nm which is the absorption maximum of the reduced acceptor. Not all of the CSS decay curves are shown (with respect to Table III. 3) for figure clarity. Smoothed data are only for presentation purposes and are not incorporated into related tables or plots that demonstrate MFE.

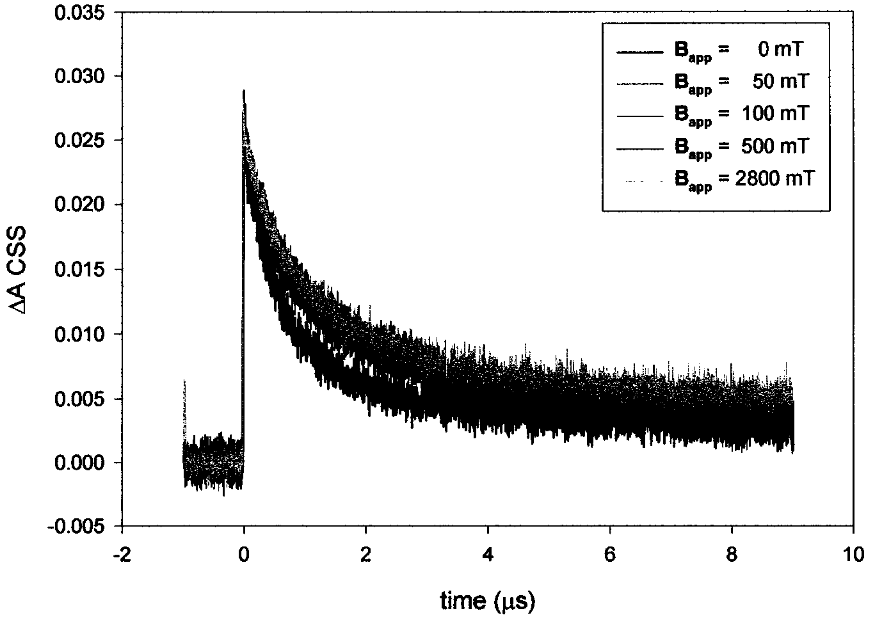

Figure 3. 14. Raw transient absorption decays of **T1** triad-sequestered PERMC sensor **C3** exhibiting an MFE. The CSS lifetimes increase and become more bi-exponential in quality as the magnetic field strength increases. The CSS decays were monitored at 388 nm, which is the absorption maximum of the reduced acceptor.

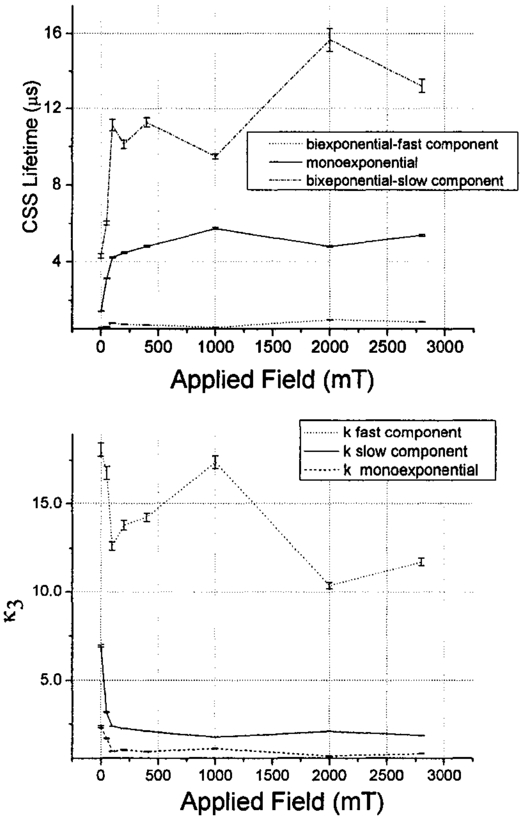

Figure 3. 15. Plot of CSS lifetimes (τ_{CSS}) of **T1** triad-sequestered PERMC **C2** obtained from both monoexponential and biexponential decay fits to the time-resolved profiles versus the applied magnetic field strength (top), and a plot of the CSS decay rate (inverse of τ_{CSS}) versus the applied magnetic field strength (bottom).

Chapter 3 References:

(1) Elliott, C. M.; Freitag, R. A.; Blaney, D. D. *J. Am. Chem. Soc.* **1985**, *107*, 4647-4655.

(2) Danielson, E.; Elliott, C. M.; Merkert, J. W.; Meyer, T. S. *J. Am. Chem. Soc.* **1987**, *109*, 2519-2520.

(3) Cooley, L. F.; Larson, S. L.; Elliott, C. M.; Kelley, D. F. *J. Phys. Chem.* **1991**, *95*, 10694-10700.

(4) Larson, S. L.; Elliott, C. M.; Kelley, D. F. *J. Phys. Chem.* **1995**, *99*, 6530-6539.

(5) Larson, S. L.; Elliott, C. M.; Kelley, D. F. *Inorg. Chem.* **1996**, *35*, 2070-2076.

(6) Pichot, F.; Beck, J. H.; Elliott, C. M. *J. Phys. Chem. A* **1999**, *103*, 6263-6267.

(7) Klumpp, T.; Linsenmann, M.; Larson, S. L.; Limoges, B. R.; Burssner, D.; Krisseinel, E. B.; Elliott, C. M.; Steiner, U. E. *J. Am. Chem. Soc.* **1999**, *121*, 1076-1087; *J. Am. Chem. Soc.* **1999**, *121*, 4092.

(8) Schmehl, R. H.; Ryu, C. K.; Elliott, C. M.; Headford, C. L. E.; Ferrere, S. *Adv. Chem. Ser.* **1990**, *226*, 211-223.

(9) Li, J. S.; Mirzamaani, M.; Bian, X. P.; Doerner, M.; Duan, S. L.; Tang, K.; Toney, M.; Arnoldsen, T.; Madison, M. *J. Appl. Phys.* **1999**, *85*, 4286-4292.

(10) Menger, F. M.; Tsuno, T. *J. Am. Chem. Soc.* **1990**, *112*, 6723-6724.

(11) Zhu, X. X.; Banana, K.; Liu, H. Y.; Krause, M.; Yang, M. *Macromolecules* **1999**, *32*, 277-281.

(12) Leporini, D.; Zhu, X. X.; Krause, M.; Jeschke, G.; Spiess, H. W. *Macromolecules* **2002**, *35*, 3977-3983.

(13) Elliott, C. M.; Steiner, U. E.; Kremer, J. J.; Hötzer, K. A. *Chem. Mater.* **2005**, *17*, 941-943.

(14) Kremer, J. J.; Lu, Y.; Elliott, C. M.; Parkinson, B. P. "Chromophore-sequestered Polymer Encapsulated Aerosol-OT Reverse Micelle Composite Materials of Aqueous and Nonaqueous Polar Phase Constitutions," (In preparation).

(15) Kaneko, M.; Fukumoto, A. *Mat. Res. Soc. Symp. Proc.* **1998**, *517*, 589-598.

(16) Lu, P. L.; Charap, S. H. *IEEE Trans. Mag.* **1994**, *30*, 4230-4235.

(17) Fontana, R. F.; MacDonald, S. A.; Santini, A. A.; Tsang, C. *IEEE Trans. Mag.* **1999**, *35*, 806-812.

(18) Belleson, J.; Grochowski, E. *The Era of Giant Magnetoresisive Heads: IBM's Magnetoresistive and Giant Magnetoresistive Head Technologies Enable Data Storage Products with the Industry's Highest Areal Densities*, 1998.

(19) Accessed TECHFAX: "IBM Deskstar 75GXP and Deskstar 40GV Hard Disk Drives," http://www.storage.ibm.com/hardsoft/diskdrdl/technolo/gmr/gmr.htm, 2000.

(20) Seigler, M. A.; Lambeth, D. N. *Mat. Res. Soc. Symp. Proc.* **1998**, *517*, 599-604.

(21) Desmulliez, M. P. Y. *Mat. Sci. Eng. B: Sol. St. Mat. Adv. Tech.* **2000**, *74*, 269-273.

(22) Kagawa, K.; Ogura, Y.; Tanida, J.; Ichioka, Y. *Appl. Opt.* **1999**, *38*, 7276-7280.

(23) Gambino, R. J.; Suzuki, T. *Magneto-optical Recording Materials*; IEEE Press: New York, NY, 2000.

(24) Khurshudov, A. *The Essential Guide to Computer Data Storage: From Floppy to DVD*; Prentice Hall Publishers: Upper Saddle River, NJ, 2001.

(25) Zhou, B.; Zhang, Y.-W.; Liao, C.-S.; Yan, C.-H.; Chen, L.-Y.; Wang, S.-Y. *J. Mag. Mag. Mat.* **2004**, *280*, 327-333.

(26) Awano, H.; Imai, S.; Ido, H.; Tani, M. U. S. Pat. Appl. Publ. 2005. JP 2003-337237.

(27) Murakami, M.; Birukawa, M. *IEEE Trans. Mag.* **2003**, *39*, 3178-3180.

(28) Sugano, S.; Kojima, N. *Springer Series in Solid-State Sciences: Magneto-optics (128)*; Springer-Verlag: Berlin, 2000.

(29) Weaver, J. C.; Vaughan, T. E.; Astumian, R. D. *Nature* **2000**, *405*, 707-709.

(30) Boskovic, C.; Brechin, E. K.; Streib, W. E.; Folting, K.; Bollinger, J. C.; Hendrickson, D. N.; Christou, G. *J. Am. Chem. Soc.* **2002**, *124*, 3725-3736.

(31) Rawls, M. T.; Elliott, C. M.; Steiner, U. E. "Spin Chemical Control of Photoinduced Electron-Transfer Processes in Ruthenium(II)-Trisbipyridine-Based Supramolecular Triads: 2. The Effect of Oxygen, Sulfur, and Selenium as the Heteroatom in the Azine Donor" (In preparation).

(32) Allcock, H. R.; Lampe, F. W. *Contemporary Polymer Chemistry*, 2nd ed.; Prentice Hall Publishing: Englewood Cliffs, NJ, 1990.

(33) Accessed (http://www.buehlerltd.com, July 2005).

(34) Lide, D. R. ed. *Chemical Rubber Company Handbook of Chemistry and Physics*, 76th ed.; CRC Press: Boca Raton, FL, 1995.

(35) De, T. K.; Maitra, A. *Adv. Coll. Inter. Sci.* **1995**, *59*, 95-193.

(36) Zulauf, M.; Eicke, H.-F. *J. Phys. Chem.* **1979**, *83*, 480-489.

(37) Sapp, S. A. Materials synthesis strategies for: microstructure self-assembly, polymer-encapsulated reverse micelles, ionic donors in bimolecular photosystems, and efficient mediators in dye-sensitized solar cells; Ph. D. Thesis, Colorado State University, 2002.

(38) Stevens, M. *Polymer Chemistry: An Introduction*, 3rd ed.; Oxford University Press: Oxford, 1999.

(39) Infelta, P. P.; Graetzel, M. *J. Chem Phys.* **1979**, *70*, 1791-1796.

(40) Atik, S. S.; Thomas, J. K. *J. Am. Chem. Soc.* **1981**, *103*, 4367-4371.

(41) Joselevich, E.; Willner, I. *J. Phys. Chem.* **1994**, *98*, 7628-7635.

(42) Riter, R. E.; Undiks, E. P.; Levinger, N. E. *J. Am. Chem. Soc.* **1998**, *120*, 6062-6067.

(43) Lang, J.; Jada, A.; Malliaris, A. *J. Phys. Chem.* **1988**, *92*, 1946-1953.

(44) Lang, J.; Lalem, N.; Zana, R. *J. Phys. Chem.* **1992**, *96*, 4667-4671.

(45) Wolf, R. A. *ACS Symp. Ser.* **1989**, *404*, 416-427.

(46) Wolf, R. A. *Polym. Mater. Sci. Eng.* **1988**, *58*, 586-589.

(47) Derecskei, B.; Derecskei-Kovacs, A.; Schelly, Z. A. *Langmuir* **1999**, *15*, 1981-1992.

(48) Silber, J. J.; Biasutti, A.; Abuin, E.; Lissi, E. *Adv. Coll. Int. Sci.* **1999**, *82*, 189-252.

(49) Karukstis, K. K.; Frazier, A. A.; Loftus, C. T.; Tuan, A. S. *J. Phys. Chem. B* **1998**, *102*, 8163-8169.

(50) Hauenstein, B. L.; Dressick, W. J.; Buell, S. L.; Demas, J. N.; DeGraff, B. A. *J. Am. Chem. Soc.* **1983**, *105*, 4251-4255.

(51) Snyder, S. W.; Buell, S. L.; Demas, J. N.; DeGraff, B. A. *J. Phys. Chem.* **1989**, *93*, 5265-5271.

(52) Arkin, M. R.; Stemp, E. D. A.; Turro, C.; Turro, N. J.; Barton, J. K. *J. Am. Chem. Soc.* **1996**, *118*, 2267-2274.

(53) García-Fresñadillo; D.; Orellana, G. *Helv. Chim. Acta* **2001**, *84*, 2708-2730.

(54) Hubig, S. M.; Rodgers, M. A. J. *J. Phys. Chem.* **1990**, *94*, 1933-1936.

(55) Markina, Z. N.; Kryukova, G. N.; Kasaikin, V. A. *Usp. Kolloidn. Khim. Fiz.-Khim. Mekh.* **1992**, 76-81.

(56) Datta, A.; Mandal, D.; Pal, S. K.; Bhattacharyya, K. *J. Phys. Chem. B* **1997**, *101*, 10221-10225.

(57) Mandal, D.; Pal, S. K.; Datta, A.; Bhattacharyya, K. *Anal. Sci.* **1998**, *14*, 199-202.

(58) Tavernier, H. L.; Barzykin, A. V.; Tachiya, M.; Fayer, M. D. *J. Phys. Chem. B* **1998**, *102*, 6078-6088.

(59) Mark, J. E. ed. *Physical Properties of Polymers Handbook*; AIP Press: Woodbury, NY, 1996.

(60) Serway, R. A. *Physics for Scientists and Engineers*, 4th ed.; Saunders College Publishing: Philadelphia, PA, 1996.

(61) Amin, M. B.; Maddhah, A. G. eds. *Handbook of Polymer Degradation*; M. Dekker Publishing: New York, NY, 1992.

(62) Colaneri, M. J.; Kevan, L.; Schmehl, R. *J. Phys. Chem.* **1989**, *92*, 397-401.

(63) Kang, Y. S.; McManus, H. J. D.; Liang, K.; Kevan, L. *J. Phys. Chem.* **1994**, *98*, 1044-1048.

(64) Harriman, A.; Heltz, V.; Ebersole, M.; van Willigen, H. *J. Phys. Chem.* **1994**, *98*, 4982-4989.

(65) Weller, A.; Staerk, H.; Treichel, R. *Faraday Discuss. Chem. Soc.* **1984**, *78*, 271-278.

(66) Scaiano, J. C.; Lougnot, D. J. *Chem. Phys. Lett.* **1984**, *105*, 535-538.

(67) Evans, C.; Ingold, K. U.; Scaiano, J. C. *J. Phys. Chem.* **1988**, *92*, 1257-1262.

(68) Basu, S.; Nath, D.; Chowdhury, M.; Winnik, M. *Chem. Phys.* **1992**, *162*, 145-153.

(69) Kleinman, M. H.; Shevchenko, T.; Bohne, C. *Photochem. Photophys.* **1998**, *67*, 198-205.

(70) Hesselink, L.; Stinson, D. G.; Thornton, R. L.; Malmhall, R. F. U. S. Pat. Appl. Publ. **2004** US2004202054.

(71) Hertz, E.; Holton, C.; Meisner, K.; Paye, C. U. S. Pat. Appl. Publ. **2005** US2004863823.

(72) Ohta, N. *Nippon Oyo Jiki Gakkaishi* **1996**, *20*, 817-825.

Chapter 4.

Chromophore-sequestered Polymer Encapsulated Reverse Micelle Composite Materials of Cationic, Zwitterionic, and Mixed Surfactant Systems.

Introduction.

Poly(styrene-*co*-divinylbenzene) encapsulated reverse micelle composite materials (PERMCs) have been developed as optical sensors over the past decade.[1-2] The composites are made by polymerizing the styrene:divinylbenzene nonpolar phases of composite precursor reverse micellar solutions (CPRMSs). The materials synthesis strategy was adapted from the work of Menger and coworkers and Zhu and coworkers[3-7] The PERMCs are macroscopically solid and contain nanoscopic-sized micelle-sequestered fluid domains wherein polar probe molecules reside in chemical environments which approximate that of bulk solution. Thus far, both the tris(bipyridine)ruthenium(II) chloride, $[Ru(bpy)_3]Cl_2$, chromophore and Donor-Chromophore-Acceptor, $D\text{-}C^{2+}\text{-}A^{2+}$, triad species (with $[Ru(bpy)_3]$ as the chromophore) have been sequestered inside the PERMC fluid polar phase domains.[2,8] Aerosol-OT was the first surfactant used because it forms the most stable reverse micelles.[9] In this way, AOT does not prematurely terminate the radical polymerization of the CPRMS nonpolar phase; the nonpolar phase polymerization is integral to the formation of PERMCs. Corresponding PERMC nonpolar phases consisting of longer, non-terminated polymers do not scatter light as much as prematurely terminated polymers.[10] The transparent optical quality of the PERMCs with AOT surfactant systems is satisfactory. Such properties are required to complete optical measurements.

The data collected on chromophore-sequestered and triad-sequestered PERMCs provides evidence demonstrating that the polar species reside within polymer encapsulated AOT reverse micelles. Chromophore-sequestered PERMCs display emission maxima centered at 610 nm (λ_{em}) and emission lifetimes (τ_{em}) on the order of 600 ns. Such 600 ns emission lifetimes approximate the chromophore's emission lifetime in degassed bulk solvent conditions.[11]

The dependence of the sequestered chromophore's chemical environment on PERMC composition is characterized in this chapter. Such studies can be conducted by either changing the sequestered polar species, the polar phase, or the surfactant system of the PERMCs. The $[Ru(bpy)_3]Cl_2$ chromophore species is not varied because of its well-understood emission qualities.[11] The polar phase is not varied, because water has a satisfactorily large dielectric constant to facilitate both its partitioning into the reverse micelle and its chromophore solvation.[12] Changing to a cationic surfactant will force the chromophore into a more fluid environment located at the center of the micelle rather than immobilize it at the surfactant-polar phase interface via electrostatic and hydrophobic interactions.[13-14] In general, cationic surfactants form larger radius reverse micelles than their anionic counterparts.[15] Such larger micellar sizes facilitate faster electron transfer and rates and faster solvent dynamic processes.[16] Therefore, the sequestered probes are more sensitive to external stimuli such as magnetic fields.

The problem encountered in the course of preparing PERMCs of cationic surfactant systems is due to the more difficult CPRMS nonpolar phase polymerization.[17-18] The difficulty arises because cationic surfactant-based reverse micelles are less stable than anionic counterparts. Cationic surfactants mainly have one long alkyl chain while

AOT has a branched hydrophobic tail conducive to extensive sodium ion and water structuring in the micelle core.[19] Moreover, the presence of sequestered cationic species increases the induced critical micelle concentration (i_{cmc}).[13-14] Accordingly, some cationic surfactants require alcohol cosurfactants.[20] Such cosurfactants as polymerization Chain Transfer (CT) agents. Therefore, the cationic surfactants and the corresponding cosurfactants are more prone to terminating the CPRMS nonpolar phase polymerization via collisional exchange of micellar materials.[21-23] The resulting PERMCs of poor optical quality are useless for the desired optical sensing applications. Even upon obtaining high optical quality cationic- and zwitterionic-surfactant-based PERMC materials, it is necessary to establish that the cationic species reside within the reverse micelles.

Herein, the materials synthesis strategies and characterizations of $[Ru(bpy)_3]Cl_2$ chromophore-sequestered poly(styrene-*co*-divinylbenzene) encapsulated reverse micelle composite materials are presented for the following cationic and zwitterionic surfactant systems: cetyltrimethylammonium bromide (CTAB) with a cosurfactant of 1-octanol (C_8OH) in a 1:5 ratio (P = 5.00) (**S1**), cetyldimethylbenzylammonium chloride (CDBA) (**S2**), hexadecylpyridinium bromide (HDPB) (**S3**), and finally phosphatidylcholine from soybean extract (or lecithin) (**S4**) (Figure 4. 1). In addition, a series of PERMCs were prepared with 3:2 Aerosol-OT:trioctylphosphine mixed anionic surfactant systems (**S5**) in an attempt to mitigate the electrostatic attractions between surfactant and sequestered chromophore species responsible for immobilizing the probe at the surfactant-polar phase interface (Figure 4. 1). Thermalgravimetric analysis (TGA) was performed on PERMCs to determine the onset of decomposition temperature (T_{dec}) as a function of composite constitution. Thermal analysis serves as an indirect detection method to determine the extent of the polar phase and surfactants' interference with the CPRMS nonpolar phase polymerization. Dynamic Light Scattering (DLS) particle sizing studies of CPRMSs at room temperature and at their respective polymerization temperatures assessed hydrodynamic micellar radii. These experiments ensured that intact micelles contained the polar probe species coincident with a change in measured radius upon chromophore sequestration. Static emission spectroscopy probed the $[Ru(bpy)_3]Cl_2$ in the PERMCs to determine the relative polarity of the chemical environment about the chromophore. The dynamic emission lifetime (τ_{em}) measurements of the sequestered $[Ru(bpy)_3]Cl_2$ species gauged the extent of any bulk solution environment present. The emission lifetimes of $[Ru(bpy)_3]Cl_2$ in deaerated water and as a solid are 0.6 and 6.0 μs, respectively.[11]

Experimental Section.

Materials. The preparation, purification, and isolation of $[Ru(bpy)_3]Cl_2$ has been reported previously.[24] A 10.00 mM $[Ru(bpy)_3]Cl_2$ stock solution was prepared in water. This served as the polar phase for the CPRMSs and the PERMCs. Dehibit 200 was purchased from Polysciences Inc. and was used as received. Activated neutral alumina, styrene (99 %) and technical grade divinylbenzene (80 % pure with the major impurity being 4-ethylstyrene) were purchased from Aldrich and used as received. Styrene and divinylbenzene were mixed in a 2:1 ratio to constitute the nonpolar phase of the CPRMSs. Then the mixture was sequentially eluted through separate columns of neutral alumina and Dehibit 200®. The radical polymerization initiator 2,2'-azobis(2,4-dimethylpentanenitrile) (ADPN) was provided by Professor Marc M. Greenberg (JHU).

Preparation of PERMCs with 1:5 Cetyltrimethylammonium bromide:1-octanol Surfactant Systems (C1 Series). The procedure for the composite preparation is schematically represented (Figure 4. 2). Anhydrous 1-octanol (99+ %) was used as received from Aldrich. Cetyltrimethylammonium bromide (CTAB) was purchased from Aldrich. The surfactant was recrystallized three times from 8:2 ethyl acetate:methanol to yield white flakey crystals which were kept in a sealed jar stored in a desiccators. The recrystallization ensured that all water would come from the 10.00 mM $[Ru(bpy)_3]Cl_2$ water solution polar phase. Four portions of 0.0363 g (1.00×10^{-4} mol) of CTAB were weighed out and placed into four 15 x 40 mm 4.0 mL Fisherbrand screwcap vials. Then, 80.0 μL (0.0656 g, 5.037×10^{-4} mol) of 1-octanol was dispensed into these four vials using a 100 μL Gastight® 1710 glass syringe yielding a P value ([cosurfactant]/[surfactant]) equal to 5.00 for all CPRMSs (**S1**). Next, 2.00 mL of 2:1 styrene:divinylbenzene nonpolar phase (effectively 75 % styrene according to reagent purities) was then injected into each vial containing the surfactant and cosurfactant using a 2.00 mL glass syringe. A VWR Scientific® 3 x 10 mm magnetic stirbar was added to each mixture. The mixtures were placed on a hot plate (set to heat a 250 mL beaker of water to 40 °C) with the stirrer mechanism set on low. The polar phase was then injected into each mixture in volumes of 1.80, 3.15, 4.50, and 5.76 μL to produce CPRMSs with W_0 values of 1.00, 1.75, 2.50, and 3.25, respectively (**C1-1.00**, **C1-1.75**, **C1-2.50**, and **C1-3.25**). The surfactant entirely dissolved upon adding the polar phase while continuously stirring and heating. Finally, the cloudy opaque orange solutions became translucent then clear. Once clear, the CPRMSs were sealed with 11 x 17 mm septa and then purged with a slow stream of nitrogen to facilitate thermal polymerization and to ensure no oxygen quenching of the sequestered chromophores' emission. The CPRMSs' nonpolar phase 45.0 °C thermal polymerization occurred over an eight day period.

Preparation of PERMCs with Cetyldimethylbenzylammonium bromide Surfactant Systems (C2 Series). The procedure for the composite preparation is schematically represented (Figure 4. 2). Cetyldimethylbenzylammonium bromide (**S2**) (98 %) was purchased from Aldrich. The surfactant was recrystallized in 2:1 ethyl acetate:methanol to effect flakey white crystals. Next, 0.0395 g of CDBA (1.00 x 10^{-4} mol) was weighed out and added into a 15 x 45 mm 4.0 mL Fisherbrand screwcap vial. Then, 2.00 mL of 2:1 styrene:divinylbenzene was injected into the vial containing the solid. The surfactant dissolved upon the injection of 9.0 μL of 10.00 mM $[Ru(bpy)_3]Cl_2$ in doubly deionized water polar phase via a 100 μL Gastight® 1710 glass syringe (**C2-5.00**) into the mixture with subsequent mechanical agitation on a Vari-Whirl® mechanical agitator. This caused the cloudy opaque orange solution to become transparent. Approximately 1.0 wt. % of 2,2'-azobis(2,4-dimethylpentane)nitrile (ADPN) (0.010 g, 8.46 x 10^{-5} mol) was added as a solid. The CPRMS was sealed with an 11 x 17 mm septum, then purged with a slow stream of nitrogen. The CPRMS was placed in a 37.0 °C sand bath to radically polymerize the nonpolar phase of the CPRMS over a period of four days. Only one composite is presented herein because composites of alternate W_0 values were not optically clear. Three replicates of this PERMC were made.

Preparation of PERMCs with Hexadecylpyridinium bromide Surfactant Systems (C3 Series). The procedure for the composite preparation is schematically represented (Figure 4. 2). Hexadecylpyridinium bromide hydrate (HDPB) (**S3**) (97 – 100 %) was purchased from Aldrich. The surfactant was recrystallized three times from 8:2 ethyl acetate:methanol. Two portions of 0.0383 g (1.00 x 10^{-4} mol) of HDPB was weighed out and placed into two 15 x 40 mm 4.0 mL Fisherbrand screwcap vials. A volume of 2.00 mL of the nonpolar phase 2:1 styrene:divinylbenzene was injected into each of these vials containing the surfactant using a 2.00 mL glass syringe. A VWR Scientific® 3 x 10 mm magnetic stirbar was added to both mixtures which were then placed on a hot plate with the stirring mechanism set on low. The polar phase was then injected into the mixtures using a 100 μL Gastight® 1710 glass syringe in volumes of 9.0 and 18.0 μL to effect CPRMSs with W_0 values of 5.00 and 10.00, respectively (**C3-1.00** and **C3-5.00**). The surfactant entirely dissolved upon the addition of the water polar phase. Stirring and heating yielded clear CPRMSs. The CPRMSs were sealed with 11 x 17 mm septa and then purged with a slow stream of nitrogen. The polymerization of the nonpolar phases of the CPRMSs occurred over an eight day period in a 45.0 °C sand bath.

Preparation of PERMCs with Phosphatidylcholine (Extracted From Soy Lecithin) Surfactant Systems (C4 Series). The procedure for the composite preparation is schematically represented (Figure 4. 2). Refined Lecithin (**S4**) was purchased from Alfa Aesar and was used as received. The surfactant is not a pure compound. Rather, the purchased lecithin consists of a mixture of hydrophobic tails of different isomers and molecular weights with only the zwitterionic head group being the same throughout. The average molecular weight was taken to be 727 g/mol. Thus, three portions of 0.0727 g lecithin were weighed out and put into three 4.0 mL 15 x 40 mm^2 screw-cap vials. Three portions 2.00 mL 2:1 styrene:divinylbenzene were injected into each vial which dissolved the surfactant to yield a golden-orange colored mixture. Volumes of 1.0, 9.0 and 18.0 μL of 10.00 mM $[Ru(bpy)_3]Cl_2$ water solution were injected into the three vials using a 100 μL Gastight® 1710 glass syringe to prepare CPRMSs with W_0 values of 1.00, 5.00, and 10.00, respectively (**C4-1.00**, **C4-5.00**, and **C4-10.00**). A Vari-Whirl® agitator was used to obtain clear CPRMSs. These vials were sealed with 7 x 11 mm septa and then purged with a slow stream of nitrogen. Thermally-assisted radical polymerization of the CPRMSs' nonpolar phases was carried out in a 45.0 °C sand bath set over eight days.

Preparation of PERMCs with 3:2 Aerosol-OT (AOT):trioctylphosphine oxide (TOPO) Surfactant Systems (C5 Series). The procedure for the composite preparation is schematically represented (Figure 2. 2). Sodium bis(2-ethylhexyl)sulfosuccinate (AOT) (98 %) and trioctylphosphine oxide (99 %) were used as received from Aldrich. A stock solution of (30.00 mM AOT + 20.00 mM TOPO) (**S5**), in 2:1 styrene:divinybenzene (effectively 75 % styrene according to reagent purities) was prepared as follows. Masses of 0.3334 g of 0.46 % water weight AOT (7.45 x 10^{-4} mol) and 0.1930 g (4.99 x 10^{-4} mol) of TOPO were weighed out and placed in a 25.00 mL volumetric flask which was then diluted to the calibration mark with the 2:1 styrene:divinylbenzene nonpolar phase. Four 2.00 mL aliquots of this 50.00 mM surfactant solution were then dispensed into four 4.0 mL 15 x 40 mm^2 Fisherbrand screw-cap vials using a 2.00 mL glass syringe. Volumes of 1.8, 9.0, 18.0, and 27.0 μL of 10.00 mM $[Ru(bpy)_3]Cl_2$ in water were injected into each of these vials using a 100 μL Gastight® 1710 glass syringe to effect micellar solutions with W_0 values of 1.00, 5.00, 10.00, and 15.00, respectively (**C5-1.00, C5-5.00, C5-10.00, C5-15.00**). Clear CPRMSs were obtained by mechanically agitating solutions on a Vari-Whirl® mixer. Approximately 1.0 wt. % ADPN (0.010 g, 8.46 x 10^{-5} mol) was added as a solid to each of the CPRMSs. The solutions were sealed with 7 x 11 mm septa and then purged with a slow stream of nitrogen. The radical polymerization of the CPRMSs was carried out in a 37.0 °C sand bath set over a four day period.

Polymer Encapsulated Reverse Micelle Composite (PERMC) Finishing. Consult Chapter 2.[25]

Composite Precursor Reverse Micellar Solution (CPRMS) Dynamic Light Scattering (DLS) Particle Sizing. The CPRMSs were particle sized in similar fashion to the CPRMSs described in Chapter 2. The difference in the refractive indices of the nonpolar and polar phases, at 1.5470 and 1.000 respectively, confirms the viability of using DLS to determine micellar radii.[12]

Thermalgravimetric Analysis (TGA) of Chromophore-sequestered Polymer Encapsulated Reverse Micelle Composite (PERMC) Series. Thermograms were collected on three reference samples and five representative PERMCs of alternate surfactant systems using a thermalgravimetric analyzer (TA Instruments® TGA 2950) to determine the decomposition temperature (T_{dec}). Two of the references were poly(styrene-*co*-divinylbenzene) (**I**) and 50.00 mM AOT dispersed in poly(styrene-*co*-divinylbenzene) (**II**). A previously characterized PERMC made from the nonpolar phase polymerization of a 50.00 mM AOT CPRMS in 2:1 styrene:divinylbenzene to which 9.0 μL of 20.00 mM $[Ru(bpy)_3]Cl_2$ in water solution was added was the third reference (**III**). Thermal analysis on the **C1-2.50, C2-5.00, C3-5.00, C4-5.00**, and **C5-5.00** PERMCs was completed. All thermally analyzed alternate surfactant composites, besides that of **C2-2.50**, had W_0 values of 5.00. The references and PERMCs were ground and polished to smaller dimensions on the order (1.0 x 5.0 x 5.0) mm^3. The masses of the samples were commonly 25 mg. The reverse micelles containing liquid can remain intact at the expense of differential heating effects across the width of the PERMC insulators. No effort was undertaken to exactly reproduce the PERMCs' dimensions or weights across all reference samples and composites thermally analyzed, because T_{dec} is independent of extensive factors. The samples were dabbed clean with ethanol and placed in a tared platinum pan which had been cleaned with a ceramic brush. The furnace was closed under a 100 cm^3/minute constant flushing helium gas stream. After an equilibration period of five minutes at 30 °C, the temperature of the oven was increased to 450 °C at a rate of 10 degrees per minute. Accounts of the entire loss of sample mass with increasing temperature for the 25 mg samples are not presented herein, because of instrumental limitations. Specifically, problems were encountered concerning the sweeping of large amount of decomposition gases from the oven. Data was exported as x-y pairs into ASCII format for presentation in Microsoft Excel®.

Static Emission Spectroscopy of Chromophore-sequestered Polymer Encapsulated Reverse Micelle Composite (PERMC) Series. All spectra were collected using the method and instruments described in Chapter 2.

Emission Lifetime (τ_{em}) Determinations of Chromophore-sequestered Polymer Encapsulated Reverse Micelle Composite (PERMC) Series. The laser system used for time-resolved emission spectroscopy was described in Chapter 2 (Figure 2. 3).[1]

Results and Discussion.

Component Concentration and Polymerization Method-relevant PERMC Preparations. The 50.00 mM surfactant and 10.00 mM tris(bipyridine)ruthenium(II) chloride ($[Ru(bpy)_3]Cl_2$) chromophore constituent concentrations used to prepare composite precursor cationic and zwitterionic reverse micellar solutions were crucial to project success (Table IV. 1). According to Poisson statistical calculations using these respective constituent concentrations,[26-28] there will be no interspecies relaxation owing to the presence of a second chromophore in a polymer encapsulated reverse micelle. The critical micelle concentrations (cmc) are less than 50.00 mM for all surfactants systems employed.[9,29-33] Using higher surfactant concentrations can deleteriously cause free surfactant molecules to terminate nonpolar phase CPRMS polymerizations. In convenient fashion, the 50.00 mM surfactant concentrations allows for direct comparisons to be made to the polymer encapsulated anionic AOT surfactant-based reverse micelle composite analogs.[1]

The small W_0 values are essential for the following reasons. According to Lang and coworkers and Markina and coworkers, the exchange of sequestered micellar material (which in this case can terminate CPRMS nonpolar phase polymerizations) increases as both the length of the surfactant tail increases and temperature increases.[21-23] To further exacerbate this phenomenon, the necessary elevated nonpolar phase CPRMS polymerization temperatures induce a larger degree of dynamic equilibrium to all constituents as a consequence of increased micellar collisions. Consequently, the micellar stability is compromised as the number of intermicellar collisions increase. Micellar instability induces CPRMS nonpolar phase polymerization termination yielding PERMCs of poor optical quality. Most water is bound to surfactant at these small W_0 values.[34] However, all CPRMSs of W_0 values larger than the maximum W_0 value herein (Table IV. 1) are of poor optical quality.

The CPRMS polymerization method depended on the identity of the surfactant and cosurfactant. A thermally assisted radical-induced nonpolar phase polymerization of the **C1** series is not feasible. The 1-octanol cosurfactant is a CT agent which can prematurely terminate the CPRMS nonpolar phase radical-induced polymerization yielding poor optical quality PERMCs. Instead, a modest 45.0 °C thermal polymerization was employed which follows the Mayo Mechanism.[35] B.-H. Lee has characterized such CTAB reverse micellar systems at elevated temperatures.[36] The nonpolar phase of the **C1** series CPRMSs polymerized over an eight day period without compromising the resulting PERMCs' optical quality. The preparation of PERMC series **C2** – **C5** proceeded by thermally assisted radical induced polymerizations of the corresponding CPRMSs at 37.0, 45.0, 45.0, and 37.0 °C, respectively (Table IV. 1). The N-benzyl and N-pyridinium moieties of **S2** and **S3**, respectively, decrease the electrostatic repulsions between adjacent surfactant monomers composing micelles; thus, cosurfactants are not required.[37] The lecithin surfactant-based PERMCs (**C4**) contain micelles which have positive charges on the terminal parts of the surfactant polar head groups and negative charges on the head groups closer to the hydrophobic tails (Figure 4. 1). The structure of the micelles promotes double ion contact pair binding with $[Ru(bpy)_3]Cl_2$ thereby reducing the i_{cmc} and increasing micellar stability.[38-39]

Overall, the goal of creating chromophore-sequestered PERMCs of cationic, zwitterionic, and anionic surfactant systems has been achieved at the expense of the maximum attainable W_0 values. The optical quality of one representative chromophore-sequestered PERMC from each alternate surfactant system is presented (Figure 4. 3).

Dynamic Light Scattering Particle Sizing Analysis. No Dynamic Light Scattering (DLS) particle sizing data can be collected on the respective CPRMSs corresponding to PERMC series **C1** and **C3**. Maintaining the optical clarity of the CPRMSs throughout the DLS experimental time scale was not feasible for these samples because of the necessary stir-heat conditions (consult Experimental Section). Hydrodynamic radii were collected on CPRMSs corresponding to PERMC series **C2**, **C4**, and **C5** at room temperature as well as at elevated temperatures (Figures 4. 4, 4. 5, and 4. 6, respectively).

Thermal Analysis Studies on Representative Chromophore-sequestered PERMCs. Thermalgravimetric analysis (TGA) was performed on representative PERMCs of alternate surfactant constitutions (**C1-2.50**, **C2-5.00**, **C3-5.00**, **C4-5.00**, and **C5-5.00**). Supplemental TGA studies were performed on poly(styrene-*co*-divinylbenzene) (**I**), 50.00 mM AOT dispersed in poly(styrene-co-divinylbenzene) (**II**), and an AOT surfactant-based PERMC (**III**). The experiments determined each PERMCs' thermal decomposition temperature (T_{dec}). The T_{dec} is at the inflection point on a 'mass wt. % v. T' plot. Qualitative interpretations of T_{dec} are offered herein.

In general, the T_{dec} is proportional to polymer molecular weight.[40-43] Accordingly, the T_{dec} of a PERMC is larger when there is less termination of growing radical polymer chains of the CPRMSs nonpolar phase by surfactant, cosurfactant, or polar phase solvent species. Samples **I** and **II** have T_{dec} values that are among the largest of all, because of the absence of foreign surfactant and polar phase species (Figure 4. 7).[41-44]

The T_{dec} values of the representative PERMCs are less than **I** and **II**. For example, the T_{dec} of **C1-2.50** is ca. 100 °C less than that of **I**. This result demonstrates that the 1-octanol cosurfactant undergoes H atom transfer to growing polymer chains.

Simultaneously, the loss of cosurfactant to this CT mechanism adversely affects the structural integrity of the **S1** reverse micelles in the corresponding CPRMS. The high dielectric constant of the nonpolar phase itself (with respect to the more commonly used isooctane) exacerbates the CT phenomena. Composite **C2-5.00** exhibits a similar 150 °C decrease in T_{dec} with respect to **I**. The onset of the T_{dec} occurs over two distinct temperature regimes. Both the T_{dec} values of **C2-5.00** and **C3-5.00** are larger than **C1-2.50** since CT phenomena are exclusive to the **C1** series.

The T_{dec} of the zwitterionic and anionic surfactant-based PERMCs **C4-5.00** and **C5-5.00**, respectively, are on the order of **I**. Zwitterionic surfactants sequestering cationic probes such as $[Ru(bpy)_3]Cl_2$ lower the i_{cmc} with respect to PERMCs of cationic surfactant systems. As a result, solvent and surfactant species terminate growing radical chains to a lesser degree. The T_{dec} of the mixed surfactant system **C5-5.00** is smaller than only its AOT surfactant-based counterpart **III**. The TOPO cosurfactant is not entirely engaging in micellar sequestration of the polar phase in lieu of participating in the CPRMS nonpolar phase growing radical chain termination processes.

Characterization of the C1 PERMC Series. The emission spectra of $[Ru(bpy)_3]Cl_2$ chromophores in the **C1** series PERMCs all feature broad bands and have larger λ_{em} values than the probe in bulk water (Figure 4. 8A, Table IV. 2).[11] Thus, the ^{3}MLCT excited state of the sequestered chromophore is emitting from multiple vibrational energy levels which is consistent with fluid environments.[45] In general, the λ_{em} increases as the polarity of the chemical environment about the chromophore increases.[46-47] Therefore, the sequestered chromophore is subjected to a more polar environment in the **C1** series PERMCs than in bulk water. The enhanced polarity arises from extensive solvent structuring in the small micelles caused by the surfactant head groups. There is no discernable trend relating W_0 to λ_{em} for the **C1** series, given the small range of PERMC W_0 values. The **C1** series composite of the largest W_0 value (**C1-3.20**) has a second emission maxima resolving at lower wavelengths. The presence of a second band in the emission spectrum is indicative of a separate chemical environment about the species.[46-48] This second **C1-3.20** emission maximum indicates that the chromophore is in a less polar chemical environment. In particular for $[Ru(bpy)_3]Cl_2$ sequestered chromophores, Rack and coworkers have determined that the blue-shifted emission maximum is due to a weaker ligand field which stabilizes the d-d orbitals and destabilizes the ^{3}MLCT states, consequently increasing the energy gap between the ground state and the LUMO.[49] This blue-shifted emission resolving at large W_0 values indicates that the chromophore partitions more extensively into a less polar environment as the W_0 increases.

The dynamic emission lifetimes decays of the polymer encapsulated 1:5 CTAB:C_8OH sequestered $[Ru(bpy)_3]Cl_2$ probes for the **C1** series PERMCs all follow single exponential fits ($R^2 > 0.95$), and have τ_{em} values ranging from 650 to 750 ns (Figure 4. 9A, Table IV. 2). The single exponential decay kinetics indicate that sequestered chromophores are subject to one distinct chemical environment.[1] The τ_{em} values for the **C1** PERMC series are ca. 300 ns less than the recorded lifetimes of $[Ru(bpy)_3]Cl_2$ chromophore-sequestered AOT surfactant-based PERMCs at like W_0 values.[1] The positive charges of the N-trimethylammonium head groups composing the micellar wall in the **C1** series force the chromophore into more fluid chemical environments. In other words, electrostatic repulsions predominate over hydrophobic interactions between the lipophilic bipyridine ligands of the chromophore and the hydrophobic tails of **S1**. As a result, the chromophore is more exposed to collisions with solvent which facilitates quicker emissive relaxation processes.[45] In conclusion, one can simulate bulk water solution environments for the sequestered $[Ru(bpy)_3]Cl_2$ chromophore, and its D-C^{2+}-A^{2+} derivatives, by using **S1**-based PERMCs of small W_0 values in addition to AOT surfactant-based composites of large W_0 values.

Characterization of the C2 PERMC Series. The emission spectrum of the $[Ru(bpy)_3]Cl_2$ chromophore in the **C2** composite features a broad band (Figure 4. 8B, Table IV. 2). The broad emission band confirms that the chromophores are emitting from multiple vibrational energy levels consistent with fluid media.[45] Therefore, the chromophore is sequestered inside the reverse micellar fluid cores which themselves are encapsulated by a nonpolar phase of poly(styrene-*co*-divinylbenzene). The λ_{em} is centered at a lower wavelength than the **C1** series PERMCs. The N-benzyl moiety on the **S2** surfactant headgroup increases the hydrophobicity of the micellar wall and thus decreases the dipole-dipole structuring of the sequestered polar phase solvent. In this way, the N-benzyl headgroup of **S2** acts in the capacity of a cosurfactant.

The emission profile of the **C2** composite follows single exponential decay kinetics with a measured time constant of 601 ns which is the same lifetime of the chromophore in degassed bulk water solution (Figure 4. 9B, Table IV. 2).[11] The τ_{em} of **C2-5.00** is 180 ns less than the previously reported τ_{em} for AOT surfactant-based of like W_0 values.[1] The chemical environment exerted on the chromophore in composite **C2-5.00** more simulates bulk solution conditions than any of the **C1** series composites.

Characterization of the C3 PERMC Series. The emission spectra of sequestered $[Ru(bpy)_3]Cl_2$ chromophores in the **C3** series PERMCs all feature broad bands and have

λ_{em} values which approximate the **C1** series PERMCs. The N-pyridinium head group of **S3** structures the water in the fluid phase to a greater degree than the N-benzyl head group of **S2**. Therefore, the sequestered chromophore experiences a more polar environment with respect to that of bulk water. The lipophilic pi-pi interactions between the sequestered chromophore and the surfactant headgroups force the chromophore to remain entirely in the reverse micellar fluid solution. The subject of pi-pi stacking has been extensively studied and has been understood to occur either by face-face or face-off-face alignments of the ring systems.[50-51] The exclusively fluid chemical environment about the chromophore causes the emission maxima for composite series **C3** to red-shift with respect to the AOT surfactant-based PERMCs where chromophore micellar embedment is more prevalent. A second, less intense emission maximum of the polymer encapsulated **S3**-sequestered chromophore centered near 585.0 nm resolves further as W_0 increases, vide supra (Figure 4. 8C, Table IV. 2).[46-49]

The emission lifetimes of the sequestered $[Ru(bpy)_3]Cl_2$ chromophores in the **C3** composite series all follow single exponential decay fits. The τ_{em} values of composites **C3-1.00** and **C3-5.00** that are 310 ns and 100 ns smaller, respectively, than their AOT surfactant-based PERMC counterparts at like W_0 values (Figure 4. 9C, Table IV. 2).[1] The τ_{em} values approximate fluid solution chemical environments more effectively than AOT surfactant-based PERMCs of like W_0 values.

Characterization of the C4 PERMC Series. The emission spectra of the $[Ru(bpy)_3]Cl_2$ chromophores in the **C4** composite series all feature broad bands with λ_{em} values that are blue-shifted with respect to the **C1-C3** series (Figure 4. 8D, Table IV. 2). The λ_{em} values are also blue-shifted with respect to the known λ_{em} of the probe in bulk water.[11] The double ion contact pairs among the zwitterionic surfactant head groups and the chromophore causes the chromophore to embed in the hydrophobic layers to a greater degree than in PERMCs of AOT surfactant systems.[52] Therefore, the electrostatically bound chromophore is subjected to a less polar environment in the **C4** series than those chemical environments characteristic of the **C1-C3** series.[39]

The sequestered chromophore's emission lifetimes for the **C4** series are on the order of AOT surfactant-based PERMCs (Figure 4. 9D, Table IV. 2).[1] The double ion contact layer composed of zwitterionic surfactant head groups, chromophores, and counteranions in the **C4** series PERMCs is stronger than the analogous single ion contact pair in AOT surfactant-based PERMCs. Thus, the sequestered chromophores have less degrees of freedom in **C4** PERMCs than in **C1-C3** PERMCs, and therewith are less subject to solvent collisions which facilitate emissive relaxation processes.[45]

Characterization of the C5 PERMC Series. The static emission spectra of the polymer encapsulated **S5** sequestered chromophores of all **C5** series composites all show broad emission bands indicative of a solution environments (Figure 4. 8E, Table IV. 2). The λ_{em} values are red-shifted with respect to the known $[Ru(bpy)_3]Cl_2$ λ_{em} in bulk water. As such, the **S5** micelles promote ion contact pair formation between the AOT surfactants and the sequestered chromophore. The λ_{em} values of the **C5** series PERMCs red-shift by 16.5 nm as the W_0 changes from 1.00 to 15.00. This behavior is similar to what has been documented for AOT surfactant-based PERMCs.[1] The polarity of the chemical environment exerted on the probe increases λ_{em}, because more of the chromophore is exposed to fluid polar phase as W_0 increases.[46-47]

The λ_{em} values of the sequestered $[Ru(bpy)_3]Cl_2$ species all follow monoexponential decays and decrease with increasing (Figure 4. 9E, Table IV. 2). The ^{3}MLCT can relax at a faster rate by having more collisional encounters with sequestered solvent molecules as the size of the micelle increases.[45] The τ_{em} values of **C5-1.00, C5-5.00, C5-10.00**, and **C5-15.00** are 200, 100, 70, and 100 ns shorter than their AOT-based composite analogs, respectively.[1] The TOPO cosurfactant mitigates the ion contact pair between AOT and $[Ru(bpy)_3]Cl_2$. Demas and coworkers established that the increase in $[Ru(bpy)_3]Cl_2$ τ_{em} values upon micellization is due to decreased ^{3}MLCT deactivation rates via photoactive d-d states.[53] The bulk solution limit is reached at a W_0 10.00.

Conclusions.

$[Ru(bpy)_3]Cl_2$ chromophore-sequestered poly(styrene-*co*-divinylbenzene) encapsulated reverse micelle composite materials (PERMCs) of cationic, anionic, and zwitterionic surfactant systems have been prepared. The maximum W_0 attainable was compromised with respect to AOT surfactant-based PERMCs to preserve optical quality. Thermalgravimetric analysis studies on the composites demonstrated that the decomposition temperature (T_{dec}) of the composite materials decreased in response to the increase in the surfactant-assisted termination of the CPRMS nonpolar phase polymerizations. The emission behavior exhibited by sequestered chromophores in the PERMCs of cationic surfactant systems was on the order of bulk solution behavior at all W_0 values; the emission behavior exhibited by sequestered chromophores in PERMCs of zwitterionic and anionic surfactants systems approached bulk solution conditions only as W_0 increased (Figure 4. 10).

Chapter 4.

Tables

Table IV. 1. Constitutions of $[Ru(bpy)_3]Cl_2$ chromophore-sequestered PERMCs of alternate surfactant systems.

PERMC[a]	[Surfactant]	[Co-surfactant]	W_0	Polymerization[b]	T_p (°C)	t_p (days)
C1-1.00	50 mM CTAB	250 mM C_8OH	1.00	thermal	45	8
C1-1.75	50 mM CTAB	250 mM C_8OH	1.75	thermal	45	8
C1-2.50	50 mM CTAB	250 mM C_8OH	2.50	thermal	45	8
C1-3.20	50 mM CTAB	250 mM C_8OH	3.20	thermal	45	8
C2-5.00	50 mM CDBA	(c)	5.00	radical	38	4
C3-1.00	50 mM HDPB	(c)	1.00	thermal	45	8
C3-5.00	50 mM HDPB	(c)	5.00	thermal	45	8
C4-1.00	50 mM Lecithin	(c)	1.00	thermal	45	8
C4-5.00	50 mM Lecithin	(c)	5.00	thermal	45	8
C4-10.00	50 mM Lecithin	(c)	10.00	thermal	45	8
C5-1.00	30 mM AOT	20 mM TOPO	1.00	radical	38	4
C5-5.00	30 mM AOT	20 mM TOPO	5.00	radical	38	4
C5-10.00	30 mM AOT	20 mM TOPO	10.00	radical	38	4
C5-15.00	30 mM AOT	20 mM TOPO	15.00	radical	38	4

(a) The polar phase for all PERMCs is 10.00 mM $[Ru(bpy)_3]Cl_2$. The CPRMS (initial) nonpolar phase is 2:1 sty:dvb. The PERMC (final) nonpolar phase after polymerization is poly(styrene-*co*-divinylbenzene).

(b) Thermal polymerizations follow the Mayo Mechanism.[35] Radical polymerizations follow from the addition of 1.0 wt. % ADPN radical initiator.

(c) No cosurfactant was used.

Table IV. 2. Static and dynamic emission characterization of chromophore-sequestered PERMCs of alternate surfactant systems.

PERMC	λ_{em}(arb. units)[a]	λ_{em} (nm)	τ_{em} (ns)[b]	σ[b]	R^2[b]
C1-1.00	7.68E+06	623.0	735.5	12.1	0.9803
C1-1.75	8.70E+06	625.5	664.1	14.7	0.9782
C1-2.50	5.81E+06	618.5	748.4	8.4	0.9887
C1-3.20	4.36E+06	629.0	685.7	10.6	0.9763
C2-5.00	8.91E+06	611.5	601	10.9	0.9845
C3-1.00	6.22E+06	626.0	802.5	3.6	0.9987
C3-5.00	4.33E+06	624.5	653.6	5.8	0.9932
C4-1.00	8.20E+06	< 550	1399	14.3	0.9957
C4-5.00	9.85E+06	605.0	1372	4.8	0.9946
C4-10.00	1.29E+07	598.0	1193	7.7	0.9985
C5-1.00	5.70E+06	623.0	989.3	5.5	0.9898
C5-5.00	8.62E+06	622.5	875.9	5.5	0.9949
C5-10.00	6.79E+06	642.5	563.9	5.8	0.9865
C5-15.00	9.10E+06	639.5	419	10.0	0.9853

(a) Values reported not absolute insomuch as fluorescence intensities are dependent upon sample pathlength (thickness) which is irreproducible due to irreproducible PERMC placement in the fluorimeter.

(b) The emission lifetimes, as well as the accompanying standard deviation (σ) and linear regression factors, were obtained from monoexponential decay fits to the time-resolved profiles.

Chapter 4.

Figures

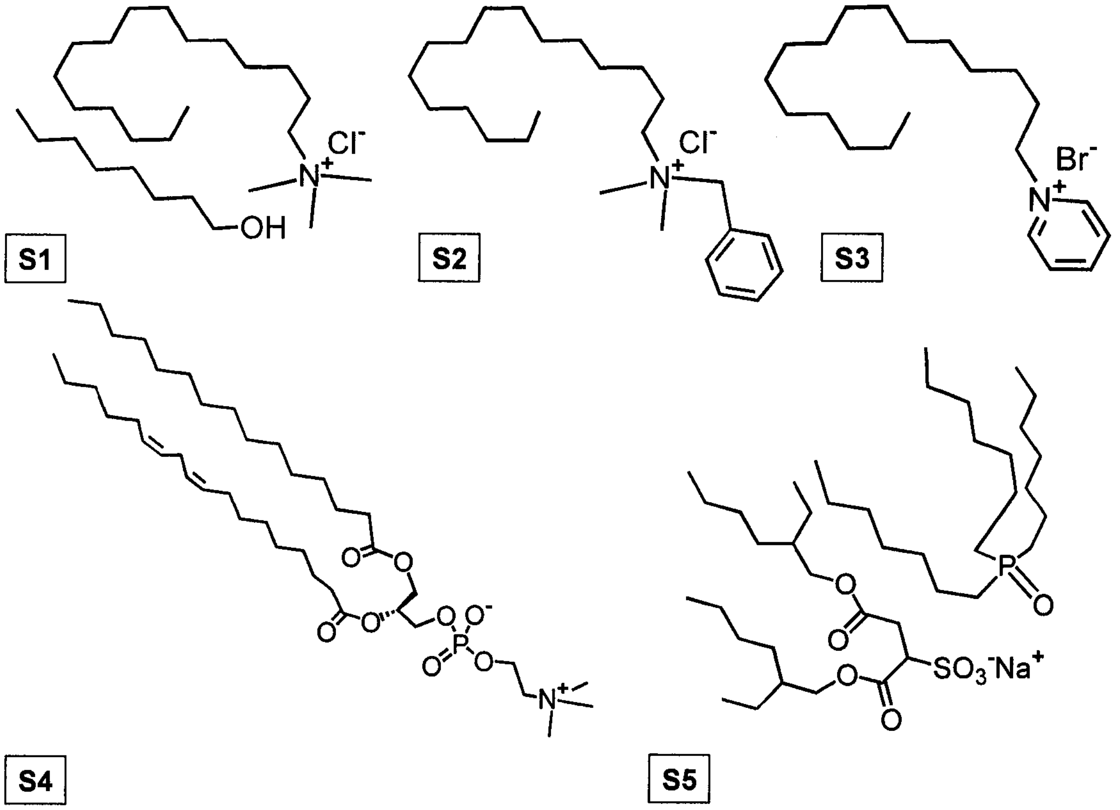

Figure 4. 1. Chemical structures of the surfactants used to make the $[Ru(bpy)_3]Cl_2$ chromophore-sequestered polymer encapsulated reverse micelle composite series **C1-C5** (see Table IV. 1): (**S1**) cetyltrimethylammonium bromide:1-octanol (P = 5.00) (1 CTAB: 5 C_8OH); (**S2**) cetyldimethylbenzylammonium chloride (CDBA); (**S3**) hexadecylpyridinium bromide (HDPB); (**S4**) phosphatidylcholine, or refined soy lecithin (a mixture of isomers); and (**S5**) Aerosol-OT:trioctylphosphine oxide (P = 0.66) (3 AOT: 2 TOPO). The curved surfactant hydrophobic tails are for presentational purposes only. The hydrophobic tails elongate upon surfactant aggregation into reverse micelles.

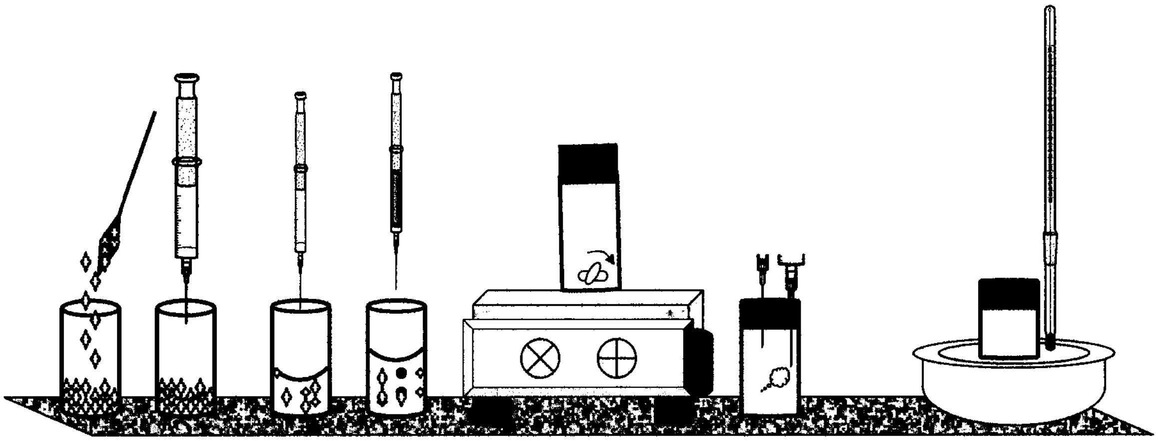

[Surfactant]	0.0363g dried recrystallized CTAB for a 50.00 m<u>M</u> solution
[Co-surfactant]	80 μL C_8OH for a 250.00 m<u>M</u> solution
Nonpolar Phase	2.0 mL of 2:1 styrene:divinylbenzene
[Molecular Sensor]	20.00 mM $[Ru(II)(bpy)_3]Cl_2$ or 20.00 m<u>M</u> Triad
In Polar Phase	H_2O
Mixing	Stir-heat
Gas purging	N_2 gas purged for 5 min.
Polymerization Conditions	$T_p = 45\,^{\circ}C$; $t_p = 96$ hrs
Nonpolar Phase Polymer	poly(styrene-*co* -divinylbenzene)

Figure 4. 2. A schematic diagram showing the steps necessary to prepare cationic surfactant-based PERMCs. First, the recrystallized CTAB solid surfactant is added to the vial in the quantity needed to prepare a 50.00 mM CPRMS (A). If necessary, a microliter volume of 1-octanol cosurfactant is added to achieve the desired P (= [cosurfactant] ÷ [surfactant]) ratio (B). Next, the styrene:divinylbenzene nonpolar phase is added on the order of milliliters (C). The polar phase is added on the order of microliters (D). The CPRMS turns clear after modest heating and vigorous stirring (E). The CPRMS is sealed and purged with nitrogen (F). The CPRMS is placed in a 45.0 °C sand bath for thermal polymerization (without the assistance of a radical initiator) (G). The accompanying table recapitulates the amounts of each constituent and the preparation conditions.

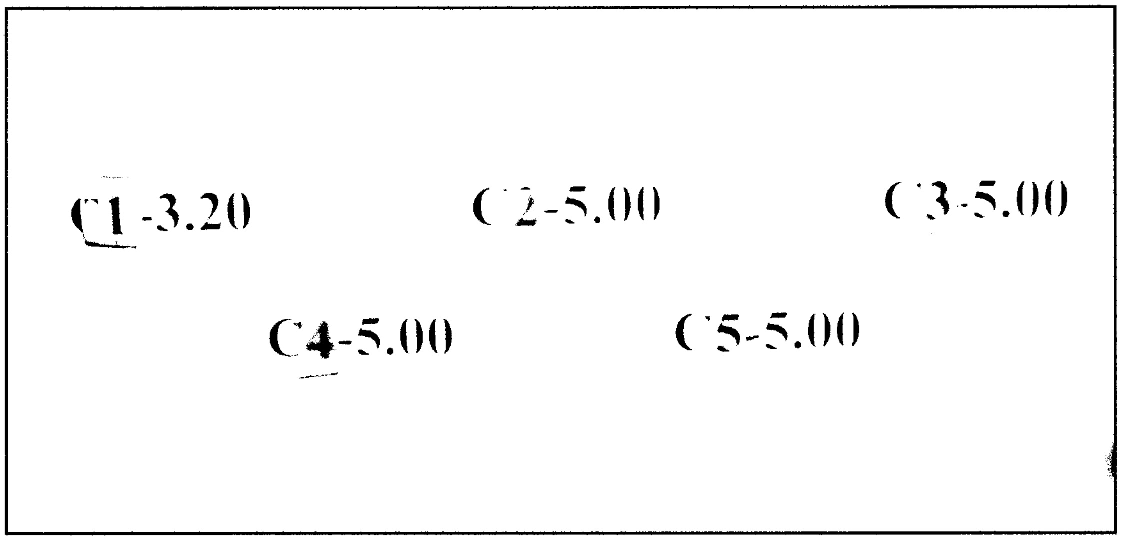

Figure 4. 3. A digital photograph exhibiting the transparent optical quality of the analyzed chromophore-sequestered PERMCs **C1-2.75**, **C2-5.00**, **C3-5.00**, **C4-5.00**, and **C5-5.00** (see Table IV. 1). The CPRMS nonpolar phase polymerizations producing the **C1-2.75** and **C3-5.00** PERMCs were thermally induced, while the CPRMS nonpolar phase polymerizations producing the **C2-5.00**, **C4-5.00**, and **C5-5.00** PERMCs were radically induced with the addition of 1.0 wt. % of 2,2'-azobis(2,4-dimethylpentanenitrile) (ADPN) initiator.

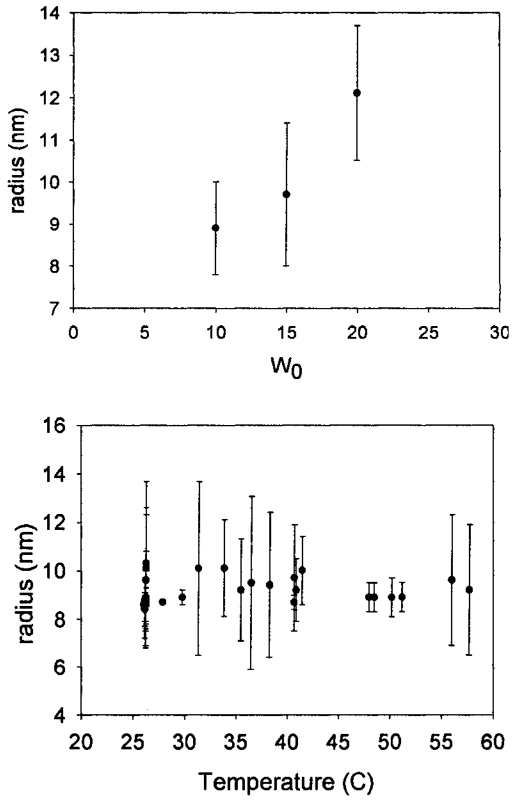

Figure 4. 4. DLS measurements taken on CDBA surfactant-based CPRMSs plotted against W_0 (top) and temperature (bottom). The error bars are large in size, because of reasons explained in the text of Chapter 2.

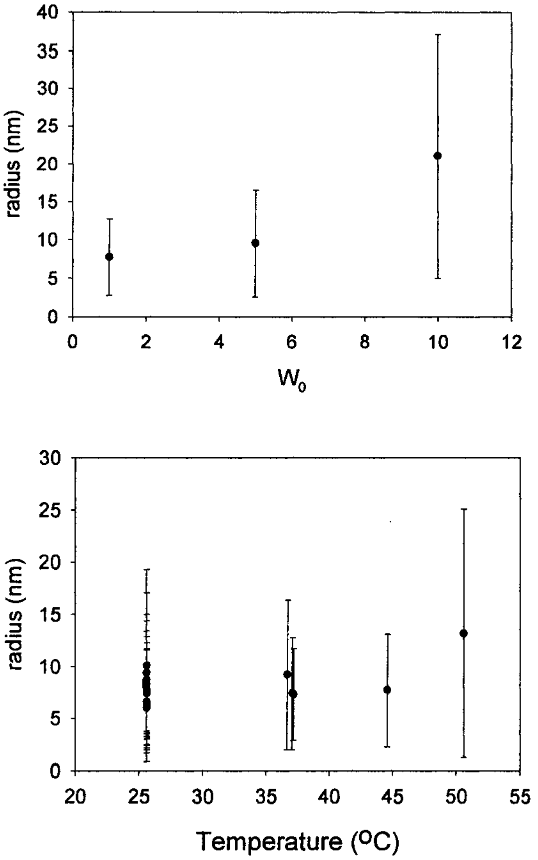

Figure 4. 5. DLS measurements taken on phosphatidylcholine surfactant-based CPRMSs plotted against W_0 (top) and temperature (bottom).

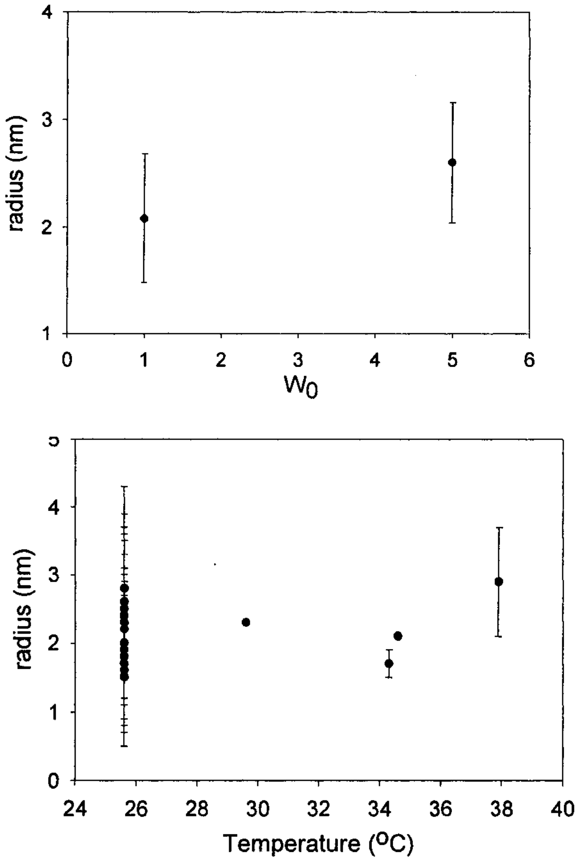

Figure 4. 6. DLS measurements taken on 3:2 AOT:TOPO surfactant-based CPRMSs plotted against W_0 (top) and temperature (bottom).

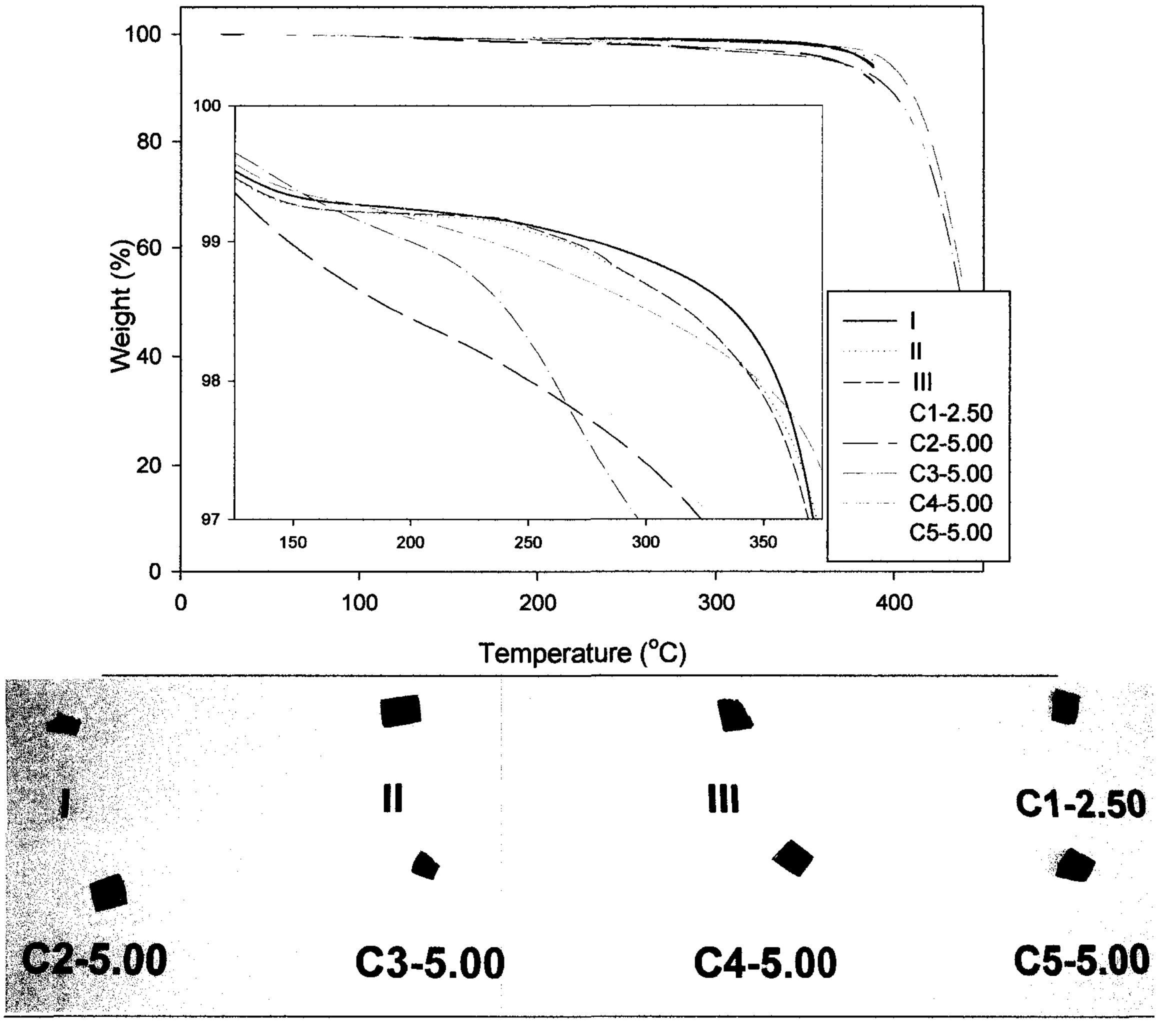

Figure 4. 7. Thermalgravimetric analysis of poly(styrene-*co*-divinylbenzene) (I), poly(styrene-*co*-divinylbenzene) with 50.00 mM Aerosol-OT dispersed in it (II), and representative chromophore-sequestered PERMCs (top). The inset shows the beginning of the thermal decompositions temperature (T_{dec}) which varies for each composite. The T_{dec} of the representative PERMCs is dependent upon the particular surfactant system employed and increases as follows: cationic < anionic < poly(styrene-*co*-divinylbenzene). The components of cationic surfactant system CPRMSs prematurely terminate the nonpolar phase polymerizations thus yielding lower molecular weight polymers which consequently have lower T_{dec} values.[41-44] The T_{dec} values are studied in a qualitative fashion only. A digital photograph of the thermal analysis samples (after experimental completion) is presented (bottom).

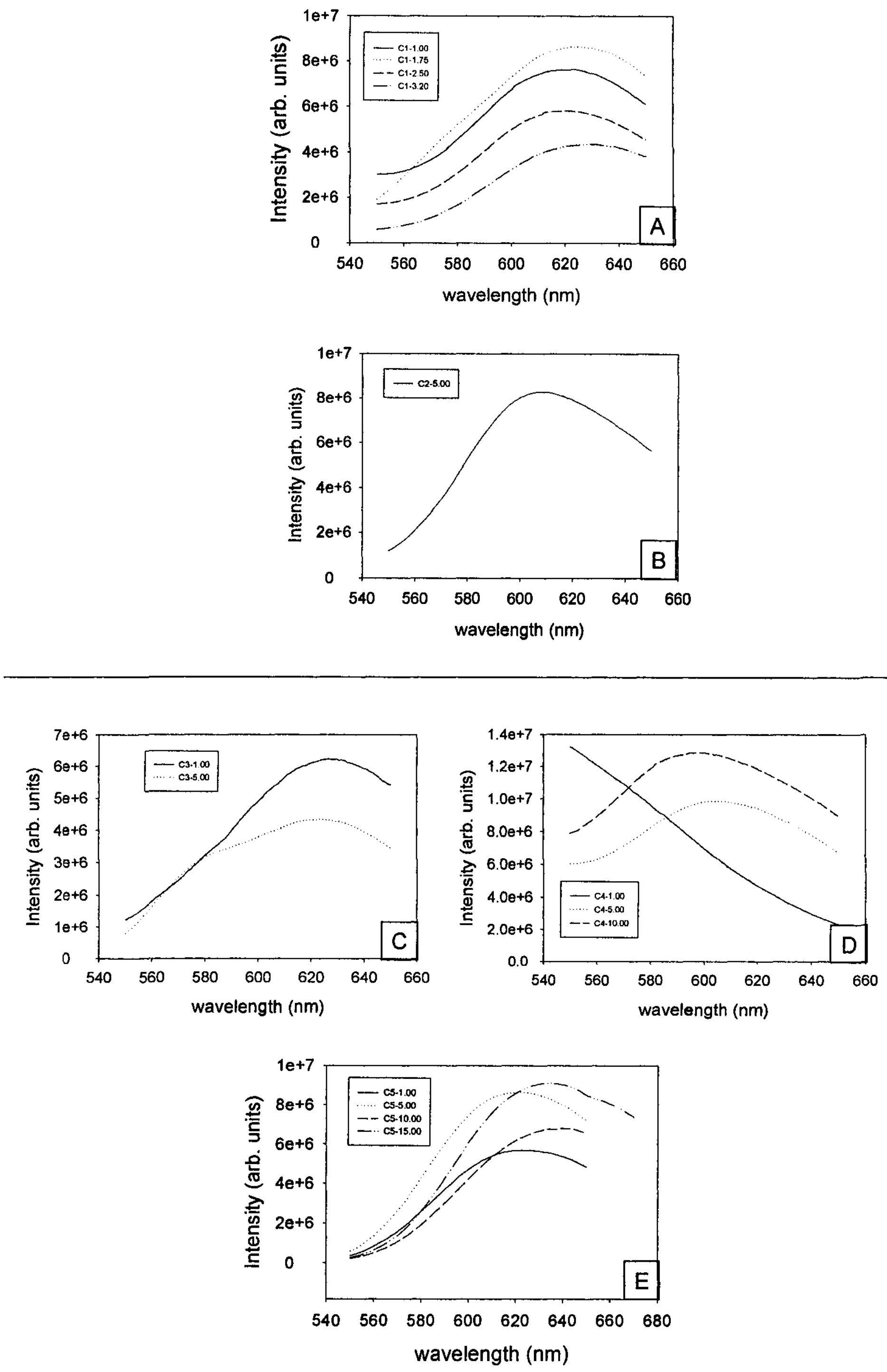

Figure 4. 8. Static emission spectra of [Ru(bpy)$_3$]Cl$_2$ chromophore-sequestered PERMCs. A: **C1** series composites. B: **C2** series composite. C: **C3** series composites. D: **C4** series composites. E: **C5** series composites.

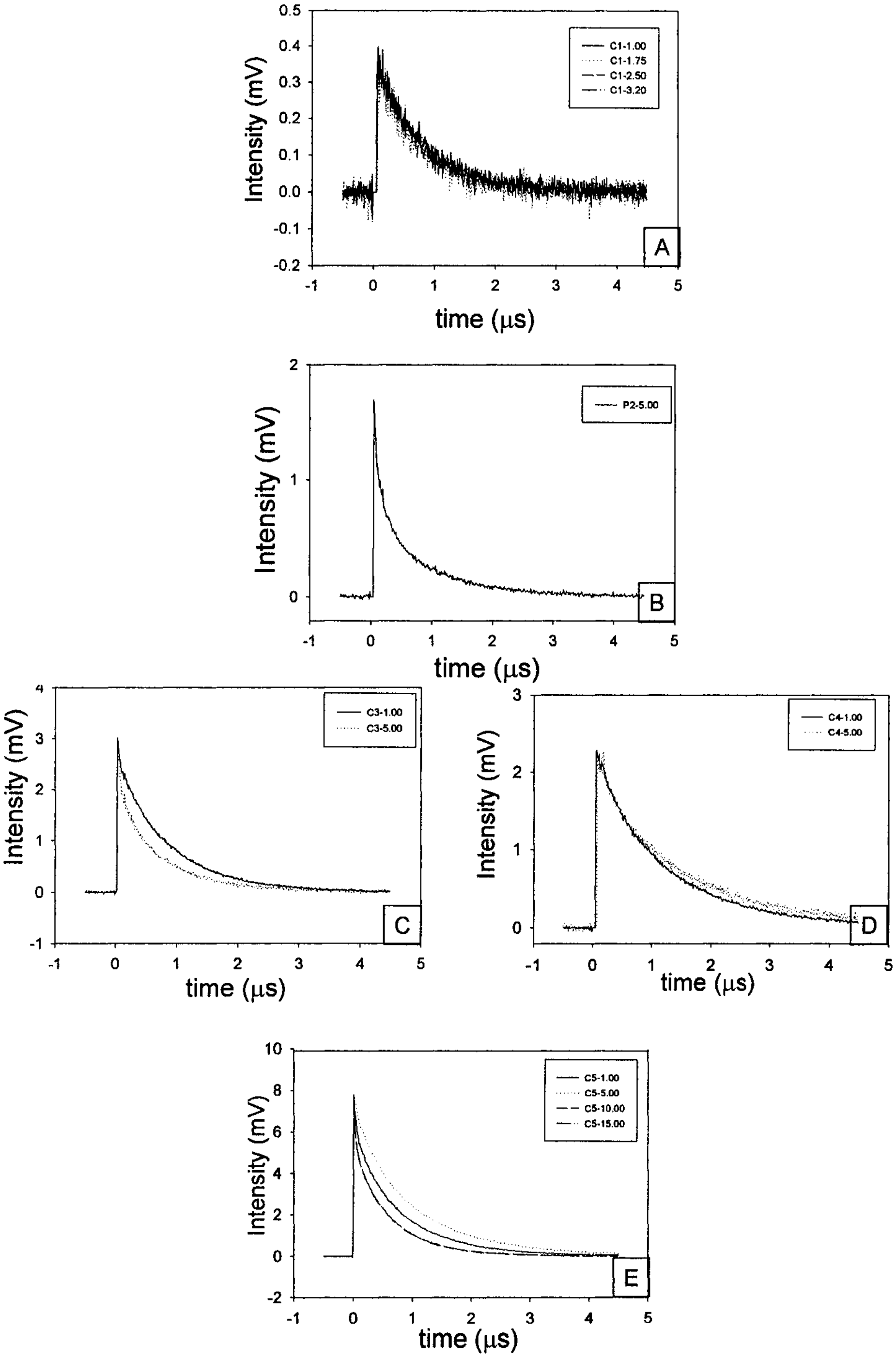

Figure 4. 9. Intensity-normalized time-resolved emission decays of [Ru(bpy)$_3$]Cl$_2$ chromophore-sequestered PERMCs. A: **C1** series composites. B: **C2** series composite. C: **C3** series composites. D: **C4** series composites. E: **C5** series composites.

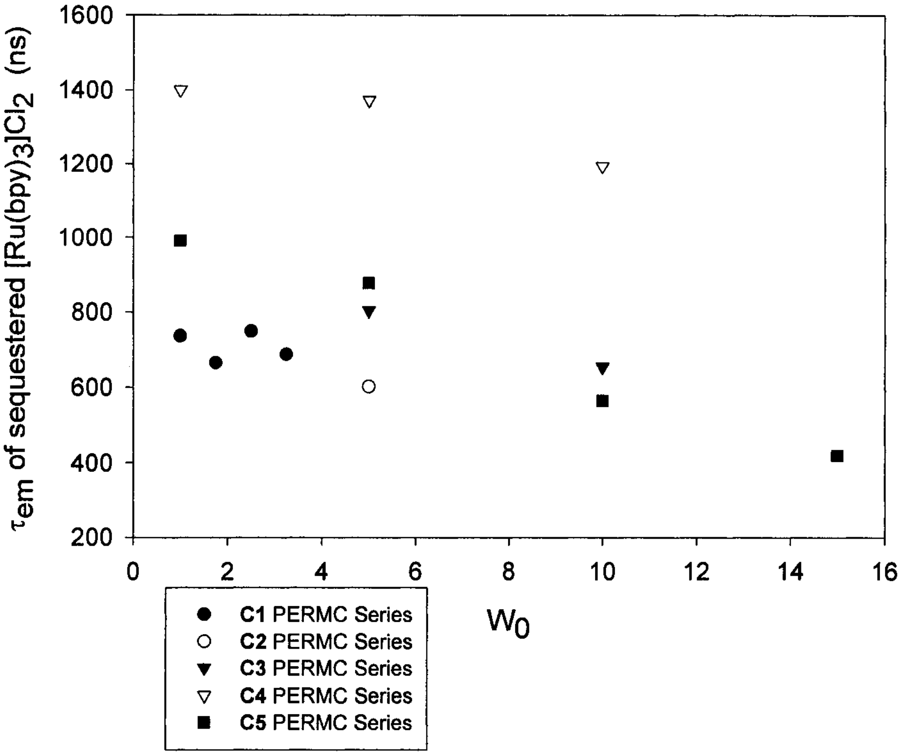

Figure 4. 10. Plot of sequestered chromophores' emission lifetimes versus W_0 for PERMC series **C1-C5.**

Chapter 4 References:

(1) Kremer, J. J.; Lu, Y.; Elliott, C. M.; Parkinson, B. P. "Chromophore-sequestered Polymer Encapsulated Aerosol-OT Reverse Micelle Composite Materials of Aqueous and Nonaqueous Polar Phase Constitutions," (In preparation).

(2) Elliott, C. M.; Steiner, U. E.; Kremer, J. J.; Hötzer, K. A. *Chem. Mater.* **2005**, *17*, 941-943.

(3) Menger, F. M.; Tsuno, T. *J. Am. Chem. Soc.* **1990**, *112*, 6723-6724.

(4) Menger, F. M.; Tsuno, T.; Hammond, G. S. *J. Am. Chem. Soc.* **1990**, *112*, 1264-1265.

(5) Zhu, X. X.; Banana, K.; Yen, R. *Macromolecules* **1997**, *30*, 3031-3035.

(6) Zhu, X. X.; Banana, K.; Liu, H. Y.; Krause, M.; Yang, M. *Macromolecules* **1999**, *32*, 277-281.

(7) Leporini, D.; Zhu, X. X.; Krause, M.; Jeschke, G.; Spiess, H. W. *Macromolecules* **2002**, *35*, 3977-3983.

(8) Kremer, J. J.; Elliott, C. M.; Hötzer, K. A.; Steiner, U. E. "Triad-sequestered Polymer Encapsulated Reverse Micelle Composite Materials as Optically Addressable Magnetic Field Sensors" (In preparation).

(9) De, T. K.; Maitra, A. *Adv. Coll. Inter. Sci.* **1995**, *59*, 95-193.

(10) Stevens, M. P. *Polymer Chemistry: An Introduction*, 3rd ed.; Oxford University Press: New York, NY, 1999.

(11) Kalyanasundarum, K. *Photochemistry and Photophysics of Polypyridine and Porphyrin Complexes*; Academic Press: London, 1992.

(12) Lide, D. R. ed. *Chemical Rubber Company Handbook of Chemistry and Physics*, 76th ed.; CRC Press: Boca Raton, FL, 1995.

(13) Hauenstein, B. L. Jr.; Dressick, W. J.; Gilbert, T. J.; Demas, J. N.; DeGraff, B. A. *J. Phys. Chem.* **1984**, *88*, 1902-1905.

(14) Snyder, S. W.; Buell, S. L.; Demas, J. N.; DeGraff, B. A. *J. Phys. Chem.* **1989**, *93*, 5265-5271.

(15) Palazzo, G.; Lopez, F.; Guistini, M.; Colafemmina, G.; Ceglie, A. *J. Phys. Chem. B* **2003**, *107*, 1924-1931.

(16) Tavernier, H. L.; Barzykin, A. V.; Tachiya, M.; Fayer, M. D. *J. Phys. Chem. B* **1998**, *102*, 6078-6088.

(17) Ambler, M. R.; McIntyre, D. *J. App. Pol. Sci.* **1977**, *21*, 3237-3250.

(18) Ambler, M. R.; McIntyre, D. *J. App. Pol. Sci.* **1977**, *21*, 2269-2282.

(19) Silber, J. J.; Biasutti, A.; Abuin, E.; Lissi, E. *Adv. Coll. Int. Sci.* **1999**, *82*, 189-252.

(20) Corbeil, E.; Levinger, N. E. *Langmuir* **2003**, *19*, 7264-7270.

(21) Lang, J.; Jada, A.; Malliaris, A. *J. Phys. Chem.* **1988**, *92*, 1946-1953.

(22) Lang, J.; Lalem, N.; Zana, R. *J. Phys. Chem.* **1992**, *96*, 4667-4671.

(23) Markina, Z. N.; Kryukova, G. N.; Kasaikin, V. A. *Usp. Kolloidn. Khim. Fiz.-Khim. Mekh.* **1992**, 76-81.

(24) Burstall, F. H. *J. Chem. Soc.* **1936**, 173-177.

(25) Accessed (http://www.buehlerltd.com, July 2005).

(26) Infelta, P. P.; Graetzel, M. *J. Chem. Phys.* **1979**, *70*, 1791-1796.

(27) Atik, S. S.; Thomas, J. K. *J. Am. Chem. Soc.* **1981**, *103*, 4367-4371.

(28) Joselevich, E.; Willner, I. *J Phys. Chem.* **1994**, *98*, 7628-7635.

(29) Izquierdo, C.; Moya, M. L.; Usero, J. L.; Casado, J. *J. Monat. Chem.* **1992**, *123*, 383-389.

(30) Lah, J.; Phar, C.; Vesnaver, G. *J. Phys. Chem. B* **2000**, *104*, 2522-2526.

(31) Pisarcik, M.; Devinsky, F.; Lacko, I. *Coll. Surf. A: Phys. Eng. Asp.* **2000**, *172*, 139-144.

(32) Hoffman, H.; Nagel, R.; Platz, G.; Ulbricht, W. *Coll. Polym. Sci.* **1976**, *254*, 812-834.

(33) Evans, R. M.; Attwood, D.; Chatham, S. M.; Far, S. J. *J. Pharm. Pharamac.* **1990**, *42*, 601-605.

(34) Kernen, P.; Agosti, R. D.; Strasser, R. J.; Darszon, A. *Biochem. Biophys. Acta* **1997**, *1321*, 71-78.

(35) Lizotte, J. R.; Erwin, B. M.; Colby, R. H.; Long, T. H. *J. Polym. Sci. A* **2002**, *44*, 583-590.

(36) Lee, B.-H. *J. Kor. Chem. Soc.* **1994**, *38*, 539-546.

(37) Cuccovia, I. M.; Dias, L. G.; Maximiano, F. A.; Chaimovich, H. *Langmuir* **2001**, *17*, 1060-1068.

(38) Hauenstein, B. L.; Dressick, W. J.; Buell, S. L.; Demas, J. N.; DeGraff, B. A. *J. Am. Chem. Soc.* **1983**, *105*, 4251-4255.

(39) Arkin, M. R.; Stemp, E. D. A.; Turro, C.; Turro, N. J.; Barton, J. K. *J. Am. Chem. Soc.* **1996**, *118*, 2267-2274.

(40) Kotka, B. V.; Valade, J. L.; Martin, W. N. *J. Appl. Polym. Sci.* **1973**, *17*, 1- 19.

(41) Nishizaki, H. *J. Appl. Polym. Sci.* **1980**, *25*, 2869-2877.

(42) Carrasco, F.; Pagès, P. *J. Appl. Polym. Sci.* **1996**, *61*, 187-197.

(43) Shirota, H.; Horie, K. *J. Phys. Chem. B* **1999**, *103*, 1437-1443.

(44) Shim, S. E.; Yang, S.; Choi, H. H.; Choe, S. *J. Polym. Sci A: Polym. Chem.* **2004**, *42*, 835-845.

(45) Drago, R. S. *Physical Methods for Chemists*, 2nd ed.; Surfside Scientific Publishers: Gainesville, FL, 1992.

(46) Raju, B. B.; Costa, S. M. B. *J. Phys. Chem. B* **1999**, *103*, 4309-4317.

(47) Raju, B. B.; Costa, S. M. B. *Spec. Acta A* **2000**, *56,* 1703-1710.

(48) Togashi, D.; Costa, S. M. B. *Phys. Chem. Chem. Phys.* **2000**, 22, 5437-5444.

(49) Rack, J. J.; McCleskey, T. M.; Birnbaum, E. R. *J. Phys. Chem. B* **2002**, *106*, 632-636.

(50) Janiak, C. *J. Chem. Soc. Dalton Trans.* **2000**, *239-241*, 3885-3896.

(51) Hunter, C. A.; Lawson, K. R.; Perkins, J.; Urch, C. J. *J. Chem. Soc. Perkin Trans.* **2001**, *2*, 651-669.

(52) Kumar, V. V.; Raghunathan, P. *Lipids* **1986**, *21*, 764-768.

(53) Dressick, W. J.; Cline III, J.; Demas, J. N.; DeGraff, B. A. *J. Am. Chem. Soc.* **1986**, *108*, 7567-7574.

Chapter 5.

Triad-sequestered Polymer Encapsulated Reverse Micelle Composite Materials of Cationic and Mixed Surfactant Systems as Optical Magnetic Field Sensors.

Introduction.

Polymer encapsulated Aerosol-OT (AOT) reverse micelle composite (PERMC) magnetic field sensors were introduced in Chapter 3. A recapitulation is in order. The ^{3}CSS state was observed for triad-sequestered PERMCs, but the corresponding τ_{CSS} values at 0 mT were an order of magnitude larger than the bulk solution τ_{CSS} value at 0 mT.[1] The longer τ_{CSS} values indicated that fewer collisional encounters occurred between the ^{3}CSS $A^{\bullet+}$ and $D^{\bullet+}$ moieties upon PERMC sequestration. Nevertheless, the sequestered triads exhibited substantial MFEs which increased the τ_{CSS} by one order of magnitude.[1]

Alternative PERMC synthesis strategies can be employed to increase electron transfer rates, decrease the τ_{CSS} at 0 mT, and thus further enhance the MFE. In particular, the surfactant composing the reverse micelles can be tuned in an effort to lessen the electrostatic and hydrophobic interactions between the triad and the micelles. In general, reverse micelles composed of cationic surfactant systems are larger in size than reverse micelles of anionic surfactant systems, and therefore promote faster electron transfer and relaxation rates.[2-3] For instance, Fayer and coworkers have determined that electron transfer rates are larger in cationic surfactant media because such surfactants generally have longer alkyl chain lengths which lower the solvent reorganization energy.[4] Photoyields are also larger in cationic reverse micelles than in anionic reverse micelles.[5]

Difficulties are encountered in the course of non-AOT surfactant-based PERMC preparation. Anionic AOT was initially used because it readily formed structurally stable micelles.[6] In addition, the AOT induced critical micelle concentration (i_{cmc}) was lowered due to the cationic triad sequestration. In contrast, it is more difficult to sequester these same cationic triads into reverse micelles composed of cationic surfactants, because of the respective increase in i_{cmc}.[7] A larger surfactant population does not participate in reverse micellar formation because of the larger i_{cmc}. Such surfactant species can terminate the composite precursor reverse micellar solution (CPRMS) nonpolar phase polymerizations. Moreover, cationic surfactants often require cosurfactants[8] which can also interfere in the CPRMS nonpolar phase polymerization.

Reproducible $[Ru(bpy)_3]Cl_2$ chromophore-sequestered PERMC materials synthesis strategies employing alternate surfactant systems were established before triad-sequestered PERMC magnetic field sensor analogs were prepared. Consult Chapter 4.[9] The sequestration of the cationic $[Ru(bpy)_3]Cl_2$ inside reverse micelles of cationic surfactants required verification. At the same time, the optical clarity of the chromophore-sequestered PERMCs had to be preserved. The $[Ru(bpy)_3]Cl_2$ chromophore was selected because of its well-understood emission qualities, and because it is in the D-C^{2+}-A^{2+} triads.[10-11] Three cationic surfactant systems were studied: cetyltrimethylammonium bromide:1-octanol ($CTAB:C_8OH$), cetyldimethylbenzylammonium chloride (CDBA), and hexadecylpyridinium bromide (HDPB) (Figure 5. 1). Phosphatidylcholine and Aerosol-OT:trioctylphosphine oxide

(TOPO) zwitterionic and mixed anionic surfactant systems, respectively, were examined to investigate the effect of mitigating triad-surfactant interactions (Figure 5. 1). Everything else being equal, the emission lifetimes (τ_{em}) of sequestered $[Ru(bpy)_3]Cl_2$ were shorter for PERMCs of cationic surfactant systems than PERMCs of AOT surfactant systems.[9] In contrast, the τ_{em} values of the sequestered $[Ru(bpy)_3]Cl_2$ were slightly shorter for PERMCs of mixed anionic surfactant systems than PERMCs of AOT surfactant systems

In this chapter, triad-sequestered PERMCs with surfactant systems other than pure AOT are prepared and the respective MFEs are characterized. A Triton X-100 surfactant-based triad-sequestered PERMC was also tested. Triton X-100 has an electrically neutral head group (Figure 5. 1).

Experimental Section.

Materials. Consult Chapter 3.

Preparation of the 1:5 Cetyltrimethylammonium bromide:1-octanol Surfactant-based PERMC Sensor (C1). Consult Figure 4. 2.

Preparation of the Cetyldimethylbenzylammonium bromide Surfactant-based PERMC Sensor (C2). Consult Figure 4. 2.

Preparation of the Hexadecylpyridinium bromide Surfactant-based PERMC Sensor (C3). Consult Figure 4. 2.

Preparation of the 3:2 Aerosol-OT:trioctylphosphine oxide Surfactant-based PERMC Sensor (C4). Consult Figure 2. 2.

Preparation of the Triton X-100 Surfactant-based PERMC Sensor (C5). Consult Figure 4. 2. Triton X-100 (Scintillation grade) was used as received from Eastman. First, 0.1543 g of Triton X-100 was weighed by difference into a 5.00 mL volumetric flask. The liquid surfactant was then diluted with the 2:1 styrene:divinylbenzene (effectively 75 % styrene according to reagent purities) nonpolar phase to the calibration mark to prepare a 50.00 mM Triton X-100 surfactant stock solution. First, 2.00 mL of 50.00 mM Triton X-100 was injected into a 15 x 44 mm 4 mL Fisher cap scintillation vial using a 2.00 mL glass syringe. A VWR Scientific® 3 x 10 mm magnetic stirbar was added to the mixture and then placed on a hot plate (set to heat a beaker of water to 45.0 °C) with the stirring mechanism set on low. A polar phase volume of 9.0 µL of 20.00 mM **T1** in water was injected into the solution using a 1710 Gastight® 100 µL glass syringe to prepare the micellar solution whose W_0 value was 5.00. The vial containing the clear reverse micellar solution was sealed with a 7 x 11 mm septum and then was purged with a slow steady stream of nitrogen to both facilitate thermal polymerization and to ensure that no dissolved oxygen remained which can react with photogenerated CSSs. The thermal polymerization of the nonpolar phase of the solution composite precursor was carried out in a 45.0 °C sand bath over a period of eight days while still stirring the reverse micellar solution with a magnetic stirrer placed underneath the sand bath. During this time, the physical state of the composite precursor solution changed through that of a viscous solution to a gel to a tacky polymer until finally cured into composite **C5**.

Polymer Encapsulated Reverse Micelle Composite (PERMC) Finishing. Consult Chapter 2.

Dynamic Light Scattering (DLS) Particle Sizing Analysis of Composite Precursor Reverse Micellar Solutions (CPRMSs). Consult Chapter 2.

Time-resolved Transient Absorption Spectroscopy Determinations of the Triad-sequestered Polymer Encapsulated Reverse Micelle Composite (PERMC) Sensor Magnetic Field Effects. Consult Figure 3. 5.

Results and Discussion.

Component Concentration and Polymerization Method-specific PERMC Preparations. Consult Chapter 4. The W_0 values of the triad-sequestered PERMCs presented herein are larger than corresponding W_0 values for chromophore ($[Ru(bpy)_3]Cl_2$)-sequestered PERMCs.[11] This is due to the more hydrophobic donor moieties of the triad which mitigate electrostatic repulsions between the cationic triad and surfactant head groups and thus decrease the i_{cmc}. Triad-sequestered PERMCs of CTAB:C_8OH, CDBA, HDPB, AOT:TOPO, and Triton X-100 surfactant systems, composites **C1**-**C5** respectively, were prepared from the polymerization of the 2:1 styrene:divinylbenzene nonpolar phases of corresponding CPRMSs of W_0 values 2.00, 15.00, 15.00, 15.00, and 5.00, respectively (Figure 5. 1, Table V. 1). Composites of larger W_0 values than those reported herein are poorer in optical quality and as such are not amenable to spectroscopic experiments.

The triad-sequestered CPRMS polymerization schemes followed from the analogous chromophore-sequestered CPRMSs polymerization schemes. Consult Chapter 4. Obtaining optically clear triad-sequestered CPRMSs of the Triton X-100 surfactant system was only achieved at temperatures of 50 °C with stirring. Such elevated temperatures facilitated the CPRMS nonpolar phase thermal polymerization to yield **C5**. A digital photograph demonstrating the non-light scattering nature of triad-sequestered PERMC optical magnetic field sensors **C1-C5** is provided herein (Figure 5. 2).

Dynamic Light Scattering (DLS) Particle Sizing Analysis of CPRMSs. Results from Dynamic Light Scattering particle sizing are reported for CPRMSs corresponding to PERMCs **C2** and **C4**. The CPRMSs corresponding to PERMCs **C1, C3** and **C5** can only be kept clear by continuously stirring and heating. This precludes DLS analysis. Ten micellar readings obtained at 25.0 °C are plotted for each radius. The micelles in the CPRMS corresponding to **C2** are larger and more monodisperse than those of **C4** (Figure 5. 3).

Preliminaries Regarding the Optical Detection of Magnetic Field Effects for PERMC Sensors. Time-resolved transient absorption CSS decay measurements determined the presence of photogenerated CSSs and any MFEs therefrom. The rate of CSS decay is monitored at 388 nm (the absorption maximum of the $A^{+\bullet}$ in the CSS). The increase in τ_{CSS} as a function of the physical state of the CPRMS nonpolar phase was explained in Chapter 3. All time-resolved transient absorption measurements examined the same 5 mm^3 volume in the interior of the optical sensor. The signal-to-noise for each CSS profile collected was optimized while simultaneously ensuring that the PERMC sensor did not burn in the 45 mW CSS photoexcitation beam during the experimental time scales. Any MFEs detected coincident with PERMC sample burning would not be representative of the true sample. The MFEs are quantitatively represented by fitting the CSS time profiles to monoexponential and biexponential decay functions. Consult Chapter 3.

Magnetic Field Sensing Capabilities of PERMC Sensor C1. A CSS was observed for composite **C1** upon photoexcitation with 450 nm light (Figure 5. 4). Thus, the 1:5 CTAB:C_8OH surfactant system provided sufficient molecular motion to the sequestered $[Ru(4\text{-}POZ)_2(4\text{-}DQ^{2+})](NO_3)_4$ triad to facilitate the formation and relaxation of the photoexcited biradical ^{3}CSS back to the ground state. The ^{3}CSS is contingent upon the presence of a fluid medium to mediate the collisional encounters between the oxidized donor and reduced acceptor moieties, $D^{+\bullet}$ and $A^{+\bullet}$ respectively. Signal-to-noise was compromised because of the low W_0 value of **C1**. The τ_{CSS} of composite **C1** under no applied field is 1.180 μs. This is a factor of 0.86 smaller than the τ_{CSS} of the $[Ru(4\text{-}POZ)_2(4\text{-}DQ^{2+})](NO_3)_4$ triad-sequestered AOT surfactant-based PERMC of W_0 15.00. Composite **C1** does not show an MFE (Table V. 2).

Magnetic Field Sensing Capabilities of PERMC Sensor C2. A CSS was observed for the **C2** sensor. This indicates that the triads are located in fluid micellar environments. The monoexponential τ_{CSS} of **C2** under no applied field is 0.9702 μs. This is a factor of 0.67 as large as the τ_{CSS} value obtained from the $[Ru(4\text{-}POZ)_2(4\text{-}DQ^{2+})](NO_3)_4$ triad-sequestered AOT surfactant-based PERMC of W_0 15.00. This shorter τ_{CSS} of **C2** under no applied field indicates that there is a larger frequency of collisions between the CSS $D^{+\bullet}$ and $A^{+\bullet}$ moieties. Such dynamics arise from the larger size of the CDBA reverse micelles coincident with lessened hydrophobic and electrostatic interactions between the cationic triad and the cationic surfactants.

Composite **C2** displays an MFE. The τ_{CSS} elongates as the field strength increases (Figure 5. 5). The MFE is reversible. In other words, the shortest τ_{CSS} monoexponential decay lifetime of 0.9702 μs is the same (to within one standard deviation) both before and after the application of an externally applied magnetic field. The time-resolved CSS profiles become more biexponential as magnetic field strengths increase.

A quantitative account of the MFE of **C2** is considered below. The slow components of the CSS decays elongate as the field strength increases, but only up to the saturation field strength which is ca. 25 mT (Table V. 2). Negligible MFE sensitivity remains at fields above 100 mT (Figure 5. 5). Meanwhile, the fast decay components of the biexponentially fit CSS lifetimes hold constant at ca. 0.44 μs across the range of field strengths examined. The MFE magnitude is dampened because of a tailing feature in the CSS profiles evident at longer time scales. The tailing feature is consistent with an incomplete CSS decay back to a ΔA value of zero (Figure 5. 5). The tailing feature of the CSS decays is attributed to either the continual presence of the $A^{+\bullet}$ moiety once the photoexcited triad returns to its ground state or an unknown photogenerated species which absorbs light at 388 nm. The MFE of composite **C2** is unlike that of the $[Ru(4\text{-}POZ)_2(4\text{-}DQ^{2+})](NO_3)_4$ triad-sequestered AOT surfactant-based PERMC insomuch as the MFE saturation field strength occurs at weaker field strengths for the former. The exact reason why this phenomenon holds is unclear at present.

Magnetic Field Sensing Capabilities of PERMC Sensor C3. A CSS was observed for composite **C3** (Figure 5. 6). Accordingly, the water polar phase domains which sequester $[Ru(4\text{-}POZ)_2(4\text{-}DQ^{2+})](NO_3)_4$ triads must still be intact inside PERMC **C3**. The 0.8432 μs τ_{CSS} for HDPB surfactant-based composite **C3** is the smallest of all representative PERMCs at 0 mT. The τ_{CSS} of composite **C3** under no applied field is a factor of 0.60 as large as the $[Ru(4\text{-}POZ)_2(4\text{-}DQ^{2+})](NO_3)_4$ triad-sequestered AOT surfactant-based PERMC τ_{CSS} of W_0 15.00 at 0 mT. The surfactant is directly responsible for such τ_{CSS} behavior at 0 mT. Composite **C3** has N-pyridinium surfactant polar head groups which strongly interact through lipophilic pi-pi stacking with the CSS donor and acceptor. Thus, these normally lipophilic pendant donor groups will now remain closer to, if not entirely in, the sequestered fluid water polar phase rather than being embedded in the surfactant hydrophobic tails. The number of collisional encounters between the CSS $D^{+\bullet}$ and $A^{+\bullet}$ moieties increases consequently decreasing in τ_{CSS} at 0 mT. The result shows the importance of tailoring the surfactant system to the polar probes of interest.

Composite **C3** exhibits an MFE which is similar to that of **C2**. Time-resolved transient absorption CSS profiles were collected at different magnetic field strengths (Figure 5. 6). The long component of the τ_{CSS} increases as field strength increases. The fast component of the τ_{CSS} holds constant at ca. 0.430 μs across all field strengths examined. As the strength of the magnetic field increases, the CSS decay becomes more biexponential in quality, and the τ_{CSS} elongates.

The MFE is quantitatively represented upon plotting τ_{CSS} values versus the externally applied field strengths (Figure 5. 6, Table V. 2). The MFE magnitude of **C3** is smaller than $[Ru(4\text{-}POZ)_2(4\text{-}DQ^{2+})](NO_3)_4$ triad-sequestered AOT surfactant-based PERMC, because of the presence of a tailing feature at long times ($t > 5$ μs). A further deviation in the solid sensor's capabilities, as compared to degassed bulk solution conditions, arises from the MFE saturating at weak field strengths of < 100 mT.

To conclude, the representative $[Ru(4\text{-}POZ)_2(4\text{-}DQ^{2+})](NO_3)_4$ triad-sequestered polymer encapsulated CDBA and HDPB reverse micelle composite magnetic field sensors, **C2** and **C3** respectively, in the very least, are 'null' sensors for the presence of externally applied magnetic fields ≥ 25 mT. Changes in transient absorption spectra can substitute as the optical magnetic field transducer

Magnetic Field Sensing Capabilities of PERMC Sensor C4. A CSS was observed for the AOT:TOPO sequestered $[Ru(4\text{-}POZ)_2(4\text{-}DQ^{2+})](NO_3)_4$ triads in composite **C4**. The triads are located within micellar fluid media (Figure 5. 7). However, the CSS decay of composite **C4**--under no externally applied field--follows biexponential kinetics. At 0 mT, the short and long components of the CSS lifetime were determined to be 0.444 and 4.769 μs, respectively (Table V. 2). Therefore, the triad is in two distinct chemical environments attributing to the two different rates of CSS decay at 0 mT.

The long component of the CSS lifetime (under 'field-off' conditions) shows a modest field effect, but only over 1700 mT. The MFE is modest in this case, because of the already large (> 4 μs) τ_{CSS} under no applied field. The loss of field sensitivity derives from the decrease in frequency of collisional encounters between CSS $D^{+\bullet}$ and $A^{+\bullet}$ moieties coincident with smaller micelle sizes.

The magnitude of the MFE can be quantitatively displayed upon plotting the τ_{CSS} slow and fast components of versus field strength (Figure 5. 7). The slow component of the CSS decay (under 'field-off' conditions) increases by ca. two microseconds over 1.7 T to 4.765 μs at the saturation field strength. The fast component of CSS decay is independent of field strength.

Magnetic Field Sensing Capabilities of PERMC Sensor C5. No CSS is observed for composite **C5**. The triad in a fluid chemical environment. It has been previously reported by Demas and coworkers that Triton X-100 cannot partition $[Ru(bpy)_3]Cl_2$ in water from an isooctane nonpolar phase.[12] Yet, at the outset, it had been hoped that the either the increased lipophilicity of the donor groups of the triad or the large positive charge of the triad would facilitate its micellar sequestration. Instead, the triad is embedded in the larger poly(ethyleneoxide) polar head group. Related phenomena have been observed by Bhattacharya and coworkers.[13]

Conclusions.

Donor-Chromophore-Acceptor $[Ru(4\text{-}POZ)_2(4\text{-}DQ^{2+})](NO_3)_4$ triad-sequestered PERMCs of alternate surfactant systems have been prepared. Selected sensors can optically detect magnetic fields through detecting photoexcited triad CSS states ($D^{+\bullet}$-C^{2+}-$A^{+\bullet}$). Composite **C1** employing a CTAB:C_8OH surfactant system showed no MFE. Composites **C2** and **C3**, employing cationic CDBA and HDPB surfactant systems respectively, showed MFEs which saturated at weak field strengths. Composite **C4** employing an AOT:TOPO surfactant:cosurfactant anionic surfactant system showed a modest MFE over 1700 mT. Composite **C5** employing Triton X-100, an electrically neutral surfactant system, showed no CSS and thus no MFE. The $[Ru(4\text{-}POZ)_2(4\text{-}DQ^{2+})](NO_3)_4$ triad-sequestered PERMCs of AOT, CDBA, HDPB, and AOT:TOPO surfactant systems represent a new class of optical-based organic magnetic field sensors.

Chapter 5.

Tables

Table V. 1. Composition of triad-sequestered CPRMSs and PERMCs of alternate surfactant systems.

PERMC	Nonpolar phase	Polar phase[a]	[surfactant]	[co-surfactant]	W_0	Polymerization[b]	T_P (°C)	t_P (hours)
C1	poly(styrene-co-divinylbenzene)	20.00 mM T1 in H_2O	50.00 mM CTAB	250 mM 1-octanol	2.00	thermal	45	192
C2	poly(styrene-co-divinylbenzene)	20.00 mM T1 in H_2O	50.00 mM CDBA	(c)	15.00	radical	38	96
C3	poly(styrene-co-divinylbenzene)	20.00 mM T1 in H_2O	50.00 mM HDPB	(c)	15.00	radical	45	48
C4	poly(styrene-co-divinylbenzene)	20.00 mM T1 in H_2O	37.75 mM AOT	12.25 mM TOPO	15.00	radical	38	96
C5	poly(styrene-co-divinylbenzene)	20.00 mM T1 in H_2O	50.00 mM Triton X-100	(c)	5.00	thermal	50	192

(a) The **T1** triad is $[Ru(II)(4\text{-}POZ)_2(4\text{-}DQ^{2+})](NO_3^-)_4$.

(b) Thermal polymerizations follow the Mayo Mechanism.[46-47] Radical polymerizations follow from the addition of 1.0 wt. % ADPN radical initiator.

(c) No cosurfactant was used.

Table V. 2. The Magnetic Field Effect of triad-sequestered PERMCs of alternate surfactant systems.

$\Delta A = A\exp(-tx)$						$\Delta A = A_{fast}\exp(-xt_{fast}) + A_{slow}\exp(-xt_{slow})$						
PERMC	**Field Strength (mT)^a**	**A**	**t (μs)**	**σ^b**	**$R^{2\,b}$**	**A_{fast}**	**t_{fast} (μs)**	**σ**	**A_{slow}**	**t_{slow} (μs)**	**σ^b**	**$R^{2\,b}$**
C1	0	0.0125	1.1864	0.0165	0.9127	0.0058	0.4645	0.0359	0.0088	2.2179	0.1597	0.9415
	10	0.0127	1.1935	0.0149	0.932	0.0093	0.3286	0.0448	0.0053	1.5358	0.0594	0.9493
	20	0.012	1.1828	0.0169	0.9092	0.077	0.4171	0.0384	0.0065	1.9612	0.1213	0.9342
	50	0.0126	0.9879	0.0127	0.9388	0.0112	0.1213	0.0222	0.0039	1.0997	0.0226	0.9459
	100	0.0124	1.0417	0.014	0.9277	0.0078	0.3921	0.0535	0.0062	1.4693	0.00893	0.9385
	1000	0.0116	1.1814	0.0166	0.9124	0.007	0.3647	0.0342	0.0069	1.8153	0.0885	0.9371
C2	0	0.00293	0.97024	0.01756	0.93123	0.00112	2.13469	0.10817	0.00285	0.36397	0.01718	0.97897
	15	0.00265	1.26214	0.02239	0.92313	0.00122	2.51864	0.11352	0.00242	0.39267	0.01908	0.97955
	20	0.00222	1.81728	0.03023	0.91699	0.00127	3.23985	0.11818	0.00181	0.42135	0.02039	0.98158
	250	0.00242	2.07303	0.03925	0.88789	0.00155	3.46149	0.11241	0.00219	0.34055	0.01782	0.97283
	1000	0.00249	2.01801	0.03769	0.89117	0.00144	3.7684	0.14385	0.00215	0.40471	0.01878	0.97783
C3	0	0.00397	0.84321	0.0222	0.85785	0.00501	0.31632	0.00834	0.00097	3.58211	0.20848	0.98114
	24	0.00312	1.60038	0.03504	0.86496	0.00339	0.45267	0.01795	0.00121	4.6606	0.33396	0.97482
	55	0.00457	0.60809	0.01033	0.97375	0.00452	0.40193	0.0117	0.00153	5.06521	0.25129	0.98325
	103	0.00347	1.93387	0.04094	0.86265	0.00374	0.43988	0.01533	0.00163	4.84776	0.24145	0.98168
	250	0.00329	1.49044	0.03025	0.88808	0.00385	0.37384	0.01284	0.00169	3.92372	0.14486	0.98258
	502	0.00336	1.53001	0.03284	0.87289	0.00378	0.47147	0.01859	0.0012	4.75612	0.38128	0.97574
	1007	0.00314	1.68092	0.0365	0.86492	0.00354	0.44566	0.01756	0.0013	4.57518	0.29459	0.97632
C4	0	0.0038	2.58581	0.04516	0.89434	0.00291	0.44018	0.01572	0.00241	4.76945	0.13881	0.98708
	34	0.00301	3.35482	0.06276	0.87326	0.00216	0.36154	0.01289	0.0022	5.55646	0.12442	0.9849
	127	0.00309	3.21448	0.06194	0.86668	0.00232	0.42885	0.01658	0.00209	6.03366	0.19646	0.98192
	1202	0.00336	3.14237	0.05654	0.88331	0.00245	0.41863	0.0156	0.00233	5.52315	0.14991	0.9852
	1793	0.00274	4.09151	0.08677	0.83687	0.00188	0.37061	0.01646	0.00205	7.1653	0.22974	0.97213
C5	0	CSS detected										

(a) The 'round number' magnetic field strengths were generated by adjusting the direct current power source in circuit with the electromagnet (Figure 3. 5).

(b) The standard deviations and linear regression values reported were obtained for the corresponding fit functions (located at the top of the table) run in Origin 7.0®.

Chapter 5.

Figures

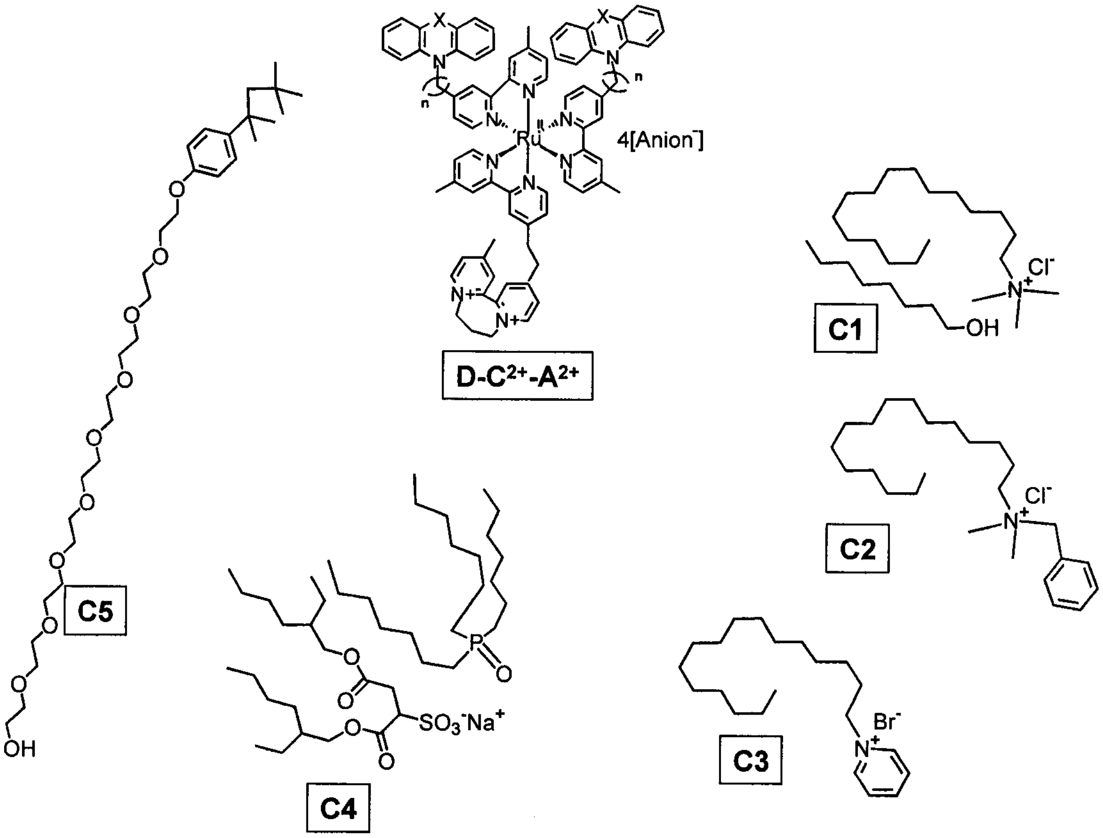

Figure 5. 1. Clockwise from the top: The **T1** Donor-Chromophore-Acceptor (D-C^{2+}-A^{2+}) triad $[Ru(II)(4\text{-}DQ^{2+})_2(4\text{-}POZ)_2](NO_3^-)_4$ which is the molecular-level magnetic field sensing species and the surfactant systems employed in the polymer encapsulated reverse micelle composites (PERMCs) **C1-C5**: cetyltrimethylammonium bromide:1-octanol (5 CTAB: 1 C_8OH) (P = [cosurfactant]/[surfactant] = 5.00) (**C1**), cetyldimethylbenzylammonium chloride (CDBA) (**C2**), hexadecylpyridinium bromide (HDPB) (**C3**), Aerosol-OT:trioctylphosphine oxide (P = 0.66) (3 AOT: 2 TOPO) (**C4**), and Triton X-100 (**C5**).

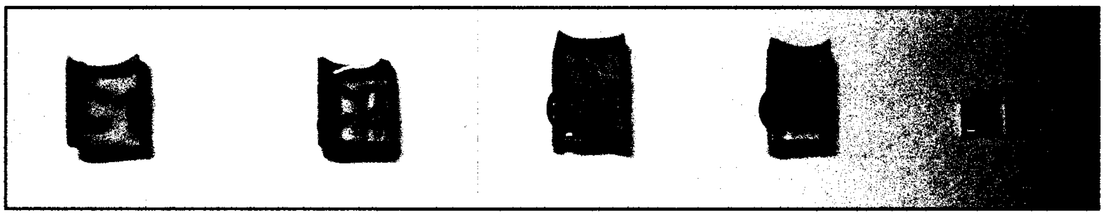

Figure 5. 2. A digital photograph exhibiting the optical quality of the analyzed triad-sequestered PERMC sensors **C1-C5.** The orange color of the composites is due to the metal-to-ligand charge-transfer (MLCT) absorbance of the sequestered triads within the composites. The transparent nature of the composites is due to the absence of both micellar aggregates and regions of microcrystallites composed of shorter, prematurely-terminated poly(styrene-*co*-divinylbenzene) chains. The dimensions of each of these features in the above composites are below the light scattering limit.

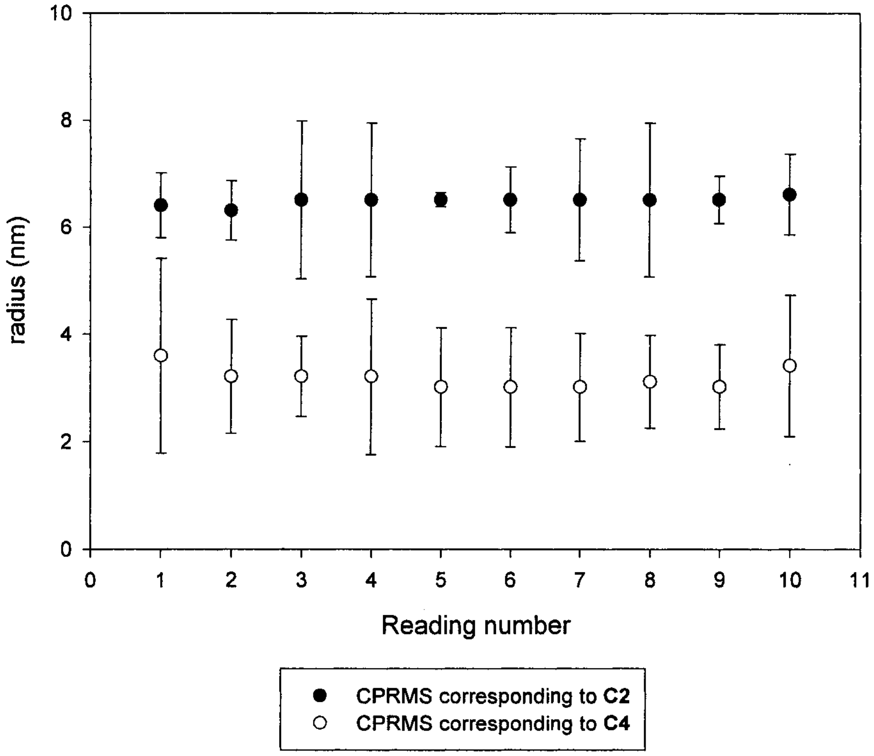

Figure 5. 3. Successive DLS particle sizing measurements taken on triad-sequestered CPRMSs corresponding to PERMCs **C2** and **C4** plotted against the reading number. The radii of the micelles in the CPRMS corresponding to PERMC **C2** are larger and more monodisperse than those of the mixed anionic surfactant system corresponding to PERMC **C4**. Micellar radii data on CPRMSs corresponding to PERMCs **C1**, **C3**, and **C5** cannot be obtained because of difficulties in the course of maintaining the optical quality of the concerned solutions at 25.0 °C (Consult Figure 4. 2).

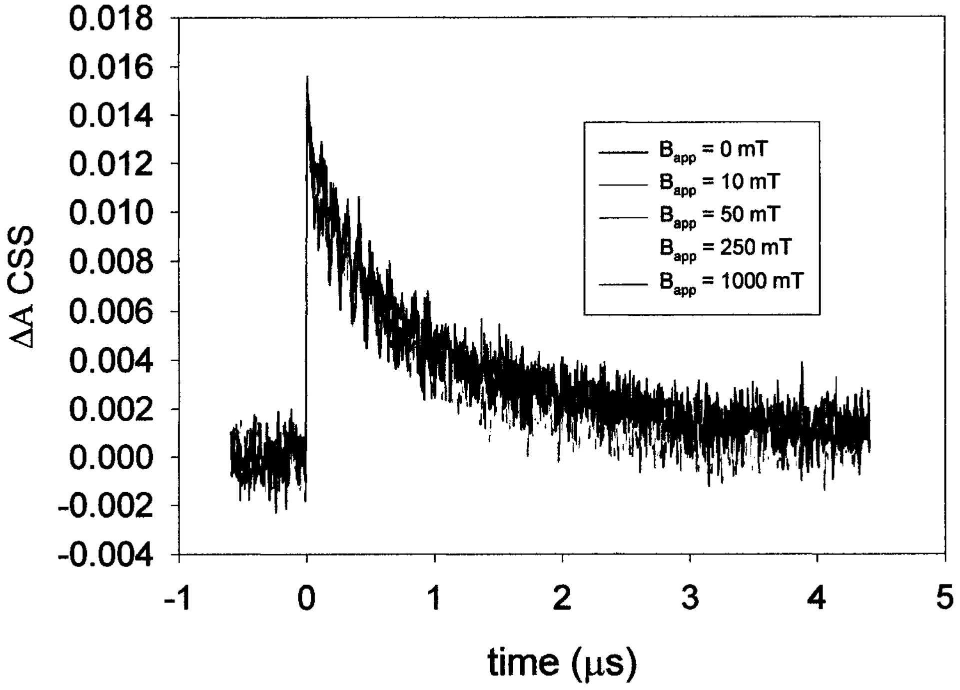

Figure 5. 4. Raw transient absorption decays of **T1** triad-sequestered PERMC **C1** demonstrating a negligible MFE. The CSS decays were monitored at 388 nm which is the absorption maximum of the reduced acceptor ($A^{+\bullet}$). The S:N is poor because of the low concentration of **T1** in the PERMC.

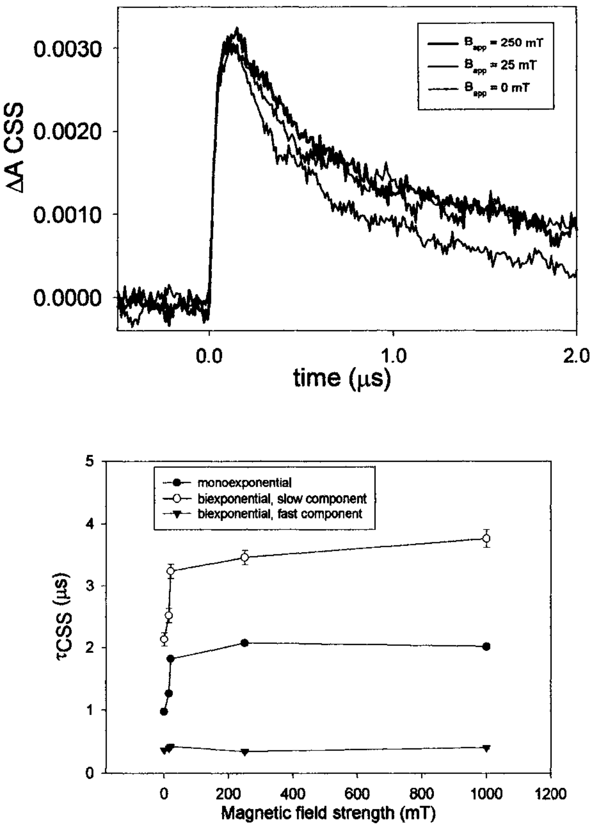

Figure 5. 5. Raw transient absorption decays of **T1** triad-sequestered PERMC **C2** demonstrating a considerable MFE (top) and a plot of τ_{CSS} values obtained from both monoexponential and biexponential decay fits versus the applied magnetic field strength (bottom). The MFE saturates at relatively low fields, whereupon the τ_{CSS} of solid composite **C2** does not appreciably elongate as field strengths exceed 100 mT. The CSS decays were monitored at 388 nm which is the absorption maximum of the reduced acceptor ($A^{+\bullet}$).

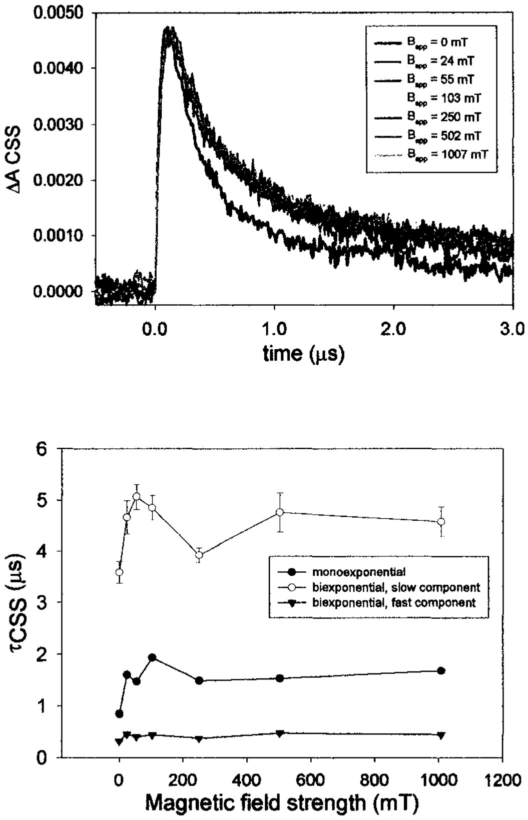

Figure 5. 6. Raw transient absorption decays of **T1** triad-sequestered PERMC **C3** demonstrating a considerable MFE (top) and a plot of τ_{CSS} values obtained from both monoexponential and biexponential decay fits versus the applied magnetic field strength (bottom). The MFE saturates at relatively low fields, whereupon the τ_{CSS} of solid composite **C3** does not appreciably elongate as field strengths exceed 50 mT. The CSS decays were monitored at 388 nm which is the absorption maximum of the reduced acceptor ($A^{+\bullet}$).

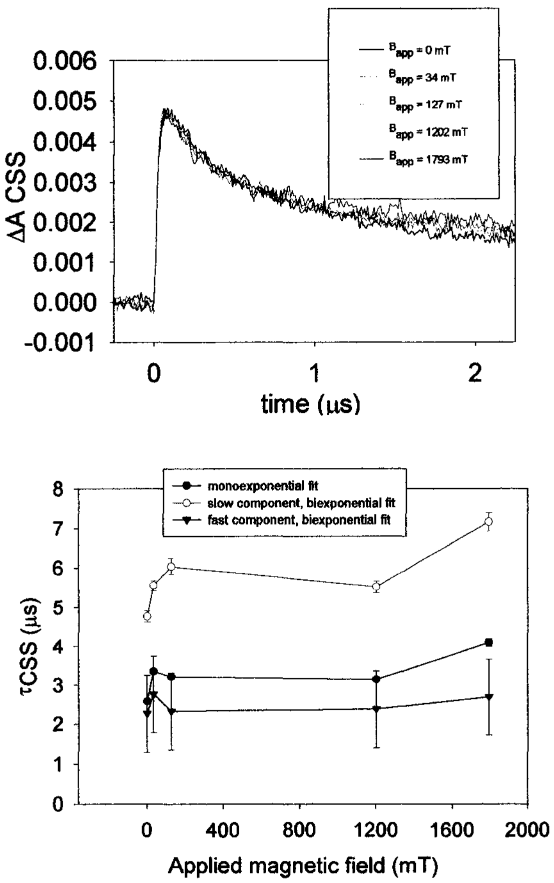

Figure 5. 7. Raw transient absorption decays of **T1** triad-sequestered PERMC **C4** demonstrating a modest MFE (top) and a plot of τ_{CSS} values obtained from both monoexponential and biexponential decay fits versus the applied magnetic field strength (bottom). AN MFE is observed only over a large 1.7 T range. The CSS decays were monitored at 388 nm which is the absorption maximum of the reduced acceptor ($A^{+\bullet}$).

Chapter 5 References:

(1) Kremer, J. J.; Elliott, C. M.; Hötzer, K. A.; Steiner, U. E. "Triad-sequestered Polymer Encapsulated Reverse Micelle Composite Materials of Cationic and Mixed Surfactant Systems as Magnetic Field Sensors" (In preparation).

(2) Palazzo, G.; Lopez, F.; Guistini, M.; Colafemmina, G.; Ceglie, A. *J. Phys. Chem. B* **2003**, *107*, 1924-1931.

(3) Tavernier, H. L.; Barzykin, A. V.; Tachiya, M.; Fayer, M. D. *J. Phys. Chem. B* **1998**, *102*, 6078-6088.

(4) Weidemaier, K.; Tavernier, H. L.; Fayer, M. D. *J. Phys. Chem. B* **1997**, *101*, 9352-9361.

(5) Kang, Y. S.; McManus, H. J. D.; Liang, K.; Kevan, L. *J. Phys. Chem.* **1994**, 98, 1044-1048.

(6) Porter, M. R. *Handbook of Surfactants*; Chapman and Hall: New York, NY, 1991.

(7) Snyder, S. W.; Buell, S. L.; Demas, J. N.; DeGraff, B. A. *J. Phys. Chem.* **1989**, *93*, 5265-5271.

(8) Corbeil, E. M.; Riter, R. E.; Levinger, N. E. *J. Phys. Chem. B* **2004**, *108*, 10777-10784.

(9) Kremer, J. J.; Elliott. C. M. "Chromophore-sequestered Polymer Encapsulated Reverse Micelle Composite Materials of Cationic, Zwitterionic, and Mixed Surfactant Systems" (In preparation).

(10) Klumpp, T.; Linsenmann, M.; Larson, S. L.; Limoges, B. R.; Burssner, D.; Krisseinel, E. B.; Elliott, C. M.; Steiner, U. E. *J. Am. Chem. Soc.* **1999**, *121*, 1076-1087.

(11) Elliott, C. M.; Freitag, R. A.; Blaney, D. D. *J. Am. Chem. Soc.* **1985**, *107*, 4647-4655.

(12) Mandal, K.; Hauenstein, B. L. Jr.; Demas, J. N.; DeGraff, B. A. *J. Phys. Chem.* **1983**, *87*, 328-331.

(13) Bhattacharyya, K. *Molec. Supramolec. Photochem.* **1999**, *3*, 283-339.